REPUBLIQUE DU CAMEROUN
Paix – Travail – Patrie

UNIVERSITE DE YAOUNDE I

FACULTE DES SCIENCES

CENTRE DE RECHERCHE ET DE FORMATION DOCTORALE EN SCIENCES, TECHNOLOGIE ET GEOSCIENCES

UNITE DE RECHERCHE ET DE FORMATION DOCTORALE EN CHIMIE ET APPLICATIONS

REPUBLIC OF CAMEROON
Peace – Work – Fatherland

UNIVERSITY OF YAOUNDE I

FACULTY OF SCIENCE

POSTGRADUATE SCHOOL OF SCIENCE, TECHNOLOGY AND GEOSCIENCE

RESEARCH AND POSTGRADUATE TRAINING UNIT OF CHEMISTRY AND ITS APPLICATIONS

LABORATORY OF APPLIED INORGANIC CHEMISTRY
LABORATOIRE DE CHIMIE INORGANIQUE APPLIQUE

Mn(II), Co(II) and Cu(II) Complexes of 1,10-Phenanthroline with co-ligands: Synthesis, Characterisation, Thermal and Biological Properties

A Thesis Submitted in partial fulfilment of the requirements for the award of a Doctorate/PhD degree in Chemistry

Specialty: Inorganic Chemistry
Option: Coordination Chemistry

By:
Donatus BEKINDAKA ENI
Registration No.: 05S234
MSc Chemistry (UYI)

Supervised by:
AGWARA Moïse ONDOH, PhD,
(Professor)

2021

ATTESTATION OF THESIS CORRECTION

We, the undersigned KETCHA Joseph MBADCAM (Examiner), EMADAKAlphonse (Examiner), AGWARA Moise ONDOH (Supervisor) and NDIFON Peter TEKE (President), attest that this PhD thesis defended publicly on Thursday 1st April 2021 at 1 pm in the Multimedia Hall of the Faculty of Science, University of Yaounde I, by Donatus BEKINDAKA ENI on the Topic:**"Mn(II), Co(II) and Cu(II) complexes of 1,10-phenanthroline and co-ligands: Synthesis, Characterization, Thermal and Biological Properties",** for the award of a Doctorate/PhDin Inorganic Chemistry, has been corrected in conformity with the recommendations of defense jury.

In this testimony whereof, this attestation is issued.

Yaounde, 8th June2021

Examiners

KETCHA Joseph MBADCAM
Professor

EMADAK Alphonse
Associate Professor

Supervisor

AGWARA Moise ONDOH
Professor

President

NDIFON Peter TEKE
Professor

DEDICATION

This thesis is dedicated to

my parents Mr/Mrs ENI John Manfred

and

my daughters ISUMBE Irene BEKINDAKA and NYAMA Lorene ENI

ACKNOWLEDGEMENT

I take this opportunity to express my profound gratitude and indebtedness to my supervisor Prof. Agwara Moïse Ondoh for mentorship, guidance, support, encouragement, and inspiration throughout my doctoral work.

My profound gratitude goes to my research mentor Dr Mbom Divine Yufanyi, of the University of Bamenda for the technical support and time, which helped in making this research work a success.

I would also like to express my gratitude to the Head of Department of Inorganic Chemistry and the head of the Laboratory of Coordination Chemistry for allowing me to use the facilities of the department and the Laboratory.

I wish to express my appreciation to the staff of the Department of Inorganic Chemistry of the University of Yaounde I for training, assistance, suggestions and useful discussions during my research work.

Special thanks to Dr Rajamony Jagan of the Institute of Technology, Madras, Chennai, India; Dr Kevin Klausmeyer, Department of Chemistry and Biochemistry Baylor University, USA for assistance with the single crystal structures and data; and Dr. Peter Lönnecke, Institute of Inorganic Chemistry, Faculty of Chemistry and Mineralogy, Universität Leipzig, Germany.

I am also thankful to Prof. Fabrice Fekam Boyom of the Department of Biochemistry, University of Yaounde I for assisting with the antimicrobial test on the complexes.

My appreciations go to Dr Che Dieudonne Tabong, Dr Amah Colette and Dr Ntum Sally Judith, Dr Sado Yanick Gaelle for their immense help, and cooperation throughout this work.

Special thanks to my research mates of the Department of Inorganic Chemistry for their collaboration, support, suggestions, as well as the good and motivating work atmosphere created during research.

Gratitude to my mothers; Mrs ENI Sarah and Mrs ENI Christiana, my uncles; Mr ENI Cletus and Mr EKOKO Julius, my lovely wife; Mrs ENI ISUMBE Maria and my elder sister Miss ENI Beatrice for their wonderful support. I am extremely thankful to Hon. Chief MBILE Norbert for his moral, financial and fatherly support throughout my studies.

TABLE OF CONTENTS

LIST OF TABLES

LIST OF FIGURES

LIST OF ABBREVIATIONS

BMCA	Bis(methoxycarbimido)aminato
CCDC	Cambridge Crystallographic Data Centre
CN	Coordination Network
CP	Coordination Polymers
dca	Dicyanamide Anion
dcg	Dicyanoguanidinate Anion
FTIR	Fourier Transform Infrared
HUS	Haemolytic Uremic Syndrome
LMP	Laboratory of Molecular Pharmacology
MH	Mueller-Hinton
MIC	Minimum Inhibition Concentration
NCCLS	National Committee for Clinical Laboratory Standards
Phen	1,10-Phenanthroline
PXRD	Powdered X-Ray Diffraction
RB	Reference Antibiotics
RF	Reference Antifungal

ABSTRACT

Five novel complexes were synthesised in a stoichiometric reaction ratio 1:2:2 of the metal(II) salt, 1,10-phenanthroline and co-ligand (dicyanamide, azide and nitrate) respectively, in a methanol/H_2O milieu at 85 °C under reflux in air. The obtained complexes; $[Mn(phen)_2(NO_3)_2]$ (**1**), $[Mn(phen)_2(N_3)_2]$ (**2**), $[Mn(phen)_2(dca)_2]$ (**3**), [Cu(phen)(BMCA)](NO_3) (**4**); BMCA = bis(methoxycarbimido)aminato ligand and $[Co(phen)_2(NO_3)](dcg)\cdot(H_2O)$ (**5**); dcg = dicyanoguanidinate anion have been fully characterised using elemental analysis, infrared and UV-Vis spectroscopy, room temperature magnetic susceptibility measurements and thermal analytical techniques. Crystal structures for the complexes have been obtained and were determined by single crystal X-ray diffraction. Complexes **1** and **2** crystallize in an orthorhombic crystal system with space group *Pbcn* while complex **3** crystallizes in the monoclinic crystal system with space group $P2_1/c$. Complexes **4** and **5** crystallise in the monoclinic crystal system and the structures are stabilised by extended hydrogen bonding networks as well as aromatic π–π stacking interactions. Dicyanamide anion was transformed in **4** and **5** to bis(methoxycarbimido)aminato (BMCA) ligand and dicyanoguanidinate (dcg) anions, respectively. These metal-promoted or mediated transformations proceed through a nucleophilic attack of the nitrile groups of dicyanamide on methanol (case of BMCA), or on another dicyanamide (case of dcg). The magnetic moments of **1**-**3** are consistent with d^5 high spin octahedral geometry. The magnetic moment of **4**, is 1.75 B.M corresponding to one unpaired electron which is slightly greater than the spin only value of 1.73 B.M for d^1. That of **5**, is 3.92 B.M which is in agreement with d^7 high spin Co(II) ion octahedral geometry. The thermal properties of the complexes have also been evaluated. The TGA thermograms of all the complexes show that they are stable up to 200 °C. The composition of the residue of **4** after thermal decomposition was characterised by powder X-ray diffraction (PXRD). The PXRD plot clearly shows (111), (200) and (220) peaks for Cu phase. Theoretical calculation were performed on the Cu(II) and Co(II) complexes which experienced dca transformation using DFT-B3LYP/6-31G(d,p) level theory. The complexes were screened for *in vitro* antibacterial and antifungal activities by the disc diffusion method. Complexes which show high activity against the microorganisms tested, their minimum inhibitory concentration values were determined using microdilution method with two-folded serial dilutions. The MIC values indicate that the complexes showed greater activity against the fungi strains and some bacteria strains tested compared to that of the reference antifungal-fluconazole and antibacterial-cloxacillin.

RESUME

Cinq nouveaux complexes ont été synthétisés et caractérisés par les techniques d'analyse élémentaire (C, H et N), de spectroscopie (UV-visible et infrarouge), de test de solubilité, de mesures de conductivité, d'analyse thermogravimétrique et de mesure de la susceptibilité magnétique à température ambiante. La structure cristallographique sur monocristal des complexes $[Mn(phen)_2(NO_3)_2]$ (**1**), $[Mn(phen)_2(N_3)_2]$ (**2**), $[Mn(phen)_2(dca)_2]$ (**3**), $[Cu(phen)(BMCA)](NO_3)$ (**4**); BMCA = anion bis(methoxycarbimido)aminato et $[Co(phen)_2(NO_3)](dcg^-)\cdot(H_2O)$ (**5**); dcg = anion dicyanoguanidinate ont été obtenue. Les complexes **1** et **2** cristallisent dans le système orthorhombique avec le groupe d'espace *Pbcn* tandis que le complexe **3** cristallise dans un système monoclinique avec le groupe d'espace $P2_1/c$. Les complexes **4** et **5** cristallisent dans un système monoclinique et les structures sont stabilisées par des liaisons hydrogène et l'interaction aromatique π–π du noyau aromatique. L'anion dicyanamide a été transformé en **4** et **5** aux ligand bis(methoxycarbimido)aminato (BMCA) et anion dicyanoguanidinate (dcg) respectivement. Cette transformation métal-promu procède par une attaque nucléophile du groupement nitrile de dicyanamide sur le méthanol (cas de BMCA) ou sur un autre anion de dicyanamide (cas de dcg). Le moment magnétique des complexes **1-3** sont compatibles avec les spins élevés d^5 avec une géométrie octaédrique. Le moment magnétique de **4** est de 1.75 B.M correspondant à un électron impair qui est légèrement plus grand que le spin à la valeur de 1.73 B.M pour d^1. Celui du **5** est de 3.92 B.M qui est en accord avec le spin élevé d^7 de l'ion Co(II) avec pour géométrie octaédrique. Les propriétés thermiques des complexes ont également été évaluées. Les thermogrammes de l'analyse thermogravimétrique de tous les complexes montrent qu'ils sont stables à 200 °C. La composition du résidu du complexe de cuivre a été caractérisée par la diffraction des rayons-X sur poudre et sa courbe a montré clairement la phase du cuivre aux pics (111), (200) et (220). La méthode de calcul théorique par DFT-B3LYP/6-31G(d,p) a été utilisée pour l'analyse des complexes Cu(II) et Co(II). Les résultats montrent qu'il y a adéquation entre les géométries théorique et expérimentale. Les gaps d'énergie entre les orbitales HOMO et LUMO pour les complexes Cu(II) et Co(II) indiquent que le complexe Co(II) est plus stable que le complexe Cu(II). Les complexes ont été soumis aux tests antibactériens et antifongiques suivant la méthode de diffusion de disque. La concentration minimale inhibitrice indique que les complexes montrent des activités supérieures à celle des levures et certain bactérie comparable à là de référence antifongique-fluconazole et antibiotique-cloxacillin.

GENERAL INTRODUCTION

Scientific interest in the synthesis and characterisation of new coordination compounds with desired physicochemical and biological properties has increased recently [1-9]. The intriguing structural diversities of these compound has made them find applications in optical devices [7, 10], magnetic devices [10-14], gas storage [5, 9, 13-15], ion exchange [4, 7, 9], antimicrobial agents [1, 5], luminescence devices [14-16], bio-sensing [1, 17], nanomaterials [1, 18], molecular separation [4, 5, 9, 13] and catalysis [9, 11-13, 17]. The concepts of crystal engineering and supramolecular chemistry aimed at controlling the way molecules assemble in the solid state have been used to synthesised structures with oriented properties [7, 16, 19]. These structures with tailored biological properties are obtained through judicious choice of the ligands, the metal ions, the counter ion, the solvent, and the reaction conditions [1, 2, 9, 20-22].

The construction of supramolecular systems is principally based on the non-covalent interactions such as hydrogen bonding [2, 13, 15, 23-28], π-π stacking [1, 4, 12, 15, 22, 23, 27-29], dipole-dipole interaction [4, 30], hydrophobic interactions, Van der Waals interactions [25, 31-35], cation-π and anion-π interactions [19, 36] and ion-ion interactions [37]. These non-covalent interactions have been used as effective and versatile tools for the construction of structures having well defined characteristic properties [37-39]. The non-covalent interactions also play an important role in the overall arrangement of the structure and influence the properties [1, 40, 41]. These interactions are also essential in some biochemical processes like replication of DNA, the folding of proteins, the specific recognition of substrates by enzymes and the detection of molecular signals [38, 42, 43].

Interest in the biological and medicinal properties of coordination compounds is due to the fact that some metal-based drugs are biologically more active than the organic drug molecules [44-46]. The metal-based drugs enhance the solubility and bioavailability, reduce systemic toxicity and increase the potency with multiple mode of actions of the drug [47]. The mode of action of these metal-based drugs prevents drug resistance by increasing cellular efflux, avoid drug modification or inactivation and avert target modification [46, 47].

The use of antibiotics and chemotherapeutics to control infectious diseases caused by different pathogenic microorganisms has been complicated by emerging infectious diseases and the growing number of multi-drug resistant microbial pathogens [48, 49]. The increasing resistance of microbes to antibacterial and antifungal drugs has necessitated the search for new compounds to target pathogenic microbes [50, 51]. The strategies that have been employed to tackle this resistance problem include the structural modification of existing antimicrobial drugs and the development of entirely new classes of antimicrobial agents [52-54]. In this thesis, focus is on

the application of Mn(II), Co(II) and Cu(II) complexes of 1,10-phenanthroline and co-ligands as antimicrobial agents against resistant pathogens. Mn(II), Co(II) and Cu(II) ions have attracted our attention because they can adopt variable coordination numbers (from 4 to 6) and geometries. These metal ions in some complexes possess magnetic and biological properties [14, 55-61].

N-donor ligands are of interest to this work due to their applications in biology [62, 63], pharmacology [55, 62, 64], and magnetism [62, 65-67]. Nitrogen-containing heterocycles such as 1,10-phenanthroline have been found to possess diverse pharmacological activities since the ligands play a significant role in many biological systems, and is a component of several vitamins and drugs [1, 58]. 1,10-phenanthroline (phen) and its derivatives differ in their chelating ability mainly as a result of the difference in geometry and conformation of the free molecules [68]. In addition to its versatile and classical chelating nature [58, 69-71] in phen is a biologically important ligand, and some of its metal complexes have been shown to be effective against various strains of microorganisms [48, 72-77]. This chelating bidentate N,N'-donor ligand is a versatile starting material for metal-organic framework, and some of its complexes exhibit luminescence, antimicrobial and magnetic properties [64, 78-80].

In this thesis, the complexes of Mn(II), Co(II) and Cu(II) with phen and co-ligands (dicyanamide, azide and nitrate ions) have been synthesised and characterised by elemental analyses, spectroscopic methods (FTIR, UV-visible), room temperature magnetic susceptibility and thermal analytical techniques. The single crystal X-ray structures have also been determined. The antimicrobial activities of these complexes on some resistant bacterial and fungal strains have been evaluated.

This thesis is divided into five sections starting with a general introduction. Chapter one focuses on a literature review of the metal complexes of phen. It also presents the motivation, aim and objectives of the work. Chapter two details the experimental methods used, while the results and discussion are presented in chapter three. This is closely followed by a general conclusion and perspectives for further work.

CHAPTER 1
LITERATURE REVIEW

1.1- Supramolecular Chemistry and Crystal Engineering

Supramolecular chemistry is one of the most important innovations in inorganic, organic and biochemistry in the last decades and offers high control over the process of molecular self-assembly (reversibility, directionality, specificity and cooperativity due to its unique nature) [81-83]. Supramolecular chemistry has expanded rapidly both in terms of potential applications and in its relevance to analogous biological systems [84, 85]. The concept of supramolecular chemistry was introduced by Jean-Marie Lehn as the "chemistry of molecular assemblies and of the intermolecular bond" in 1979, or as the "chemistry beyond the molecule". Other definitions of supramolecular chemistry include "the chemistry of non- covalent bond" and "non-molecular chemistry". Originally, supramolecular chemistry was defined in terms of the non-covalent interactions between a "host" and a "guest" molecule. However, the rapid expansion in supramolecular chemistry has resulted in evolution of "host-guest" principle. Supramolecular chemistry now encompasses not only "host-guest" systems but also molecular recognition, so-called "self-processes" such as self-assembly and self-organization to molecular devices and machines [81, 86-88]. The formation of "supermolecules" relies on the ability of molecular entities to identify each other and self-assemble by means of non-covalent interactions (e.g. dipole-dipole, hydrogen bonding) [89, 90]. Since intermolecular interactions, such as metal ion coordination, electrostatic forces, hydrogen bonding, van der Waals interactions, donor-acceptor interactions, etc. are in general weaker than covalent bonds, the supramolecular entities are dynamic materials by nature allowing error-checking and resulting in defect-free products. The construction of supramolecular architectures is performed by breaking or making intermolecular bonds under thermodynamic control which has provided an alternative and complementary synthetic strategy to covalent chemistry [87, 91].

Supramolecular chemistry and crystal engineering practised at the Å and nm scale are the meeting point of 'top down' chiselling and 'bottom up' construction of nanostructures for materials science and technology. Understanding structure–property correlation and finding the optimal material for a particular application is the goal in these studies [85]. When applied to crystalline solids, the paradigm shift leads directly from supramolecular chemistry to crystal engineering which is the understanding of intermolecular interactions in the context of crystal packing and in the utilisation of such understanding in the design of new solids with desired or tailored physical and chemical properties [87, 92].

Crystal engineering is described as the design and construction of crystalline solids, both organic and metal-organic, with the goal of expressing a specific function or property within

the solid [89]. Crystal engineering was born in the field of solid-state organic chemistry in the context of studying the solid-state photo-dimerization of cinnamic acid [23]. Coordination polymers and metal-organic frameworks are among the most prolific research areas of inorganic chemistry and crystal engineering which constitute an interdisciplinary field with their origins from inorganic and coordination chemistry [65, 93-95]. Studies in this area of research have expanded rapidly in the last three decades, and are now also attracting the interest of the chemical industry. The term "Crystal Engineering" was first introduced by Pepinsky in 1955 and was then elaborated by Schmidt (1950-1970). Schmidt addressed the issue of crystal packing in the context of organic solid-state photochemical reactions of cinnamic acids and amides [96-98]. According to Desiraju, crystal engineering is the understanding of intermolecular interactions in the context of crystal packing and the utilization of such understanding in the design of new solids with desired physical and chemical properties [96, 99]. Crystal engineering has grown and developed over the past 50 years as a natural outcome of the interplay between crystallography and chemistry [98].

Crystal engineering overlap considerable with supramolecular chemistry and yet it is a distinct discipline. In a broader sense, the concepts of crystal engineering are applicable to any kind of intermolecular assembly, for example, protein-ligand recognition. The subject today includes three distinct activities, which form a continuous sequence. Firstly, it involves the study of intermolecular interactions; followed by the study of packing modes, in the context of these interactions and with the aim of defining a design strategy; and lastly, the study of the crystal properties and their fine-tuning with deliberate variations in the packing [96, 97].

The rational design of functional solid materials from metal ions and multifunctional ligands as building blocks with intermolecular interactions for the self-assembly has attracted considerable attention in crystal engineering due to their potential applications in catalysis, separations, optoelectronics, conductivity, porosity, chirality, luminescence, magnetism, spin-transition, non-linear optics and antimicrobials [64, 96, 100, 101]. The rich structural diversity present in such compounds in-turn facilitates systematic evaluation of structure-property relationships [102]. In the design and preparation of new crystalline structures, the expansion of crystal engineering as a research field has gone parallel with a significant interest in the origin and nature of intermolecular interactions [97]. The reality of the idea in 1955 saw little interest until the 1970s by which the improvement of X-ray methodologies enabled more precise determination of the spatial arrangement of molecules within a crystal, allowing photochemists to more thoroughly explore the effects of light on molecules in the solid state [89].

The realm of crystal engineering has consequently achieved great success in the self-assembly of molecules by increasing the number of components, polar bridging groups with variable spacer and counter-ions which decide whether one-dimensional (1D) molecular chains can interlock to form two-dimensional (2D) networks which in turn could be cross-linked into three-dimensional (3D) networks [30]. Coordination polymers (CPs), coordination networks (CNs), metal-organic frameworks (MOFs), organic-inorganic hybrid solids are some of the terminologies extensively encountered in this discipline where dimensionality, nature of interactions, permanent porosity draw a line of demarcation among them [99].

1.2- Non-covalent Interactions

An understanding and quantification of intermolecular interactions is of importance both for the rational planning of new supramolecular systems, including intelligent materials, as well as for developing new biologically active agents [84, 103]. The strongest bonds that are present in organic molecules are covalent bonds. A typical carbon-carbon (C-C) covalent bond has a bond length of 1.54 Å (bond energy: 85 kcal·mol^{-1}), meaning considerable energy must be expended to break the bonds [104]. Due to their strength and directionality, covalent bonds are not classified as one driving force for the formation of self-assembled systems [105]. Although the covalent bonds determine the skeleton or the disposition of atoms inside a molecule (its primary structure), the non-covalent interactions can control or organise the conformation, aggregation, the tertiary and quaternary structure of the molecule, its stabilisation and particular properties [36].

Non-covalent interactions between molecules are weak intermolecular contacts that govern the physicochemical properties of molecular systems in the condensed phase and play a pivotal role in the design of a new material with specific properties [39, 106, 107]. Johannes Diderik van der Waals in 1873 was the first to postulate the existence of intermolecular forces. In the early twentieth century, non-covalent bonds were understood in greater detail with the hydrogen bond being described firstly by Latimer and Rodebush in 1920 and later by Linus Pauling in an extended treatment [108]. These non-covalent intermolecular bonds are known to govern self-assembly of molecules through a balance of attractive and repulsive interactions leading to the formation of larger and ordered supramolecules [109]. These supramolecular interactions (hydrogen bonding, π–π stacking, host-guest interaction, ionic interaction, etc.), have long been used as effective and versatile tools for the construction of supramolecular polymers having intriguing responsive properties due to their non-covalent and dynamic nature [4, 37]. The weak

intermolecular interactions between molecular building units enforce a self-assembling process to generate molecular networks of different dimensionality with specific architectural and functional behaviours [30].

From crystal engineering point of view, the strong directional intermolecular interactions are more helpful to design target crystal structures and control the molecular organisation in the solid state. This approach is based on the premise that if these interactions dominate the crystal field, then the solid-state structure should follow from the directional preferences associated with the interactions [110]. The action of non-covalent interactions is greatly affected in different ways by the local environment of the atoms involved but the geometrical effects are important for the structure and function of the molecules. In fact, non-covalent interactions are the main tool in chemical and biochemical processes controlling the central parts of living systems [36, 111]. Although the different types of non-covalent interactions individually have their own place in synthetic transformations, their cooperation is particularly more attractive and advantageous (for example, to facilitate a complexation reaction and enhance the catalytic, photoluminescence, biological properties of the isolated coordination compounds) [36].

1.2.1- Hydrogen bonds

Among the various non-covalent interactions, hydrogen bonds appeared to be the most widely studied in the combinations of multiple interactions [36, 37, 96]. According to IUPAC recommendation 2011 [106], a hydrogen bond is defined as an attractive interaction between a bonded hydrogen atom from a molecule or a molecular fragment; X−H···A in which X is more electronegative than H, where A is O, N, or S [96, 106, 112]. This definition readily permits the inclusion of interactions C−H···O, C−H···N, and C−H···π as hydrogen bonds [113-115]. The X to A distance was found to be less than the sum of the van der Waals radii of X and A, and this shortening of the distance was taken as an infallible indicator of hydrogen bonding [98]. Hydrogen bonds are therefore formed when a hydrogen atom covalently bonded to an electronegative atom (hydrogen donor or electron acceptor) interacts with the lone pair of electrons from another electronegative atom (hydrogen acceptor or electron donor), from an adjacent molecule or within different parts of the same molecule.

The strength of the hydrogen bond is dependent on both the donor-acceptor distance and the electronegativity with typical bond energy varying between 1 to 40 kcal·mol^{-1}. Hydrogen bonds are classified into three categories based on their donor-acceptor distances and bond strength; strong (donor-acceptor distance 2.2-2.5 Å and bond energy 40-15 kcal/mol), moderate (donor-

acceptor distance 2.5-3.2 Å and bond energy 15-5 kcal/mol) and weak (donor-acceptor distance 3.2-4.0 Å and bond energy 4-1 kcal/mol) hydrogen bonds [85, 116, 117]. The strong hydrogen bonds which are mostly covalent (e.g. O–H···O, O–H···N, N–H···N, N–H···O, etc.) are important elements in crystal engineering. However, in the absence of these directional forces, the moderate or weak interactions involving C–H···X (X = O, N, Cl, F, π, etc.) are mainly responsible for crystal packing which has been investigated to determine their influence on the molecular self-assembly. It is known that the -CH group is able to form hydrogen bonds and it has been shown that C–H···O, C–H···N, C–H···Cl and C–H···F interactions, among others, may have a key role in the crystal packing. Furthermore, there are even weaker interactions than the ones described above, for example, the X–H···π (X = O, N, C) interactions, but still, they are important for the packing of organic crystals [118].

M. C. Etter in 1990 identified the hydrogen bond as being both directional and strong, thus important as a determinant of crystal structures [98]. The directionality of hydrogen bonds includes them among the most important instruments for selective molecular recognition [96]. Among the non-covalent interactions, hydrogen bonds are the most common type of non-covalent interactions used by organic tectons to control the secondary coordination sphere of metal ions [36]. For example, the monocomponent structure which contain infinite O–H···O–H···O–H··· cooperative synthons (Fig. 4) is linked with molecular connectors such as phenyl and biphenyl, and supramolecular connectors such as the acid dimer in 4-hydroxybenzoic acid. The cocrystal design was based on the anticipation that dicarboxylic acids would form supramolecular connectors with 4-hydroxybenzamide mediated by acid···amide synthons, leaving the O–H··· O–H···O–H··· infinite synthons free to form [98].

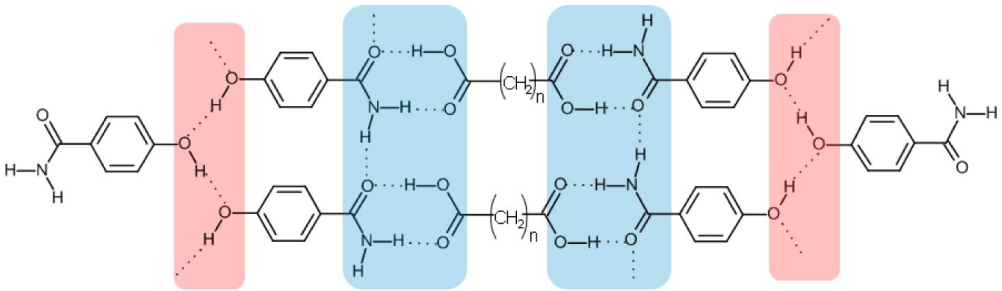

Figure 1: Synthon insulation in cocrystals of 4-hydroxybenzamide and dicarboxylic acids [98].

In this regard, the strong hydrogen bonds, e.g., O/N–H···O/N with their highly directional characteristics (Fig. 5) are found to be very effective in the supramolecular assembly of molecules. The stronger hydrogen bonds possess increasing covalent character and show a tendency of having more cooperative effects through mutual polarisation of the groups [84,

117]. The stabilisation energy of a hydrogen bond lies approximately in the range of 40–5 kcal/mol (the higher range corresponds to ionic hydrogen bonds). Hence, the strongest hydrogen bond can provide energetic stabilisation similar in magnitude to a covalent bond, while the weakest one can be close to that of van der Waals interactions [106]. Stronger than van der Waals forces, the hydrogen bonding is a special type of dipole-dipole interaction. The evidence of the existence of weak hydrogen bonds like C–H···O, C–H···N, C–H···π(C), O/N–H···π(C) are now well established in modern supramolecular chemistry (Fig. 1.5) and are being utilized in the systematic design of materials [38].

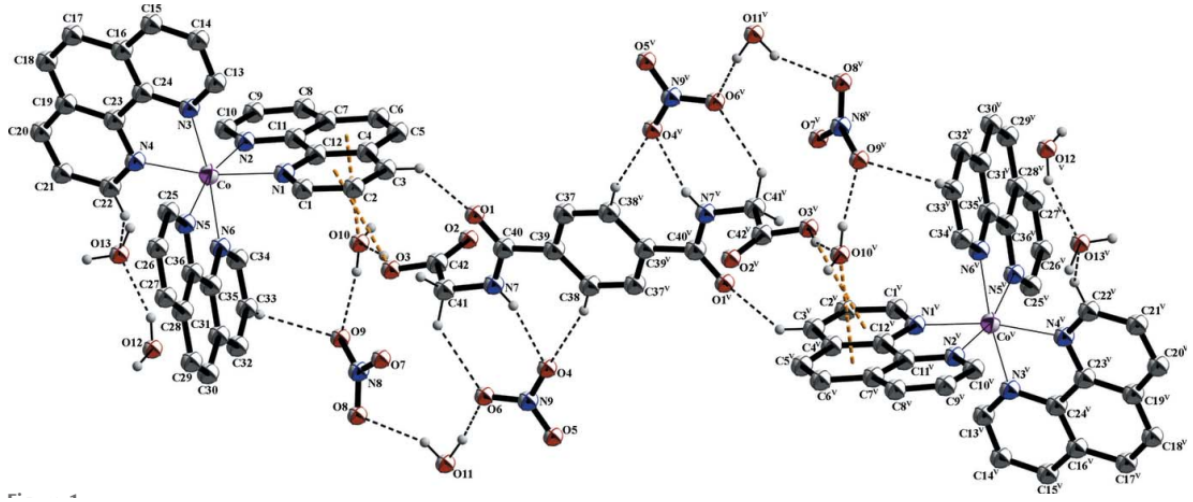

Figure 2: The molecular entity of $[Co(C_{12}H_8N_2)_3]_2(NO_3)_4C_{12}H_{12}N_2O_6{\cdot}8H_2O$ [38]

Though hydrogen bonds are weaker interactions than covalent bonds, they are crucial for the determination of structure of biological macromolecules such as DNA and proteins, since they are directly in charge of the secondary structure of these molecules and affect their interactions with other molecules like water [104].

The relative stability of most supramolecular compounds is due to the formation of hydrogen bonds. For example, in the complexes $[LnCl(H_2O)_3L(phen)]{\cdot}nCH_3CN$ {(n = 0 for 2, n = 2 for 3, n = 1.5 for 4, n = 0 for 5, n = 1.5 for 6, n = 1.5 for 7) (Ln = Dy, Ho, Er, Tm, Yb, Lu for 2–7, respectively) and (L=tetrakis(O-isopropyl)methylenediphosphonate, phen=1,10-phenanthroline)}, the formation of hydrogen bonds (C–H···Cl and O–H···Cl) is simplified as having a two-dimensional mesh 4.8^2 topology as depicted in Figure 6 [4].

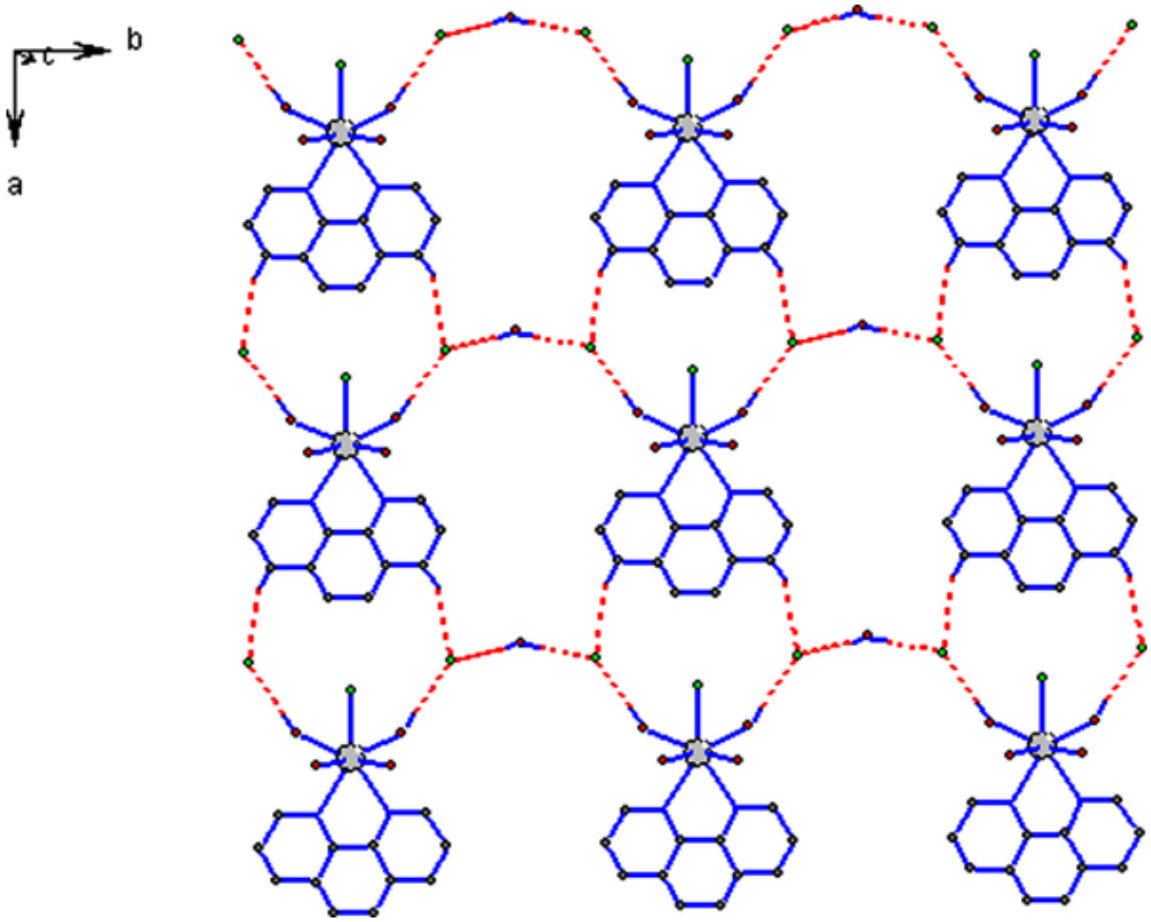

Figure 3: Schematic representation of the two-dimensional mesh 4.8^2 topology formed by hydrogen bonds (C–H···Cl and O–H···Cl) [4].

1.2.2- Aromatic or π–π stacking interactions

The fundamental understanding of the nature of the non-covalent bond is of utmost importance in the identification of molecules capable of self-assembling in solution and of self-organising in the solid state [109]. The self-assembly which relies on several molecular recognition in solution is driven mainly by π–π interactions that occur between a π-electron-deficient unit and a π-electron-rich unit and, to a marginally lesser extent, by weak hydrogen bonding and edge-to-face T-type interactions [119]. The term π–π interaction or π stacking refers to the non-covalent interactions involving a π-electron-rich unit with a cation, an anion, or another π-system containing a π-bond with the energy of interactions estimated at 2–10 kcal mol^{-1} [85, 120]. This energy of interactions between π–systems largely depends on the chemical nature of units [105]. The π–π interaction or π stacking can also be defined as an attractive interaction between two stacked aromatic rings. Hunter and Sanders in 1990 described the π–π interactions simply as electrostatic interactions. Electrons in π bonds of aromatic rings form a quadrupole moment (i.e., two dipoles aligned so that no net dipole can be distinguished) due to the stronger electronegativity of sp^2 carbons compared to hydrogen atoms [105]. The π–π stacking

interactions between π–donors, such as hydroquinone, resorcinol or dioxynaphthalene residues, and π–accepting ring systems, such as bipyridinium or π–extended viologen units, can govern the self-assembly of a variety of complexes and interlocked molecular compounds in both the solid and solution states [106, 119, 121].

Since many stacking complexes are based on Coulomb forces and are characteristically a combination of electron-poor and electron-rich units [84], the use of ligands with an aromatic moiety in complexation can provide π–π stacking, π–cation or π–anion types of non-covalent interactions. The strength of these interactions falls in a varied range and in some particular instances can be even slightly stronger than a weak covalent bond. Metal–π interactions (with electrostatic origin) can constitute non-covalent interactions [36].

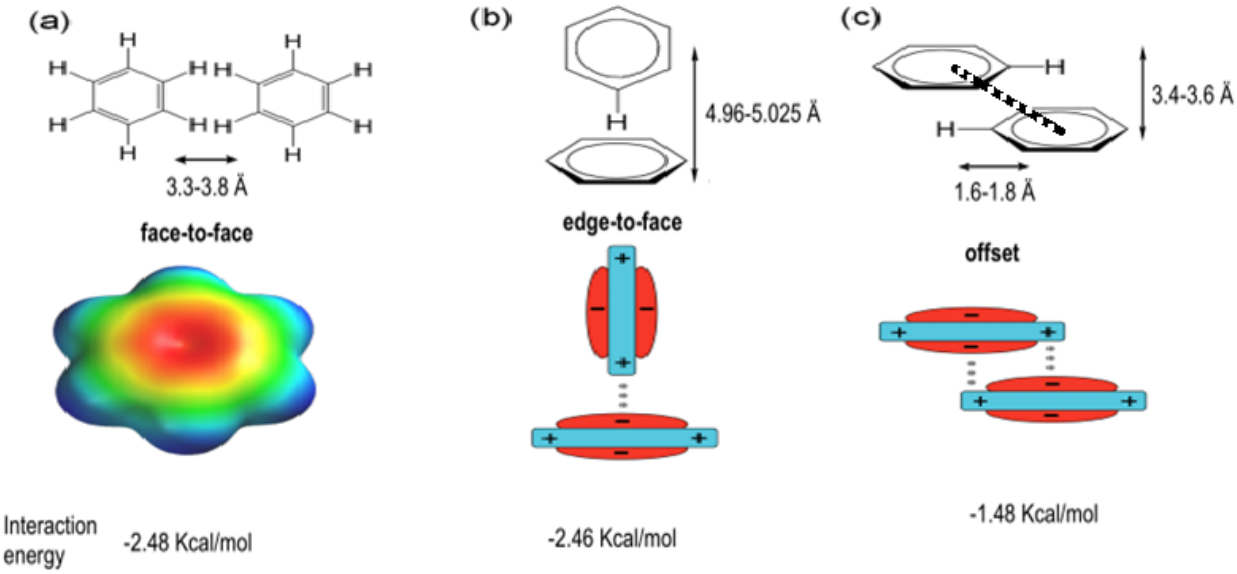

Figure 4: (**a**) Electrostatic potential surface of a benzene molecule (**b**) and (**c**) schematic representations of interaction geometries of a benzene dimer [109].

Nitrogen-containing heterocycles such as bipyridine and phenanthroline are metal-coordinating, electron-deficient aromatic systems and predestined for π–π stacking as π–acceptors can lead to remarkable properties [122].

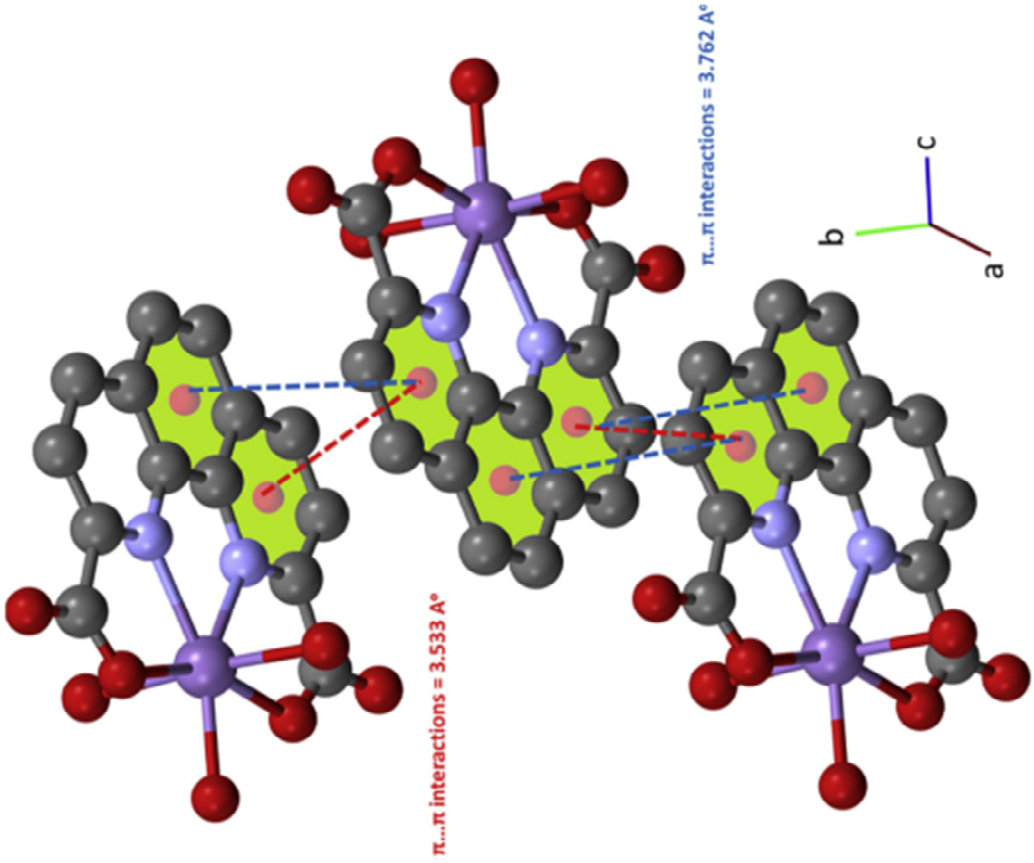

Figure 5: The perspective view of the π···π intermolecular interactions along the b axis in triaqua(1,10-phenanthroline-2,9-dicarboxylato)manganese(II) dihydrate complex [122].

The relative stability of most supramolecular compounds does not only result from the formation of hydrogen bonds but can also be reinforced by π–π stacking interactions. For example, the dinuclear compound $[(CeCl_2Lphen)_2(l\text{-}Cl)_2]\cdot CH_3CN$, (L = tetrakis(O-isopropyl)methylenediphosphonate, phen = 1,10-phenanthroline) displays a two-dimensional mesh 6^3 topology by forming by π–π interactions as illustrated in Figure 1.9 [4].

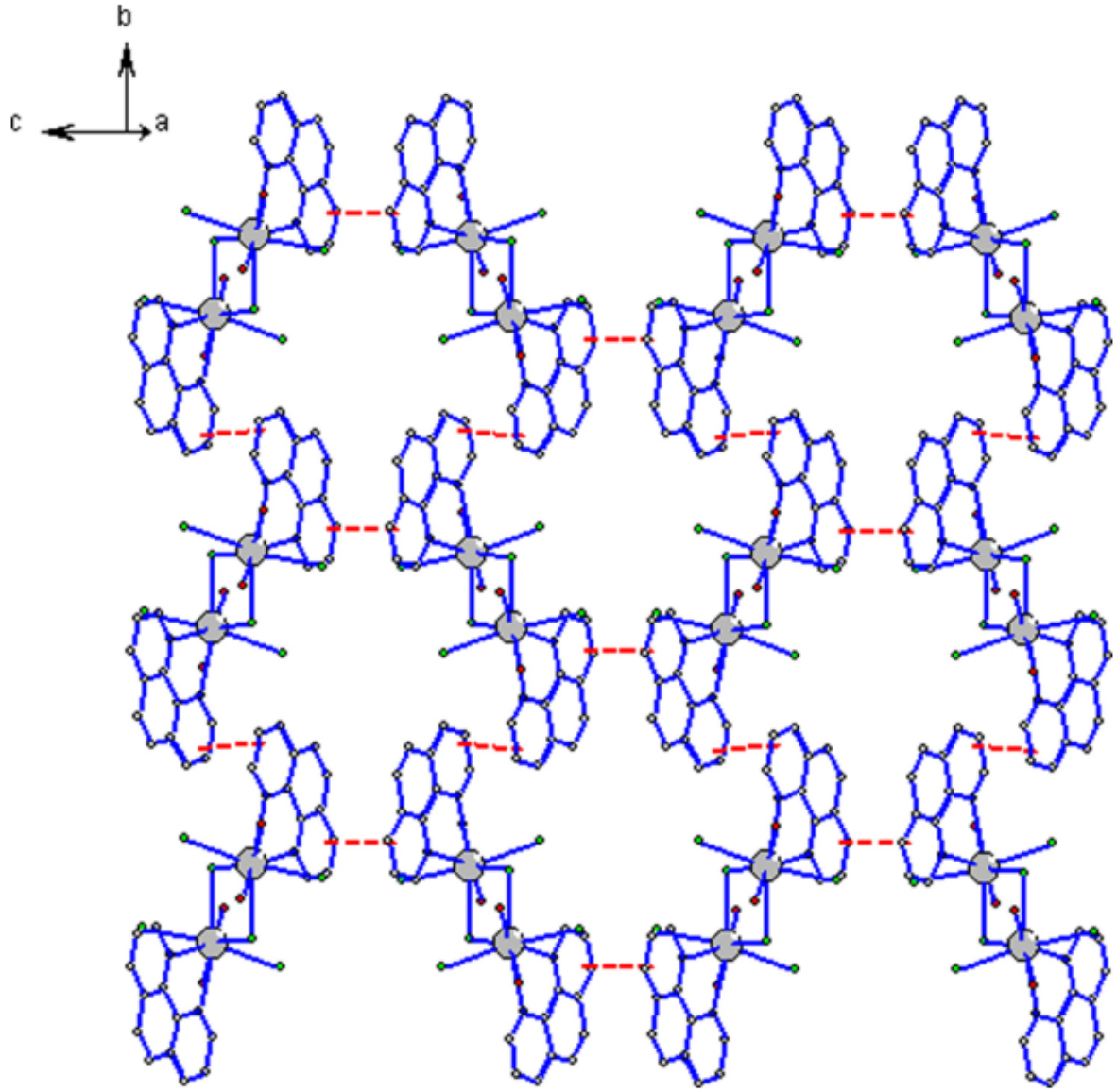

Figure 6: Schematic representation of the two-dimensional mesh 6^3 topology formed by π–π interactions [4].

1.2.3- Metal-aromatic interactions

Many transition metal cations can accept π–electrons from unsaturated organic molecules and, thus, form very stable organometallic molecules. The metal cation is known to form comparatively weak interactions with aromatic molecules; hence, measurements of association constants of the metal with simple aromatic hydrocarbons lead to a conclusion that the broader a conjugated electronic system the stronger the metal–π interaction. The energy of metal-aromatic interactions is not known with precision but estimated around 2–10 kcal mol^{-1} [85, 90, 120].

1.3- Metals in Biological Systems

Many metal ions are known to play very important roles in biological processes in the human body [74, 123]. The interaction of metal ions with nucleic acids and nucleic acid constituents are important for biological action [124, 125]. These metal ions play essential roles in about one-third of enzymes by modifying electron-flow in a substrate or enzyme, thus effectively controlling an enzyme-catalysed reaction. They can also serve to bind and orient substrate with respect to functional groups in the active site and can provide a site for redox activity if the metal has several valence states [58, 74, 126]. A biochemical reaction catalysed by a particular metalloenzyme would proceed very slowly without the appropriate metal ion [127]. Apart from the huge success of platinum-based drugs, some other metal compounds such as manganese [76, 128, 129], cobalt [75, 130, 131], and copper [75, 129, 132, 133] complexes have shown some potential for chemotherapy by accelerating drug action [125]. Many drugs administered in the form of metallic complexes possess modified pharmacological and toxicological properties [48].

Metal ions are generally positively charged and act as electrophiles, seeking the possibility of sharing electron pairs with other atoms so that a bond or charge-charge interaction can be formed. The transition metal complexes of multi-dentate nitrogen-donor ligands have received much attention recently due to the enhanced thermodynamic and kinetic stability of the resulting complexes and their application in various activities such as anticancer, antitubercular and antimicrobial agents [44]. One aspect of the behaviour "*in vivo*" of metals, which cannot be over-emphasized, is their chemistry, which is essentially that of the formation of the complex ion. The properties such as the effective size and solubility of a metal ion *in vivo* are a function of ligand and solvent present as well as the metal ions themselves. Most importantly, the correct metal ion balance in various *in vivo* compartments is very essential for the proper functioning of the specific metal-containing-sites in many enzymes and proteins. For example, if the concentrations of some metal ions are raised considerably above the normal, blocking of transport sites can occur and symptoms more normally attributed to depletion of certain metal ions can appear [134].

1.3.1- Manganese

Interest in the coordination chemistry of Mn(II) compounds has increased due to their significant role as redox sites in biological systems such as pyruvate carboxylase, oxaloacetate decarboxylase, superoxide dismutases and diamine oxidases [135]. Manganese activates

enzymes that help in using some vital nutrients in the human body as a constituent in some metalloenzymes:

- Arginase (present in the liver that creates urea which breaks down proteins and amino acids and is also responsible for expelling extra nitrogen from the body through the urine),
- Glutamine synthetase (plays an important role in synthesizing glutamine, an amino acid that helps in improving mental function, controlling blood sugar, and maintaining muscle mass),
- Phosphoenolpyruvate decarboxylase (involved in the metabolism of blood sugar), and
- Manganese-dependent superoxide dismutase (present only in the body's mitochondria which performs an antioxidant function by protecting the tissues from the damaging effects of free radicals) [126, 136].

Although manganese has an important biological role in the human body, only 15-20 milligrams of this trace mineral is present mostly in the bones and some amount is found in the kidneys, liver, pancreas, pituitary glands, and adrenal glands [137]. Manganese acts as a catalyst in the synthesis of fatty acids and cholesterol and in the metabolism of protein and carbohydrate. It may also play a role in the production of sex hormones and in maintaining the reproductive health of an individual. Another important function of manganese may be in the production of the thyroid hormone called thyroxine, which is responsible for controlling the rate of metabolism, regulating the rate of oxygen use by cells, and generating body heat. Manganese also plays a role in maintaining healthy nerve tissues [136, 137].

Since manganese plays an important role in the human body, its deficiency can have an impact on the major physiological processes. Poor dietary intake of this nutrient is the most common cause of manganese deficiency. Excessive sweating and chronic liver or gallbladder disorders are also some causes of manganese deficiency. The deficiency of this nutrient can cause nausea, vomiting, high blood sugar levels, bone loss, low cholesterol levels, difficulties of the reproductive system, dizziness, and hearing loss in adults. In infants, it has been found to cause paralysis, blindness, convulsions, and deafness. However, manganese deficiency occurs very rarely in humans [138]. The important biological role of manganese in humans emphasizes the fact that it should be a part of one's daily diet. The recommended daily intake of manganese for adults is between 1.8 to 11 milligrams [136]. You can get the required amount of manganese by consuming mustard greens, kale, raspberries, spinach, molasses, garlic, grapes, summer squash, green beans, brown rice, turmeric, strawberries, and maple syrup.

1.3.2- Cobalt

Cobalt is an essential trace element found in the liver, kidney and bones. The presence of cobalt in the active centre of vitamin B_{12}, which participates indirectly in the regulation of the DNA synthesis, is its most important role *in vivo* which is indispensable in the metabolism of folic acid and fatty acids [139]. The adult human body contains 2-5 milligrams of vitamin B_{12} and its derivatives [138]. Besides, cobalt is involved in the production of red blood cell (erythrocytes), and it is useful in the prevention of anaemia. It is also important for the proper functioning of the nervous system as it can help in creating a myelin sheath [2, 58]. In addition to its role in cobalamin, cobalt is a part of some metalloproteinases that in their structure does not contain *Corinne* (characteristic for the cobalamin -which binds cobalt) such as *methionine aminopeptidase-II* and *nitrile hydratase*.

In contrast to nickel, iron, and manganese, one of the interesting structural aspects of working with cobalt is the range of geometries that are stable; octahedral, tetrahedral, square-pyramidal, trigonal-bipyramid and square-planar [140]. The biological relevance of cobalt compounds was initially reported sixty years ago; thereafter, a significant number of biological interesting cobalt complexes exhibiting noteworthy *in vitro* antibacterial, antifungal, antioxidant, antiproliferative and antiviral activity has been reported [58, 76, 139, 141-144].

Cobalt deficiency in humans or animals can lead to anaemia since its ion participates in the formation of red-blood-cell and may also lead to disturbances in protein metabolism and calcium and phosphorus absorption [58].

1.3.3- Copper

Copper is the third most abundant transition metal in humans found either at the active sites or as structural components of a good number of enzymes [74]. Copper is a vital dietary nutrient, although only small amounts (75-100 milligrams) of the metal are needed for the well-being of the body [145] and is present in every tissue of the body but is stored primarily in the liver, with fewer amounts found in the brain, heart, kidney, and muscles [146, 147].

Copper plays an important role in our metabolism, largely because it allows many critical enzymes to function properly [148] and is essential for maintaining the strength of the skin, blood vessels, epithelial and connective tissue throughout the body. Copper also plays a role in the production of haemoglobin, myelin, melanin and it also keeps thyroid gland functioning normally [147]. Copper can act as both an antioxidant and a pro-oxidant. Free radicals occur naturally in the body and can damage cell walls, interact with genetic material, and contribute

to the development of a number of health problems and diseases. As an antioxidant, Copper scavenges or neutralize free radicals and may reduce or help prevent some of the damage they cause [149-151]. When copper acts as a pro-oxidant at times, it promotes free radical damage and may contribute to the development of Alzheimer's disease [152]. Maintaining the proper dietary balance of Copper, along with other minerals such as zinc and manganese, is important [145].

Copper is involved in many functions of the body; therefore, its deficiency can produce an extensive range of symptoms. The deficiencies of copper can result in hernias, aneurysms, blood vessel breakage manifesting as bruising or nosebleeds, iron deficiency anaemia, osteoporosis and joint problems, brain disturbances, abnormalities in glucose and cholesterol metabolism, increased susceptibility to infections due to poor immune function [neutropenia], loss of pigment, weakness, fatigue, skin sores, poor thyroid function, irregular heartbeat and low body temperature [145, 149]. If copper is important in cellular membrane structure, then a copper deficiency could seriously alter the movement of nutrients through cell walls [145].

Excessive copper intake can cause nausea, vomiting, abdominal pain and cramps, headache, dizziness, weakness, diarrhoea, and a metallic taste in the mouth (associated with water containing copper concentrations greater than 6 mg/L) [145]. Chronic copper toxicity does not normally occur in humans because of transport systems that regulate absorption and excretion [153].

Metal ions, especially their radii and coordination geometry, determine the direction and coordination modes of the organic ligands, which is important for the structure of the complexes [154]. Several copper complexes with the best-studied example; $[Cu(phen)_2]^{2+}$ (phen =1,10-phenanthroline) has been described as cleaving DNA. The $[Cu(phen)_2]^{2+}$ is reduced *in situ* to $[Cu(phen)_2]^{+}$, which subsequently binds to the minor groove of DNA, combines with molecular oxygen, generates a non-diffusible oxidant, and finally induces strand scission by oxidation of the ribose backbone [155].

1.4- Ligands used in this work

Nitrogen-containing heterocyclic compounds play an important role, not only in life science industries but also in many other industrial fields related to special and fine chemistry [44]. Most of the N-donor heterocyclic compounds do play important roles in regulating biological activities [1, 156]. Transition metal complexes of N-donor ligands are of our interest due to their applications in biology [73, 139, 154, 157], pharmacology [158, 159], and magnetism [62,

120, 160]. In this work, 1,10-phenanthroline is used as the main ligand and the anions; dicyanamide, azide and nitrate are used as co-ligands.

1.4.1- 1,10-phenanthroline

The polypyridyl ligand; 1,10-phenanthroline (phen) and its derivatives are very important ligands in coordination and organometallic chemistry because they have a rigid framework and possess an excellent ability to chelate many metal ions via the two nitrogen donor atoms [122, 161, 162]. Their complexes provide the potential for various technological applications due to their high charge transfer mobility, bright light emission and good electro and photoactive properties [163, 164]. Phen has extended planar π systems and can be used in model compounds to mimic the non-covalent interactions in biological processes [165]. Phen and its derivatives (2,9-dimethylphenanthroline, 5,6-dimethylphenanthroline; 3,4,7,8-tetramethylphenantroline; 4,7-diphenylphenanthroline; 2,9-dimethyl-4,7-diphenylphenanthroline; and $5NO_2$-phen--5-nitrophenanthroline [72]) also play important roles in supramolecular assemblies, metallo-dendrimers, and formation of stable complexes exhibiting numerous biological activities such as antitumor, anticandida, antimycobacterial and antimicrobial activities [55, 76, 166]. Phen is also a biologically important ligand which, together with some of its metal complexes, has been shown to be effective against various strains of microorganisms [77, 167-169]. In the biological investigations aimed at discovering and developing new type of antiproliferative agents, one of the most important aspects is the interactive studies between drugs and DNA since DNA is one of the main molecular targets in the design of anticancer compounds [64]. The interaction of these complexes with DNA has gained much attention due to their possible applications as new therapeutic agents [61, 170].

1.4.1.1- Synthesis of 1,10-phenanthroline

In the late 1800's, Blau et *al* [180] first reported the synthesis of phen in the late 1800's. It was obtained using the Skraup synthetic method by heating o-phenylenediamine with glycerol, nitrobenzene and concentrated sulphuric acid (Scheme 1).

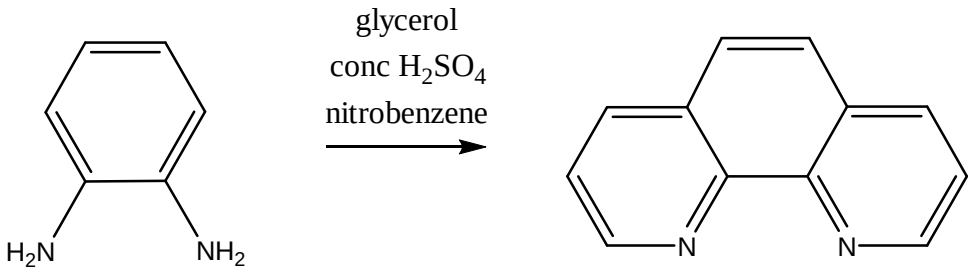

Scheme 1: Synthetic route to 1,10-phenanthroline [171, 172]

Moreover, Chelucci et *al* [173] also reported a protocol for the synthesis of substituted phen. The first two steps involve the synthesis of phen from pyridine molecules (Scheme 2).

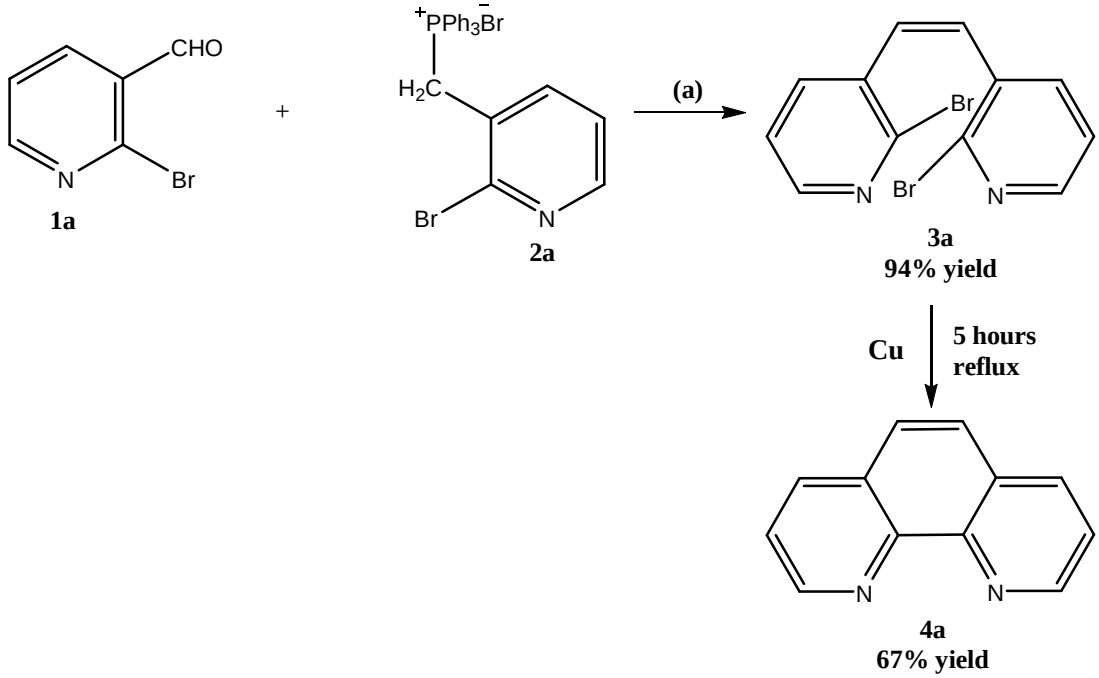

Scheme 2: Two-step synthesis of 1,10-phenanthroline [181]

1.4.1.2- Structure and bonding of 1,10-phenanthroline in complexes

Phen and its derivatives are an important class of chelating agents which has a high affinity for metal ions and possess π-acceptor capability that significantly contributes to the stabilisation of their low valent metal complexes [71, 154, 174]. It has a rigid planar framework and a well-defined structure (Fig. 10) [69]. Moreover, this heterocyclic bidentate chelating ligand bonds to metal atoms (ions) using its lone pairs of electrons on the two nitrogen atoms resulting in a five-membered ring structure. In this ligand, the σ-donation is complemented by the π-acceptor ability giving the complexes formed greater stability [58]. Complexes of this ligand have

potential technological applications due to their ability to absorb strongly in the ultraviolet spectral region, emit bright light alongside their good electro- and photoactive properties [175].

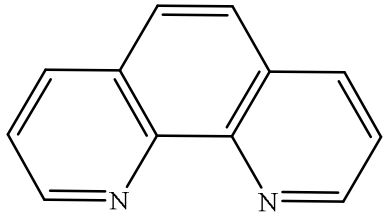

Figure 7: Structure of 1,10-Phenanthroline

1.4.1.3- Properties of 1,10-phenanthroline

Phen can exist as either a monohydrate compound, melting point (m.p.) 94 ˚C or as an anhydrous compound, m.p. 117 ˚C. It is slightly soluble in water and readily soluble in ethanol, methanol, acetone, ether, and benzene. In the structure of phen, the shortest bond lengths are the N-C bond at 1.36 Å, whilst the longest bond is C-C bond that join the pyridyl rings at 1.40 Å. Generally, phen has a strong ligand field depending on the constituent of the coordination sphere causing spin pairing. Due to its stability, most phen complexes (for example, $[Fe(phen)_3]^{2+}$) can be used for the colorimetric determination of iron [176]. Phen belongs to the phenanthrene family and is best considered as an α-diimine ligand [177].

1,10-phenanthroline is chosen for this work because:

- It has a rigid, planar framework and is a versatile polypyridine nitrogen donor ligand which has been widely studied for its coordination ability and stability in biochemical processes [61],
- It controls the supramolecular assemblies formed through the non-covalent interactions [61, 68],
- Its compounds can exhibit far better luminescence and biological properties than the free ligand [78],
- It can be used as redox indicators for oxidation-reduction titrations in the quantitative analysis [178],
- Its metal complexes can be extensively used for mapping protein and drug binding sites on DNA as well as for studying DNA structure [48, 64, 179, 180], and
- 1,10-Phen and some of its complexes have been shown to be biologically active [48, 72, 179, 181, 182].

Although there are many important factors to be considered in the development of novel materials (with interesting magnetic and biological properties), the selection of suitable centers, linking bridges, and coordinating ligands always plays a key role. Mixed ligand complexes with phen are also interesting due to their potential role as models for biological systems such as binding of small molecules to DNA [162]. The co-ligands nitrato, azido and dicyanamido have been chosen for this work, not only due to their versatile coordination modes, but also due to their remarkable ability to transmit ferro- or antiferromagnetic interactions [11, 62, 183]. These anions are not only necessary for the charge balance to the metal cations, but typically function as nodes in the scaffolds [184]. The charge number, size, and shape of balancing ions are important factors which affect the crystal growth and molecular structure [183].

1.4.2- Dicyanamido (dca) co-ligand

Dicyanamide (dca) anion also known as the bent pseudohalide [160, 185, 186] is an interesting versatile ligand which can act as a terminal monodentate, bidentate, or as a tridentate ligand [187-189]. The versatility of the anion arises from its variable coordination modes [21, 185, 186, 188, 190, 191]. Since dca has three nitrogen donor atoms, it can exhibit several possible coordination modes (Scheme 1.3) of which four modes have been substantiated by X-ray crystallography [21, 185, 188, 190, 191]. The most common coordination mode is the bridging mode with the terminal N-atoms (μ-$_{1,5}$), which has been found in many transition metal compounds and some main group metal compounds [186, 188-191]. The versatile coordination ability of dca has led to the design and synthesis of several metal-dca complexes with varied topologies and magnetic properties [192-194]. Dicyanamide has the unique ability to coordinate to metal ions through terminal monodentate, μ^2, μ^3 as well as unusual μ^4 coordination modes [160] (Scheme 1.3) where one nitrile nitrogen binds to two metal atom [185, 187]. The variability in coordination mode is a particular feature of dca, however, in most cases monodentate or bidentate coordination via the nitrile N atom occurs [83, 195-198]. The first report on its coordination compounds was published by Madelung and Kern in 1922 and its coordinating ability towards 3d transition metal ions was explored by Kohler and co-workers in the 1960s and 1980s [108, 199]. The different coordination modes of dca are presented in Scheme 3.

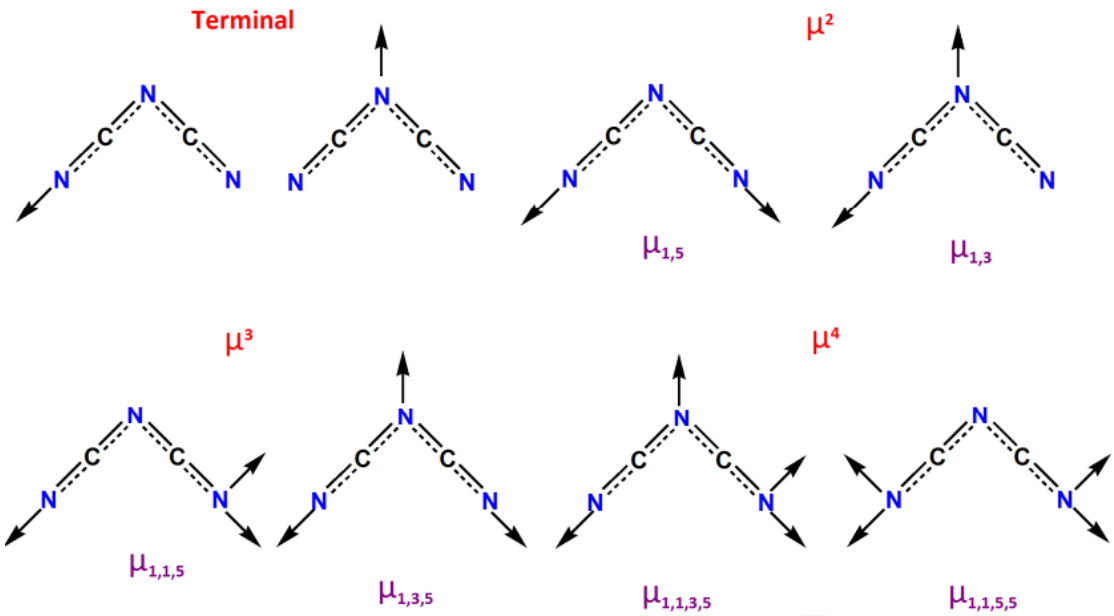

Scheme 3: Coordination modes of dicyanamide (dca) [21, 185, 188, 190, 191]

The design and synthesis of polynuclear coordination complexes, aimed at understanding the structural and chemical factors that govern the exchange coupling between paramagnetic centres using dca are of great interest in biology, chemistry, and physics [195]. A considerable number of metal complexes from zero- to three-dimensional (0D to 3D) metal-dca polymeric compounds with different structural motifs have been designed and synthesised.

Tonzing *et al*., 2006 [188] reported the isomorphous structures of $M(dca)_2(phen)(H_2O)\cdot MeOH$, (M=Mn, Fe, Co, Ni, Zn and Cd, dca=dicyanamide, phen=4,7-phenanthroline) containing 1D coordination polymer chains in which each metal atom is connected to two others by two pairs of $\mu_{1,5}$ bridging dca anions coordinating in the equatorial position.

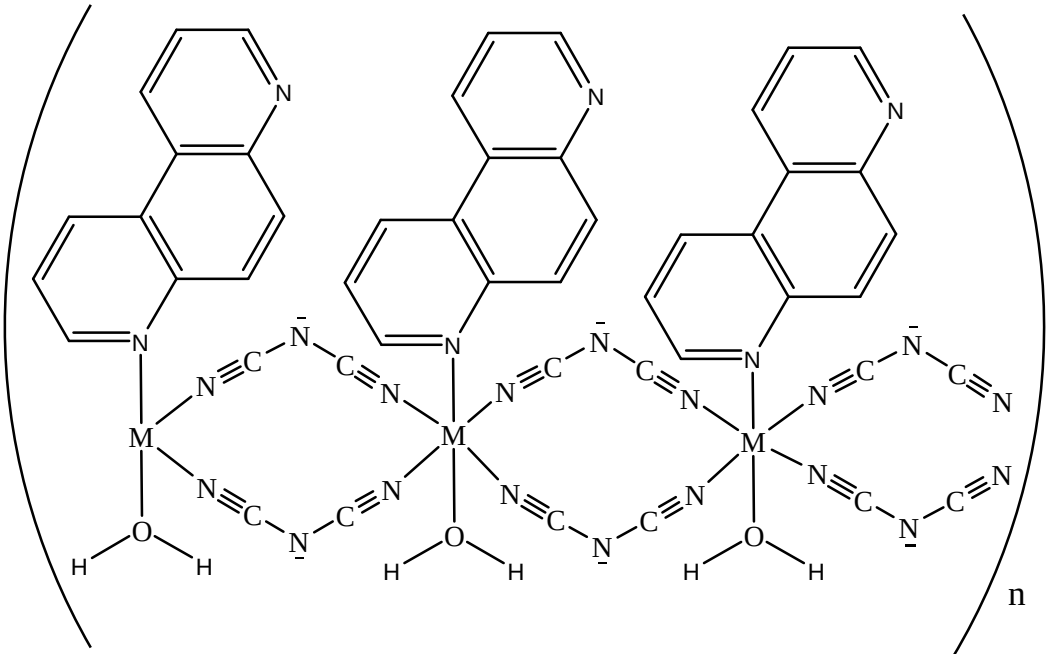

Figure 8: The 1D chain structure of $M(dca)_2(phen)(H_2O)\cdot MeOH$ [188]

The axial position of the metal occupied by the monodentate water and phen ligands were further linked into an overall 3D network by hydrogen bonding interactions between the water ligands, the uncoordinated nitrogen atoms of the phen ligands, and the intercalated methanol molecules.

Manson *et al*., 2013 [193] reported a quasi-2D antiferromagnetic $Mn(dca)_2$(o-phen) complex featuring both single- and bi-bridged Mn-dca-Mn linkages {dca=dicyanamide; o-phen=1,10-phenanthroline} with a long-range magnetic order in a low-dimensional Mn-dca polymer consisting of octahedral MnN_6 sites that are connected via four $\mu_{1,5}$-bridging dca ligands. The interdigitation of the 2D layers is readily apparent.

A 1D polynuclear copper(II) complex $[Cu(L1)\{\mu_{1,5}\text{-dca}\}]_n$ {L1H=$C_6H_5C(O)$-$NHN=C(CH_3)C_5H_4N$} showing weak antiferromagnetic interactions with J values = 0.10 on variable temperature magnetic susceptibility has also been reported [200]. A 2D layer structure of a dca complex $[Mn(\mu_{1,5}\text{-dca})_2(phen)]_n$ has also been reported (Fig. 12) showing weak antiferromagnetic interaction [201].

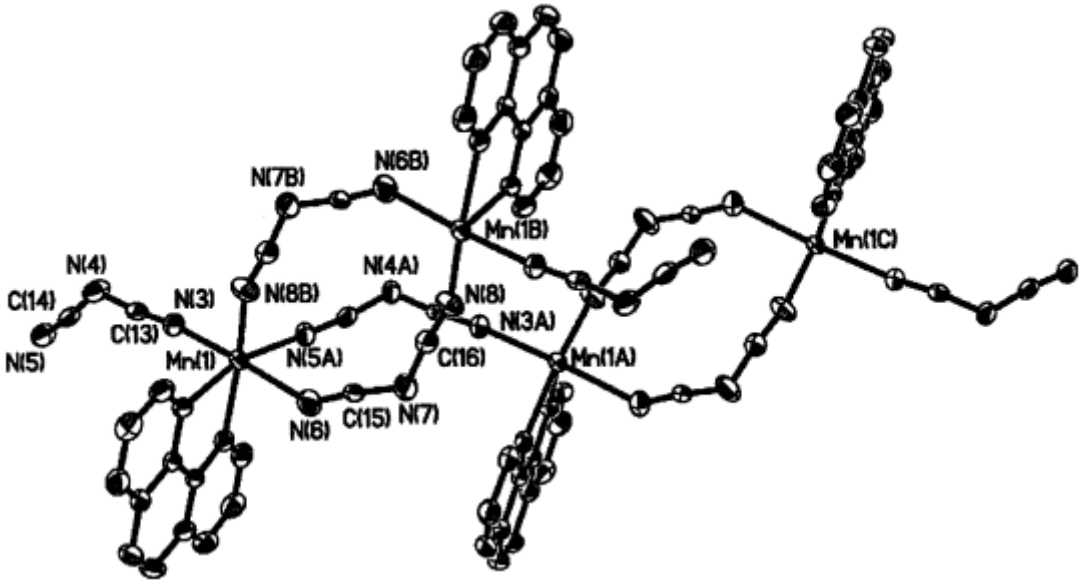

Figure 9: The atom-numbering scheme and 2D layer structure of $[Mn(\mu_{1,5}\text{-dca})_2(phen)]_n$ complex [201].

Several metal-dca complexes have been proposed as potential anticancer substances and cancer-inhibiting agents, as they demonstrate remarkable anticancer activity by strongly binding and cleaving DNA and regulating apoptosis [182]. Generally, complexes with the dca ligand possess diverse properties such as magnetic [194, 201, 202] and biological [21, 203] properties. As a long-range bridging ligand, dca does not only participate in the formation of interesting topological structures but it is also an effective medium for super-exchange coupling between two metal ions [186, 204, 205]. Depending on the synthetic condition and solvent system used, dca has been shown to undergo some transformations. These transformations are metal-mediated through a nucleophilic attack of the nitrile groups of dca on the solvent system used [206-209].

1.4.3- Azido (N_3^-) co-ligand

The azido ligand is a linear and symmetric tertiary amine which possesses equal N-N distances of average 1.154 Å [210-215]. The main source of the azide moiety is sodium azide (NaN_3); a colourless crystalline solid of density 1.85 g/cm^3, soluble in water and has a molecular weight of 65.01 g/mol with melting point 295 °C and boiling point 300 °C. This monodentate weak field ligand is a deadly chemical that exists as an odourless white solid [37].

The flexidentate azide ion has been demonstrated to be an extremely versatile ligand as well as an excellent magnetic coupler which provides complexes of great structural diversity with important physical properties [216-218]. The azido ligand has been intensively studied because of its ability to coordinate to transition metals with different coordination modes generating a

wide variety of fascinating structures with applications in functional materials [58]. It forms complexes with compounds having diverse structures spanning from discrete molecules (0D) to 3D arrays [219, 220]. The azide anion is one of the most commonly employed inorganic bridging ligands in the design of polynuclear 3d-metal complexes [214, 221, 222]. The magnetic properties of these complexes depend on the different bridging modes of the azido ligand [222-224].

Generally, the azido ligand has two bridging modes: end-on (EO) and end-to-end (EE) which mediate ferro- and anti-ferromagnetic exchange interactions, respectively [12, 26, 203, 222, 225-228]. The end-on azides have been shown to transmit antiferromagnetic exchange and end-to-end azides ferromagnetic exchange interactions [223]. Besides the most frequently encountered end-to-end ($\mu_{1,3}$-N_3, EE) and end-on ($\mu_{1,1}$-N_3, EO) double coordination modes (Scheme 4), the single; $\mu_{1,1}$ and $\mu_{1,3,}$ triple; $\mu_{1,1,1}$ and $\mu_{1,1,3,}$ and quadruple; $\mu_{1,1,1,1}$ and $\mu_{1,1,3,3}$ connection modes have also been met [213, 222].

The coordination modes range from monodentate to bridging bi-, tri- and tetra-dentate , with the μ-1,1 (end-on, EO), μ-1,3 (end-to-end, EE) and μ-1,1,3 being the most common (Scheme 2) .

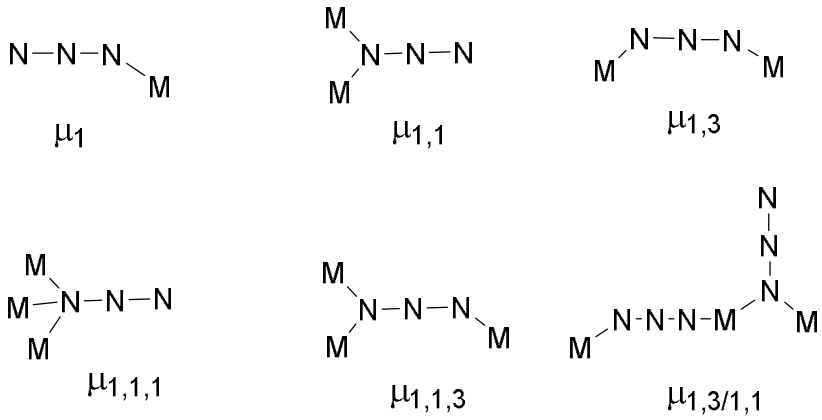

Scheme 4: Bonding modes of azide

The ability of the azido ligand to coordinate up to six metal ions leads to structural varieties of azide-complexes that range from molecular clusters to multidimensional materials (1D, 2D, and 3D) [228, 229]. The coordination pattern of azide could be either symmetric, with all equivalent metal–azide bond lengths, or may deviate from such a perfect picture as illustrated in Scheme 5.

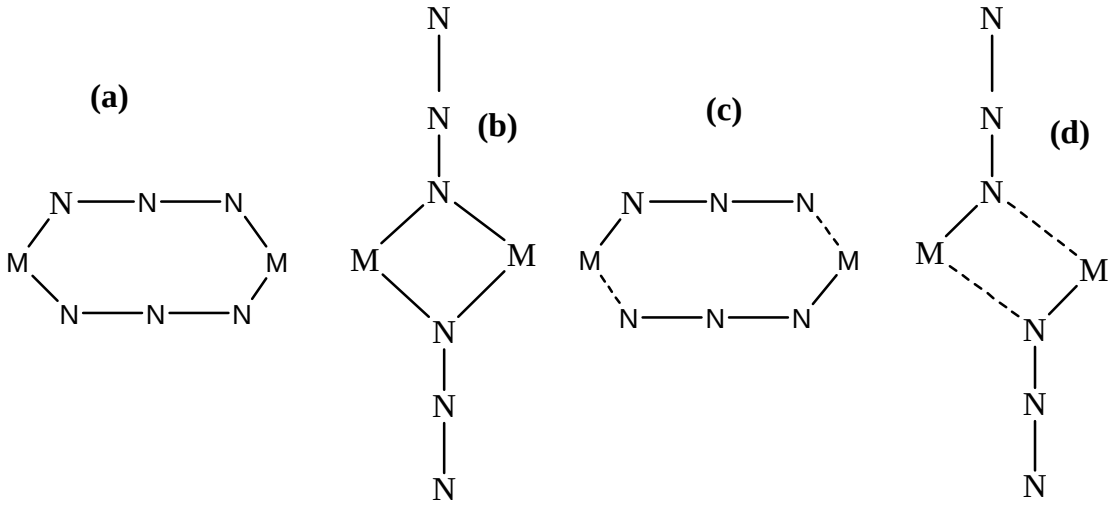

Scheme 5: Symmetric EE (a) and EO (b) and asymmetric EE (c) and EO (d) double coordination modes usually encountered for the azide ligand [213, 222].

The azido group can be introduced into transition metal complexes by metathesis reaction of NaN_3 with halogeno complexes of the transition metals [230]. The azide ion is an excellent ligand to build various polynuclear complexes with transition metals [226]. For example, Safin *et al*, 2017 [231] reported the reaction of one or two equivalents of 5-phenyl-2,2'-bipyridine (L) with a mixture of one equivalent of $CoCl_2$ and two equivalents of NaN_3 which led to the formation of mononuclear heteroleptic cobalt(III) complexes $[CoL_2(N_3)_2](N_3)_{0.55}Cl_{0.45}EtOH$ and $[CoL_2(N_3)_2]N_3{\cdot}2.5EtOH$, respectively. Both structures revealed that cobalt(III) atom were linked to the six nitrogen atoms of two L and two N_3 anions and are stabilized by intermolecular C-H···N and π···π stacking interactions.

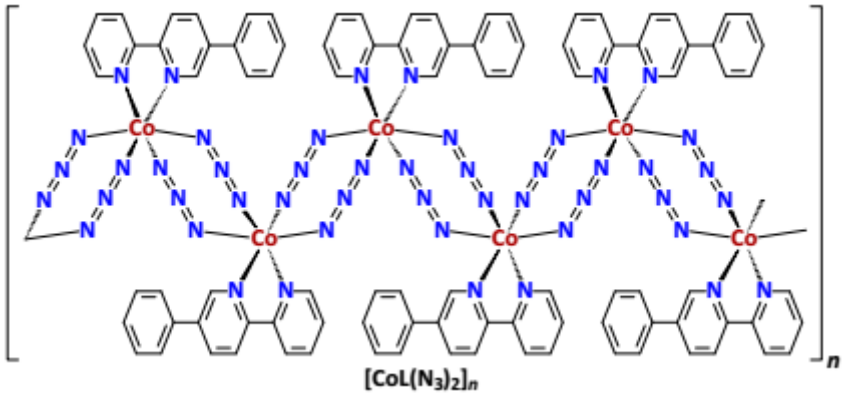

Figure 10: An azide-rich complex of Cobalt(III) with the rare 5-phenyl-2,2'-bipyridine ligand [231].

Several metal complexes have been reported with the azide acting as a bridging ligand [218, 232]. For example, the two polynuclear azido-bridged Co(II) compounds (Fig. 14) with formulas catena-$[Co(\mu_{1,3}\text{-}N_3)(N_3)(py)_2(H_2O)]_n$ and $[Co(\mu_{1,3}\text{-}N_3)2(4\text{-}acpy)_2]_n$ (py); pyridine, (4-

acpy); 4-acetylpyridine has been reported [12] with both complexes showing antiferromagnetic interactions.

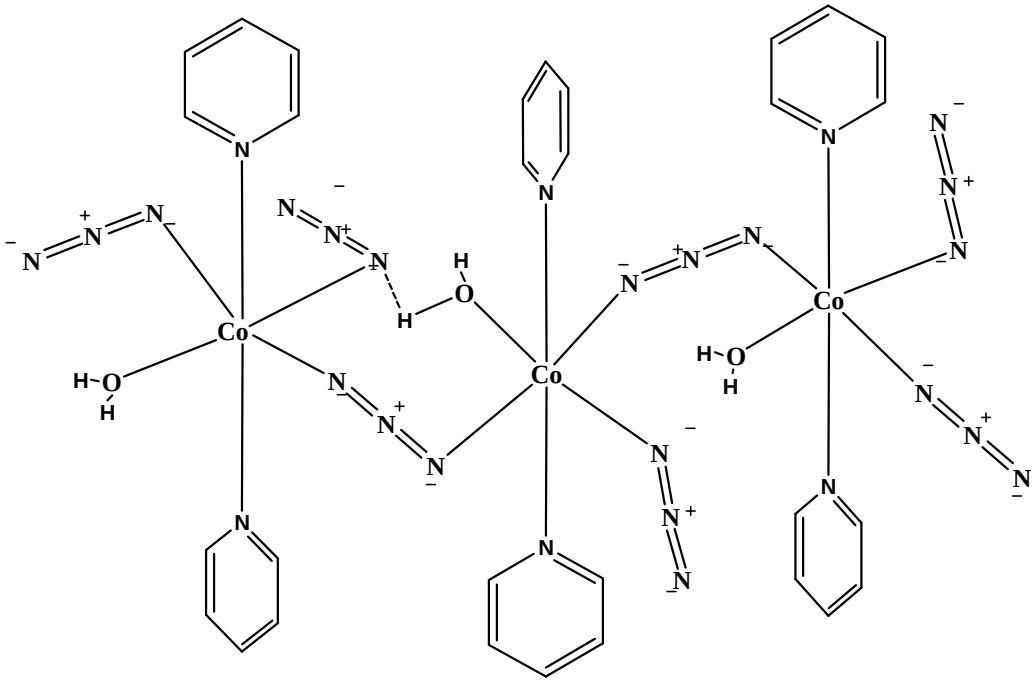

Figure 11: 1D chain system of the *catena*-[Co($\mu_{1,3}$-N_3)(N_3)(py)$_2$(H_2O)]$_n$ [12].

1.4.4- Nitrato (NO_3^-) co-ligand

Nitrates are good oxidizing agents and decompose exothermically at elevated temperatures [233]. The nitrato ligand can function as a monodentate ligand, bidentate ligand, bridging group, or ionic species in various inorganic systems. The functional characteristics probably depend on the nature and number of molecules of other ligands present [58, 61].

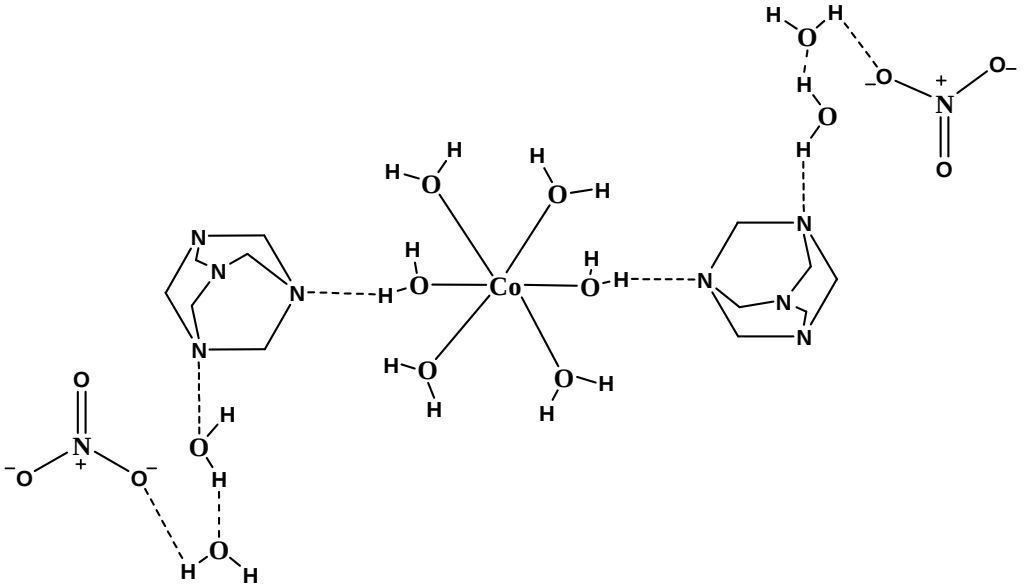

Figure 12: Metal nitrate complexes [Co(H_2O)$_4$(H_2O-HMTA)$_2$](NO_3)$_2$·4H_2O [233]

The $[Cu(phen)_2N_3](NO_3)(H_2O)$ complex (Fig. 16) are connected by π–π interactions among the phen aromatic ring giving rise to a 1D chain [234].

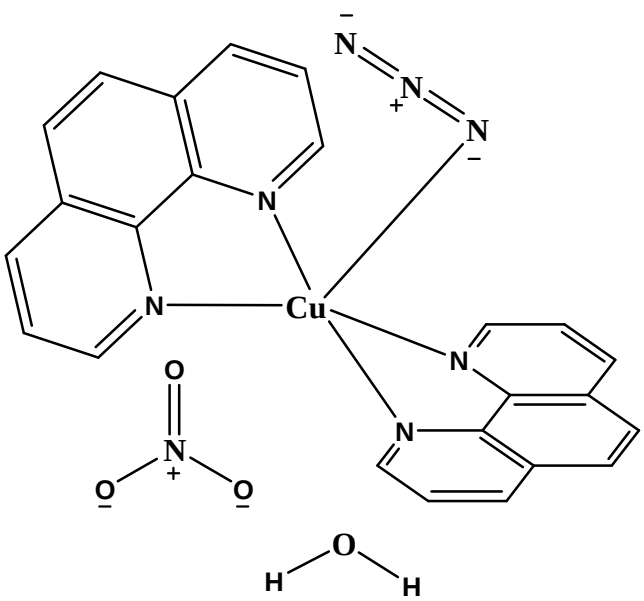

Figure 13: ORTEP view of $[Cu(phen)_2N_3](NO_3)(H_2O)$ complex [234]

1.5- Metal Complexes of 1,10-phenanthroline

The 1D, 2D, and 3D polymeric networks constructed from polydentate ligands and transition metals comprise an area that has experienced a tremendous increase in interest and is overwhelmingly dominated by the use of N-containing bridging ligands [235, 236]. The majority of compounds of phen are linked by strong directional forces such as coordination bonds and hydrogen bonds emerging as powerful tools to create new materials [183, 237]. The π–π stacking interactions between the different aromatic ring systems and C–H···π as well as O–H···O and N–H···O hydrogen bonding are observed in most cases and are consolidated by an extensive three-dimensional supramolecular network [38, 215]. The modification of the physical and chemical properties of these metal complexes can be possible through the use of mixed ligands with different donor atoms. These nitrogen-containing heterocycles are metal-coordinating, electron-deficient aromatic systems which can undergo π-π stacking interactions as π-acceptors [238]. Though hydrogen bonding still remains the most reliable and widely used means of enforcing molecular recognition, an interplay of weak intermolecular interactions (offset π stacking and C-H···π interactions) also determines the self-assembly of these molecules into 3D networks [239]. Due to the chelating nature of phen and substituted phen ligands in metal complexes, they control the supramolecular assemblies formed through chelation of the metal centre [175].

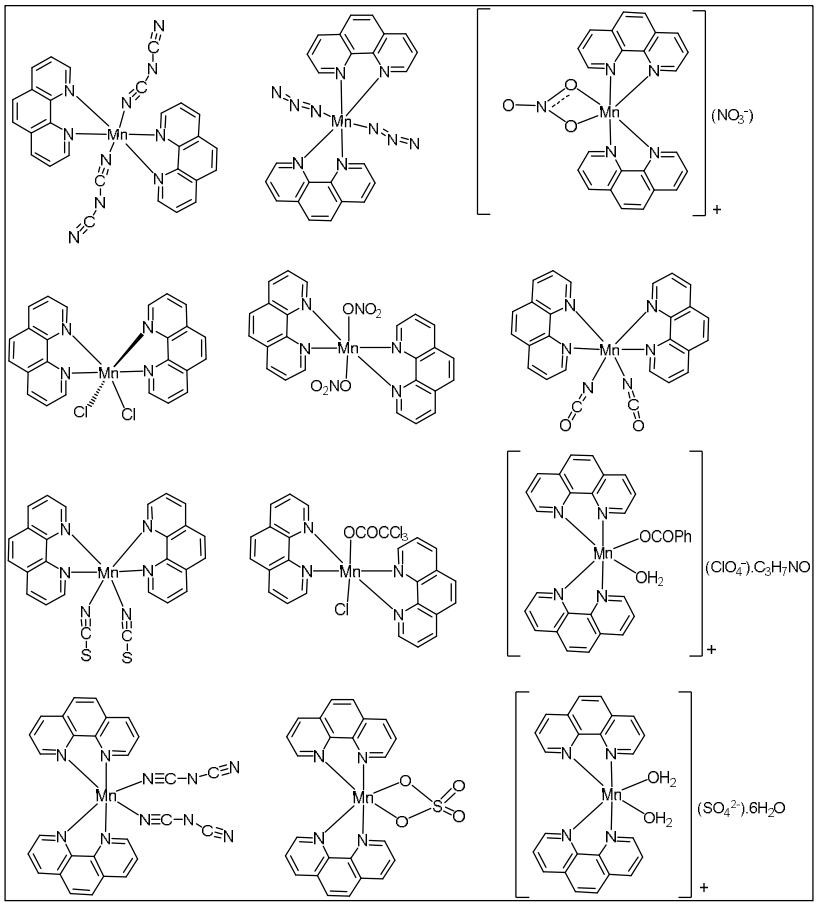

Scheme 6: Some complexes of Mn-Phen found in the literature [201, 240]

The survey of the metal complexes of phen alone around the central metal and its coordination compounds with co-ligands are presented as follow:

1.5.1- Simple Complexes of 1,10-phenanthroline

In 2006, Yesilel *et al* [241] reported the synthesis of tris(1,10-phenanthroline)cobalt(II) squarate octahydrate complex; $[Co(phen)_3]sq\ 8H_2O$ with a slightly distorted octahedral coordination geometry, involving six N-atoms from bidentate chelating phen ligands in which the Co–N bond distances ranging from 2.108 to 2.127 Å (Fig. 17).

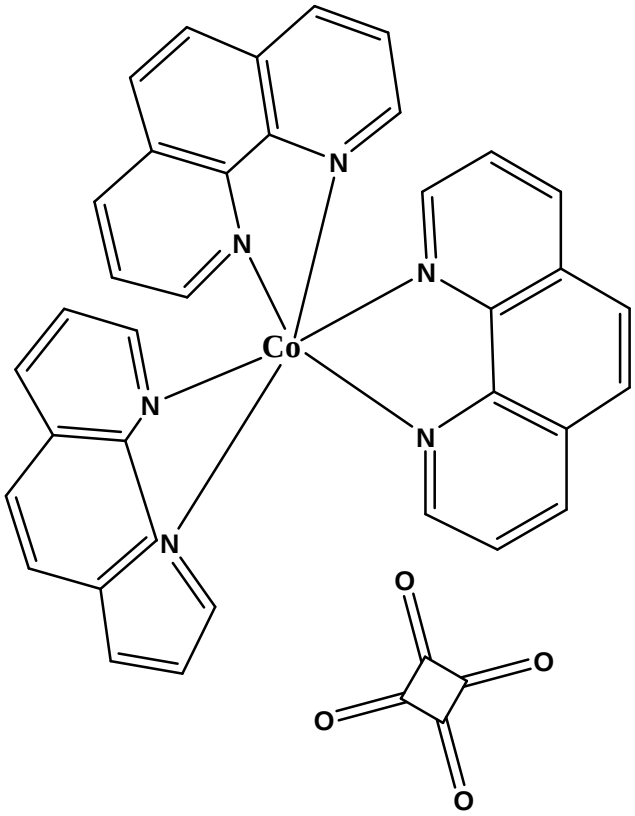

Figure 14: The molecular structure of $[Co(phen)_3]sq\ 8H_2O$ compound [241]

In the crystal packing (Fig. 18), the squarate dianions are linked to the eight solvent water molecules by means of C–H···O hydrogen-bonding interactions between the complex cation, thus extending the crystal structure in a three-dimensional network [241].

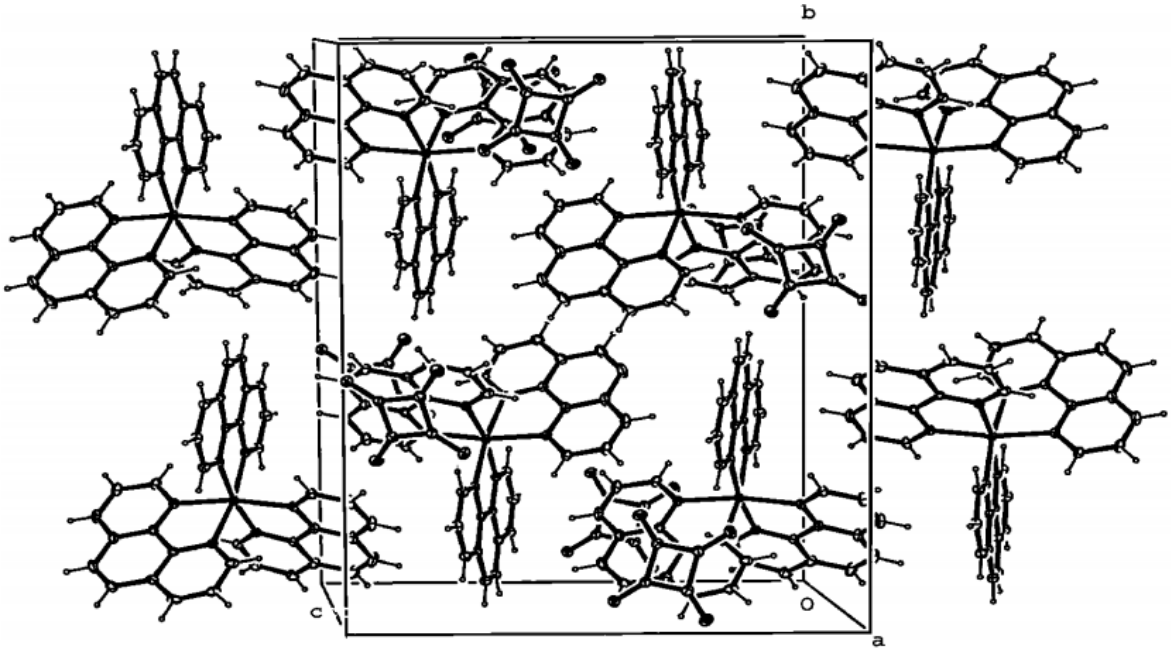

Figure 15: The crystal packing of tris(1,10-phenanthroline)cobalt(II) squarate octahydrate, $[Co(phen)_3]sq\ 8H_2O$ [241]

A similar phen compound $[Co(phen)_3]_2(NO_3)_4 \cdot C_{12}H_{12}N_2O_6 \cdot 8H_2O$, was reported by Pook *et al*., 2015 [38] containing Co(II) atom with a distorted octahedral coordination environment defined by six N atoms from three bidentate phen ligands. The two $[Co(phen)_3]^{2+}$ cations connected through the C–H···O hydrogen bonding and through lone-pair···π interactions involved the non-coordinating N,N'-(1,4-phenylenedicarbonyl)diglycine and phen molecules. Moreover, the different aromatic ring systems which are involved in the π–π stacking and C–H···π interactions, with centroid-to-centroid distances in the range 3.7094 (8)–3.9973 (9) Å stabilised the structure. The crystal structure (Fig. 19) is further stabilized by the anion···π interactions and C–H···O contacts, as well as O–H···O and N–H···O hydrogen bonds between the water molecules, the non-coordinating nitrate anions, N,N'-(1,4-phenylenedicarbonyl)diglycine and phenanthroline molecules giving rise to a three-dimensional supramolecular network. Selected π–π stacking and C–H···π interactions are shown as dashed lines [241]

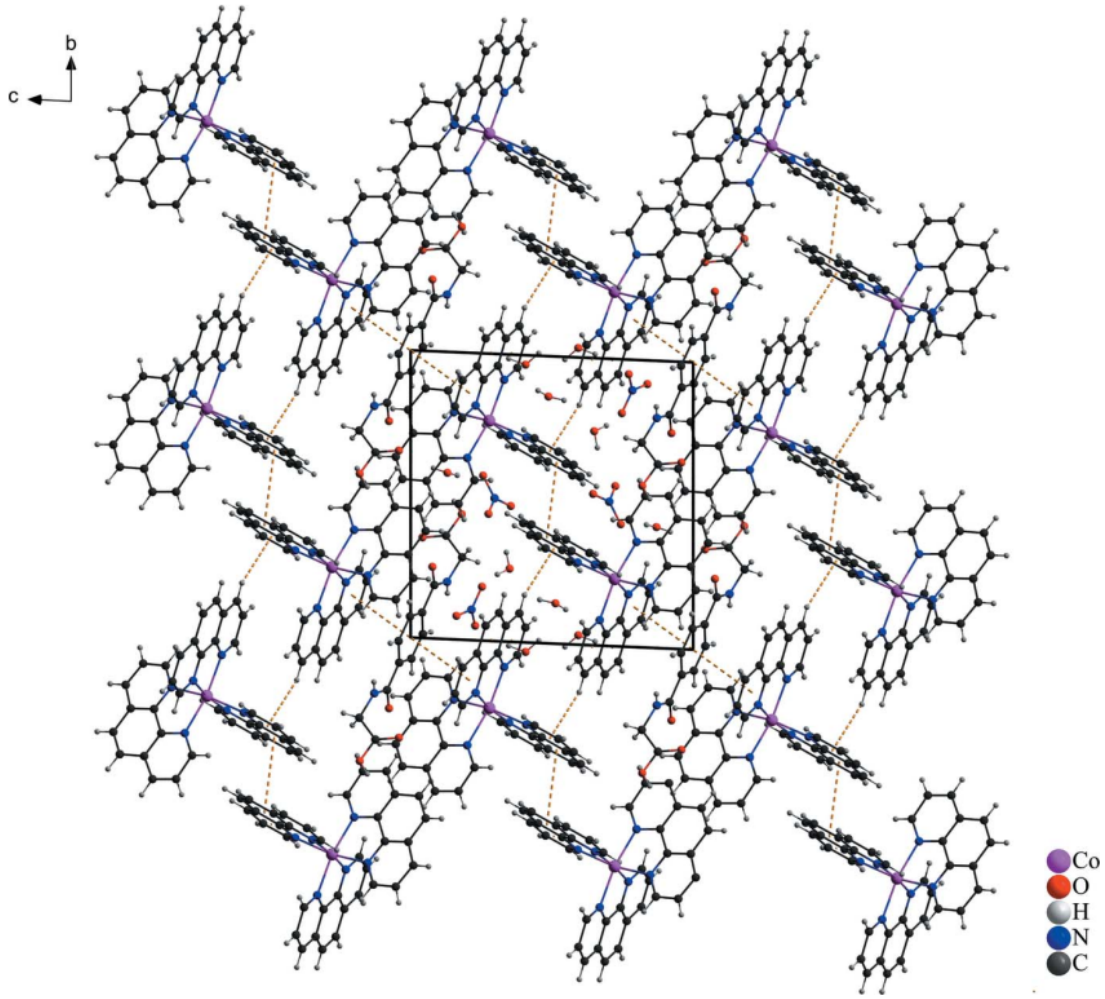

Figure 16: The crystal packing of the $[Co(phen)_3]_2(NO_3)_4 \cdot C_{12}H_{12}N_2O_6 \cdot 8H_2O$; bis[tris(1,10-phenanthroline-κ^2N,N')cobalt(II)] tetranitrate N,N'-(1,4-phenyl-enedicarbonyl)diglycine solvate octahydrate, structure in a view along the *a*-axis [38]

1.5.2- Mixed-Ligand Complexes of 1,10-phenanthroline

Mixed-ligand complexes of phen and co-ligands are also interesting due to their potential role as models for biological systems such as binding of small molecules to DNA [241]. Several complexes of phen and co-ligands have been reported in the literature.

Yesilel *et al.*, 2006 [162] reported the synthesis of cis-diaquabis(1,10-phenanthroline)zinc(II) diorotate hydrate $[Zn(H_2O)_2(phen)_2](C_5H_3N_2O_4)_2\cdot(H_2O)_{2.125}$, with the zinc ion located on a twofold axis coordinated by two aqua ligands together with a pair of bidentate phen molecules which exhibited a distorted octahedral coordination geometry. The orotate anions acted as a counter ion for charge balance (Fig. 20) and one of the water molecules acted as a co-ligand.

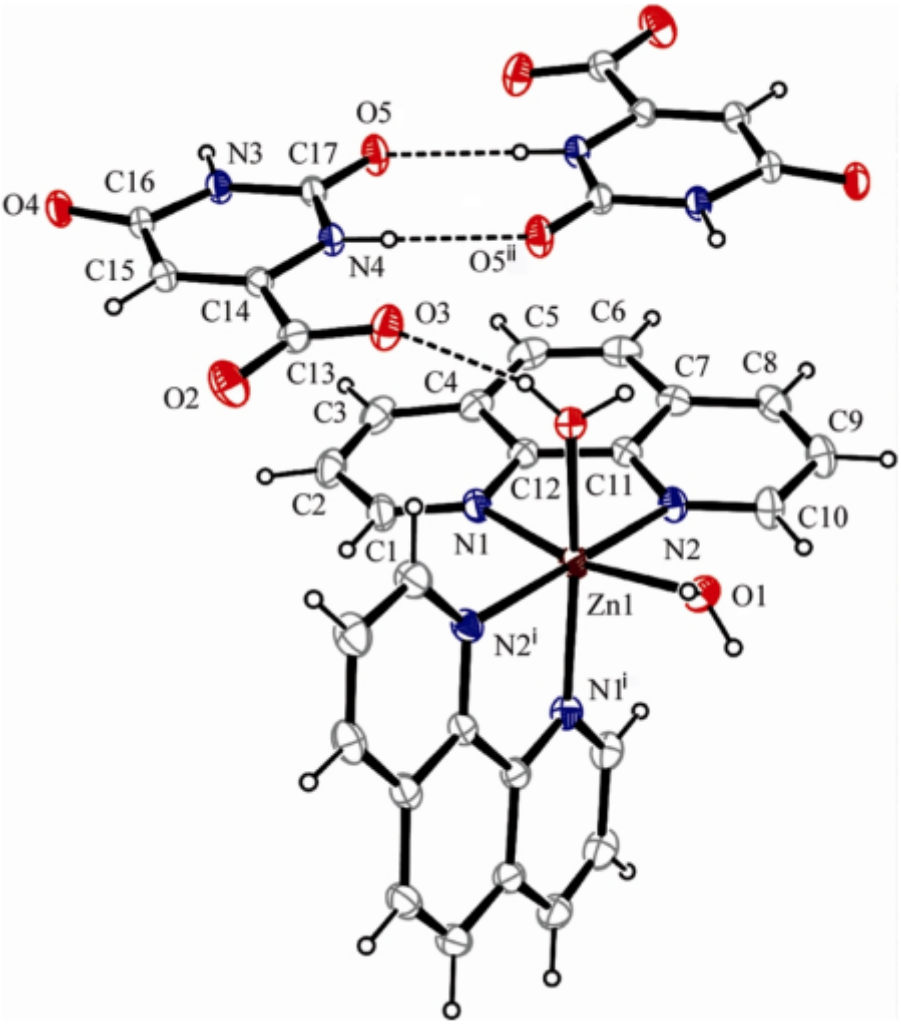

Figure 17: A view of the zinc coordination, in the title compound $[Zn(H_2O)_2(phen)_2](C_5H_3N_2O_4)_2\cdot(H_2O)_{2.125}$ [162]

In the crystal packing, both the coordinated and uncoordinated water molecules link the orotate ions to the metal complex through O–H···O hydrogen bonds. Thus, the extensive network of

hydrogen bonds together with π–π, and π–ring interactions stabilized the crystal structure and formed an infinitive three-dimensional structure.

Hu *et al.*, 2016 [242] reported a mixed-ligand complex with an asymmetric unit of $[Mn(C_7H_4BrO_2)(phen)_2(H_2O)](C_7H_4BrO_2)\cdot 2H_2O$, consisting of a monovalent $[Mn(C_7H_4BrO_2)(phen)_2(H_2O)]^+$ complex cation, a 4-bromobenzoate anion and two lattice water molecules (Fig. 21). In the complex cation, the Mn(II) ion is coordinated by four N atoms from two bidentate chelating phen ligands and two O atoms of the co-ligands; one from a 4-bromobenzoate anion and the other from the coordinating water molecule forming MnN_4O_2 distorted octahedral geometry.

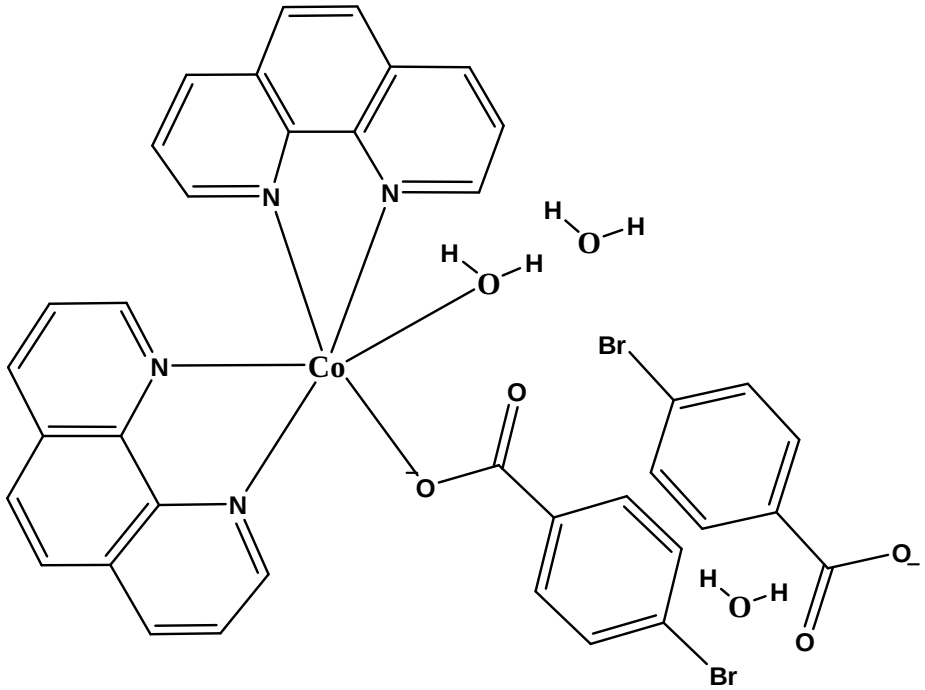

Figure 18: The molecular structure of the $[Mn(C_7H_4BrO_2)(phen)_2(H_2O)](C_7H_4BrO_2)\cdot 2H_2O$ compound [242]

In the crystal packing, the complex cations are connected to each other via O–H···O, O–H···Br and C–H···O hydrogen bonds [closest separation = 3.492(4) Å] and π–π stacking interactions [closest separation = 3.771(4) Å]. The π–π contacts are also linked to both the coordinated and non-coordinating 4-bromobenzoate anions resulted in an overall three-dimensional network structure.

Dong *et al.*, 2010 [240] presented a 3D supramolecular complex di(thiocyanato-κN)bis(1,10-phenanthroline-5,6-dione-κ2N,N')manganese(II) with molecular formula $[(C_{12}H_6N_2O_2)_2Mn(NCS)_2]_2$, formed by the reaction of 1,10-phenanthroline-5,6-dione with $Mn(NCS)_2$. Here, the metal ion is in a six-coordinated environment with a distorted octahedral

geometry. The asymmetric unit (Fig. 22) consisted of one manganese cation, two 1,10-phenanthroline-5,6-dione ligands and two thiocyanate anions co-ligands with the Mn-N bond lengths ranging from 2.117(3) Å to 2.364(2) Å.

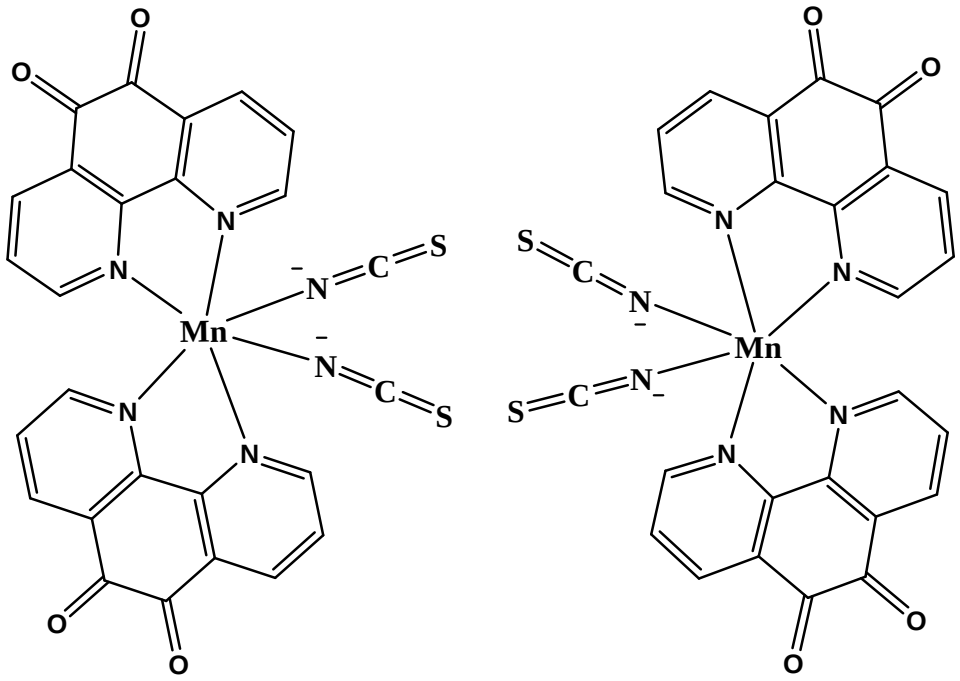

Figure 19: Molecular structure of the $[(C_{12}H_6N_2O_2)_2Mn(NCS)_2]_2$ complex [240]

In the crystal packing, the independent mononuclear units are linked to each other by C–H···O intermolecular hydrogen bonds formed between adjacent molecules resulting in a 3D supramolecular framework.

Hazari *et al.*, 2015 [243] reported a trinuclear manganese(II) entity, $[Mn_3(phen)_2(phdac)_3]\cdot 2H_2O$, (phen=1,10-phenanthroline and H_2phdac=1,4-phenylenediacetic acid) Mn(phen) moieties that sandwich another manganese atom by means of six bridging carboxylate groups in a centro-symmetric fashion (Fig. 23).

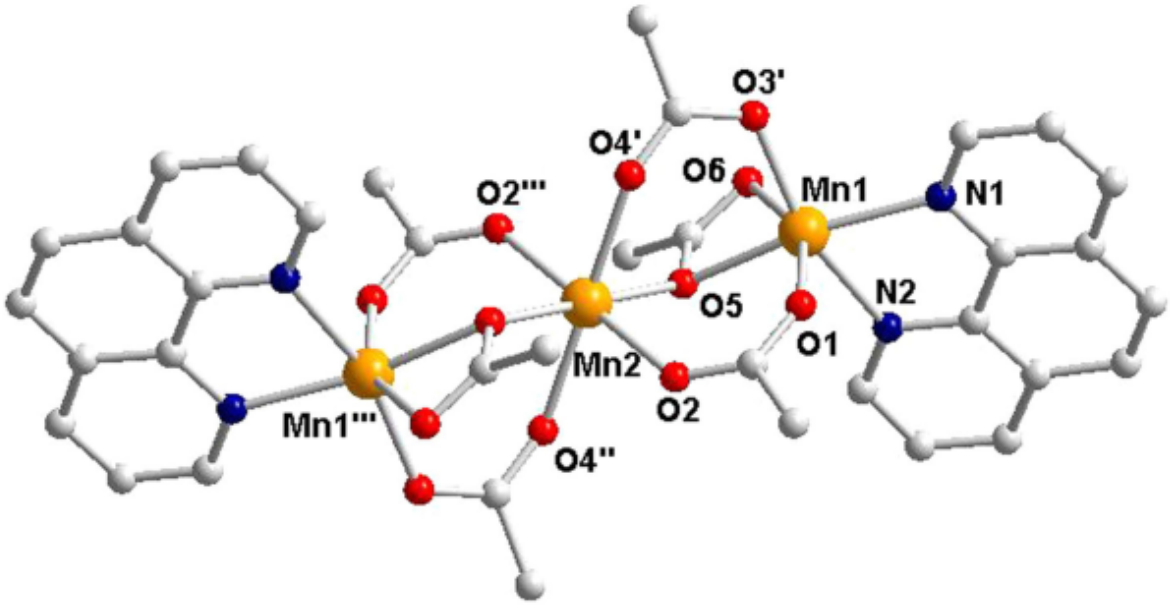

Figure 20: The centrosymmetric trinuclear unit of $[Mn_3(phen)_2(phdac)_3]\cdot 2H_2O$ [243]

The independent Mn_1 and Mn_2 centres have octahedral geometries with N_2O_4 and O_6 donor sets, respectively. The crystal packing is a 2D coordination polymer of (4,4) topology, where the trinuclear units and the facing phen rings interact through π–π interactions (centroid-to-centroid distance of 3.7438(1) Å). In addition, the lattice water molecules bridged the carboxylate oxygen atoms of the different layers by means of weak Hydrogen bonds resulting to the formation of a 3D architecture.

Sado *et al.*, 2017, synthesised an azido-bis(1,10-phenanthroline-κ^2N,N')copper(II) nitrate complex; $[Cu(phen)_2N_3]\cdot NO_3$ [61] with the molecular structure containing three monomeric cations, $[Cu(phen)_2(N_3)]^+$, three nitrate ions and one water molecule in one asymmetric unit (Fig. 24).

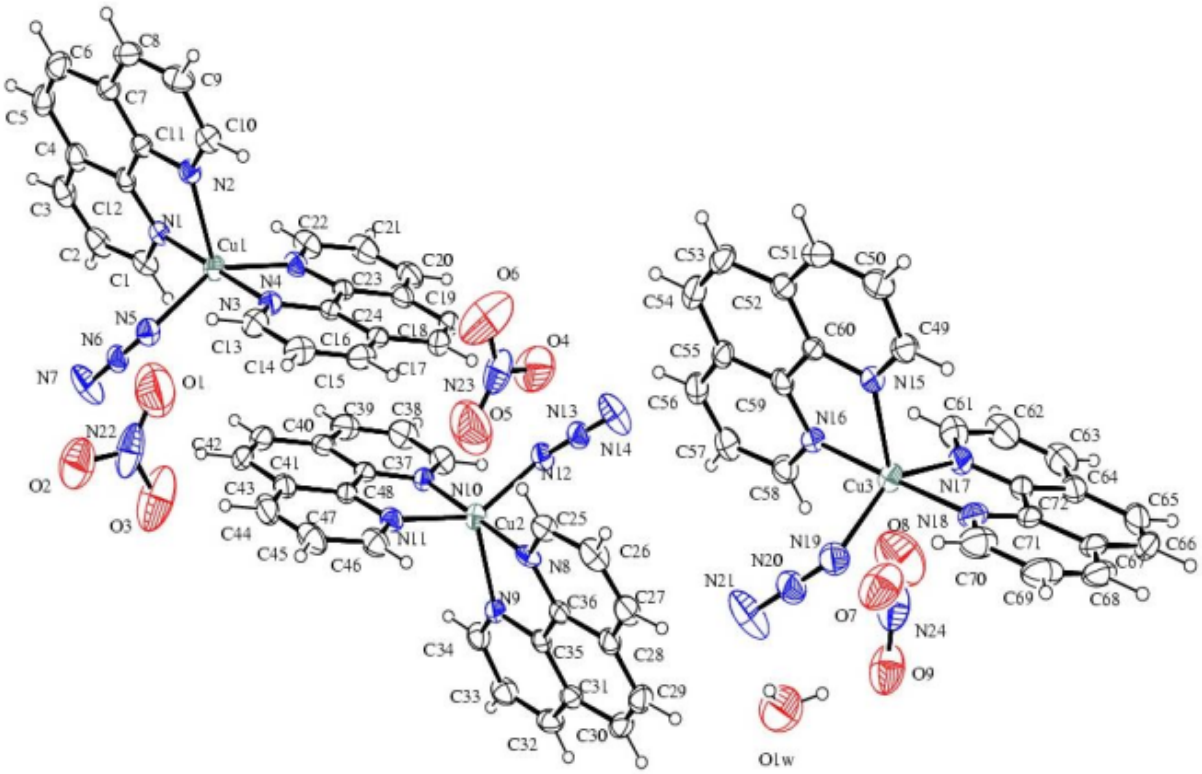

Figure 21: Crystal structure of $[Cu(phen)_2N_3]\cdot NO_3$ view along a-axis [61]

The three molecular complexes and the anions in the asymmetric unit are linked alternatively through C-H···O hydrogen bonds which generates an infinite one-dimensional chain.

The presence of nitrate O and azide N atoms in the molecular structure act as acceptor centres for the formation of C–H···O, C–H···N and water associated O–H···O hydrogen bonds. These adjacent chains, arranged in parallel are interlinked through C–H···O hydrogen bonds to generate an infinite two-dimensional supramolecular sheet, which exchange π–π interactions experienced between the phen moiety, forming an extended three-dimensional network in the solid [61].

Manson *et al*, 2013 [193] synthesised a quasi-2D antiferromagnetic $Mn(dca)_2$(o-phen) complex {dca = dicyanamide; o-phen = 1,10-phenanthroline} with a long-range magnetic order in a low-dimensional Mn-dca polymer which showed both single- and bi-bridged Mn-dca-Mn linkages (Fig. 25). Note the bibridged dimer-like $[Mn_2(dca)_2(o\text{-phen})_2]^{2+}$ units in the structure. Only the nitrogen atoms of the chelated o-phen molecule are shown for clarity

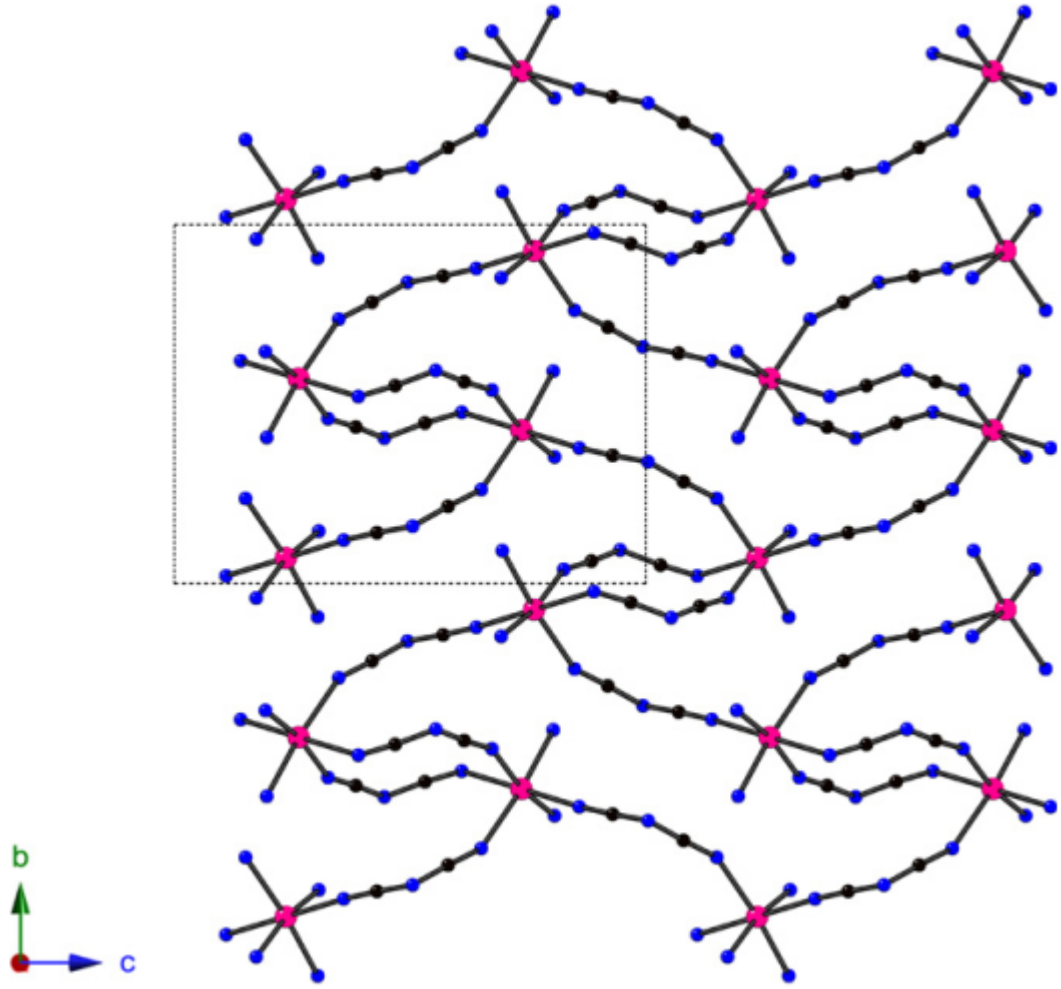

Figure 22: Two-dimensional polymeric structure of $Mn(dca)_2(o\text{-}phen)$ [193]

Sado *et al.*, 2016 [58] reported $[Co(phen)_2(N_3)_2]NO_3$ complex with an asymmetric unit (Fig. 1.26) consisting of one molecule of phen, one azide anion, one nitrate anion and one Co(III) ion. The Co–N bond lengths in CoN_6 (Fig. 26) core ranges from 1.9356(17)-1.955(2) Å for the $Co–N_{phen}$ and 1.933(3) Å for the $Co–N_{azide}$. The adjacent two-dimensional supramolecular sheets exchange π–π interactions are experienced between the phen moiety forming an extended three-dimensional network in the solid. The cobalt atoms between the stacked sheets running along the c-direction had an interlayer Co–Co distance of 7.369 Å.

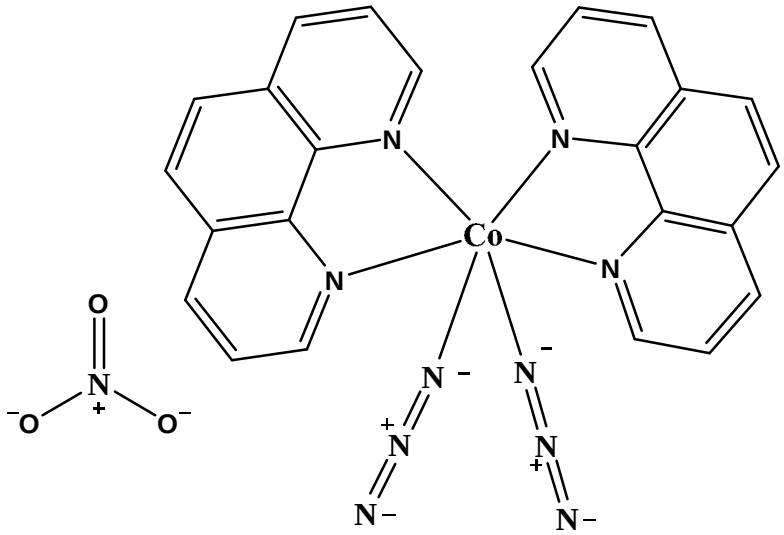

Figure 23: ORTEP view of $[Co(phen)_2(N_3)_2]NO_3$ crystal structure [58]

Čechová *et al*., 2014, reported the crystal structure of $[Mn(phen)_2Cl_2]$ complex determined at 150 K where, the manganese atoms are coordinated by four pyridine nitrogen atoms from two phen ligands and two chloride anions, resulting in a distorted cis-MnN_4Cl_2 octahedral geometry. The crystal packing connected through the C–H···Cl hydrogen bonds and π-π stacking interactions is consolidated by an extensive three-dimensional supramolecular framework [244].

Saphu *et al*., 2012 [245] reported the crystal structure (Fig. 27) of the title compound $[Mn(NO_3)_2(phen)_2]$ in which the Mn(II) atom lies on a twofold rotation axis and is six-coordinated in a distorted trans-N_4O_2 octahedral environment by four N atoms from two phen ligands and two O atoms from two nitrate anions. In the crystal packing, the molecules are linked by weak C–H···O hydrogen bonds and π–π stacking interactions consolidating into a three-dimensional supramolecular network.

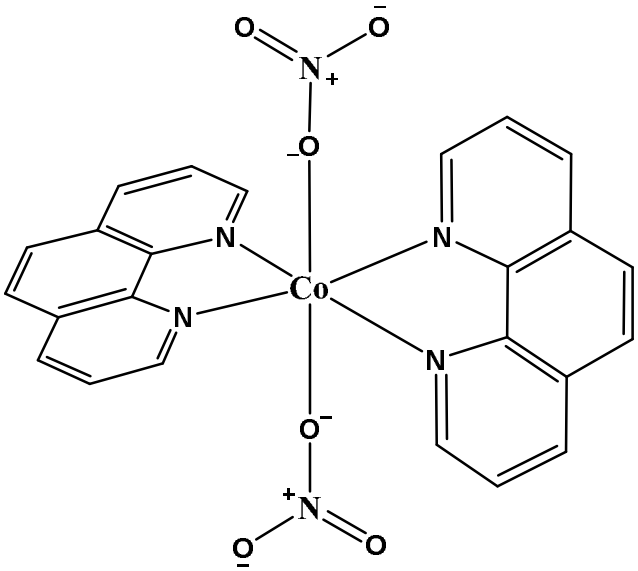

Figure 24: Asymmetric unit of the metal centers of $[Mn(NO_3)_2(C_{12}H_8N_2)_2]$ [245]

1.6- Potential Applications of Complexes of 1,10-phenanthroline

The functionalization of phen moiety enables the formation of complexes which change the spectroscopic and electronic properties of the products and therefore broadening the potential application for biological studies and molecular magnetism [58, 246]. This biologically important ligand and some of its metal complexes have been shown to be effective against various strains of microorganisms [61]. Notwithstanding, metal complexes of substituted phen ligands have demonstrated higher antimicrobial activity than that of their uncoordinated or non-substituted ligands [48, 180].

1.6.1- Molecular magnetism

Magnetic properties of coordination polymers are studied because they enable the design of lightweight molecular-based magnets. Anti-ferromagnetism, ferrimagnetism and ferromagnetism are cooperative phenomena of the magnetic spins within a solid. They require interaction or coupling between the spins of the paramagnetic centres [247].

Magnetic coordination networks should have a residual permanent magnetisation at zero-field for as high as possible critical temperature (T_C). Its structure should allow parallel coupling of the spins (↑↑↑↑, ferromagnetism) or the anti-parallel coupling of unequal spins(↑↓↑↓, ferrimagnetism) of neighbouring paramagnetic spin carriers so that an on-zero spin of the bulk material results. Anti-parallel coupling of spins (↑↓↑↓, anti-ferromagnetism) also occurs as the state of low-spin multiplicity is often more stable than the state of high-spin multiplicity. Efficient coupling in materials can occur through open shell organic ligands. In order to achieve

strong coupling between the metal centres and their unpaired electrons, short oxo, cyano or azido bridges are needed [120, 247].

The magnetic behaviour at variable temperatures on the coordination networks for Cu(II) [182, 194, 248], Co(II) [182, 249] and Mn(II) [250] complexes of phen have been reported in the literature. Studies on the ability of phen to transmit magnetic coupling have revealed the transmission of a very weak antiferromagnetic coupling [13, 193]. Other bridging ligands (e.g. dca, azide, SCN) in these compounds, which exhibit strong couplings, mediate their magnetic interactions.

The magnetic susceptibility measurements at room temperature of $[Cu(L)(phen)_2]Cl_2$ complex (1.85 BM) and that of $[Co(L)(phen)_2]Cl_2$ complex (4.84 BM) indicates consistency with the octahedral environment (L is the schiff base ligand prepared by reactiong N-(4-aminophenyl)acetamide into a solution of 4-hydroxybenzaldehyde in ethanol) [182].

The neutron diffraction measurements down to 0.5 K revealed a conventional Néel order of the Mn^{2+} magnetic moments within the ac-plane and T_N = 1.85 K for the quasi-2D antiferromagnet $Mn(dca)_2$(o-phen) complex featuring both single- and bi-bridged Mn-dca-Mn linkages [193].

The magnetic properties of $[Cu_2(dmphen)_2(dca)_4]$ complex (dmphen=2,9-dimethyl-1,10-phenanthroline, dca=dicyanamide) was as expected for two magnetically isolated spin doublets. Upon cooling, the Curie law behaviour was observed until ca. 50 K, and then, $\chi_M T$ decreases sharply to reach a value of 0.24 cm^3 mol^{-1} K at 1.9 K and a maximum was observed in the susceptibility curve at 3.0 K depicting a weak intramolecular antiferromagnetic interaction leading to a low lying singlet spin state [194].

1.6.2- Antimicrobial Activity

Metal-based drugs are a class of antimicrobial agents that have potential applications in the fight against microbial infections. Antibacterial agents are small molecules of low molecular weight and they may be natural products (such as cephalosporins, aminoglycosides or β–lactams including penicillin) or synthetic compounds (sulfonamides, nitroimidazoles, oxazolidinones, and quinolones are characteristic members). These compounds should be thermally stable before being used for the production of medicine. Thermal stability of the complexes is one of the necessary conditions associated with the production process of drugs since most of the pharmacologically active compounds used in medicine are solids and are prepared at temperatures greater than ambient temperature [78].

Phen has been used as a model ligand for many bioactive molecules due to the presence of de-shielded nitrogen atoms [78, 179]. Their metal complexes have exhibited good DNA binding affinity (as DNA cleaving agents) and non-radioactive nucleic acid probes [48, 64, 179, 180]. Phen metal complexes have been shown to possess bacteriostatic and bacteriocidal properties toward many Gram-positive bacteria [48]. Chandraleka *et al.*, 2014 presented the $[Cu(SAla)Phen]\cdot H_2O$ complex (SAla = alanine salicylaldehyde) suitable for the treatment of bacterial and fungal infections [48]. Coyle *et al.*, 2003 reported three (3) 1,10-phenanthroline complexes; $[Cu(phen)_2(mal)]\cdot 2H_2O$, $[Mn(phen)_2(mal)]\cdot 2H_2O$ and $[Ag_2(phen)_3(mal)]\cdot 2H_2O$($malH_2$ = malonic acid) showing very good fungicidal activity with minimum inhibitory concentrations (MIC's) values in the range 1.25–5.0 $\mu g/cm^3$ at a concentration of 10 $\mu g/cm^3$ [76]. Lobana *et al.*, 2014 presented four copper complexes of salicylaldehyde-N-substituted thiosemicarbazones and phen with significant growth inhibitory activity (antimicrobial activity) against *Staphylococcus aureus* (MTCC740), methicillin resistant *Staphylococcus aureus* (MRSA), *Klebsiella pneumoniae* 1 (MTCC109), *Shigella flexneri* (MTCC1457), *Pseudomonas aeruginosa* (MTCC741) and *Candida albicans* (MTCC227) [60].

1.7- Microorganisms

Microbial infection is one of the main causes of morbidity and mortality because treatment of these infections is often complicated by increasing antimicrobial resistance, drug cytotoxicity and limited drug spectrum. These challenges have prompted the search for and development of new antimicrobial agents. Antibiotic and antiseptic resistance have partly emerged due to the prevalence of bacteria in the form of biofilms [251].

Antimicrobials or antimicrobial agents are natural or synthetic compounds that inhibit the growth of or kill microorganisms (bacteria, fungi and viruses), completely in low concentrations in both human and animals. The inappropriate use of antibiotics has resulted to substantially increased resistance in the recent years and is posing an ever-increasing therapeutic problem [54]. This resistance to antibiotics can be explained in biochemical terms as the inability of a given antibiotic to reach its microbial target at an adequate concentration in order to inhibit the target's activity or kill the target. Within this scope, there are two main ways of acquiring resistance: decreasing the affinity of the target for the antibiotic (mutations in genes encoding the antimicrobial targets) and/or diminishing the active concentration of the antibiotic inside the cell [252]. For the latter, the mechanisms of resistance can be broadly classified into three categories:

- ***Production of hydrolytic or modifying enzymes***

Bacteria or fungi may acquire several genes for a metabolic pathway which ultimately produces altered bacterial cell walls that no longer contain the binding site of the antibacterial agent, or they may acquire mutations that limit access of antimicrobial agents to the intracellular target site [253].

- ***Mutations in antimicrobial transporters***

The organism may acquire gene-encoding enzymes, such as ß-Lactamases, that destroy the antibacterial agent resulting in mutations in antimicrobial transporters that may impede their entrance into the target before they can have an effect [254].

- ***Use of efflux pumps to extrude antimicrobials***

Mutations in antibiotics transporters may impede their entrance; and as such bacteria may acquire energy-dependent efflux pumps that extrude the antimicrobial agents from the cell before it can reach its target site and exert its effect. Efflux pumps were first described as a mechanism of resistance to tetracycline in *Escherichia coli* [255]. However, nowadays it is well known that efflux pumps constitute the most ubiquitous type of resistance element, present in all organisms from bacteria to mammals, among those that have been described [256].

1.7.1- Bacteria species

Bacteria species are generally classified as Gram-positive and Gram-negative. Gram-positive bacteria are those that stained dark blue or violet by Gram staining. They retain the crystal violet stain because of the high amount of peptidoglycan in the cell wall that lacks the outer membrane. Gram-negative bacteria contrary do not retain the crystal violet dye in the Gram staining protocol. The Gram-negative bacteria instead take up the counterstain and appear red or pink. The different species of bacteria used in this study are *Salmonella enterica, Shigella flexineri, Escherichia coli, Staphylococcus aureus streptococcus pneumonae, Pseudomonas aeruginosa, Klessiella pneumonae, Hemophyllus influenza, Enterococcus fecalis and Mycobacterium smegmatis.*

1.7.1.1- *Escherichia coli*

Escherichia coli is a Gram-negative bacillus in the family *Enterobacteriaceae*. Most *E. coli* are found in the intestinal tract of mammals. Pathogenic strains of this organism are distinguished from normal flora by their possession of virulence factors such as exotoxins [257]. However, there also exist many pathogenic strains of *E. coli* that can cause a variety of diarrheal, hemorrhagic colitis diseases in humans and animals. Haemorrhagic colitis occasionally

progresses to hemolytic uremic syndrome (HUS), an important cause of acute renal failure in children and morbidity and mortality in adults. In addition, *E. coli* is generally responsible for urinary tract infections, septicaemia, neonatal meningitis and gastrointestinal tract infections. It is sensitive to different antibiotic groups notably; β-lactams, aminoglycosides, first-generation quinolones, cloroquinolones and cotrimoxazole [76].

1.7.1.2- *Staphylococcus aureus*

Staphylococcus aureus is a Gram-positive spherical bacterium approximately 1 μm in diameter. Its cells form grape-like clusters since cell division takes place in more than one plane. Among the *Staphylococcal* species, *S. aureus* is by far the most virulent and pathogenic for humans. It has been estimated that approx. 20–30% of the general population are *S. aureus* carriers [258, 259]. Hospital-acquired infections with *Staphylococcus aureus*, especially methicillin-resistant *S. aureus* (MRSA) infections, are a major cause of illness and death and impose serious economic costs on patients and hospitals [260, 261].

It can be isolated from the respiratory tract of patients with cystic fibrosis. It causes diseases such as superficial infections like boils and abscesses, deep infections like septicaemia and pneumonia, toxic shock and skin exfoliation. *S. aureus* is commonly found in the nose, skin, throat and gut and many healthy people are carriers of this bacterium. It can be spread by contact and airborne routes. These strains usually do not cause pathological conditions but serious infections occur when the resistance of the host is low. This could be due to hormonal changes, debilitating illness, wounds on the skin surface, treatment with steroids or other anti-inflammatory drugs. *S. aureus* readily appears in multiple resistant forms, especially in hospitals because of the extensive use of antibiotics, thus making treatment more difficult. Treatment of choice for *S. aureus* infections are beta-lactamase stable penicillins, while vancomycin is indicated for the methicillin resistant strain [262].

1.7.1.3- *Salmonella enterica*

Salmonella enterica is a Gram-negative, rod-shaped, flagellated bacterium that is of interest due to its ability to cause infectious diseases in humans and animals. Salmonellosis is food poisoning caused by consumption of food contaminated with bacteria of the genus Salmonella. Salmonellosis is a major global cause of diarrheal, extra-intestinal diseases as well as other foodborne illnesses in both humans and animals [263]. Also, typhoid fever, caused by *Salmonella enteritis* is endemic to the developing world [264]. According to the WHO

estimates, the global typhoid fever disease burden at 11-20 million cases annually, resulting in about 128,000–161,000 deaths per year [265].

Furthermore, multidrug-resistant *S. enterica* which is resistant to the extended-spectrum third-generation cephalosporins aminoglycosides, tetracyclines, sulfonamides and chloramphenicol, have now been isolated in several countries from food, animals and humans [263].

1.7.1.4- *Shigella flexneri*

Shigella is Gram-negative, rod-shaped, immobile anaerobic and facultative enterobacteria with a weak metabolic strength. They are the class of bacteria that are found in human beings but are not part of the normal intestinal flora. Despite this, they are the cause of infected colitis in adults and severe gastrointestinal problems associated with diarrhoea and dysentery in children. Diarrhoeal diseases account for approximately 25 % of all deaths in children of age less than 5 years in developing countries [266, 267]. Moreover, Infections caused by *Shigella* species are an important cause of diarrhoeal diseases in both developing and developed countries.

1.7.1.5- *Pseudomonas aeruginosa*

It is a Gram-negative bacillus and is an obligate aerobe. It is an opportunistic pathogen, especially in hospitals, which can infect almost any body part given the right predisposition. It causes skin infections, burns and pneumonia.it is a major lung pathogen in cystic fibrosis patients. It can also cause urinary tract infections, septicaemia, osteomyelitis and endocarditis. A small percentage of normal healthy people are carriers as part of the normal flora of the gut. *P. aeruginosa* is resistant to most antibacterial agents and is only susceptible to aminoglycosides and newer beta-lactams [268, 269]. There are however strains within the species that may also acquire resistance to these agents.

1.7.1.6- *Klebsiella pneumonia*

It is a Gram-negative bacillus and is a facultative anaerobe. *Klebsiella* infections generally tend to occur in people with weakened immune systems, most commonly in the urinary tracts. It causes pneumonia in patients with predisposing medical conditions such as diabetes, as well as septicaemia and wound infections [270]. *K. pneumonia* is normally found in the gut of man and animals and in moist environments such as soil and water. Infection may be endogenous or spread by contact as this bacterium has a remarkable capacity for survival on hands. Multiple antibiotic resistance is common and treatment is difficult. Most often, two or more powerful antibiotics are used to eliminate the infection. These include cephalosporins, beta-lactamase stable penicillins and aminoglycosides [261].

1.7.2- Fungi Species

The Fungi; *Candida albicans, Candida krusei, Cryptococcus neoformans* and *Candida parapsilosis* are different fungi species used in this work. They are the main cause of candidemia, which has become one of the main agents of most bloodstream infections over the last two decades [271]. They are also the causative agents of *Candida pneumonia, vulvovaginitis* gastrointestinal fungi infections, *Septicemia*, and meningitis. Despite the high morbidity and mortality associated with candidosis, no decrease in the incidence of this infection has yet been achieved [272]. The increasing prevalence of fungal infections, especially hospital-acquired infections and infections in immune-compromised patients has heightened the need for new anti-fungal treatments. Drug-resistant fungal isolates have been reported for all known cases of antifungal drugs [273]. Thus, there is an urgent need to develop new and more effective antifungal therapies [56, 274].

1.7.2.1- *Candida albicans*

Candida albicans is a yeast and it exists as a commensal of warm-blooded animals including humans. It is a diploid (a form of yeast) and causal agent of opportunistic oral and genital infections in humans. It colonizes the mucosal surfaces of the oral and vaginal cavities and the digestive tract and is able to cause a variety of infections [76, 275].

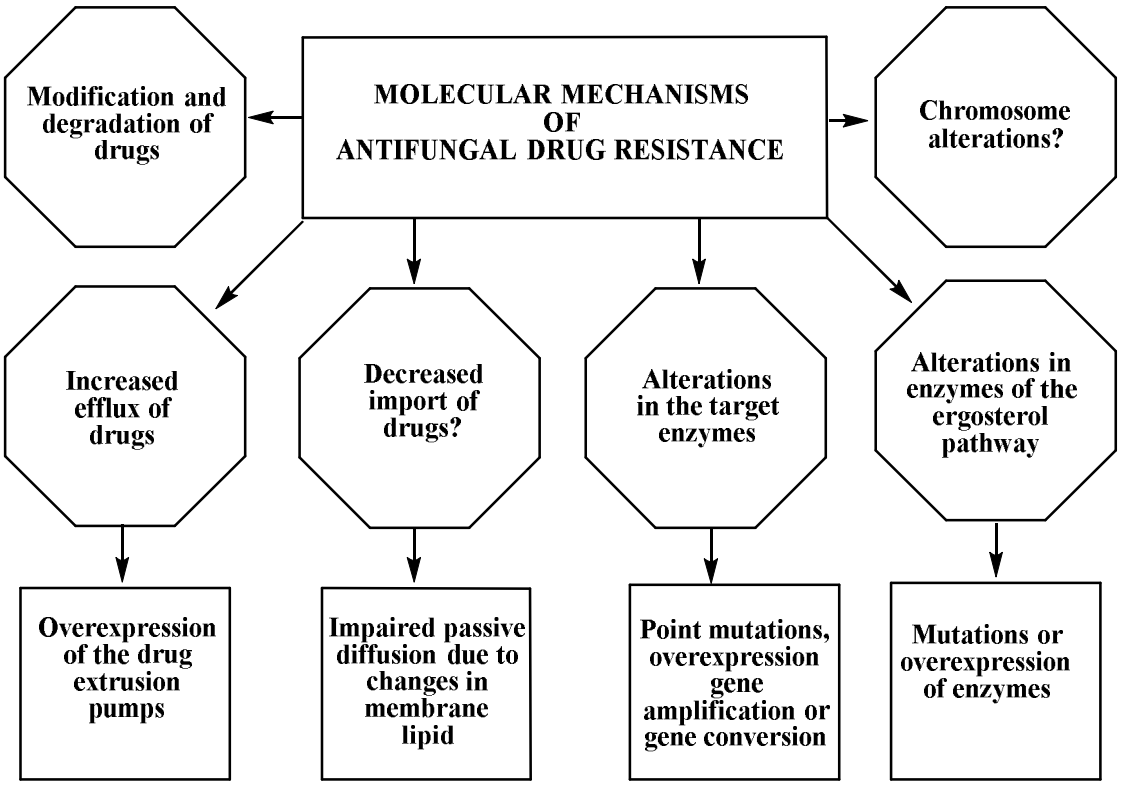

Figure 25: A schematic representation of the known molecular factors that contribute to antifungal drug resistance in *C. albicans* [59].

1.7.2.2- *Candida krusei*

Candida krusei is budding yeast involved in chocolate production in the fermentation of the cocoa bean to remove the bitter taste. *C. krusei* is an emerging fungal nosocomial pathogen primarily found in people with hematological malignancies. *C. krusei* causes vaginitis and has a natural resistance to fluconazole [276, 277].

1.7.2.3- *Candida Parapsilosis*

Candida Parapsilosis is the yeast that causes candidemia. It affects mostly critically ill neonates and surgical intensive care unit patients [276]. It is been reported that *C. parapsilosis* causes knee joint infection [278].

1.7.2.4- *Cryptococcus neoformans*

Cryptococcus neoformans or *Cryptococcus gattii* is yeast found mostly in tropical and sub-tropical climates. It is a fungus that causes *cryptococcosis*, a global invasive mycosis associated with significant morbidity and mortality. It is the causative agent in Meningitis. It has been reported that global warming may have been a factor in the emergence of *Cryptococcus neoformans* in British Columbia [272].

Treatment is usually by drug association therapy of flucytosine, fluconazole and amphotericin B [272, 279].

Table I: Some Microorganisms, diseases caused and treatment used

Microorganism	Type	Disease caused	Treatment	Resistance	Reference
Escherichia Coli	Gram negative bacillus	Cystic fibrosis (Urinary tract infections) Diarrhea Nausea Abdominal pains	Nitrofuran Penicillin Amoxilline Citrofloxacin Cotrimoxazole	Medium None None	[139, 156, 280]
Staphylococcus aureus	Gram Positive cocci	Boils, Abscesses, septicaemia, pneumonia toxic shock Impetigo	Beta-lactamase Stable penicillins Erythromicin	Low Low	[281]
Samonella typhi	Gram positive bacillus	Typhoid diarrheal	Chloramphinicol Ampicillin Ciproloxacin	High High High	[281]
Shigella flexneri	Gram negative bacillus	Diarrhea	Amoxicilline, Ampicillin Clotrimoxazole	High	[156, 281]
Candida albicans	Fungi	Vaginitis Candidiasis	Suppositories or creams containing miconazole, Clotrimazole, Nystatin, imidazole	High High	[30, 156]
Candida krusei	Fungi	Vaginitis, Candidiasis	Nystatin Amphotericin B	High Low	[139]
C.neoformans	Fungi	Pneumonia Meningitis	Flucytosine Fluconazole Amphotericin B	Moderate Low	[282, 283]
C. Parapsilosis	Fungi	Pneumonia, Knee joint infections, Candinemia	Amphotericin B Fluconazole,	Low Moderate	[100]

1.8- Theoretical Calculations

Nowadays, density functional theory (DFT) calculations provide a numerical “virtual coordination chemistry lab” able to compute even properties difficult or impossible to measure experimentally [284]. DFT calculations can predict the behaviour of a broad range of chemical, physical, and biological phenomena of importance in chemical reactivity, catalytic activity, bioactivity, photo-physics, electronic and nuclear magnetic resonance spectroscopy, linear and nonlinear optics [284, 285].

1.9- Statement of the Problem

The emergence of antifungal and antibiotic-resistant pathogens and the continuing emphasis on health care costs has provoked a renewed interest in the design and development of novel and cost-effective antimicrobial agents with increased biological activity against the resistant strains [274, 286]. The strategies currently being explored to tackle this problem include the structural modification of existing antimicrobial drugs to which resistance has developed and the development of entirely new classes of antimicrobial agents that work on different target sites [287].

Combining the chelating ability of 1,10-phenanthroline, its biological activities and the versatile bonding modes of dca^-, N_3^- and NO_3^- with that of biologically relevant metals, might improve the biological properties of the complexes thereof.

1.10- Motivation

The metal complexes of 1,10-phenanthroline have shown very interesting biological and medicinal properties [48, 56, 58, 61, 179, 246, 282]. The possibility of it using its extended π-system to form non-covalent π-interactions, which mimic various biological processes, is also of interest [238, 288]. For example, the $[Cu(phen)_2]^{2+}$ complex ion has shown antitumor activity where it inhibited DNA or RNA polymerase activities [154, 177, 289]. The $[Mn(phen)_2NO_3]NO_3{\cdot}2H_2O$ and $[Mn(phen)_2]Cl_2{\cdot}C_2H_5OH$ complexes have also shown potent *in vitro* antifungal activity superior to the state-of-the-art drug Amphotericin B [176]. Likewise, the complexes; $[Cu(en)(phen)_2]_2phen{\cdot}2Br{\cdot}8H_2O$ and $[Cu(en)(phen)_2]_2{\cdot}ClO_4^-$ (en = ethylenediamine) have exhibited antimicrobial activities compared to the known standard drugs used for *Staphylococcus aureus, Escherichia coli, Pseudomonas aeruginosa, Streptoccocus pyogeneous, Candida albicans,* and *Aspergillus niger* [132]. The most active drug tested in aqueous media is the $[Ag(phendio)_2]ClO_4$ (phendio=1,10-phenanthroline-5,6-dione) complex which have greatly inhibited the growth of the human fungal pathogen *Candida albicans* [290]. The metal complexes of 1,10-phenanthroline have been proven to be bacteriostatic and bacteriocidal toward many Gram-positive bacteria but are relatively ineffective against Gram-negative organisms.

1,10-Phenanthroline is one of the most popular bidentate N,N´-chelating agent, so far used in the development of coordination chemistry of heterocyclic nitrogen donor ligands [45, 55, 69, 74, 174]. Its rigidity makes it an entropically better chelating molecule than 2,2´-bipyridine and has been exploited to make a variety of simple geometrically diverse complexes [48, 234]. In

addition to this versatile ligand, dicyanamide (dca), azide and nitrate anions have continued to receive much research attention because of their stability and coordination versatility in the assembly of multi-dimensional coordination polymers [188, 193, 194, 201]. Dicyanamide ligand can act as the uni-, bi-, or tridentate manner and both of its homo- and heteroleptic complexes have rich topologies and magnetic properties [201, 205]. On the other hand, the azide anion can coordinate to transition metals with different coordination modes ranging from monodentate to bridging bi-, tri- and tetradentate generating a wide variety of fascinating structures (discrete molecules to 3D arrays) and their promising applications in functional materials [58]. The nitrate anion can function as a bidentate, bridging, or monodentate ligand or as an ionic species in different complexes. The bonding type is probably a function of the nature and number of other ligands present [61].

The pharmacological efficiencies of metal complexes depend on the nature of the metal ions and the ligands because the metal ions present in the complexes accelerate the drug action and efficacy of organic therapeutic agents [129]. The interaction of metal ions with drugs administrated for therapeutic purposes is a subject of considerable interest [291]. The medicinal application of metal complexes is of great interest due to the increased antimicrobial resistance with the rapid increase in multidrug-resistant microbes [48, 180, 182]. Research work [55, 58, 61], in our laboratory has focused on the antibacterial and antifungal properties of mixed-ligand complexes containing 1,10-phenanthroline and co-ligands (2,2´-bipyridine, azide and nitrate anions). The high antimicrobial activity of 1,10-phenanthroline and the upsurge of infectious diseases in our country, Cameroon, caused by some bacterial and fungal strains has motivated this research work on the antimicrobial activities of Mn(II), Co(II) and Cu(II) complexes of 1,10-phenanthroline using dca, azide and nitrate as co-ligands.

1.11- Aim and Objectives

Our interest in the area of therapeutic agents, especially on metal-based drugs, is fuelled by the search for new and effective antimicrobial agents. The aim of this work, therefore, is to synthesise and characterise Mn(II), Co(II) and Cu(II) complexes of 1,10-phenanthroline and co-ligands (dicyanamide, azide, and nitrate) as potent antimicrobial agents against the resistant microbial pathogens.

The specific objectives of this work are:

- To synthesise Mn(II), Co(II) and Cu(II) complexes of 1,10-phenanthroline and co-ligands (dicyanamide, azide and nitrate anions).

- To elucidate structures of the metal complexes using physicochemical analytical methods: elemental analyses (C, H, and N), Fourier transform infrared spectroscopy (FTIR), Ultraviolet-visible spectroscopy (UV-vis), Solubility test, Conductivity measurements, Magnetic susceptibility measurement and Single crystal X-ray crystallography.
- To study the thermal properties (TGA and DTA) of the metal complexes
- To evaluate Powered XRD on the products of thermal decomposition.
- To investigate the antibacterial and antifungal properties of the complexes on a broad range of resistant strains of microorganisms isolated from patients.

CHAPTER 2
EXPERIMENTAL

In this chapter, we describe the methods used for the synthesis of the complexes, the different analytical techniques for their characterisations and the biological applications of the complexes as potential functional materials.

2.1- Chemicals

All the chemicals were of reagent grade and were used as such without further purification.

2.1.1- Ligands

The ligands used for this thesis are 1,10-phenanthroline monohydrate $C_{12}H_8N_2 \cdot H_2O$ (≥ 99 %), sodium dicyanamide NaC_2N_3 (≥ 97 %), and sodium azide NaN_3 (≥ 99.5 %) obtained from Sigma-Aldrich.

2.1.2- Metal salts

The metal salts used for this thesis are $Mn(NO_3)_2.4H_2O$ (99 %), $Co(NO_3)_2.6H_2O$ (98 %), and $Cu(NO_3)_2.3H_2O$ (98 %) obtained from Sigma-Aldrich and Fisher Scientific.

2.1.3- Solvents

All the used solvents were dried and distilled according to standard methods. The following solvents were used for this thesis: Methanol (99.8 %) and Ethanol (99.8 %) obtained from ProLabo while DMSO (≥ 99.5 %) and Acetone (≥ 99.8 %). They were obtained from Sigma-Aldrich and distilled water was obtained from the laboratory.

2.2- Synthesis

Generally, the complexes were synthesised following the procedure reported by Sado et *al,* 2016 [61] with slight modifications. The simple metal(II)/1,10-phen complex was prepared using 1:2 molar reactant ratio while the mixed metal(II)/1,10-phen/co-ligand complexes were prepared using 1:2:2 molar reactant ratios.

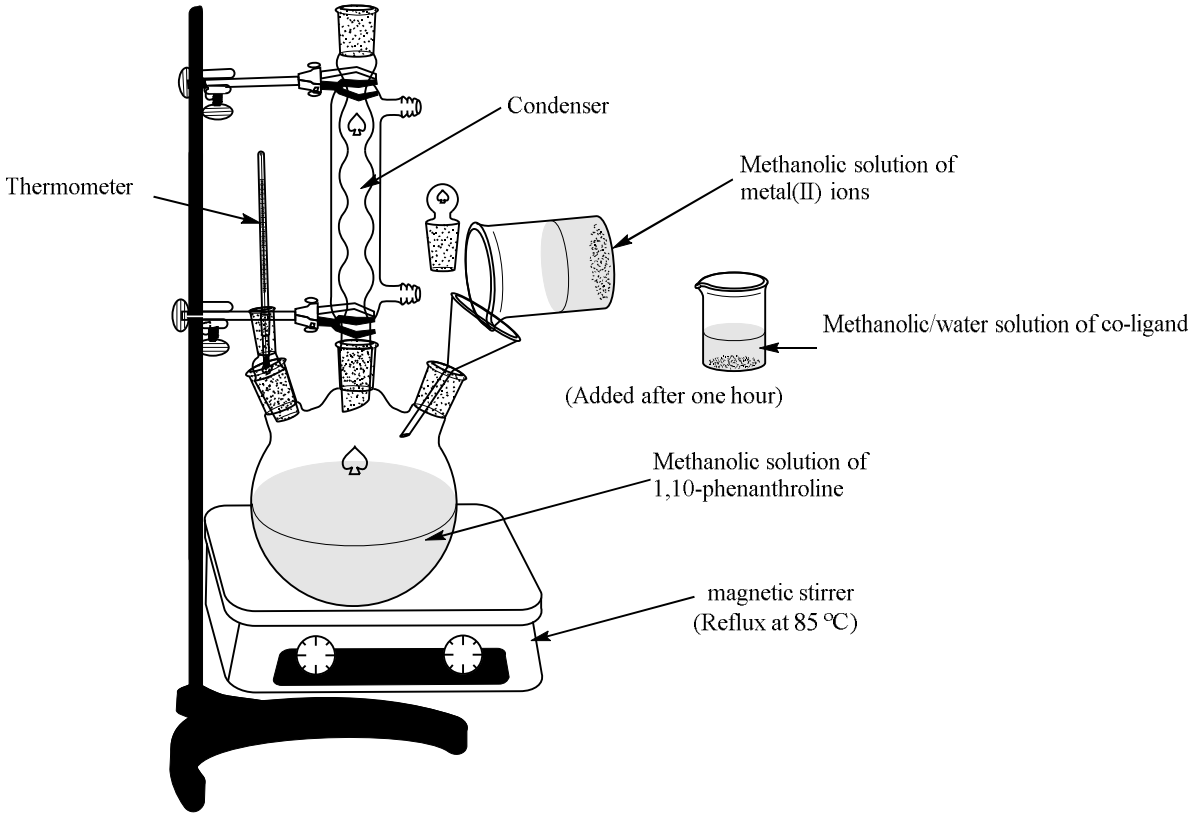

Figure 26: Experimental set-up for the synthesis of the complexes

2.2.1- Synthesis of $[Mn(Phen)_2(NO_3)_2]$ (1)

At room temperature, a solution of $Mn(NO_3)_2{\cdot}4H_2O$ (0.251 g, 1.0 mmol) in methanol (25 mL) was added dropwise to a solution of 1,10-phenanthroline (0.396 g, 2 mmol) in methanol (25 mL) with constant stirring and the reaction mixture was refluxed at 85 °C for 4 hours. The light yellow precipitate formed was filtered, washed with ethanol and dried over silica gel in a desicator. The volume of the filtrate was reduced to ca. 15 mL. At 25°C yellow crystals were obtained after two days (0.352 mg, 75 %).

2.2.2- Synthesis of $[Mn(Phen)_2(N_3)_2]$ (2)

At room temperature, a solution of $Mn(NO_3)_2{\cdot}4H_2O$ (0.251 g, 1.0 mmol) in methanol (25 mL) was added dropwise to a solution of 1,10-phenanthroline (0.396 g, 2 mmol) in methanol (25 mL) with constant stirring and the reaction mixture was refluxed at 85 °C for an hour. A solution of sodium azide (0.13 g, 2 mmol) in 10 mL water/methanol (1:4 v/v) was added dropwise to the reaction mixture and it was further refluxed for 3 h. The intense yellow precipitate formed was filtered, washed with ethanol and dried over silica gel in a desicator. The volume of the filtrate was reduced to ca. 15 mL. At 25°C yellow crystals were obtained after one day (0.525 mg, 80 %).

2.2.3- Synthesis of $[Mn(Phen)_2(dca)_2]$ (3)

At room temperature, a solution of $Mn(NO_3)_2 \cdot 4H_2O$ (0.251 g, 1.0 mmol) in methanol (25 mL) was added dropwise to a solution of 1,10-phenanthroline (0.396 g, 2 mmol) in methanol (25 mL) with constant stirring and the reaction mixture was refluxed at 85 °C for an hour. A solution of sodium dicyanamide (0.18 g, 2 mmol) in 10 mL water/methanol (1:4 v/v) was added dropwise to the reaction mixture and it was further refluxed for 3 h. The yellow precipitate formed was filtered, washed with ethanol and dried over silica gel in a desicator. The volume of the filtrate was reduced to ca. 15 mL. At 25°C light yellow crystals were obtained after one day (0.675 mg, 85 %).

2.2.4- Synthesis of $[Cu(phen)(BMCA)](NO_3)$; BMCA = bis(methoxycarbimido)aminato anion (4)

At room temperature, a solution of $Cu(NO_3)_2 \cdot 3H_2O$ (0.241 g, 1 mmol) in methanol (25 mL) was added dropwise to a solution of 1,10-phenanthroline (0.396 g, 2 mmol) in methanol (25 mL) with constant stirring and the reaction mixture was refluxed at 85°C for an hour. A solution of sodium dicyanamide (0.18 g, 2 mmol) in 10 mL water/methanol (1:4 v/v) was added dropwise to the reaction mixture and it was further refluxed for 3 h. The dark green precipitate formed was filtered, washed with methanol and dried over silica gel in a desiccator. The volume of the filtrate was reduced to ca. 10 mL. Violet-pink crystals (327 mg, 75 %) were obtained from this filtrate at 25°C after two weeks.

2.2.5- Synthesis of $[Co(phen)_2(NO_3)](dcg^-)\cdot(H_2O)$; dcg = dicyanoguanidinate anion (5)

At room temperature, a solution of $Co(NO_3)_2 \cdot 6H_2O$ (0.29 g, 1.0 mmol) in methanol (25 mL) was added dropwise to a solution of 1,10-phenanthroline (0.396 g, 2 mmol) in methanol (25 mL) with constant stirring and the reaction mixture was refluxed at 85°C for an hour. A solution of sodium dicyanamide (0.18 g, 2 mmol) in 10 mL water/methanol (1:4 v/v) was added dropwise to the reaction mixture and it was further refluxed for 3 h. The dark orange precipitate formed was filtered, washed with methanol and dried over silica gel in a desiccator. The volume of the filtrate was reduced to ca. 10 mL. At 25°C dark-orange crystals were obtained (533 mg, 80 %) after two weeks.

2.3- Characterisation

Elemental analysis (C, H, N) of the complexes were carried out on a FLASH 2000 Organic Elemental Analyzer in the Department of Chemistry of the University of Zululand, South Africa. The melting point temperatures of the complexes were obtained using the STUART Scientific Melting Point SMP1 Device with maximum temperature calibrated at 360 °C carried out in the Laboratory. The Fourier Transformed Infrared (FT-IR) spectra of the complexes and ligands were recorded from 4000-400 cm^{-1} on a PerkinElmer Spectrum Two universal attenuated total reflectance Fourier transform infrared (UATR-FT-IR) spectrometer calibration Department of Chemistry of the University of Zululand, South Africa. Thermogravimetric analysis (TGA) and differential scanning calorimetry (DSC) curves were obtained from the Laboratory of Applied Inorganic Chemistry, University of Yaounde I. Thermogravimetric analysis (TGA) and differential Thernmal Analysis (DTA) curves were obtained using a NETZSCH STA449F1 thermoanalyzer in a dynamic argon atmosphere (heating rate 10 °C·min^{-1}, flow rate 25 mL/min, aluminium oxide crucible, mass 20 mg, and a temperature range from room temperature up to 900 °C) at the Institute of Inorganic Chemistry, Faculty of Chemistry and Mineralogy, Universität Leipzig, Germany. Room temperature magnetic susceptibility measurements of the complexes were determined using the GOUY method with mercury tetrathiocyanocobalt(II) as calibrant on a Stanton Instruments Limited (Model A49). Powder XRD measurements were performed with a Stoe-StadiP powder diffractometer with a CuKα (1.540598 Å) X-ray source (0.5 °/step and 30 s/step (2 repetitions); tube power: 40 KV/40 mA; scan mode: Debye-Scherrer using a borosilicate glass capillary as sample holder during the measurement.

2.3.1- Melting Point Determination

The melting point of a material is the temperature at which it changes from a solid to a liquid state. Determining the melting point of a compound is a simple and fast method used specially to determine the purity of substances. The melting point temperatures of the complexes were obtained using the STUART Scientific Melting Point SMP1 Device with maximum temperature calibrated at 360 °C carried out in the Laboratory of Coordination Chemistry, University of Yaounde I. The samples were placed each in a capillary tube, and the capillary tube was then inserted into the melting point apparatus and heated to higher temperatures while observing through a magnifying lens for the temperature at which the compound will completely melt or decompose. Prior to use, the apparatus was calibrated with the aid of standards (Solophen: 191 °C; Saccharine: 228 °C; Dicyandiamide: 210 °C).

2.3.2- Microanalysis

The microanalysis for CHN helps us to ascertain the empirical percentage composition of each element in the complexes. Elemental analysis (C, H, N) of the complexes was carried out on a FLASH 2000 Organic Elemental Analyzer in the Department of Chemistry of the Faculty of Science and Agriculture, University of Zululand, South Africa. The samples were placed each in a tin container and dropped into a furnace at 1000 °C. The samples decomposed releasing carbon monoxide, water vapour and nitrogen dioxide with the release of oxygen gas from the furnace. The amount of each element in the sample was determined by gas chromatography. The metal content in each sample was estimated by complexometric titration using EDTA solution [292].

- **Estimation of the Metal Contents of the Complexes**

The metal content of the complexes was estimated by complexometric titrations using EDTA solution.

- ***Preparation of the samples***

The solutions of the complexes and metal oxide for metal content analyses were prepared by dissolving 0.1 g of each sample in a mixture of 2 mL of concentrated sulphuric acid and 3 mL water. The solution obtained was heated until the characteristic colour of the metal ion in the aqueous medium is obtained. The solution was then cooled at room temperature, transferred completely into a 50 mL standard volumetric flask and the volume made up to the mark with distilled water.

- ***Preparation of EDTA solution (0.01M)***

The hydrated sodium salt of ethylenediaminetetraacetic acid ($Na_2EDTA.H_2O$) was dried for one hour in an oven at 110 °C and cooled in a desiccator under vacuum. A mass of 3.724 g of the salt was dissolved in a small beaker and transferred completely into a 1000 mL standard volumetric (Erlenmeyer) flask, and the volume made up to the mark with distilled water. The EDTA solution was standardised using the primary standard of 0.01M zinc sulphate solution as shown in equation (2.1).

$$H_2Y^{2-} + Zn^{2+} \longrightarrow ZnY^{2-} + 2H^{+} \qquad (2.1)$$

For each complex, 10 mL solution of the complex was pipetted and introduced into an Erlenmeyer flask. 3 drops of murexide were added as an indicator. The resulting solution was

then titrated against EDTA. The endpoint was indicated with a colour change, for example, the cobalt complex changes from violet to blue colouration.

2.3.3- Solubility Tests

The solubility of the complexes was evaluated qualitatively in nine different solvents. The solubility of the compounds was determined in three non-polar solvents, (Toluene, Hexane and Chloroform); three polar aprotic solvents (Acetone, DMF and DMSO) and three polar protic solvents (MeOH, EtOH, and Water). To determine solubility in g/100 mL, 0.01 g of the complex was dissolved in 3 mL of solvent and then stirred magnetically for 5 minutes at room temperature.

2.3.4- Conductance Measurements

The conductance measurements were carried out in order to determine, with the help of literature if the complexes are molecular (non-electrolyte) or ionic (electrolyte).

Conductivity measurements for the complexes were carried out in dimethylsulfoxide (DMSO) using the Tacussel conductometer, model CD810 at room temperature. Solutions of the complexes were prepared by dissolving 0.001 g of each sample in 30 mL of DMSO and the solution left to equilibrate at room temperature for 15 minutes before measuring their conductivities.

2.3.5- Infrared (IR) Spectroscopy

Infrared spectroscopy is an extremely powerful technique for both qualitative and quantitative analysis and the spectrum of any substance is interpreted by the use of known group frequencies [134]. The Fourier Transformed Infrared (FT-IR) spectra of the complexes and ligands were recorded from 4000-400 cm^{-1} on a PerkinElmer Spectrum Two universal attenuated total reflectance Fourier transform infrared (UATR-FT-IR) spectrometer calibration Department of Chemistry of the University of Zululand, South Africa.

2.3.6- Electronic Absorption Spectra

The spectra of transition metal complexes depend on the transition of unpaired electrons from the ground state to an excited state. The electronic spectra were recorded on a Perkin–Elmer Lambda-25 UV–Visible spectrometer of the Laboratory of Applied Inorganic Chemistry, University of Yaounde I.

The samples were each dissolved in dimethylsulfoxide (DMSO) and placed in a quartz cuvette (1 cm) optical on two sides. The cuvette was placed in the sample holder of the spectrometer

and spectrum recorded on the monitor.

2.3.7- Thermal Analysis

Thermogravimetric Analysis (TGA) provides a quantitative measurement of weight change versus temperature. Typically, TGA is used to investigate the thermal stability and compositional analysis of materials. TGA can record directly the weight change as a function of temperature or time for transitions that involve dehydration or decomposition. Thermogravimetric analysis (TGA) and differential scanning calorimetry (DSC) curves were obtained from the Laboratory of Applied Inorganic Chemistry, University of Yaounde I. Thermogravimetric analysis (TGA) and differential Thermal Analysis (DTA) curves were obtained using a NETZSCH STA449F1 thermoanalyzer in a dynamic argon atmosphere (heating rate 10 °C·min^{-1}, flow rate 25 mL/min, aluminium oxide crucible, mass 20 mg, and a temperature range from room temperature up to 900 °C) from the Institute of Inorganic Chemistry, Faculty of Chemistry and Mineralogy, Universität Leipzig, Germany.

The sample was placed each in a crucible and put in the furnace on a quartz beam which is attached to the automatic recording balance. Any change in the weight of the sample causes the deflection of the beam which is sensed by photodiodes. When the beam is restored to the original position, the balance detects the current which is sent from the photodiodes. The current is proportional to the change of weight of the sample.

2.3.8- Magnetic Susceptibility Measurements

The measurement of the magnetic moment is one of the useful methods available to the coordination chemists for studying the electronic structure of a transition metal complex. Room temperature magnetic susceptibility measurements of the complexes were determined using the GOUY method with mercury tetrathiocyanocobalt(II) as calibrant on a Stanton Instruments Limited (Model A49) in the Department of Chemistry of the Faculty of Science and Agriculture, University of Zululand, South Africa. The magnetic measurements were performed at a temperature range of 5-300 K using a Sherwood Scientific magnetic susceptibility balance. The magnetic data of the samples were obtained by taking the difference in mass between an empty sample tube and the sample tube filled with a sample which is in the form of a reasonable fine and uniform powder. The diamagnetic corrections for the samples were estimated using Pascal's constant and the magnetic data were corrected for diamagnetic contributions using a sample holder.

The mass susceptibility; χ_g, is calculated using equation (2.3).

$$\chi_g = \frac{C_{Bal} l (R - R_o)}{10^9 m} \qquad (2.3)$$

where: l = sample length (cm)
m = sample mass (g)
R = reading for tube plus sample
Ro = empty tube reading
C_{Bal} = balance calibration constant
χ_g = mass susceptibility

2.3.9- Test for Nitrate ions

A common nitrate test, known as the brown ring test was performed by adding iron(II) sulphate to the solution, then slowly adding concentrated sulphuric acid and watching for a brown ring on the test tube, which will indicate the presence of the nitrate ion. For the preparation of the solution, 0.01 g each of the sample was dissolved in 30ml of water in a 100 mL beaker. Note that the presence of nitrite ions will interfere with this test.

2.3.10- Crystal Structure Determination

This is a versatile, non-destructive method which reveals detailed information about the chemical composition, crystallographic and microstructure of materials. The X-ray crystallography is the most powerful and unambiguous method for the determination of the structure of crystalline materials [293]. The single crystal X-ray Measurements were carried out at the Institute of Technology, Madras, Chennai, India; Department of Chemistry and Biochemistry Baylor University, USA; and Institute of Inorganic Chemistry, Faculty of Chemistry and Mineralogy, Universität Leipzig, Germany. Suitable single crystals of the complexes $[Mn(Phen)_2(NO_3)_2]$ (yellow crystal, 0.300 x 0.250 x 0.250 mm^3), $[Mn(Phen)_2(N_3)_2]$ (dark yellow crystal, 0.25 x 0.25 x 0.20 mm^3), $[Mn(Phen)_2(dca)_2]$ (light yellow crystal, 0.170 x 0.157 x 0.129 mm^3), $[Cu(Phen)dca\text{-}(OMe_2)]\cdot NO_3$ (pink crystal, 0.20 × 0.10 × 0.01 mm^3) and $[Co(Phen)_2(NO_3)]\cdot(H_2O)(dcg)$ (dark-orange crystal, 0.35 x 0.30 x 0.20 mm^3), coated with dry perfluoropolyether were mounted, each at a time, on glass fibres and fixed to the goniometer head in cold nitrogen stream (T = 173(2) K). Data collection was performed on a Bruker-Nonius X8APEX-CCD diffractometer using monochromatic radiation λ(Mo-Kα1) = 0.71073 Å, by means of ω and ϕ scans of width 0.30 and exposure time of 10 s per frame in the range $6.0 < 2\theta < 60.96$ with a detector distance of 37.5 mm.

For the complex $[Mn(Phen)_2(NO_3)_2]$, out of the 12,206 measured reflections, the final cell parameters were obtained by full-matrix least-squares techniques [294] on 2,957 observed unique reflections (Rint = 0.0264), and 168 refined parameters with final R1 = 0.0580 for reflections with I > 2α (I) and ωR2 = 0.1867 for all data. For the complex $[Mn(Phen)_2(N_3)_2]$, out of the 22,275 measured reflections, the final cell parameters were obtained by full matrix least-squares techniques on 2,029 observed unique reflections (Rint = 0.041) and 159 refined parameters with final R1 = 0.077 and for reflections with I > 2α (I) and ωR2 = 0.179 for the compound. In the case of the complex $[Mn(Phen)_2(dca)_2]$, out of the 54,213 measured reflections, the final cell parameters were obtained by full matrix least-squares techniques on 6160 observed unique reflections (Rint = 0.0564) and 352 refined parameters with final R1 = 0.0364 for reflections with I > 2α (I) and ωR2 = 0.0850 for the compound. For the complex $[Cu(Phen)dca\text{-}(OMe)_2]\cdot NO_3$, out of the 8594 measured reflections, the final cell parameters were obtained by full matrix least-squares techniques on 2366 observed unique reflections (Rint = 0.051) and 178 refined parameters with final R1 = 0.712 and for reflections with I > 2α (I) and ωR2 = 0.087 for the compound. For the complex $[Co(Phen)_2(NO_3)]\cdot(H_2O)(dcg)$, out of the 14,308 measured reflections, the final cell parameters were obtained by full matrix least-squares techniques on 6,751 observed unique reflections (Rint = 0.0253) and 400 refined parameters with final R1 = 0.0392 and for reflections with I > 2α (I) and ωR2 = 0.0941 for the compound.

X-ray data were collected with a GEMINI CCD diffractometer (Rigaku Inc.), λ(Mo-K_α) = 0.71073 Å, T=130(2) K, empirical absorption corrections with SCALE3 ABSPACK [295]. All structures were solved by dual space methods with SIR-92 [296]. Structure refinement was done with SHELXL-2016 [297, 298] by using full-matrix least-square routines against F^2. All hydrogen atoms were calculated on idealised positions. The pictures were generated with the program Mercury [299].

2.3.11- Powder X-Ray Diffraction (XRD) Spectroscopy

The powder X-ray diffraction was performed to obtain the degree of crystallinity, crystalline lattice spacing and magnetite phase purity of the decomposed products after thermal analysis. The XRD diffractograms were recorded on a Bruker D8 Advance X-ray diffractometer using a Cu Kα radiation source (λ = 0.15406 nm, 40 kV and 40 mA) at the Institute of Inorganic Chemistry, Faculty of Chemistry and Mineralogy, Universität Leipzig, Germany. Scans were taken over the 2θ range from 10° to 100° in steps of 0.01° at room temperature in open quartz sample holders. The phases were identified with the help of the Bruker DIFFRAC plus evaluation software in combination with the ICDD powder diffraction database (International

Centre for Diffraction Data).

2.3.12- Theoretical Calculations

Calculations were performed on the complexes to gain further insights into the molecular interactions in the synthesized compounds and to predict some of their electronic properties. The calculations were performed using the DFT method and the exchange-correlation functional [300] were approximated by the Becke three parameter exchange functionals [301, 302] and the Lee-Yan-Parr correlation functional [303]. The molecular orbitals of the studied molecules were described by a Pople double split valence orbitals basis set 6-31G [304] as implemented in the Gaussian 03, Revision A1 package [305]. This basis set has been polarized for all atoms to improve the flexibility of molecular orbitals [306]. The geometries obtained from the crystal structures were used as the starting point for the optimization. The optimized geometries were subjected to frequency calculations to verify that they represent energy minima. The non-covalent interactions (NCI) such as hydrogen bond and van der Waals interactions were described by two theories based on the electron distribution in the molecular system: the Bader and collaborators approach known as quantum theory of atom in molecules (QTAIM) [307] and the Contreras-Garcia and collaborators approach referred to as non-covalent interactions index [308, 309]. The multiwfn software [310] was used for this purpose.

2.3.13- Antimicrobial Studies

The antimicrobial tests were carried out in the Applied Microbiology and Molecular Pharmacology Laboratory (LMP) of the University of Yaoundé I, Cameroon. The tests were done on twenty four pathogenic micro-organisms; twenty bacterial strains: B1 = *Streptococcus pneumonae* ATCC49619; B2 = *Staphylococcus aureus* BAA917; B3 = *Staphylococcus aureus* ATCC43300; B4 = *Staphylococcus aureus* NR45003; B5 = *Staphylococcus aureus* NR46003; B6 = *Staphylococcus aureus* CP7625; B7 = *Shigella flexneri* NR518; B8 = *Salmonella enterica* NR4294; B9 = *Salmonella enterica* NR4311; B10 = *Salmonella enterica* NR13555; B11 = *Pseudomonas aeruginosa* NMC592; B12 = *Klessiella pneumonae* ATCC13883; B13 = *Klessiella pneumonae* ATCC70603; B14 = *Klessiella pneumonae* NR41916; B15 = *Escherishia coli* ATCC25922; B16 = *Escherishia coli* ATCC35218; B17 = *Enterococcus fecalis* ATCC51219; B18 = *Staphylococcus aureus* NR46374; B19 = *Hemophyllus influenza* ATCC49247; B20 = *Mycobacterium smegmatis* and four yeasts: *Candida krusei*, *Candida parasilosis*, *Candida albicans*, *Cryptococcus neoformans* obtained from Centre Pasteur Yaoundé, Cameroon.. The selected microorganisms represent the causative agents for diseases that are prevalent in our environment.

The microbial isolates were maintained on agar slant at 4 °C in the laboratory. The strains were sub-cultured on a fresh appropriate agar plate in incubators 18 hours prior to any antimicrobial test.

2.3.13.1- Sensitivity Test

The ligands, metal salts and the complexes were diluted in sterilized distilled water at 100 mg/mL and 1 mg of each test compound was placed on a sterilized filter paper disc and allowed to dry. The reference antibiotics (RB) amoxicillin, ciprofloxacin and cloxacillin and the reference antifungal (RF) drug fluconazole were also prepared in the same manner and 10 µg placed on a sterilized filter paper disc and dried, prior to testing.

2.3.13.2- Diffusion Tests

In vitro antimicrobial activity of the ligand, metal salts and complexes were evaluated using the disc-diffusion method. Mueller-Hinton (MH) agar was employed as the microbial growth medium. The antimicrobial tests were carried out as described by Berghe and Vlietinck [311] using a cell suspension of about 1.5 x 10^6 CFU/mL obtained from the McFarland Turbidity standard No. 0.5. MH agar was poured (to a height of 8 mm) into sterile 9 cm diameter Petri dishes and allowed to solidify. The solid MH agar was inoculated with bacteria strains using a platinum wire loop which had been previously sterilized by heating it red hot in a flame, cooled and then used for the application. The dishes were allowed to dry for ten minutes at 37 °C in an incubator. Sterilised forceps were used for the application of the paper discs containing the test compounds on previously inoculated MH agar dishes, with that of the RB or RF placed at the centre. The plates were kept for 30 minutes at ambient temperature to allow for pre-diffusion, and then incubated at 37 °C for 24 hours. A plate containing only the agar was also kept in the incubator to determine whether contaminants were present. Antimicrobial activity was evaluated by measuring the diameter of the growth inhibition zone (IZ) in mm around the discs. Three replicas were performed for each sample and mean values of the growth inhibition zone were calculated. Compounds with a zone of inhibition IZ < 7 mm were considered to be inactive, those in the range 7 < IZ < 20 mm as active and those with IZ > 20 mm, very active.

2.3.13.3- The Minimum Inhibitory Concentration (MIC) of the Complexes

The Minimum Inhibitory Concentration (MIC) was determined according to National Committee for Clinical Laboratory Standards (NCCLS) M38 [312, 313], a microdilution method using (12 x 8 wells) microtitre plates. This method was applied to compounds that demonstrated high activity against microorganisms using the disc diffusion method. In the well

of the first line (line 1), 100 µL of culture medium Mueller Hinton Broth (Mast Group Ltd) was introduced and 100 µL in the remaining wells of the plates. This was followed by 100 µL of the stock solution of the compounds at 2 mg/mL to the first well. The medium and sample in the first well were mixed thoroughly before transferring 100 µL of the resultant mixture to the well of the second line. Then two-fold serial dilutions of the test samples were made from line 1 until line 11 and 20 µL of inoculum standardized at 0.5 McFarland standards were introduced in the entire well containing the test substances except for the columns of blank (Column C and F) which constitute the sterility control. The concentration range was 0.00488 to 5 mg/mL for compounds. In each microtiter plate, a column with broad-spectrum with the reference antibiotic (RB); amoxicillin, ciprofloxacin, and cloxacillin while the reference antifungals (RF); fluconazole and cloxacillin with the concentration range from 0.00195 mg/mL to 2 mg/mL were used as positive control. After incubating at 37 °C for 24 hours for bacteria and 48 hours for yeasts, turbidity was observed; an indication of growth. Thus, the lowest concentration inhibiting the growth of microorganisms was considered as the Minimum Inhibitory Concentration (MIC).

CHAPTER 3
RESULTS AND DISCUSSION

3.1- Synthesis of the Complexes

The complexes were obtained in stoichiometric reaction ratio 1:2:2 of the metal(II) salt, 1,10-phenanthroline and co-ligand respectively, in a methanol/H_2O mixture at 85 °C. The obtained complexes; $[Mn(Phen)_2(NO_3)_2]$ (**1**), $[Mn(Phen)_2(N_3)_2]$ (**2**), $[Mn(Phen)_2(dca)_2]$ (**3**), $[Cu(phen)(BMCA)](NO_3)$ (**4**); BMCA = bis(methoxycarbimido)aminato anion and $[Co(phen)_2(NO_3)](dcg^-)\cdot(H_2O)$ (**5**); dcg = dicyanoguanidinate anion have been fully characterised. A transformation of the dicyanamide anion in **4** and **5** to bis(methoxycarbimido)aminate anion (BMCA) or dicyanoguanidinate anion (dcg) respectively was observed during the reaction (Scheme 7).

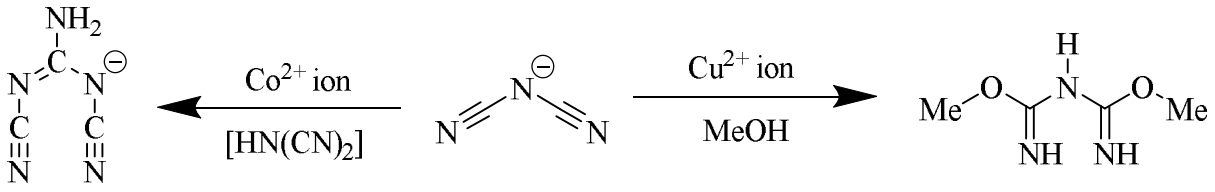

dcg Hdca dca BMCA

Scheme 7: Transformation of dca to BMCA and dcg

3.2- Physical Properties of the Complexes

Table II: Physical properties of the complexes

Complex	Nature	Colour	% Yield	Molar mass (g/mol)	Melting point / °C
$[Mn(phen)_2(NO_3)_2]$ (1)	Crystals	Yellow	75	539.37	356 ± 2
$[Mn(phen)_2(N_3)_2]$ (2)	Crystals	Intense yellow	80	499.41	/
$[Mn(phen)_2(dca)_2]$ (3)	Crystals	Light yellow	85	547.45	290 ± 2
$[Cu(phen)(BMCA)](NO_3)$ (4)	Crystals	Pink	70	435.89	202 ± 2
$[Co(phen)_2(NO_3)](\boldsymbol{dcg})\cdot(H_2O)$ (5)	Crystals	Dark orange	82	607.46	296 ± 2

The complexes **1-5** were precipitated from solution relatively quickly without solvent evaporation. All the complexes are crystalline, coloured, air-stable, non-hydroscopic as compared to the starting materials and they can be reproducibly prepared in high yields (>70 %). Their physical properties are summarised in Table II. The melting points of the complexes range from 202-360 °C. Complex **1** melted at (356 ± 2 °C) while the melting point of complex **2** could not be determined due to the explosive nature of the azido ligand. Complex **3** changed in colour upon heating from yellow to dark orange and then melted at (290 ± 2°C). Complex **4**

had a sharp melting point (202 ± 2 ºC) while complex **5** also changed in colour upon heating from dark-orange to brown and then melted at (296 ± 2 ºC). The sharp melting points of the complexes indicate their degree of purity. The change in colour of the complexes **3** and **5** with the increase in temperature could be attributed to a change in crystal structurally geometry from octahedral to tetrahedral as the complexes decompose [314, 315].

3.3- Elemental Analysis

Table III: The elemental analytical data of the complexes

Complex	**Elemental analysis: Found (Calc.)**			
	% Carbon	% Hydrogen	% Nitrogen	% Metal
1	51.88 (53.45)	2.50 (2.99)	15.57 (15.58)	10.19 (10.25)
2	56.65 (57.72)	3.03 (3.23)	29.01 (28.05)	11.51 (11.00)
3	62.29 (61.43)	2.33 (2.95)	25.92 (25.59)	9.46 (10.04)
4	44.39 (44.09)	3.85 (3.70)	19.59 (19.28)	14.58 (14.58)
5	52.60 (53.39)	3.92 (3.32)	22.67 (23.06)	9.81 (9.70)

The elemental analytical data of the complexes presented in Table III shows that the experimental values are generally in agreement with the theoretical values and to a larger extend, demonstrate the degree of purity of the complexes.

The metal content for each of the complexes were obtained by complexometric titration using EDTA [292].

3.4- Solubility Studies

Table IV: Solubility Tests of the Complexes in Different Solvents

Complex	Water ε = 78.3	Methanol ε = 32.7	Ethanol ε = 24.3	DMSO ε = 47.0	DCM ε = 9.1	THF ε = 7.6	Chloroform ε = 4.8	Hexane ε = 1.9
1	+	-	-	+	+	+	-	-
2	+	-	-	+	+	+	-	-
3	+	-	-	+	+	+	-	-
4	-	-	-	+	±	±	-	-
5	-	-	-	+	±	±	-	-

(+) Soluble (-) Insoluble (±) Sparingly soluble

Solubility, which is often said to be one of the "characteristic properties of a substance," [316] was studied qualitatively in eight different solvents; three polar protic solvents; water (**ε = 78.3**), methanol (**ε = 32.7**), and ethanol (**ε = 24.3**); three polar aprotic solvents; dimethyl sulphoxide

(**ε = 47.0**), dichloromethane (**ε = 9.1**), tetrahydrofuran (**ε = 7.6**); and two nonpolar solvents; chloroform (**ε = 4.8**) hexane (**ε = 1.9**).. The results are presented in Table IV reveals that the manganese(II) complexes (**1-3**) are found to be soluble in water, dimethyl sulfoxide (DMSO), tetrahydrofuran (THF) and dichloromethane (DCM) while the copper(II) and cobalt(II) complexes are soluble only in DMSO. The solubility of the metal compounds in DMSO was of great toxicological importance because it is one of the major factors influencing the availability and absorption of the metals [317].

3.5- Molar Conductance Measurement

Table V: Molar Conductance Data of the Complexes

Complex	Mass of sample (mg)	Molar mass ($gmol^{-1}$)	Conc. ($molL^{-1}$)	Molar Conductance ($\Omega^{-1}cm^2\ mol^{-1}$)	No. of ions
1	16	539.37	$1x10^{-3}$	11.18	0
2	15	499.41	$1x10^{-3}$	8.86	0
3	16	547.45	$1x10^{-3}$	6.54	0
4	13	435.89	$1x10^{-3}$	83.25	2
5	18	607.46	$1x10^{-3}$	82.50	2

The molar conductivity of the complexes measured at room temperature in DMSO at 10^{-3} M concentration are summarised in Table V. The molar conductivity value of each of the complexes was calculated using equation (2.2) as illustrated in section 2.3.4. The values were compared with literature to determine the type of electrolyte and the number of ions present in solution for each of the complexes. Complexes with molar conductance values, in DMSO at room temperature in the range (80-115) $\Omega^{-1}cm^2\ mol^{-1}$ are 1:1 electrolytes; (160-220) $\Omega^{-1}cm^2\ mol^{-1}$ are 2:1 electrolytes and (290-350) are 3:1 electrolytes [318]. The molar conductance values of complexes **1-3** are in the range (6.54-11.18) $\Omega^{-1}cm^2\ mol^{-1}$ indicating a non-ionic nature and are therefore considered as molecular complexes [318]. For complexes **4** and **5**, the molar conductance values are 83.25 $\Omega^{-1}cm^2\ mol^{-1}$ and 82.50 $\Omega^{-1}cm^2\ mol^{-1}$, respectively, indicating that they are both 1:1 electrolytes (two ions present) [318]. This is in agreement with the structures obtained by single crystal X-ray crystallography.

3.6- Infrared Spectroscopy

The most relevant absorption bands in the IR spectra of the ligands and the complexes (Figures 30-34) are summarised in Table VI. In the spectrum of the phen ligand, the absorption bands at

1586 and 1501 cm^{-1} assigned to $\nu_{(C=N)}$ and $\nu_{(C=C)}$ stretching vibrations respectively, are shifted in the complexes to 1580 and 1521 cm^{-1} for **1**, 1580 and 1514 cm^{-1} for **2**, 1580 and 1514 cm^{-1} for **3**, 1600 and 1520 cm^{-1} for **4**, and 1666 and 1514 cm^{-1} for **5**. These shifts indicate the participation of the C=N of phen in bonding [58, 61]. The weak band observed at 1751 cm^{-1} in **1** (Fig. 30) shows the coordination of a monodentate nitrate ion, Mn-NO_3 [319]. The vibrational bands at 3050-3075 cm^{-1} that occurred in all the complexes can be assigned to Csp^2-H stretching vibrations of the phen ligand [144].

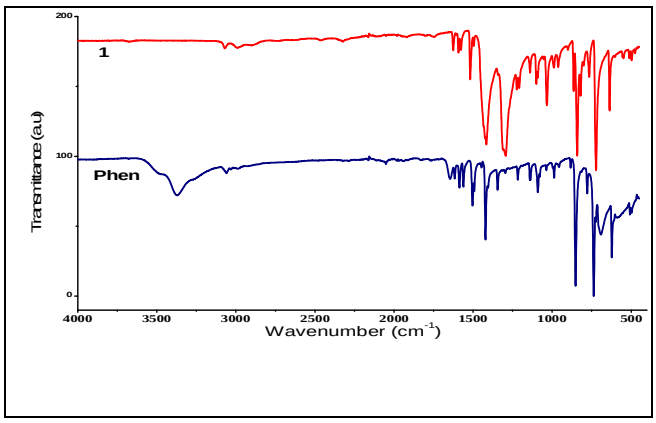

Figure 27: IR spectra of **1** and phen ligand

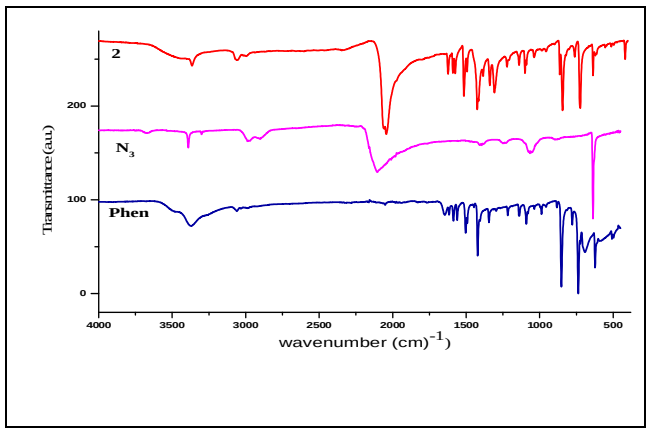

Figure 28: IR spectra of **2**, azido (N_3) and phen ligands

The strong absorption band at 2105 cm^{-1} in the spectrum of the azido ligand (Fig. 31), assigned to the asymmetric stretching vibration $\nu_{as(N_3)}$ is shifted to 2040 cm^{-1} in **2**, indicating terminal coordination of the azido ligand to the metal ion [58, 61].

The characteristic stretching vibration bands of dca (Fig. 32) are observed in the range of 2300–2100 cm^{-1}, which corresponds to the $\nu_s + \nu_{as(C\equiv N)}$ 2285 cm^{-1}, $\nu_{as(C\equiv N)}$ 2229 cm^{-1} and $\nu_{s(C\equiv N)}$ 2179 cm^{-1} [14, 191, 192, 320, 321]. In **3**, the characteristic absorption bands of dca are shifted to higher wavelengths; $\nu_s + \nu_{as(C\equiv N)}$ 2279 cm^{-1}, $\nu_{as(C\equiv N)}$ 2209 cm^{-1} and $\nu_{s(C\equiv N)}$ 2154 cm^{-1}. The shift towards higher wavelengths of these peaks, when compared with those of the free dca in its sodium salt, is consistent with terminal coordination of the ligand [320, 321].

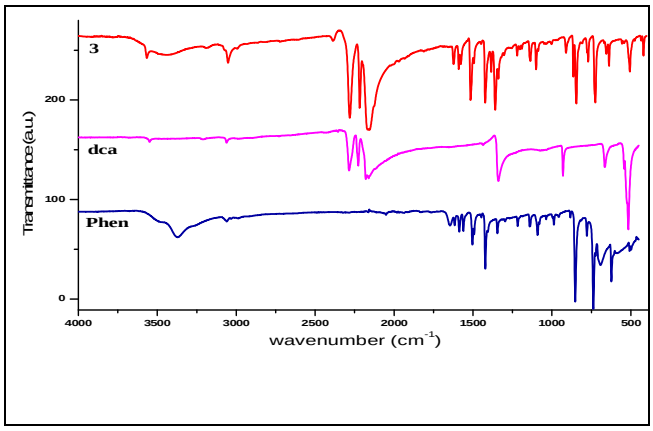

Figure 29: IR spectra of 3, dicyanamido (dca) and phen ligands

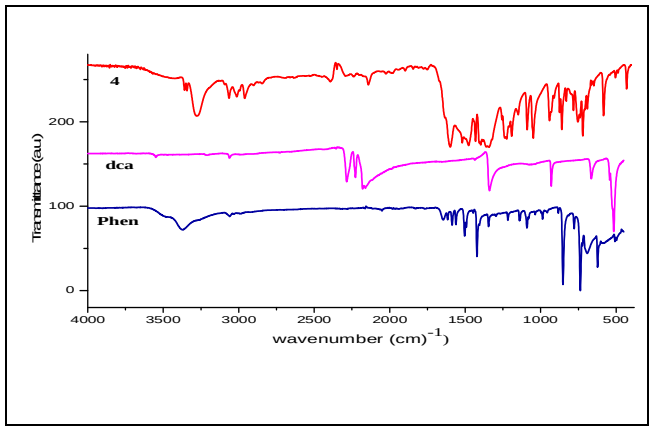

Figure 30: IR spectra of **4**, dicyanamido (dca) and phen ligands

In **4**, the very strong bands (Fig. 33) with maxima at 1600 cm^{-1} and at 1362 cm^{-1} are assigned to the $\nu_{(C=N)}$ and $\nu_{(C–N)}$ vibrations respectively. The appearance of the $\nu_{(N–H)}$ at 3275 cm^{-1} is an indication of the transformation of dca ligand [208]. The appearance of the $\nu(Csp^3–H)$ stretching and $\nu_{(C–O)}$ alkoxy vibrations at 2958 cm^{-1} and 1085 cm^{-1}, respectively, indicates the addition of methanol to dca [208]. Characteristic nitrile bands (C≡N) due to dca expected at 2173 and 2229 cm^{-1} were not observed in the spectrum. On the contrary, the characteristic C-O-CH_3 stretch at about 1200 cm^{-1} and a C-H symmetrical deformation vibration at about 1400 cm^{-1} were observed [206]. This observation is consistent with the crystal structure of the complex showing a transformation of the dca anion to bis(methoxycarbimido)aminate anion (BMCA).

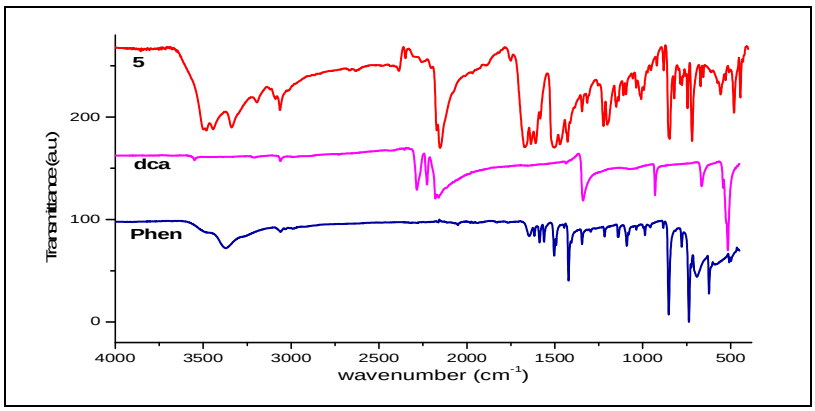

Figure 31: IR spectra of **5**, dicyanamido (dca) and phen ligands

In **5** (Fig. 34), the band at 2147 cm^{-1} and the small shoulder at 2178 cm^{-1} are the characteristic bands of dicyanoguanidinate (dcg) anion assigned to ν(C≡N) vibrations which are observed in the spectrum of dcg anion at 2138 and 2160 cm^{-1} [209]. The twin bands at 3440 and 3492 cm^{-1} assigned to the $\nu(NH_2)$ and the band at 3196 cm^{-1} assigned to the $\nu_{(N-H)}$ both from the amino

group of dcg anion indicates that the lone pairs on these N-atoms are not involved in bonding. This suggests that the N,N'-dicyanoguanidinate ($(H_2N)C(NCN)_2$) anion is present as a counter ion [209]. The new band at 1758 cm^{-1} is assigned to the ν(N-O) vibration for the nitrato ligand [209, 319]. The broad and diffuse band at about 3500 cm^{-1} is assigned to ν(O-H) vibration of a lattice water molecule.

The new bands at 512-557 cm^{-1} in all the complexes can be attributed to ν(M–N) stretching while the new bands observed in the low frequency region at 472 for **1** and 445 cm^{-1} for **5**, may be attributed to ν(M–O) [322]. These bands are possibly due to the bond between the metal ion and the nitrogen of phen and dca, and oxygen of nitrate ion.

Table VI: Relevant IR absorption bands (cm^{-1}) of the ligands and their metal complexes

Compound	$\nu_{(C=N)}$	$\nu_{(C=C)}$	$\nu_{(C\equiv N)}$	$\nu_{(C-N)}$	$\nu_{(O-H)}$	$\nu_{(N-H)}$	$\nu_{(N-H2)}$	$\nu_{(N-O)}$	$\nu_{(C-O)}$	γ(C-H) sp2 bend	γ(C-H) sp2 stretch	γ(C-H) sp3 stretch	$\nu_{(N=N=N)}$	$\nu_{(M-N)}$	$\nu_{(M-O)}$
N_3													2105vs		
dca			2285vs 2229s 2173vs	1336vs											
Phen	1586s	1501vs		1250s	3373s					854vs 738vs	3057s				
1	1580s	1521s						1751		846vs 728vs	3075			550m	472m
2	1580s	1514vs			/					848vs 722vs	3057s		2105vs	551m	
3	1580s	1514vs	2279vs 2209s 2173vs	1336vs						848vs 722vs	3050s			551m	
4	1600vs	1520s	2140s	1362		3275vs		1751	1046vs 1085vs	848s 722vs	3064s 3017s	2958s		512m	
5	1666vs	1514vs	2147vs 2178s		3334s	3196m	3492vs 3440vs	1758		848vs 722vs	3196m 3064s			551s	445s

br=broad, s=strong, vs=very strong, m=medium, w=weak.

3.7- Electronic Absorption Spectra

The significant electronic absorption bands in the spectra of the complexes shown in Figures 35-39 are summarised in Table VII.

Table VII: Significant absorption bands in the spectra of the complexes

Complex	Absorption Maxima		Band Assignment
	Wavelength nm	Wavenumber cm^{-1}	
1	340	29411	$\pi \rightarrow \pi^*$ and n-π^*
2	325	30769	$\pi \rightarrow \pi^*$
	347	28818	n-π^*
3	300	33333	$\pi \rightarrow \pi^*$
	325	30769	n-π^*
4	380	26385	$\pi \rightarrow \pi^*$ and $n \rightarrow \pi^*$
	437	22883	$^2B_{2g} \rightarrow {}^2B_{1g}$
5	360	27700	$\pi \rightarrow \pi^*$ and $n \rightarrow \pi^*$
	501	19960	$^4T_{1g} \rightarrow {}^4T_{2g}$

The Mn(II) high spin complexes are weakly coloured due to spin forbidden d-d transition (laporte forbidden). As a result of the spin forbidden d-d transition, the bands at the visible regions are not defined but rather submerged at the ultraviolet region depicting the strong intra-ligand transitions or charge transfer bands. The UV absorption spectra of **1-3** reveal bands in the region 300-350 nm (34000-29000 cm^{-1}) attributed to the ligand field ($\pi \rightarrow \pi^*$ and $n \rightarrow \pi^*$ transitions) and charge transfer (d-π^* transitions) due to the migration of electrons from the ligand orbitals to metal orbitals [323]. This is consistent with d^5 high spin Mn(II) configuration with an ^6S ground term for octahedral geometry [55, 324].

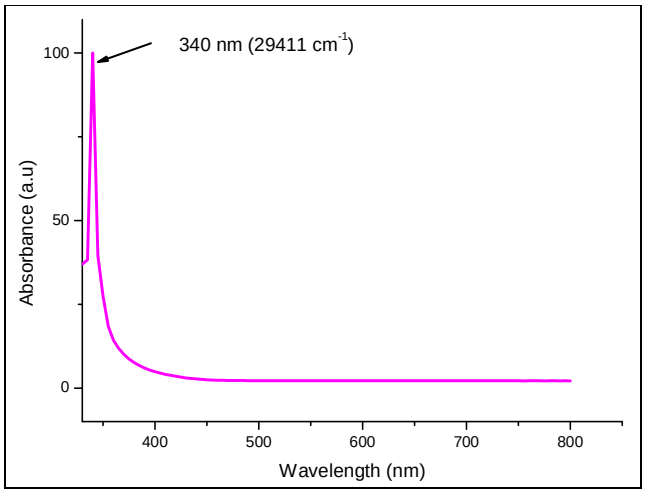

Figure 32: UV spectrum of **1**

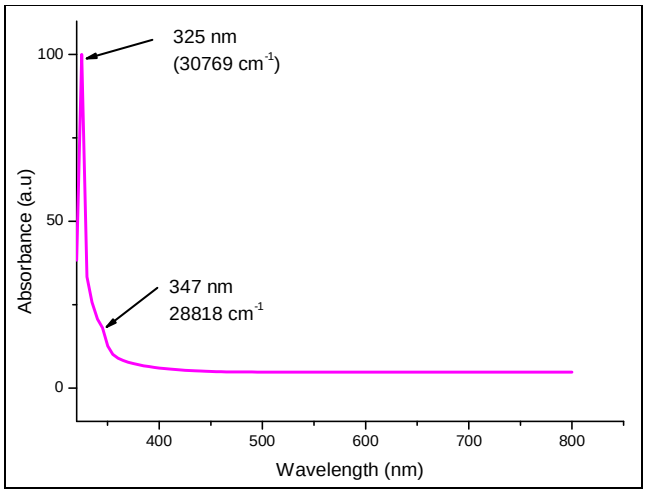

Figure 33: UV spectrum of **2**

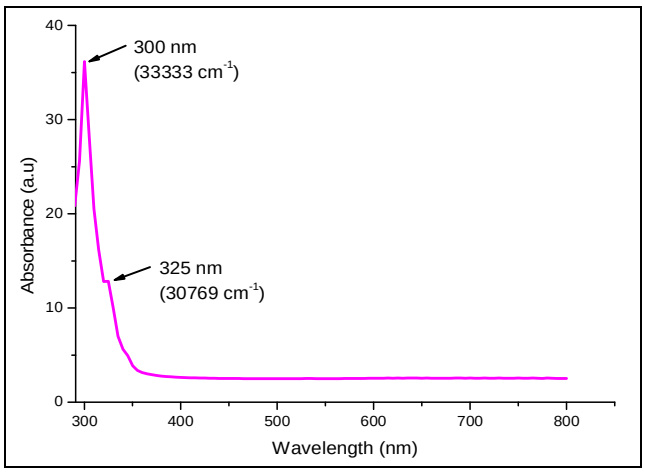

Figure 34: UV spectrum of **3**

The UV-Visible spectrum of the copper(II) complex (Fig. 38) displays a broad peak in the UV region at λ = 280 nm (26385 cm^{-1}) due to the ligand field (π→π* and n→π*) and charge transfer (d-π*) transitions [325]. The d-d transitions appear in the visible region at λ = 437 nm (22883 cm^{-1}) attributed to the transition $^2B_{2g} \rightarrow {}^2B_{1g}$. These transitions, as well as the measured value of the magnetic moment (μ_{eff} = 1.75 μ_B) suggest a square-planar stereochemistry around Cu^{2+} ions [326, 327].

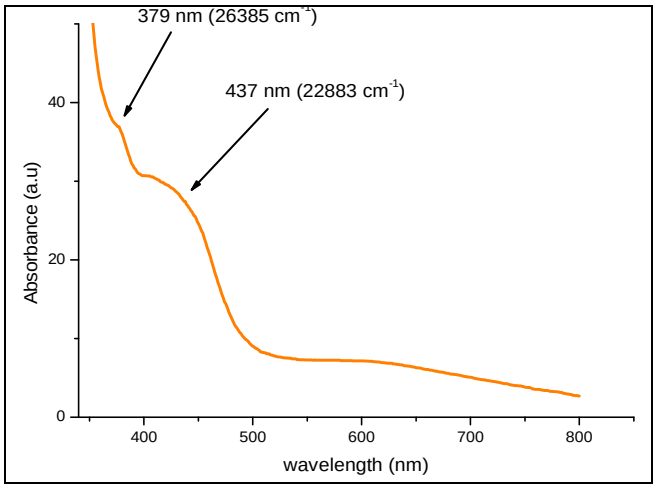

Figure 35: UV-Visible spectrum of **4**

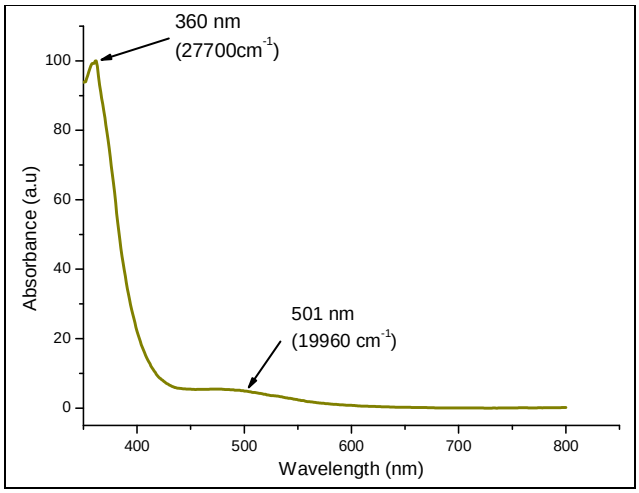

Figure 36: UV-Visible spectrum of complex **5**

The UV-Vis spectrum of 5 (Fig. 39) shows a broad peak at λ = 375 nm (26385 cm-1) which were attributed to intra-ligand (π→π* and n→π*) transitions of the coordinated phen groups due to the ligand field and charge transfer (d-π*) transitions [328]. The visible region contains peaks at λ = 501 nm (19960 cm-1) due to the d-d transition $^4T_{1g} \rightarrow {}^4T_{2g}$, suggests a distorted octahedral ligand field with moderate Jahn-Teller effect geometry around the Co(II) ion [323, 328].

The complexes **4** and **5** exhibit absorption bands at 380 nm and 360 nm respectively, in the UV region, are attributed to an intra-ligand π–π* transition of the coordinated phen groups, while the absorption spectrum in the visible region was characterised by a d-d transition at a maximum wavelength of 437 nm for **4** and 501 nm for **5** [325].

3.8- Magnetic Susceptibility Measurement

The mass susceptibility data for the complexes are presented in Table VIII.

Table VIII: Mass susceptibility data for the complexes

Complex	Temp. (°C)	m_1 (g)	m_2 (g)	m (g)	Ro	R	*l* (cm)
1	30	1.488	1.544	0.056	-757	330	2.0
2	30	1.667	1.722	0.055	-759	-379	2.6
3	30	1.665	1.698	0.033	-760	-451	1.8
4	30	1.487	1.524	0.037	-756	-759	2.4
5	30	1.665	1.730	0.065	-760	-592	2.5

The magnetic data of the samples were obtained by taking the difference in mass between an empty tube (m_1) and the tube filled with sample (m_2) which is in the form of a reasonable fine and uniform powder.

The mass susceptibility; χ_g, was calculated using equation (2.3).

$$\chi_g = \frac{C_{Bal} l (R - R_o)}{10^9 m} \qquad (2.3)$$

where: l = sample length (cm)

m = sample mass (g)

R = reading for tube plus sample

Ro = empty tube reading

C_{Bal} = balance calibration constant (1.53)

χ_g = mass susceptibility

The diamagnetic corrections for the samples were estimated using Pascal's constant and the magnetic data were corrected for diamagnetic contributions using sample holder.

For example: the mass susceptibility, χ_g for **1**, was calculated as follows:

$$\chi_g = \frac{1.53\ x\ 2.0\ (-330 + 757)}{10^9\ x\ 0.0565} = 23.33\ x\ 10^6$$

The susceptibility of ligands, χ_L for **1**, was calculated as follows:

$$\chi_L = 2(\chi_{phen}) + 2(\chi_{NO3})$$

$$\chi_L = 2(-128\ x\ 10^6) + 2(-18.7\ x\ 10^6)$$

$$\chi_L = -293.8\ x\ 10^6$$

The molar susceptibility, χ_M for **1**, was calculated as follows:

$$\chi_M = \chi_g\ x\ molar\ mass$$

$$\chi_M = 23.33\ x\ 10^6\ x\ 539.73$$

$$\chi_M = 13868.8\ x\ 10^6$$

The magnetic susceptibility, χ_A for **1**, was then calculated as follows:

$$\chi_A = \chi_M - \chi_L$$

$$\chi_A = (13868.8 + 293.8)\ x\ 10^6$$

$$\chi_A = 14162.6\ x\ 10^6$$

The magnetic moments, μeff for **1**, was calculated from the magnetic susceptibility and the temperature using equation (3.4) as follows:

$$\mu eff = 2.83(\chi_A T)^{1/2}\ B.M$$

$$\mu eff = 2.83(14162.6\ x\ 303)^{1/2} B.M$$

$$\mu eff = 5.86\ B.M$$

where: B.M is Bohr Magneton

The room temperature magnetic moments summarised in Table IX were then calculated from the magnetic susceptibility (χ_A) by the treatments of the gram magnetic susceptibility (χ_g) into the molar magnetic susceptibility (χ_M) then multiply by Paschal constant for the elements and the metals.

Table IX: Magnetic moments of the complexes

Compound	Mass susceptibility (χ_g) x10^{-6}	Molar susceptibility (χ_m) x10^{-6}	Susceptibility of ligand (χ_L) x10^{-6}	Magnetic susceptibility (χ_A) x10^{-6}	Magnetic moment (μ_{eff}) B.M.
1	23.33	13868.00	-293.80	14162.60	5.86
2	27.48	13725.90	-282.02	14007.80	5.83
3	25.79	14117.30	-310.20	14427.50	5.92
4	2.38	1038.2	-220.25	1258.5	1.75
5	9.89	6005.44	-327.12	6332.56	3.92

The room temperature magnetic moments of the Mn(II) complexes (**1-3)** are 5.86, 5.83 and 5.92 B.M., respectively. These values are consistent with high spin (d^5) octahedral geometry and are indicative of five unpaired electrons in a Mn(II) ion. The high-spin d^5 configuration gives an essentially spin-only temperature independent magnetic moment value of ~5.9 B.M with the octahedral $^6A_{1g}$ ground term for the high-spin system [324]. The magnetic moment of the Cu(II) complex (**4)**, is 1.75 B.M corresponding to one unpaired electron which is slightly greater than the spin only value of 1.73 B.M offers possibility of square planar or tetrahedral geometry [316, 323]. The magnetic moment values of high spin octahedral Co(II) complexes have been reported to be in the range of 3.87–4.2 B.M [322]. In this study, the observed magnetic moment value for **5** is 3.92 B.M. This is in good agreement with high spin (d^7) octahedral geometry [322].

3.9- Description of Crystal Structures of the Complexes

3.9.1- Crystal Structure of $[Mn(phen)_2(NO_3)_2]$ (1)

Complex **1** crystallizes in the orthorhombic crystal system with space group *Pbcn* with four molecules in the unit cell. The ORTEP representation of the crystal structure of **1**; [dinitrato-bis(1,10-phenanthroline-κ^2*N*,*N*')manganese(II)] is shown in Figure 40 and the packing diagram in Figure 41. The crystallographic data and structure refinement parameters of **1,** is presented in Table X. Selected bond lengths and angles are presented in Table XI while the H-bond parameters are given in Table XII.

Table X: Crystal data and structure refinement parameters for **1**

Complex	**1**
Chemical formula	$C_{24}H_{16}MnN_6O_6$
M_r	539.37
Crystal system, space group	Orthorhombic, *Pbcn*
Temperature (K)	296
a, *b*, *c* (Å)	12.5477 (14), 10.1607 (10), 17.695 (2)
β (°)	
V (Å^3)	2256.0 (4)
Z	4
Radiation type	Mo *K*α
μ (mm^{-1})	0.64
Crystal size (mm)	0.30 × 0.25 × 0.25
Diffractometer	Bruker kappa apex2 CCD Diffractometer
Absorption correction	Multi-scan *SADABS* (Bruker, 2012)
T_{min}, T_{max}	0.831, 0.856
No. of measured, independent and observed [$I > 2\sigma(I)$] reflections	12206, 2957, 1774
R_{int}	0.026
$(\sin \theta/\lambda)_{max}$ (Å^{-1})	0.703
$R[F^2 > 2\sigma(F^2)]$, $wR(F^2)$, S	0.058, 0.187, 1.02
No. of reflections	2957
No. of parameters	168
No. of restraints	0
H-atom treatment	H-atom parameters constrained
$\Delta\rho_{max}$, $\Delta\rho_{min}$ (e Å^{-3})	0.67, −0.55

The asymmetric unit of **1** consists of one phen molecule, one nitrate ion and one Mn(II) ion and the other half of the asymmetric unit is generated by inversion symmetry. The Mn(II) ion is coordinated by four N atoms from two chelating phen ligands and two O atoms from two nitrate ions giving a MnN_4O_2 coordination sphere with a distorted octahedral geometry. Three phen N atoms [N(1)-Mn(1) 2.319(3) Å, N(2)-Mn(1) 2.289(3) Å, Mn(1)-N(2)#1 2.289(3) Å] and one nitrate O atom [O(1)-Mn(1) 2.422(6) Å] form the equatorial plane, whereas symmetry related fourth phen N atom [Mn(1)-N(1)#1 2.319(3)] and the second nitrate ion [Mn(1)-O(1)#1

2.422(7)] are in apical positions. The 5-membered chelating rings of Mn(II) and N atoms of phen exhibit a near perfect plane; the N2−C11–C12–N1 torsion angle is 0.84(4)° for **1**. The Mn–N bond lengths are in the range 2.289(3)–2.319(3) Å, which are similar to values reported in the literature [314, 315]. The N(2)-Mn(1)-N(1)#1 bond angle of 88.70(10)° indicates that the N(2)–Mn(1) and Mn(1)–N(1)#1 bonds are in different planes, almost perpendicular to each other. The N(2)-Mn(1)-N(1) chelating angle is 72.14(10)°. The bond lengths in the phenanthroline ring range from 1.328(6)–1.438(4) Å in C–C and from 1.323(4)–1.352(4) Å in C–N and this is similar to literature reported values for phenanthroline complexes [314, 315].

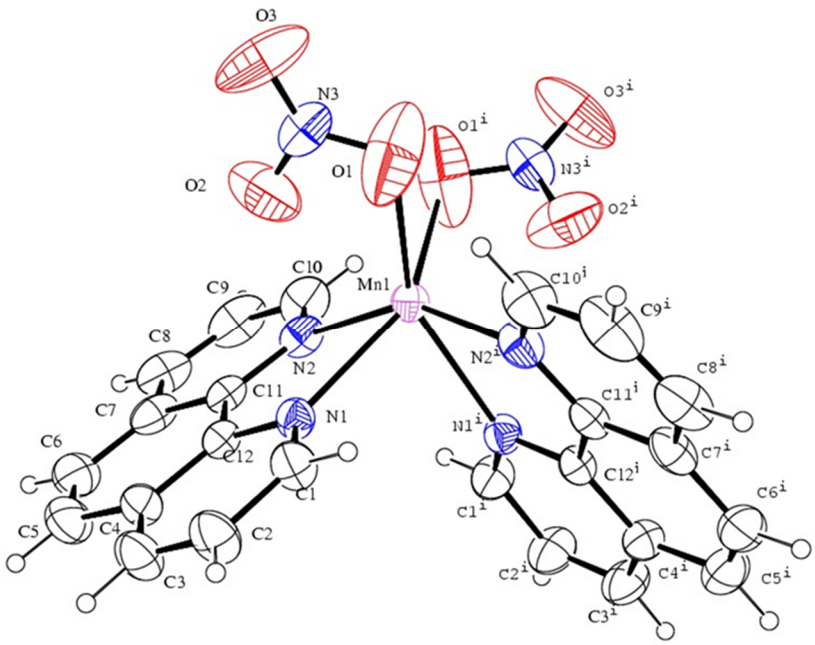

Figure 37: ORTEP view of the crystal structure of [dinitrato-bis(1,10-phenanthroline-κ^2N,N')manganese(II) (**1**)

The packing in the unit cell is based on intermolecular hydrogen bonding and π–π stacking interactions. Cooperation between extensive series of C–H···O hydrogen bonds [244, 329] (Table XII) and face-to-face π–π [C9–C4 3.369(6) Å; symmetry code -1/2+x,-1/2+y,3/2-z] stacking interactions [330], between adjacent phen ligands, stabilize the structure and assemble complex **1** into an interesting 3D supramolecular structure. It is noteworthy to mention that a polymorph of **1** is known [245]. The comparative crystal data of the complexes are presented in Table XIII.

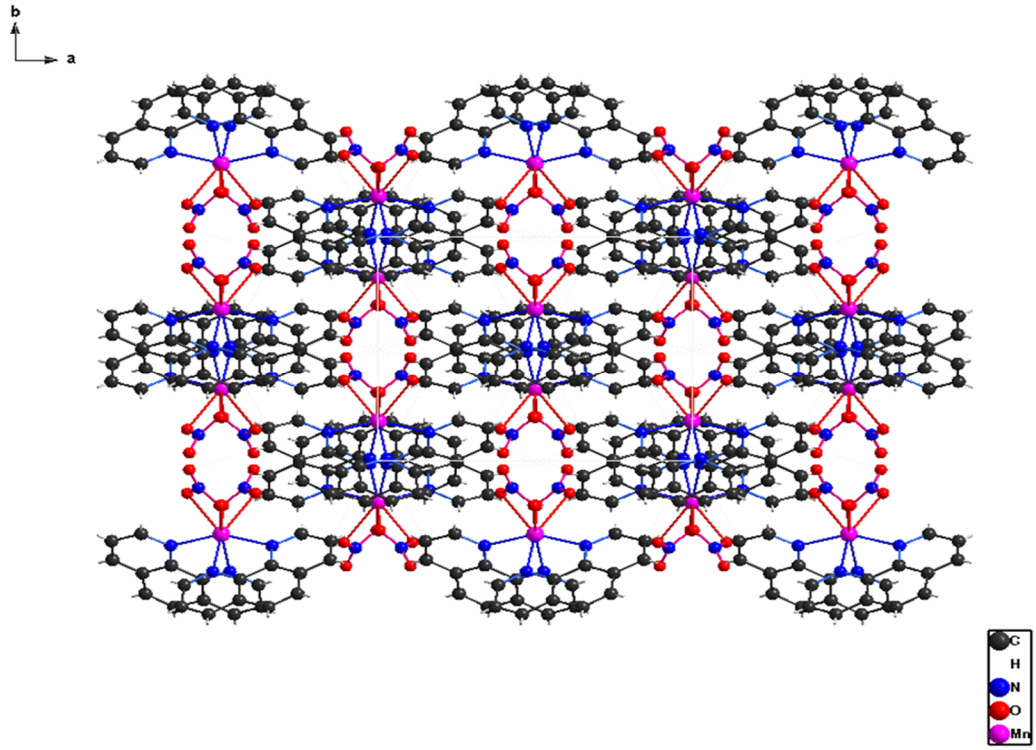

Figure 38: Packing diagram of **1** seen along the crystallographic c-axis

Table XI: Selected bond lengths and bond angles for complex **1**

Bond	Length (Å)	Bond	Angle (°)
N(1)-Mn(1)	2.319(3)	N(2)#1-Mn(1)-N(2)	153.72(15)
N(2)-Mn(1)	2.289(3)	N(2)#1-Mn(1)-N(1)#1	72.14(10)
O(1)-Mn(1)	2.422(6)	N(2)-Mn(1)-N(1)#1	88.70(10)
O(2)-Mn(1)	2.495(6)	N(2)#1-Mn(1)-N(1)	88.70(10)
Mn(1)-N(2)#1	2.289(3)	N(2)-Mn(1)-N(1)	72.14(10)
Mn(1)-N(1)#1	2.319(3)	N(1)#1-Mn(1)-N(1)	87.09(14)
Mn(1)-O(1)#1	2.422(7)	N(2)#1-Mn(1)-O(1)#1	122.84(14)
		N(2)-Mn(1)-O(1)#1	78.61(15)
		N(1)#1-Mn(1)-O(1)#1	104.40(18)
		N(1)-Mn(1)-O(1)#1	148.31(14)
		N(2)#1-Mn(1)-O(1)	78.61(15)

Table XII: Hydrogen-bond geometry (Å, °) for **1**

D–H···*A*	*D*–H	H···*A*	*D*···*A*	*D*–H···*A*
C10–H10···O1^{i}	0.93	2.34	2.935 (8)	122
C3–H3···O2^{ii}	0.93	2.65	3.460(6)	144.1
C6–H6···O3^{iii}	0.931	2.719	3.394(7)	130.1
C6–H6···O3^{iv}	0.931	2.579	3.381(5)	144.5

Symmetry code: (i) −*x*, *y*, −*z*+3/2; (ii) -x,-y,1-z ; (iii) -1/2+x,1/2-y,1-z ; (iv) -1/2+x,-1/2+y,3/2-z

Table XIII: Comparative crystal data of 1 with that of a known polymorph

Complex	1 (this work)	$[Mn(NO_3)_2(C_{12}H_8N_2)_2]$ [308]
Chemical formula	$C_{24}H_{16}MnN_6O_6$	$C_{24}H_{16}MnN_6O_6$
M_r	539.37	539.37
Crystal system, space group	Orthorhombic, *Pbcn*	Monoclinic, C2/c
Temperature (K)	296	298
a	12.5477 (14)	11.6191 (6)
b	10.1607 (10)	15.1164 (8)
c (Å)	17.695 (2)	13.4526 (7)
β (°)	90	105.387 (1)
V (Å^3)	2256.0 (4)	2278.1 (2)
Z	4	4

3.9.2- Crystal Structure of $[Mn(phen)_2(N_3)_2)]$ (2)

Complex **2** crystallizes in the orthorhombic crystal system with space group *Pbcn* with four molecules in the unit cell. The ORTEP representation of the crystal structure of complex **2** [diazido-bis(1,10-phen-κ^2N,N′)manganese(II)] is shown in Figure 42 and the packing diagram in Figure 43. The crystallographic data and structure refinement parameters of **2,** is presented in Table XIV. Selected bond lengths and angles are presented in Table XV while the H-bond parameters are given in Table XVI.

Table XIV: Crystal data and structure refinement parameters for **2**

Complex	**2**
Chemical formula	$C_{24}H_{16}MnN_{10}$
M_r	499.41
Crystal system, space group	Orthorhombic, *Pbcn*
Temperature (K)	296
a, *b*, *c* (Å)	13.395 (2), 9.6457 (14), 16.979 (3)
β (°)	
V (Å^3)	2193.8 (6)
Z	4
Radiation type	Mo *K*α
μ (mm^{-1})	0.64
Crystal size (mm)	0.25 × 0.25 × 0.20
Diffractometer	Bruker kappa apex2 CCD Diffractometer
Absorption correction	Multi-scan *SADABS* (Bruker, 2012)
T_{min}, T_{max}	0.861, 0.941
No. of measured, independent and observed [$I > 2\sigma(I)$] reflections	22275, 2029, 1349
R_{int}	0.041
$(\sin \theta/\lambda)_{max}$ (Å^{-1})	0.606
$R[F^2 > 2\sigma(F^2)]$, $wR(F^2)$, S	0.077, 0.179, 1.17
No. of reflections	2029
No. of parameters	159
No. of restraints	0
H-atom treatment	H-atom parameters constrained
$\Delta\rho_{max}$, $\Delta\rho_{min}$ (e Å^{-3})	0.71, −0.52

The asymmetric unit consists of one molecule of phen, one azide anion, one Mn(II) ion and the other half of the asymmetric unit is generated by inversion symmetry. Chemically, each Mn atom is six-coordinate with four N atoms of two phen molecules [Mn1–N1 2.320(4) Å, Mn1–N1^i 2.320(4) Å, Mn1–N2 2.268(4) Å, Mn1–N2^i 2.268(4) Å] and two terminal N atoms from two azide anions [Mn1–N3 2.130(6) Å, Mn1–N3^i 2.130(6) Å] giving a distorted octahedral geometry around the Mn atom with MnN_6 chromophore. The azido ligands have a cis configuration in the structure. This observation is similar to literature reports of the same

structure obtained by different synthetic methods but with slightly different crystal parameters [215, 331].

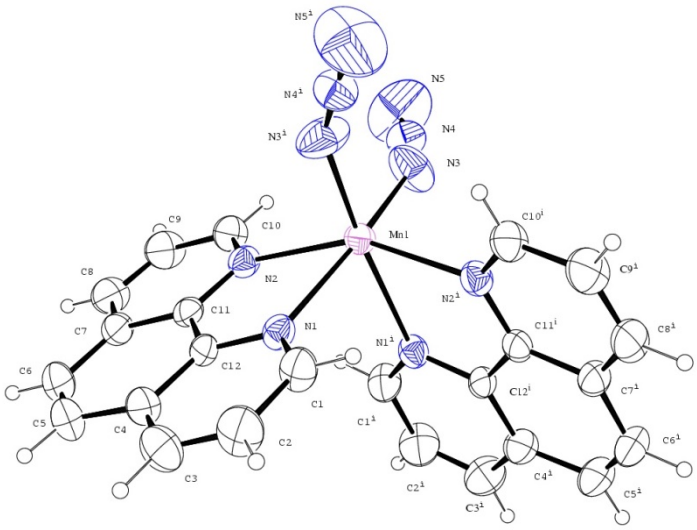

Figure 39: ORTEP view of crystal structure of [diazido-bis(1,10-phenanthroline-κ^2N,N')manganese(II) (**2**)

The axial positions are occupied by the $N3^i$ from one azide and $N1^i$ from a phen molecule [$N3^i$–Mn1–$N1^i$ 167.17(19)°] while the equatorial plane is formed by the coordinating atoms N1, N2 from one phen molecule, $N2^i$ from the second phen molecule and N3 from an azide ion. The bond angles in the equatorial plane deviate noticeably from the ideal value of 90°, with two larger, 101.1(2)° for N3–Mn1–$N2^i$, 95.7(2)° for N3–Mn1–N2 and two smaller angles of 89.03(15)° for $N2^i$–Mn1–N1 and 72.16(16)° for N2–Mn1–N1. This deviation in bond angles coupled with the observation that the Mn–$N_{(azide)}$ bonds are slightly shorter than the Mn-$N_{(phen)}$ bonds indicate a highly distorted square-planar arrangement in the equatorial plane. There are two long Mn-$N_{(phen)}$ bonds [Mn1–N1 2.320(4) Å] and two short ones [Mn1–N2 2.268(4) Å]. The two phen ligands which form five-membered chelate rings with Mn exhibit near perfect planes [torsion angle N2–C11–C12–N1 is −0.8(7)°] and are oriented in two different molecular planes [215, 244, 332]. The N5–N4–N3 bond angle of 178.8(9)° indicates that the azide anion is almost linear. The C8–H8···N3 H-bonds between the nitrogen atom of an azide ion and one phen ligand coupled with π–π stacking interactions between the phen ring systems are observed and consolidate an extensive three-dimensional supramolecular network.

Table XV: Selected bond lengths and angles for **2**

Bond	Length (Å)	Bond	Angle (°)
Mn1–N3	2.130 (6)	N3–Mn1–N3^{i}	97.9 (4)
Mn1–N3^{i}	2.130 (6)	N3–Mn1–N2^{i}	101.1 (2)
Mn1–N2^{i}	2.268 (4)	N3i–Mn1–N2^{i}	95.7 (2)
Mn1–N2	2.268 (4)	N3–Mn1–N2	95.7 (2)
Mn1–N1^{i}	2.320 (4)	N3i–Mn1–N2	101.1 (2)
Mn1–N1	2.320 (4)	N2i–Mn1–N2	154.3 (2)
		N3–Mn1–N1^{i}	88.8 (2)
		N3i–Mn1–N1^{i}	167.17 (19)
		N2i–Mn1–N1^{i}	72.16 (16)
		N2–Mn1–N1^{i}	89.03 (15)
		N3–Mn1–N1	167.17 (19)
		N3i–Mn1–N1	88.8 (2)
		N2i–Mn1–N1	89.03 (15)
		N2–Mn1–N1	72.16 (16)
		N1i–Mn1–N1	86.8 (2)

Table XVI: Hydrogen-bond geometry for **2** (Å, º)

D–H···*A*	*D*–H	H···*A*	*D*···*A*	*D*–H···*A*
C8–H8···N3	0.931	2.552	3.342(8)	143

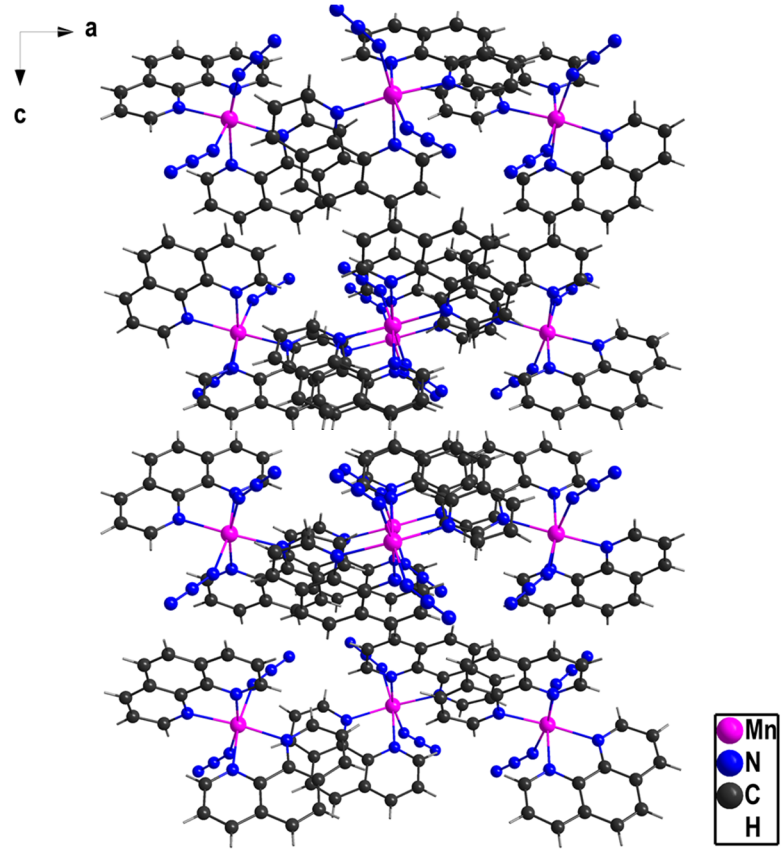

Figure 40: Packing diagram of **2** seen along the crystallographic b-axis

3.9.3- Crystal structure of [Mn(Phen)$_2$(dca)$_2$)] (3)

Complex **3**, bis(dicyanamido)bis(1,10-phenanthroline)manganese(II), crystallizes in the monoclinic crystal system with space group $P2_1/c$ with four molecules in the unit cell. The ORTEP view of the crystal structure of **3** together with the atom numbering scheme used in the corresponding tables are shown in Figure 44 and the crystal packing diagram seen along the crystallographic *b*-axes is shown in Figure 45. The crystallographic data and structure refinement parameters of **3**, is presented in Table XVII. Selected bond lengths and angles are presented in Table XVIII while the H-bond parameters are given in Table XIX.

Table XVII: Crystal data and structure refinement parameters for **3**

Complex	**3**
Chemical formula	$C_{28}H_{16}MnN_{10}$
M_r	547.45
Crystal system, space group	Monoclinic, $P2_1/c$
Temperature (K)	150
a, *b*, *c* (Å)	9.8716 (8), 14.6636 (8), 17.6165 (11)
β (°)	104.364 (3)
V (Å^3)	2470.3 (3)
Z	4
Radiation type	Mo $K\alpha$
μ (mm^{-1})	0.57
Crystal size (mm)	0.17 × 0.16 × 0.13
Diffractometer	Bruker *APEX*-II CCD diffractometer
Absorption correction	Multi-scan *SADABS*
T_{min}, T_{max}	0.847, 0.867
No. of measured, independent and observed [$I > 2\sigma(I)$] reflections	54213, 6160, 4835
R_{int}	0.056
$(\sin\theta/\lambda)_{max}$ (Å^{-1})	0.668
$R[F^2 > 2\sigma(F^2)]$, $wR(F^2)$, S	0.036, 0.085, 1.06
No. of reflections	6160
No. of parameters	352
No. of restraints	0
H-atom treatment	H-atom parameters constrained
$\Delta\rho_{max}$, $\Delta\rho_{min}$ (e Å^{-3})	0.37, −0.39

The asymmetric unit consists of two 1,10-phenanthroline molecules, two monodentate non-bridging dca anions, and one Mn(II) ion. A similar structure with slightly different parameters, obtained by a 1:1:1 reaction of $Mn(OAc)_2{\cdot}4H_2O$, Na(dca), and phen in an ethanol/water mixture, has been reported [333].

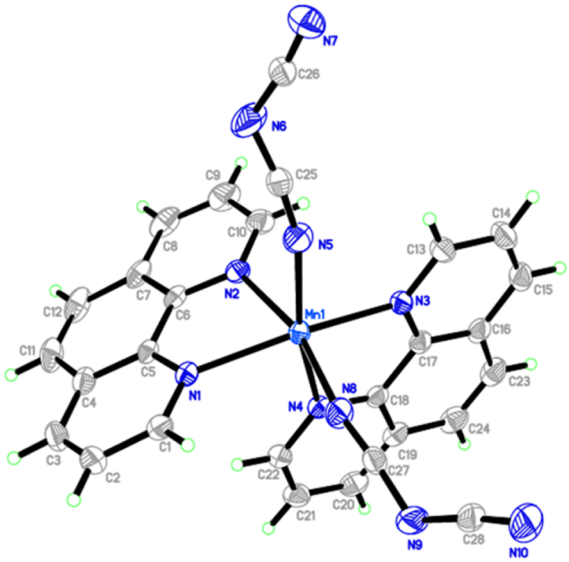

Figure 41: ORTEP view of crystal structure of **3**

Chemically, each manganese atom is six-coordinate; bonded to four N-atoms of two phen molecules [Mn1–N1 2.2593(14) Å, Mn1–N2 2.2897(13) Å, Mn1–N3 2.2549(14) Å, Mn1–N4 2.3214(14) Å] and two terminal N-atoms from two dca anions [Mn1–N5 2.1505(16) Å, Mn1–N8 2.1552(15) Å] giving a distorted octahedral geometry around the Mn atom with MnN6 chromophore. The axial positions are occupied by the N2 atom of one phen ring and the N8 atom of one azide ion [N(8)–Mn(1)–N(2) 165.68(5)°] while the equatorial plane is formed by the coordinating atoms N1, N3, N4 from two different phen molecules and N5 from the another dca anion. The Mn–N(phen) [2.2549(14)-2.3214(14) Å] and the Mn–N(dca) [2.1505(16)-2.1552(15) Å] are in agreement with values reported in the literature [193, 333]. The longer Mn-N(phen) bonds [Mn(1)–N(2) 2.2897(13), Mn(1)–N(4) 2.3214(14)] are trans to each other [N(2) –Mn(1)–N(4) 85.19(5)°]. The N(5)–Mn(1)–N(8) bond angle of 98.21(6)2(6)° indicates that the Mn1–N5 and N8–Mn1 bonds are in two different molecular planes almost perpendicular to each other. The dca anions do not coordinate linearly [N8–C27–N9 173.4(2)°, N5—C25—N6 171.7(2)°] to the metal centre as observed in other Mn-dca complexes [193, 333]. The two phen ligands which form five-membered chelate rings with Mn are oriented in two different molecular planes.

Table XVIII: Selected Bond lengths (Å) and angles (°) for **3**

Bond	Length (Å)	Bond	Angle (°)
Mn(1)–N(5)	2.1505(16)	N(5) –Mn(1) –N(8)	98.21(6)
Mn(1) –N(8)	2.1552(15)	N(5) –Mn(1) –N(3)	93.37(6)
Mn(1) –N(3)	2.2549(14)	N(8) –Mn(1) –N(3)	98.65(5)
Mn(1) –N(1)	2.2593(14)	N(5) –Mn(1) –N(1)	104.32(6)
Mn(1) –N(2)	2.2897(13)	N(8) –Mn(1) –N(1)	93.31(5)
Mn(1) –N(4)	2.3214(14)	N(3) –Mn(1) –N(1)	157.00(5)
		N(5) –Mn(1) –N(2)	89.05(6)
		N(8) –Mn(1) –N(2)	165.68(5)
		N(3) –Mn(1) –N(2)	93.19(5)
		N(1) –Mn(1) –N(2)	72.87(5)
		N(5) –Mn(1) –N(4)	164.65(6)
		N(8) –Mn(1) –N(4)	90.62(6)
		N(3) –Mn(1) –N(4)	72.81(5)
		N(1) –Mn(1) –N(4)	87.57(5)
		N(2) –Mn(1) –N(4)	85.19(5)
		C(1) –N(1) –Mn(1)	125.75(11)
		C(5) –N(1) –Mn(1)	115.56(11)
		C(27) –N(8) –Mn(1)	163.57(15)

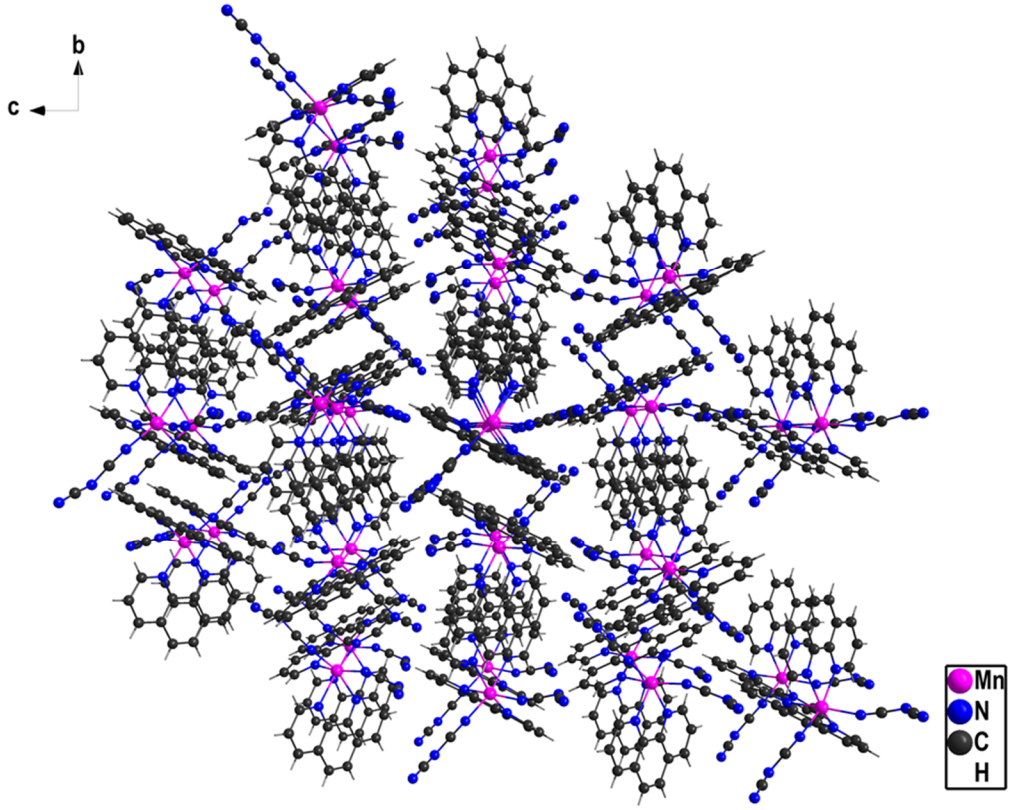

Figure 42: Packing diagram of **3** seen along the crystallographic a-axis

The packing in the unit cell is based on intermolecular hydrogen bonding and π–π stacking interactions. Cooperation between π–π stacking interactions of phen rings of adjacent molecules and an extensive series of weak C–H···$N_{(dca)}$ hydrogen bonds (Table 3.18) between neighbouring molecules further stabilize the structure and form an extended three-dimensional network [193].

Table XIX: Hydrogen-bond geometry for **3** (Å, º)

D–H···*A*	*D*–H	H···*A*	*D*···*A*	*D*–H···*A*
C1–H1···N7^{i}	0.95	2.516	3.372	150
C3–H3···N6^{ii}	0.951	2.567	3.473	159.6
C20–H20···N7^{iii}	0.95	2.708	3.292	120.4
C21–H21···N7^{iv}	0.95	2.567	3.224	126.5
C10–H10···N9^{v}	0.95	2.657	3.439	140
C8–H8···N10^{vi}	0.951	2.406	3.336	165.8
C12–H12···N5^{vii}	0.949	2.662	3.546	155.1

i)1-x,1-y,1-z; ii) 2-x,1-y,1-z; iii) -1+x,1.5-y,-1/2+z; iv) -1+x,1.5-y,-1/2+z; v) x,1.5-y,-1/2+z; vi) -1+x,1.5-y,1/2+z ; vii) -1+x,y,z

3.9.4- Crystal Structure of [Cu(phen)(BMCA)]·NO_3 (4)

Complex **4** crystallizes in the monoclinic crystal system with space group C2/c with four molecules in the unit cell. The molecular structure and atom-labelling scheme used in the corresponding tables of the crystal structure [{bis(methoxycarbimido)aminato-κ^2N,N'}(1,10-phenanthroline-κ^2N,N')copper(II)] nitrate; [Cu(phen)(BMCA)]·NO_3 is shown in Figure 46 and the packing diagram in Figure 47. The crystallographic data and structure refinement parameters of **4** are presented in Table XX. The selected bond lengths and bond angles are presented in Table XXI while the H-bond parameters are given in Table XXII.

Table XX: Crystal data and structure refinement parameters for **4**

Complex	**4**
Chemical formula	$C_{16}H_{16}CuN_5O_2^+ \cdot NO_3^-$
M_r	435.89
Crystal system, space group	Monoclinic, C2/c
Temperature (K)	130(2)
a, *b*, *c* (Å)	17.0517 (12), 14.5051 (5), 7.0537 (3)
β (º)	102.252(4)
V (Å^3)	1705.17 (12)
Z	4
Radiation type	Mo *K*α
μ (mm^{-1})	1.33
Crystal size (mm)	0.20 × 0.10 × 0.01
Diffractometer	Bruker kappa apex2 CCD Diffractometer
Absorption correction	Multi-scan *SADABS* (Bruker, 2012)
T_{min}, T_{max}	0.993, 1.000
No. of measured, independent and observed [$I > 2\sigma(I)$] reflections	8594, 2366, 1861
R_{int}	0.051
$(\sin\theta/\lambda)_{max}$ (Å^{-1})	0.712
$R[F^2 > 2\sigma(F^2)]$, $wR(F^2)$, S	0.047, 0.087, 1.04
No. of reflections	2366
No. of parameters	178
No. of restraints	7
H-atom treatment	All H-atom parameters refined
$\Delta\rho_{max}$, $\Delta\rho_{min}$ (e Å^{-3})	0.35, −0.43

The asymmetric unit consists of one Cu(II) cation, one bis(methoxycarbimido)aminato (BMCA) anion, one phen molecule, and one nitrate counter anion. BMCA and the phen ligand are coordinating at Cu in a planar fashion, but both planes are not coplanar. Least squares planes for these two units are shifted by an angle of 36.55(3)°. The Cu–N_{phen} bond distances are 1.998(2) Å which are comparable to those reported in the literature [209, 334-337]. The Cu–

N_{BMCA} bond lengths fall in the range 1.892(2) – 1.998(2) Å but are quite shorter compared to those of related complexes (1.928(3)–1.932(3) Å) [209, 334-336]. Cu(1), BCMA and phen are located on a twofold axis. It forms two metallocycles; a six-membered ring with the BMCA anion and a five-membered ring with the phen molecule. The two CH_3O groups of the BMCA ligand are in *syn-syn* conformation in the complex. Parallel π-stacking interactions, between adjacent phen ligands, stabilize the structure and assemble complex **4** into an interesting 3D structure [338].

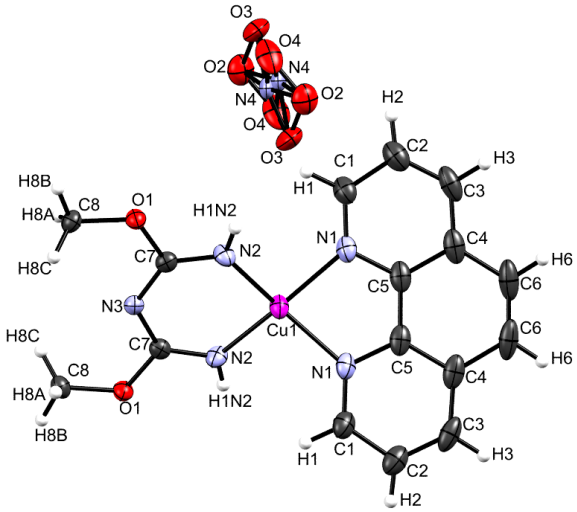

Figure 43: Molecular structure and atom-labelling scheme for [{bis(methoxycarbimido)aminato-κ^2N,N'}(1,10-phenanthroline-κ^2N,N')copper(II)] nitrate; **4,** with ellipsoids drawn at 50% probability level. H atoms are omitted for clarity

The packing in the unit cell is based on intermolecular hydrogen bonding and π–π stacking interactions. Cooperation between extensive series of N–H···O hydrogen bonds [38, 215] (Table XXII) and face-to-face π–π [N(3)–O(3) 3.195(4) Å; symmetry code 1 x+1,-y+3/2,z+1/2] stacking interactions, between adjacent phen ligands, stabilize the structure and assemble complex **4** into an interesting 3D supramolecular structure. It is noteworthy to mention that a polymorph of **4** is known [245].

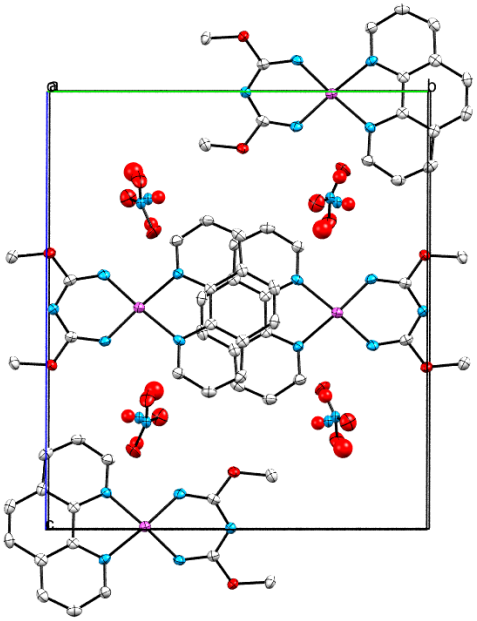

Figure 44: Packing diagram of **4** seen along the crystallographic a-axis

Table XXI: The selected bond lengths (Å) and bond angles (°) for **4**

Bond length (Å)		Bond angle (°)	
Cu(1)-N(4)	1.891(3)	N(4)-Cu(1)-N(3)	91.52(11)
Cu(1)-N(3)	1.893(3)	N(4)-Cu(1)-N(2)	154.32(13)
Cu(1)-N(2)	1.994(3)	N(3)-Cu(1)-N(2)	98.62(11)
Cu(1)-N(1)	2.003(3)	N(4)-Cu(1)-N(1)	98.48(11)
O(1)-C(14)	1.351(3)	N(3)-Cu(1)-N(1)	154.57(12)
O(1)-C(13)	1.443(4)	N(2)-Cu(1)-N(1)	82.28(10)
O(2)-C(15)	1.354(3)		
O(2)-C(16)	1.439(4)		
N(5)-C(15)	1.329(4)		
N(5)-C(14)	1.332(4)		

Table XXII: Hydrogen bonds for **4** [Å and °]

D-H···A	d(D-H)	d(H···A)	d(D···A)	<(DHA)
N(3)-H(1N3)···O(3)#1	0.72(3)	2.47(3)	3.195(4)	176(4)
N(4)-H(1N4)···O(4)	0.78(3)	2.31(3)	3.028(4)	154(4)

Symmetry transformations used to generate equivalent atoms:
#1 x+1,-y+3/2,z+1/2

3.7.5- Crystal Structure of $[Co(phen)_2(NO_3)](dcg)\cdot(H_2O)$ (5)

Complex **5** crystallizes in the monoclinic crystal system with space group Cc with four molecules in the unit cell. The molecular structure and atom-labelling scheme used in the corresponding tables of the crystal structure [(nitrato-κ^2O,O')(1,10-phenanthroline-κ^2N,N')cobalt(II)] dicyanoguanidinate; $[Co(Phen)_2(NO_3)](dcg)\cdot H_2O$ is shown in Figure 48 and the packing diagram in Figure 49. The crystallographic data and structure refinement parameters of the complex are presented in Table XXIII. The selected bond lengths and bond angles are presented in Table XXIV while the H-bond parameters are given in Table XXV.

Table XXIII: Crystal data and structure refinement parameters for **5**

Complex	**5**
Chemical formula	$C_{27}H_{20}CoN_{10}O_4$
M_r	607.46
Crystal system, space group	Monoclinic, *Cc*
Temperature (K)	130(2)
a, *b*, *c* (Å)	13.2779 (3), 14.9105 (3), 12.6468 (3)
β (º)	99.501(2)
V (Å^3)	2469.47(10)
Z	4
Radiation type	Mo *K*α
μ (mm^{-1})	0.755
Crystal size (mm)	0.35× 0.30 × 0.20
Diffractometer	Bruker kappa apex2 CCD Diffractometer
Absorption correction	Multi-scan *SADABS* (Bruker, 2012)
T_{min}, T_{max}	0.97588, 1.00000
No. of measured, independent and observed [$I > 2\sigma(I)$] reflections	14308, 6751, 1244
R_{int}	0.0253
$(\sin \theta/\lambda)_{max}$ (Å^{-1})	0.0392
$R[F^2 > 2\sigma(F^2)]$, $wR(F^2)$, S	0.0470, 0.0941, 1.029
No. of reflections	6751
No. of parameters	400
No. of restraints	6
H-atom treatment	H-atom parameters constrained
$\Delta\rho_{max}$, $\Delta\rho_{min}$ (e Å^{-3})	0.475, −0.755

The asymmetric unit consists of one Co(II) cation, one nitrate anion, two phen molecules, one lattice water molecule and one dicyanoguanidinate counter anion. As illustrated in Figure 48, the Co atom is chelated by two oxygen atoms from one nitrate anion and also coordinated to four N atoms from two phen ligands to complete a distorted octahedral environment with a CoO_2N_4 chromophore. The Co–O bond lengths vary from 1.888(4) Å to 1.890(4) Å, while the Co–N bond distances fall in the range of 1.927(4)–1.957(4) Å. The deviation of the bond angles

O(1)-Co(1)-O(2) - O(2)-Co(1)-N(3)(69.67(8)–99.26(17)˚) and O(2)-Co(1)-N(1) - N(4)-Co(1)-N(2) (167.32(17)–175.65(9)˚) (Table XXIV) from the ideal values (90˚, 180˚) for a regular octahedron, indicates that the coordination polyhedron of Co(II) ions is highly distorted octahedron. These angles, as well as Co–N and Co–O bond lengths, are quite similar to those of related complexes [13, 58, 209]. The distortion is also thought to result from the high-spin $3d^7$ ion of cobalt(II) which gives a $^4F_{9/2}$ ground term in octahedral ligand fields [13]. This distortion is also a consequence of the rigidity of the ligands. All ligands are coordinating in a chelate fashion.

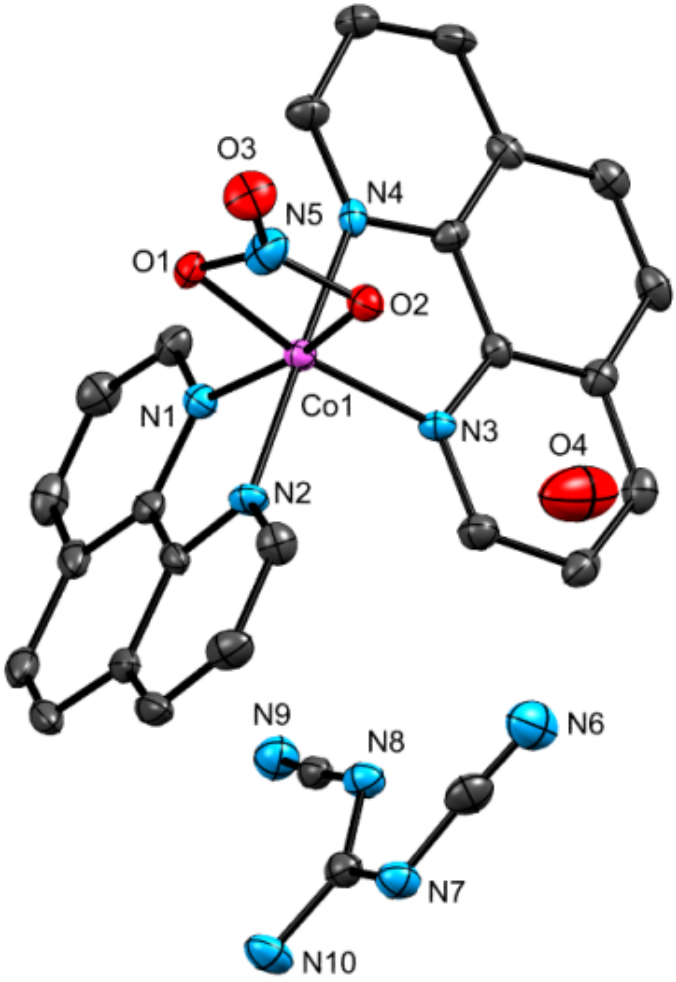

Figure 45: Molecular structure and atom-labelling scheme for [(nitrato-κ^2O,O')(1,10-phenanthroline-κ^2N,N')cobalt(II)] dicyanoguanidinate; **5** with ellipsoids drawn at 50% probability level. H atoms are omitted for clarity

For the certainty of the charge of N,N'-dicyanoguanidine (dcg), the molar conductance Λ_M = 82.5 $ohm^{-1}cm^2mol^{-1}$ of the complex **5** measured at room temperature in DMSO solvent with 10^{-3} M concentration confirmed a 1:1 electrolyte [162] as reported early in this work. Therefore, N,N'-dicyanoguanidine ($(H_2N)C(NCN)_2$) is present as a counter anion, which originated from

the reaction of two dca anions. However, the subsequent elimination of the cyano group leading to dcg anion was not observed before and its mechanism is unclear. Notwithstanding, dicyanoguanidine (both in its neutral and anionic form) has been characterized in the literature [209].

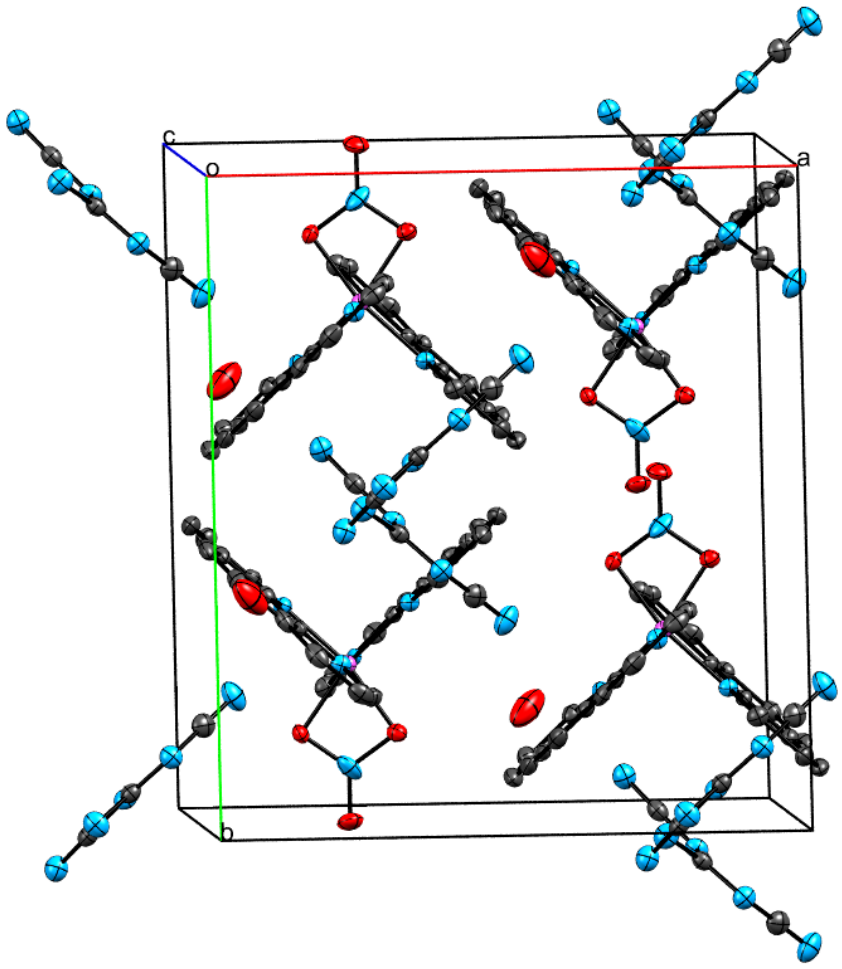

Figure 46: Packing diagram of **5** seen along the crystallographic a-axis

In addition, C–N···Cg (π–ring) contacts between planar dcg anions and planar rings of phen ligands contribute to the stabilization of the dimeric cationic units. Due to these types of interactions, the chains parallel to the a-axis are formed (Fig. 49). The parallel π stacking interactions between phen ligands and numerous N–H···N, C–H···N and C–H···O hydrogen bonds extend the structure into a three-dimensional network.

Table XXIV: The selected bond lengths (Å) and bond angles (°) for **5**

Bond length (Å)		Bond angle (°)	
Co(1)-O(1)	1.888(4)	O(1)-Co(1)-O(2)	69.67(8)
Co(1)-O(2)	1.890(4)	O(1)-Co(1)-N(4)	91.74(16)
Co(1)-N(4)	1.927(4)	O(2)-Co(1)-N(4)	90.78(15)
Co(1)-N(2)	1.937(4)	O(1)-Co(1)-N(2)	91.76(16)
Co(1)-N(1)	1.956(5)	O(2)-Co(1)-N(2)	92.87(17)
Co(1)-N(3)	1.957(4)	N(4)-Co(1)-N(2)	175.65(9)
Co(1)-N(5)	2.320(3)	O(1)-Co(1)-N(1)	98.15(17)
		O(2)-Co(1)-N(1)	167.32(17)
		N(4)-Co(1)-N(1)	93.18(17)
		N(2)-Co(1)-N(1)	83.75(18)
		O(1)-Co(1)-N(3)	168.13(17)
		O(2)-Co(1)-N(3)	99.26(17)
		N(4)-Co(1)-N(3)	83.93(17)

Table XXV: Hydrogen bonds for **5** [Å and °].

D-H···A	d(D-H)	d(H···A)	d(D···A)	<(DHA)
O(4)-H(3O4)···N(6)	0.95(4)	1.96(6)	2.895(6)	165(13)
O(4)-H(2O4)···N(9)#1	0.95(4)	2.04(5)	2.905(6)	151(7)
N(10)-H(1N)···N(9)#2	0.81(6)	2.35(6)	3.116(6)	158(6)
N(10)-H(1N)···C(27)#2	0.81(6)	2.89(6)	3.651(8)	158(5)
N(10)-H(2N)···C(11)#2	0.83(5)	2.77(5)	3.564(7)	161(4)
N(10)-H(2N)···C(12)#2	0.83(5)	2.75(5)	3.471(6)	147(4)

Symmetry transformations used to generate equivalent atoms:
#1 x+1/2,y-1/2,z #2 x,-y+1,z-1/2

The adjacent $[Co(phen)_2(NO_3)]^+$ cations are joined to each other by face to face π–π stacking interactions between phen ligands, and isolated dimeric units are formed. Adjacent dimeric units are fused together by a N=O···Cg interaction between the non-coordinated oxygen atom of the nitrato ligand and appropriate heterocyclic part of phen ligand of neighbouring dimeric unit. In addition, C–N···Cg (π–ring) contacts between planar dcg anions and planar rings of phen ligands contribute to the stabilization of the dimeric cationic units. Due to these types of interactions, the chains parallel to the b axis are formed. The isolated chains are further bound to a three-dimensional network by numerous N–H···N, C–H···N and C–H···O hydrogen bonds [209].

3.10- Metal-mediated dca transformations

These metal-promoted transformations proceed through a nucleophilic attack of the nitrile groups of dca on methanol (case of BMCA), or on another dca (case of dcg), as previously reported [206-209]. The BMCA ligand is isoelectronic with acetyl-acetonate [339].

These metal-promoted transformation reactions are a function of the reaction temperature, the transition metal ion used, and the molar ratio of dca^-/nucleophile on the product [207].

3.10.1-Copper-Mediated dca Transformation

The overall reaction for the addition of methanol to dca anion in the Cu(II) complex is presented in equation 3.6.

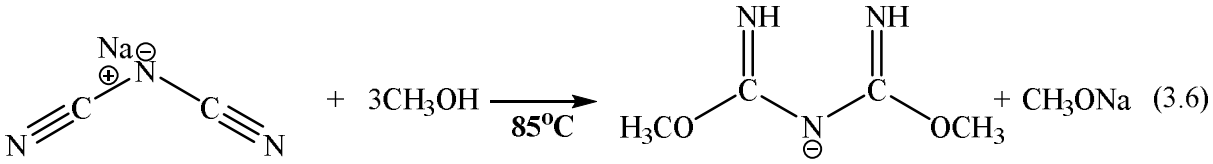

(3.6)

The proposed mechanism for the transformation of dca (dca) to bis(methoxycarbimido)aminate anion (BMCA) is divided into two parts; i) the formation of the nucleophile and ii) the attack of the nucleophile to methanol.

- Formation of the nucleophile

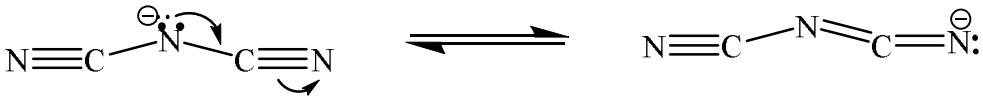

(3.7)

- Attack of the nucleophile to methanol

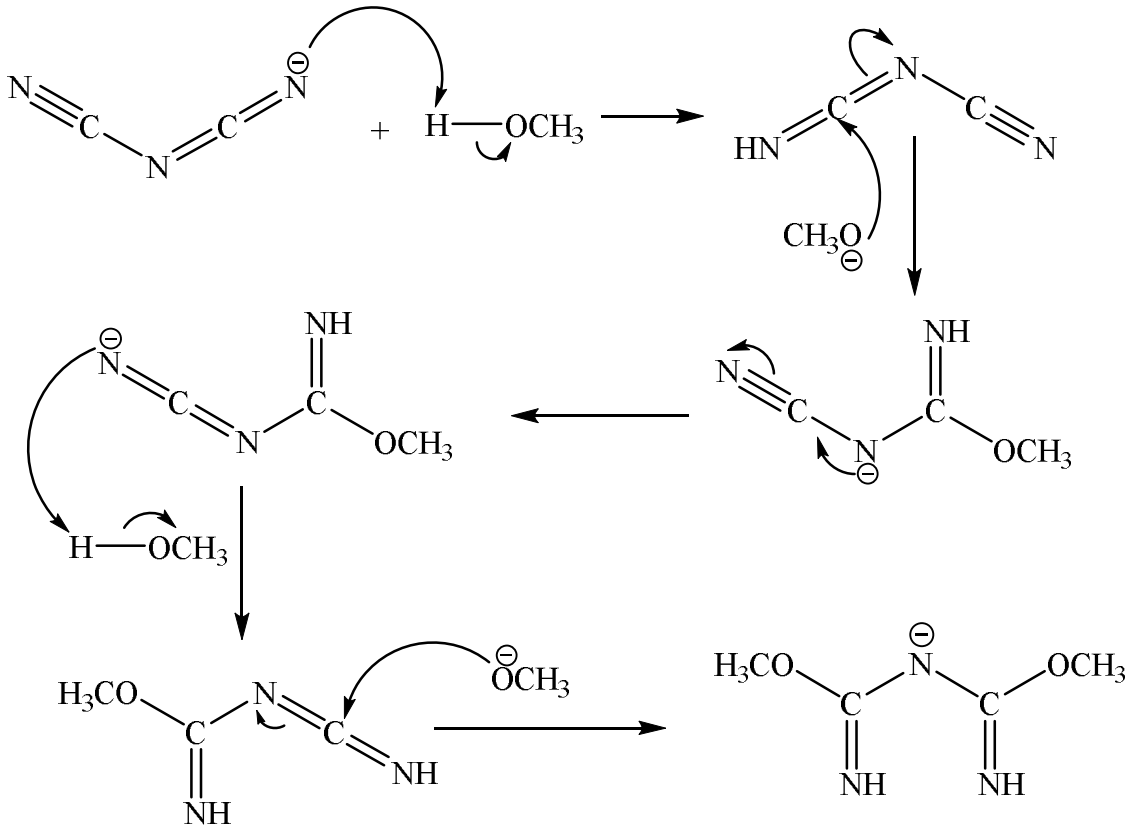

Scheme 8: Proposed mechanism of nucleophilic addition of methanol to dca anion in the Cu(II) complex [206, 208]

3.10.2- Cobalt-mediated dca transformation

The overall reaction for the formation of N,N'-dicyanoguanidinate anion from two dca anion in the Co(II) complex is presented in equation 3.8.

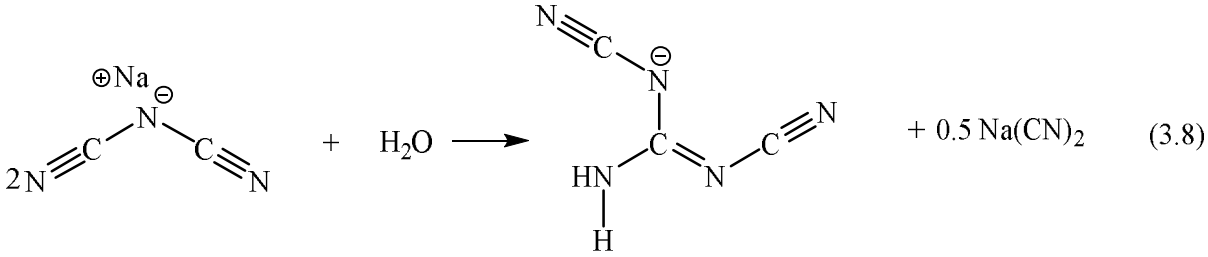

(3.8)

The proposed mechanism for the transformation of two dca anions to N,N'-dicyanoguanidinate anion is divided into two parts; i) the protonation of dca anions and ii) nucleophilic addition of Hdca molecules

- Protonation of dicyanamide anions

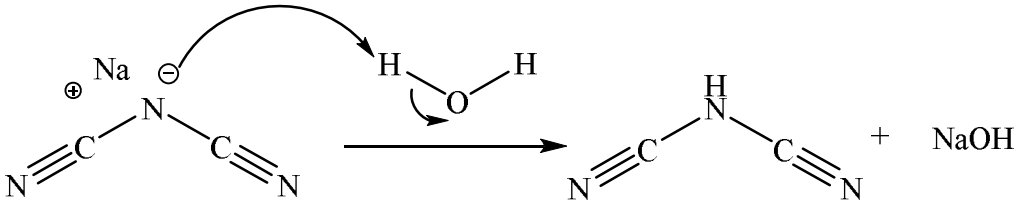

(3.9)

- Nucleophilic addition of dca molecules

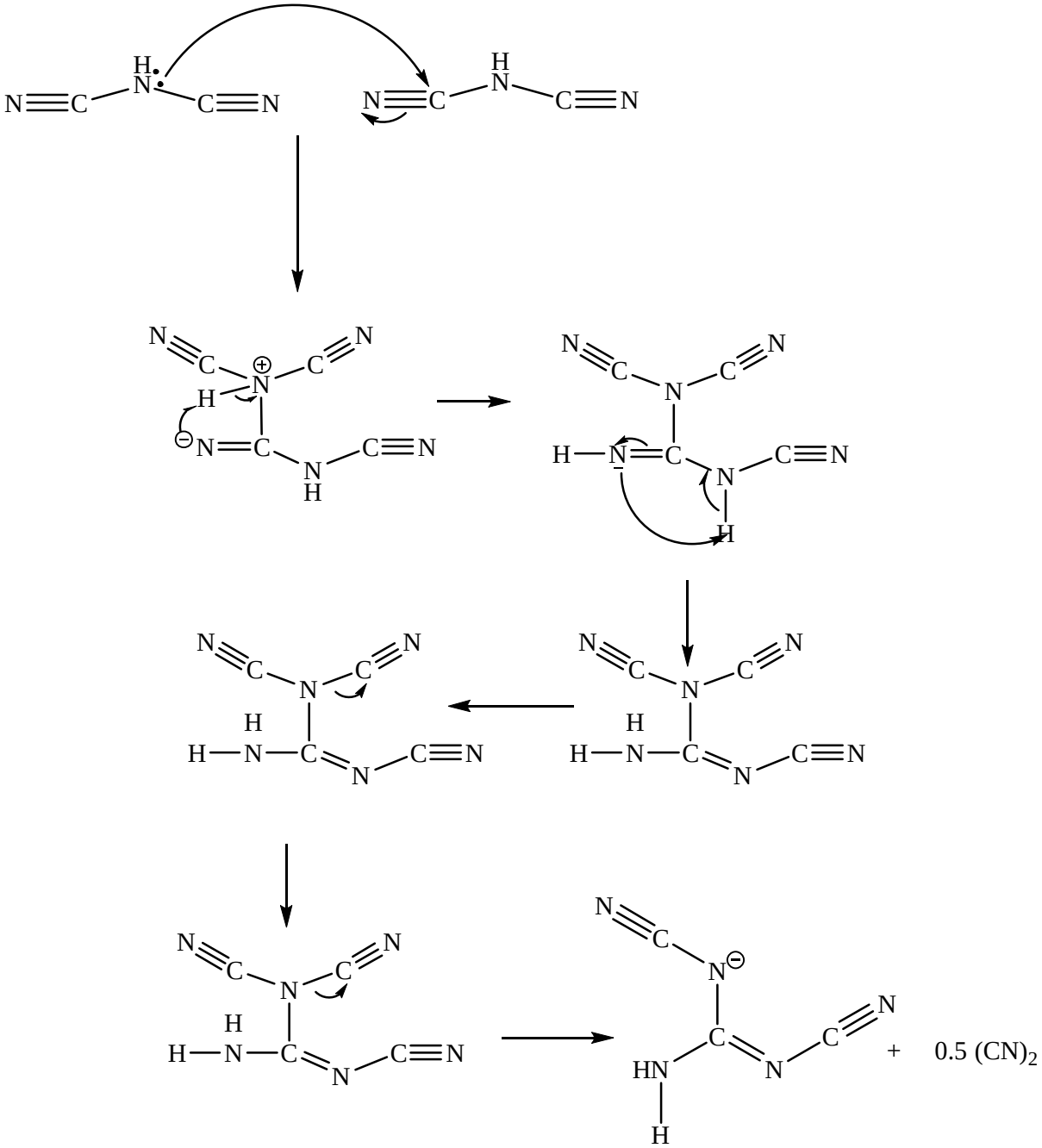

Scheme 9: Proposed Mechanism for the formation of N,N'-Dicyanoguanidinate anion from two dicyanamide anions [209, 320]

N,N'-dicyanoguanidine (dcg) is present in **5** as a counter anion. The molar conductance (Λ_M = 82.5 $ohm^{-1}cm^2mol^{-1}$) of **5**, measured at room temperature in DMSO, indicates that it is a 1:1 electrolyte [162]. N,N'-dicyanoguanidinate anion results from the nucleophilic reaction of two dca anions, with the subsequent elimination of the cyano group (Scheme 9). However, the mechanism is of the elimination of the cyano group leading to the dcg anion is unclear. Dicyanoguanidine (both in its neutral and anionic form) has been characterized in the literature [209].

3.11- Thermal Studies of the complexes

The thermal properties of the complexes were determined in both air and inert atmosphere at a heating rate of 10˚C/ min from 30 °C to 900 °C. Under air atmosphere, thermal gravimetric analysis (TGA) and differential scanning calorimetry (DSC) were carried out on the complexes primarily to determine the composition of materials, know their thermal stability and also to determine extent of weight loss or gain due to decomposition, oxidation or dehydration [132]. The thermal behaviours of the complexes in air are presented in Figures 50-53 and summarised in Table XXVI.

Table XXVI: Thermo-analytical data (TGA, DSC) in oxygen atmosphere of the complexes

Complex	Step	TGA			DTA	
		Temperature range (°C)	% Found (% Calc.).	Probable products	Peak temp./°C	Nature
1	I	340-450	89.68 (89.81)	2phen and $2NO_3$	380	Endothermic
		450-	10.32 (13.15)	MnO		
3	I	256-400	84.56	2phen and 2 dca	296	Endothermic
	II	400-650	(89.96)		520	Endothermic
		650-	15.44 (12.96)	MnO		
4	I	160-280	55.35 (55.56)	1phen and $1NO_3$	241	Endothermic
	II	280-555	16.29 (15.61)	BMCA	470	Endothermic
		555-	28.36 (21.91)	CuO_2		
5	I	279-325	13.11 (13.17)	H_2O and $1NO_3$	309	Endothermic
	II	325-542	75.89 (77.12)	2phen and dcg	436	Endothermic
		542-	11 (12.33)	CoO		

The TGA curve of **1** (Fig. 50) shows that it is stable up to 300 °C and decomposes in a single step, from 340 to 450 °C, with a mass loss of 89.68 % (Calc. 89.81 %) attributed to the decomposition of two phen molecules and two nitrates into some solid and a mixture of gaseous products. This step corresponds to a sharp endothermic DSC peak at 380°C. The composition of the residue (13.15 %) was calculated to be MnO_2 (Found 10.32 %) [241].

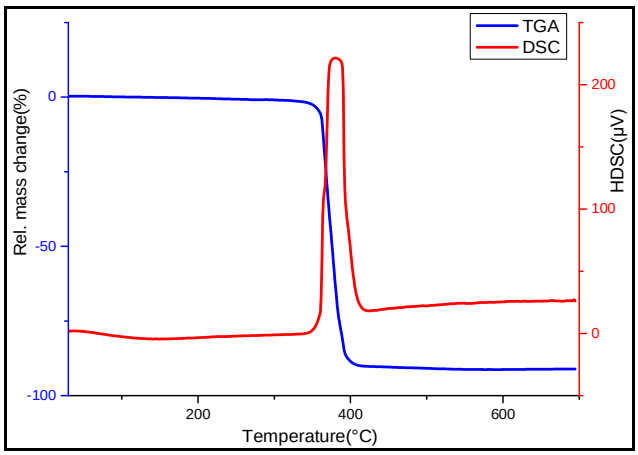

Figure 47: TGA-DSC Curves of **1**

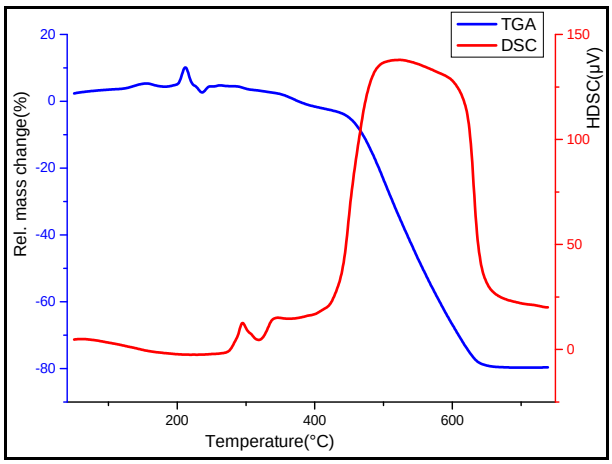

Figure 48: TGA-DSC Curves of **3**

The TGA curve of **3** (Fig. 51), shows that it is stable up to 180 °C. An oxidation process took place at 250 °C with an exothermic DSC peak at 210 °C. The thermogram displays two continuous steps decomposition from 250 °C to 650 °C, with a mass loss of 84.56 % (Calc. 89.96) assigned to the decomposition of two phen molecules and two dca ions into some solid and a mixture of gaseous products. This decomposition steps correspond to endothermic DSC peaks at 296 °C and 520 °C. The composition of the residue (12.96 %) was calculated to be MnO_2 (Found 10.32 %) [241].

The TGA curve of **4** (Fig. 52) displays that it is stable up to 241 °C and decomposes in the first step, from 160 °C to 280 °C with a mass loss of 55.35 % (calc. 55.56%) attributed to the decomposition of one molecule of phen and the nitrate ion into some solid and a mixture of gaseous products. In the last step, there is an endothermic mass loss of 16.29% (280–555 °C, calc. 15.61 %) attributed to the complete decomposition of organic residue at 470 °C. The composition of the residue (21.91 %) was calculated to be CuO_2 (Found 28.36 %) [132, 241].

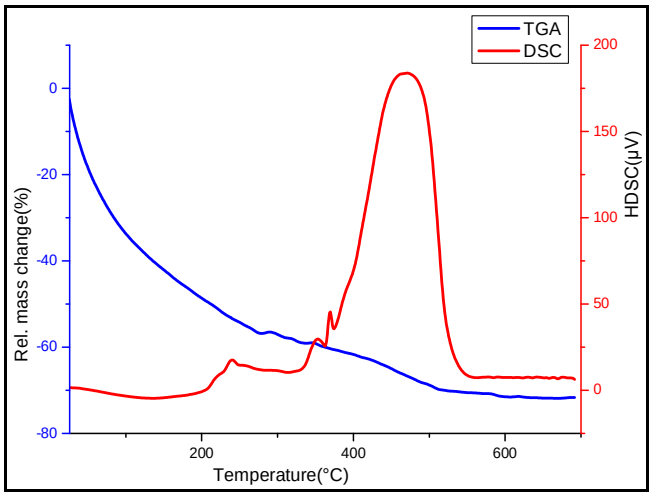

Figure 49: TG-DSC Curves of **4**

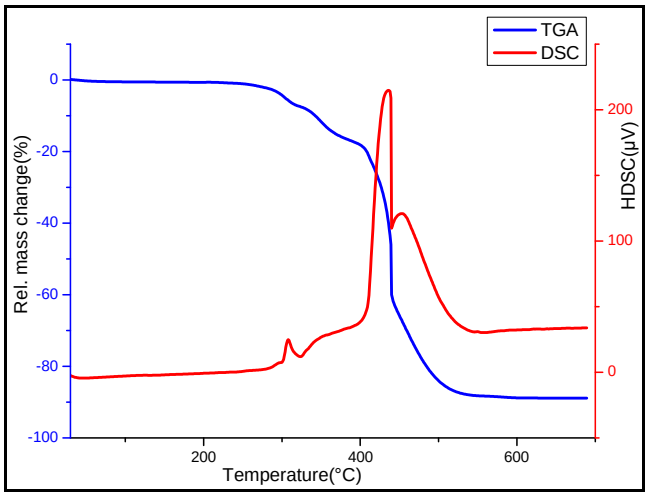

Figure 50: TG-DSC Curves of **5**

The TGA curve of **5** (Fig. 53) displays that it is stable up to 307 °C and decomposes in the first step, from 279°C to 325 °C with a mass loss of 13.11 % (calc. 13.17 %) attributed to the decomposition of one water molecule of crystallisation and nitrate ion. This step corresponds to a sharp and exothermic DSC peak at 436 °C. In the last step, there is an endothermic mass loss of 75.89 % (325–542 °C, calc. 77.12 %) attributed to the decomposition of the two molecules of the phen molecule and the dicyanoguanidinate (dcg) ion into a mixture of gaseous products. The composition of the residue (12.33 %) was calculated to be CoO (Found 11 %).

The thermal behaviour of the complexes under inert atmosphere was also investigated by TG-DTA.

The TG curve of **1** (Fig. 54) shows that it is stable up to 300 °C then decomposes in several steps. The first and major decomposition step is from 300 °C to 370 °C with a mass loss of 48.61 % is attributed to the decomposition of one phen ring and one nitrate into some solid and a mixture of gaseous products. This step corresponds to a sharp exothermic DTA peak at 370 °C. The second and third stages from 380–720 °C and 730–900 °C are weak mass loss processes considered to be further decomposition of the second nitrate with mass loss of 10.38 % (calculated 11.49 %). These two stages correspond to two exothermic peaks, one broad and one shallow in the DTA curve with peak temperatures 480 °C and 880 °C, respectively. The residual mass (41 %) is probably composed of Mn and nitrogen in a carbon residue.

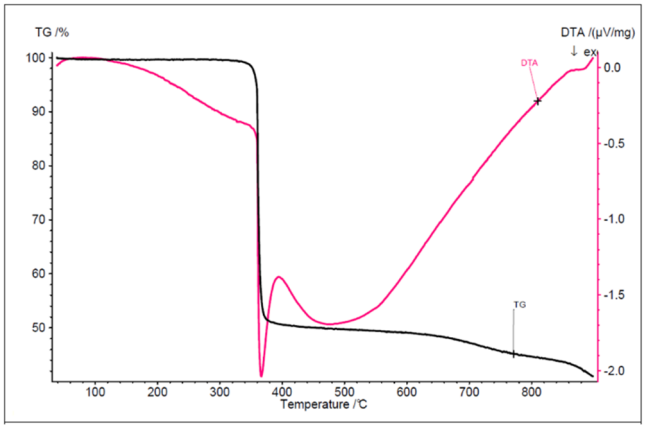

Figure 51: TG-DTA Curves of **1**

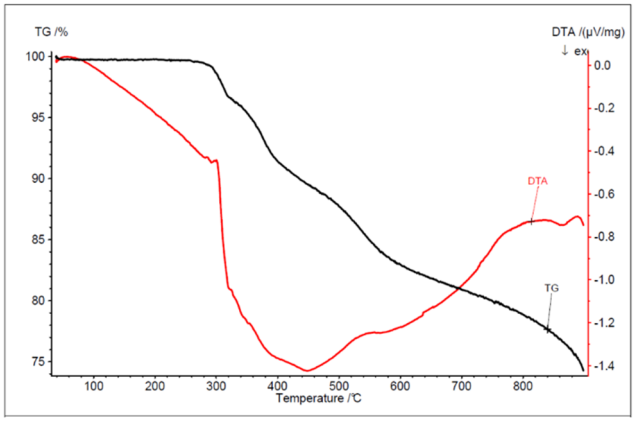

Figure 52: TG-DTA Curves of **3**

The TG curve of **3** (Fig. 55) shows that it stables up to 320 °C. The first decomposition step is endothermic, as shown on the DTA curve, followed by a series of decomposition steps from 330 to 600 °C with a cumulative mass loss of 17.10 %. This is attributed to partial decomposition of the solid. This corresponds to a broad exothermic peak in the DTA centred at 450 °C. The last decomposition step from 600 to 900 °C is another weak mass loss step 8.56 %, considered to be further decomposition of the product. The residual mass is 74.34 % indicating a high carbon content.

In **4** (Fig. 56), the TG curve displays the first endothermic oxidation at DTA = 252 °C with a mass loss of 43.25 % (190–340 °C, calc. 44.0 %) attributed to the release of the BMCA; {bis(methoxycarbimido)aminato} and the nitrate ions in the form of gases. The last stage (340–700 °C) is due to the complete endothermic decomposition of the remaining components $Cu(phen)^{2+}$ complex ion. The residue was analysed by PXRD indexed to a Cu phase, with Cu_2O impurity (Fig. 58) [132, 340, 341].

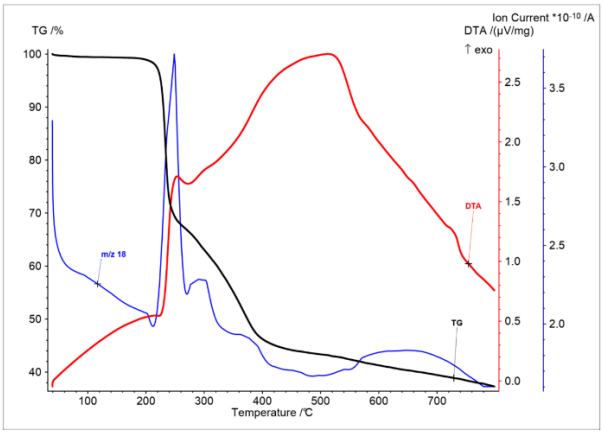

Figure 53: TG-DTA Curves of **4**

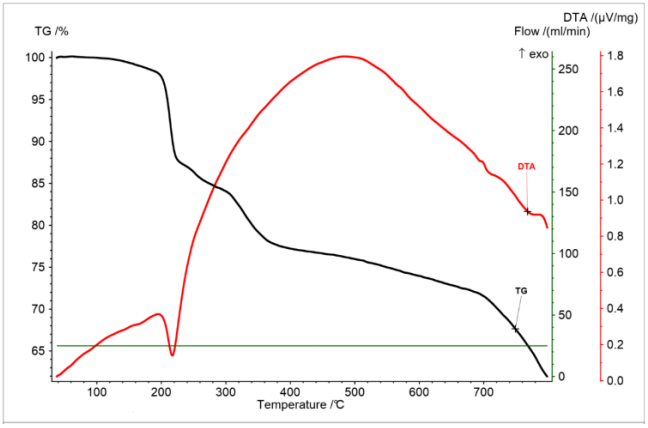

Figure 54: TG-DTA Curves of **5**

The TG curve of **5** (Fig. 57) displays the first exothermic DTA peak at 218 °C with weight loss: 12.28% (120–235 °C, calc. 13.17%) attributed to the release of the lattice water molecule and the nitrato ligand. The last step from 235-700°C, with an endothermic DTA peak at 470 °C, is due to the complete decomposition of $[Co(phen)_2(dcg^-)]^+$ complex ion. A black powder remains as final decomposition product. This indicates a high carbon content in the residue. Complexes **4** and **5** are very stable up to 200°C.

3.12- Powdered X-ray Diffraction of the decomposition product of 4

The composition of the TG residue from **4** was characterised by X-ray diffraction. Figure 58 shows the XRD plot. The PXRD pattern of the residue indicates that the residue is crystalline and a mixture of two phases. The residue has a well-defined diffraction pattern and matched well with the powder diffraction patterns of [04-0836] Cu phase and [05-0667] Cu_2O impurity [341]. The XRD plot clearly shows (111), (200) and (220) peaks for Cu phase [341-343].

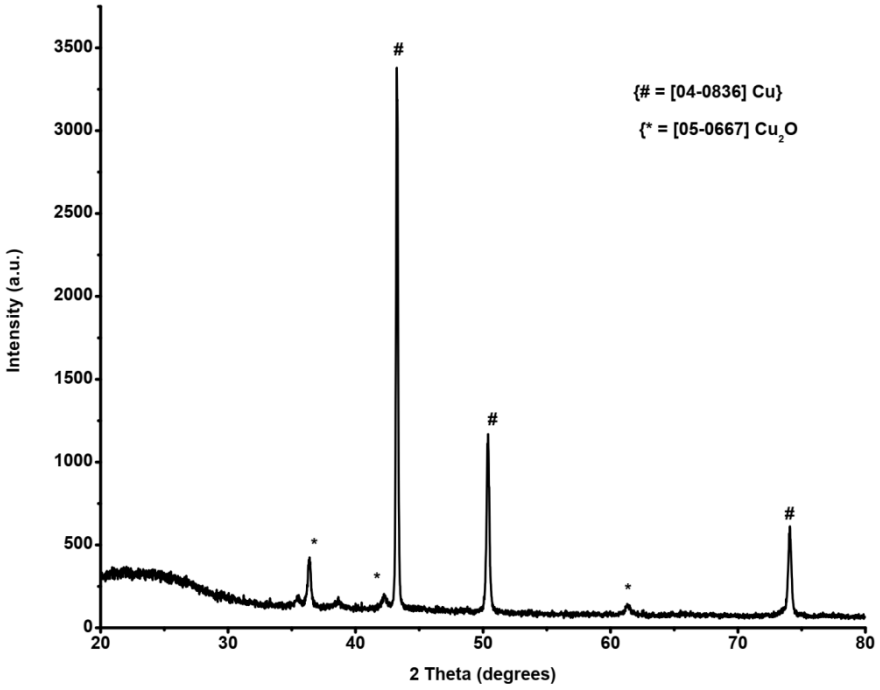

Figure 55: PXRD pattern of the residue of **4**

The high carbon content in the residue reduces the initially formed Cu(II) oxide through Cu(I) oxide to Cu metal as illustrated in equation (3.10).

$$CuO_{(s)} \xrightarrow{C_{(s)}} Cu_2O_{(s)} \xrightarrow{C_{(s)}} Cu_{(s)} \qquad (3.10)$$

3.13- Theoretical Calculations

The optimized geometries of **4** and **5** (Fig. 59) were obtained from DFT-B3LYP/6-31G(d,p) level of theory. The calculated and experimental bond lengths for **4** and **5** are presented in Table XXVII. The results show that, the deviation of calculated M-N (M = Co(II), Cu(II)), N-O and C-X (X=C, N and O) bond lengths are in the range 0.004-0.028 Å, except for O2-N5 where it is 0.079 Å. In the case of C-H bond lengths, the deviation is in the range 0.075-0.14 Å. The most important deviation 0.494 Å was obtained for the Co-O2 bond of **5**. The linear correlation between experimental and calculated bond lengths gave a regression coefficient of 0.979 and a standard deviation of 0.05 for **4** and 0.977 with 0.06 standard deviation for **5**. These results show that there is a good agreement between experimental and calculated geometries and thereby indicate that the used level of theory used is adequate to describe the properties of the concerned molecules.

Table XXVII: Experimental and calculated bond lengths (Å) of molecules **4** and **5**

5			**4**		
Bond	**Cal**	**Exp**	**Bond**	**Cal**	**Exp**
Co-O1	1,920	1,889	Cu-N1	1,978	2,003
Co-O2	2,384	1,890	Cu-N2	2,025	1,995
Co-N1	2,154	1,956	Cu-N3	1,890	1,894
Co-N2	1,939	1,938	Cu-N4	1,875	1,891
Co-N3	1,933	1,957	C1-C2	1,427	1,431
Co-N4	1,945	1,926	C1-C9	1,400	1,389
C1-C2	1,432	1,406	C2-C6	1,407	1,396
C1-C9	1,407	1,389	C3-C4	1,402	1,395
C2-C6	1,405	1,416	C4-C5	1,378	1,356
C3-C4	1,401	1,410	C5-C6	1,408	1,413
C4-C5	1,375	1,373	C6-C7	1,430	1,424
C5-C6	1,408	1,392	C7-C8	1,362	1,348
C6-C7	1,431	1,430	C8-C9	1,430	1,436
C7-C8	1,358	1,340	C9-C10	1,414	1,421
C8-C9	1,430	1,441	C10-C11	1,371	1,361
C9-C10	1,406	1,411	C11-C12	1,411	1,391
C13-C14	1,420	1,427	N3-H	1,015	0,720
C13-C21	1,401	1,404	N4-H	1,038	0,78
C14-C18	1,404	1,385	C4-H	1,085	0,95
C1O-C11	1,376	1,359	C5-H	1,088	0,87
C11-C12	1,403	1,394	C7-H	1,088	0,95
C16-C17	1,378	1,362	C8-H	1,088	0,87
C17-C18	1,407	1,420	C10-H	1,088	0,95
C18-C19	1,431	1,432	C11-H	1,086	0,85
C19-C20	1,361	1,365	C12-H	1,092	0,97
C20-C21	1,432	1,432	C13-H	1,095	0,97
C21-C22	1,410	1,397	C13-H	1,094	0,98
C22-C23	1,373	1,377	C13-H	1,092	0,96

C23-C24	1,405	1,406	C16-H	1,091	0,97
C15-C16	1,402	1,407	C16-H	1,095	1,02
C3-H3	1,087	0,950	C16-H	1,095	0,91
C4-H4	1,085	0,950	O3-N6	1,273	1,246
C5-H5	1,088	0,950	O4-N6	1,252	1,232
C7-H7	1,088	0,950	O5-N6	1,232	1,225
C8-H8	1,087	0,950	N1-C1	1,354	1,362
C10-H10	1,088	0,950	N1-C12	1,324	1,325
C11-H11	1,086	0,950	N2-C2	1,355	1,358
C12-H12	1,090	0,950	N2-C3	1,323	1,331
C15-H15	1,088	0,950	N3-C14	1,323	1,301
C16-H16	1,085	0,951	N4-C15	1,304	1,305
C17-H17	1,088	0,950	N5-C14	1,317	1,332
C24-H24	1,088	0,950	N5-C15	1,342	1,328
C20-H20	1,088	0,950	O1-C13	1,420	1,443
C19-H19	1,088	0,950	O1-C14	1,347	1,352
C22-H22	1,088	0,950	O2-C15	1,335	1,354
C23-H23	1,087	0,949	O2-C16	1,417	1,440
Ow-H2	0,960	0,94			
Ow-H3	0,978	1,00			
N10-H1	1,008	0,81			
N10-H2	1,010	0,81			
O1-N5	1,304	1,325			
O2-N5	1,247	1,326			
O3-N5	1,209	1,216			

Non-covalent interactions have been described using NCI index plot since it is able to reveal very weak interactions and to distinguish between attractive and repulsive interactions as well as strong and weak NCI [308, 309]. This plot (Fig. 60) represents the distribution of the electron density in the region of weak density (less than 0.05). The inspection of the NCI isosurface of molecule **4** indicates the presence of a moderate hydrogen bond between O3---H-N4 (1.872 Å /161.1°) and a weak hydrogen bond between O4---H11-C11 (2.035 Å/140.2°). Also, it reveals the presence of an attractive weak interaction (green surface) between O2 and C11. The QTAIM analysis of the molecular graph of this molecule (Fig. 61) shows the existence of bond critical point (BCP) for these three interactions and some of the parameters of these BCPs are presented in Table XXVIII. The values of the energy of these two interactions, their electron density, ρ (between 0.002-0.04 a.u.) and Laplacian of electron density, $\nabla^2\rho$ (between 0.024-0.139 a.u.) [344, 345] confirm their hydrogen bond character and that O3---H-N4 is stronger than O4---H11-C11.

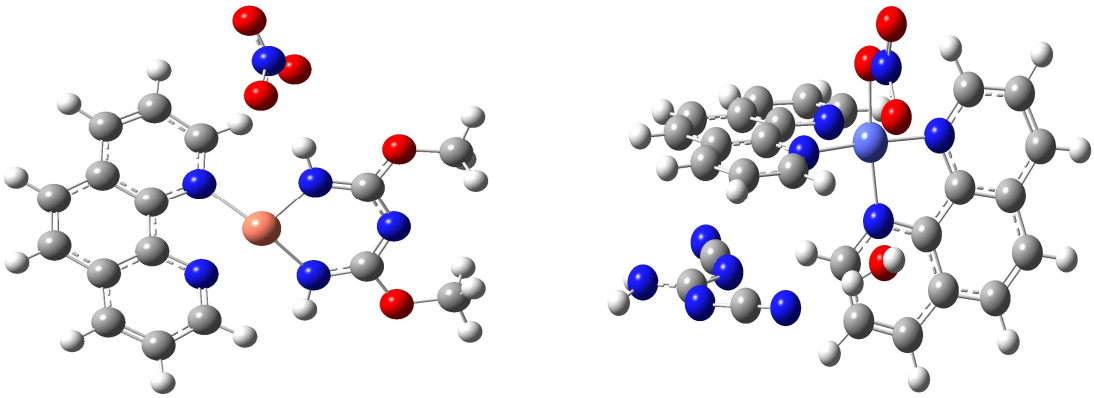

Figure 56: Optimized geometries of molecules **4** (left) and **5** (right)

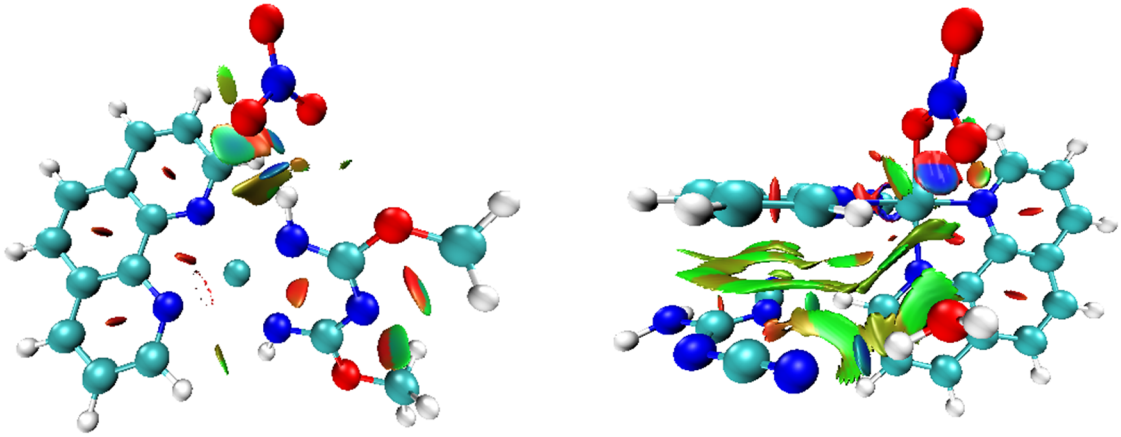

Figure 57: Plot of NCI isosurface for molecules of **4** (left) and **5** (right)

The blue region of these plots represents the strong attractive interactions (hydrogen bond), the green region indicates weak attractive interactions (van der Waals interactions and dispersing hydrogen bond) and the red region the strong repulsion interactions (steric effects).

Table XXVIII: Electron Density ρ(r) (a.u.), Laplacian of electron density $\nabla^2\rho(r)$ (a.u.), potential energy density V® (a.u.) and bond energy E_{HB} (kJ/mol) at the BCP of hydrogen bonds in the molecules

		ρ(r)	**∇^2 ρ(r)**	**V®**	**E_{HB}**
4	O3-HN4	0.03204	0.08784	-0,02388	-31
	O4-HC12	0.02468	0.07328	-0,01944	-26
5	CH----N	0.01660	0.04691	-0,01083	-14
	HOH---N	0.02846	0.08199	-0,01936	-25
	O2NO-Co	0.03548	0.13473	-0,04393	-58

The NCI plot of **5** (Fig. 60) indicates the presence of two hydrogen bonds N6---H-OH, (1.916/165.1°) and N8---H24-C24 (2,282 Å /142,6°) but the latter is very weak compared to the former. This plot also exhibits a very large green surface indicating the existence of many van der Waals interactions in this complex. These vans der Waals interactions are mostly found between the counter ion dca, the water molecule and the ligands. The QTAIM analysis of **4** reveals the presence of a BCP between N6---H-OH, and N8---H24-C24 and many others between the counter ion and the ligand.

Table XXIX: Most Relevant Vibrational Bands in the complexes and ligands

Compound	**Dca**	**Phen**	**4**	**Scaled**	**5**	**Scaled**
ν(C=N)		1586s	1600vs	1606.188 1614.981	1666vs	1607.165 1604.234
ν(C=C)		1501vs	1520s	1536	1514vs	1533
ν(C≡N)	2285vs 2229s 2173vs		2140s		2147vs 2178s	2231.468 2250.031
ν(N-H)			3275vs	3188.928 3499.614	3196m	
ν(NH2)					3492vs 3440vs	3514.269 3654.957
ν(N-O)			1751	1570.039	1758	1668.716
ν(C-O)			1046vs 1085vs	1087.401 1102.056		
γ(C-H) sp2 stretch		3057s	3064s 3017s	3106.86 3142.032	3196m 3064s	3083.412 3151.802
γ(C-H) sp3 stretch			2958s	2968.126 2974.965		
ν(M-N)			512m	638.958	551s	635.05 644.82

The values of the most relevant vibrational bands found in complexes **4** and **5** calculated at DFT-B3LYP/6-31G(d,p) level of theory are also presented in Table XXIX. The Gauss View 5.0.8 molecular visualization program was used to assign the calculated harmonic vibrational frequency bands. The theoretical values of the frequencies were scaled by a factor of 0.977 to reduce the basis set and method limitations to reproduce experimental vibrational frequencies. The theoretical spectrum of molecule **4** shows two absorption bands in the high frequency region (above 3000 cm^{-1}) assigned to the vibration of the two N-H bonds of dca. The lowest value 3189 cm^{-1} corresponds to the vibration of the N-H which is involved in N-H---O3

hydrogen bond. This value is lower than the experimental value probably because of the overestimation of the energy of N-H---O3 hydrogen bond by the level of theory as observed during geometry analysis. For the same reason, the calculated vibration frequency of N-O bond is also lower than the experimental value. The two bands observed in the region above 3000 cm^{-1} in the spectrum of molecule **5** corresponds to the symmetric (3514 cm^{-1}) and asymmetric (3655 cm^{-1}) N-H stretch. The harmonic frequency vibrations of C=N and N-O bonds obtained for molecule **5** are lower than the experimental values while the value of C---N is significantly higher. However, for most vibration frequencies of molecule **4**, there is a good agreement with experimental values. The shapes (drawn with Gauss View graphical interface software) and the distribution of the HOMO and LUMO of the complexes are shown in Figure 62.

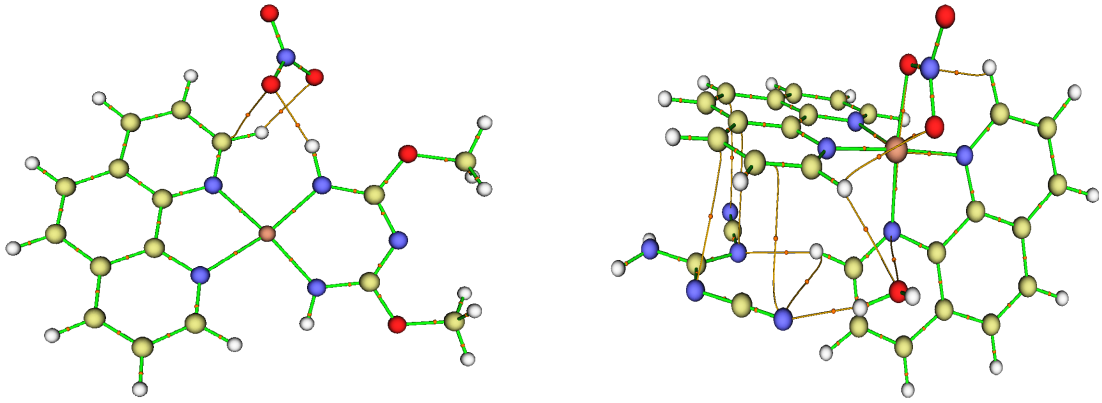

Figure 58: Molecular graph of molecules **4** and **5** plotted using VMD 1.9.2. The orange lines and spheres are bond paths and bond critical points respectively.

The HOMO of the two complexes are localized on the counter ions with mainly π-type orbitals. From the orbital composition analysis by Hirshfeld method, the oxygen of nitrate anion of **4** contributes up to 78% of the HOMO and in the case of **5**, the HOMO is composed of 78% of the atoms N6, N7, N8 and N9 and 16% C25, C26 and C27. The LUMO of **4** is localized on phen and copper atom and the Hirshfeld orbital composition analysis reveals that this orbital is composed of 12% of π*-type orbitals of the N5, 15% of d* orbital of Cu, and 60% of π*-type of carbon atoms of phen. However, the main contributors are C1 to C5. The π*-type orbital of N4 contributes only for 4% to the LUMO of **4**. The LUMO of **5** is also delocalized on the surface of phen and the π*-type orbital of carbon of phen involved, contribute for about 75% of this LUMO. The π*-type orbitals of N3 and N4 contribute for 4 and 14%, respectively which is practically the same in **4**. The contribution of d*-type orbitals of Co(II) ion to the LUMO of **5** is insignificant (3%). The distribution obtained by the isosurface is in agreement with the Hirshfeld orbital analysis composition.

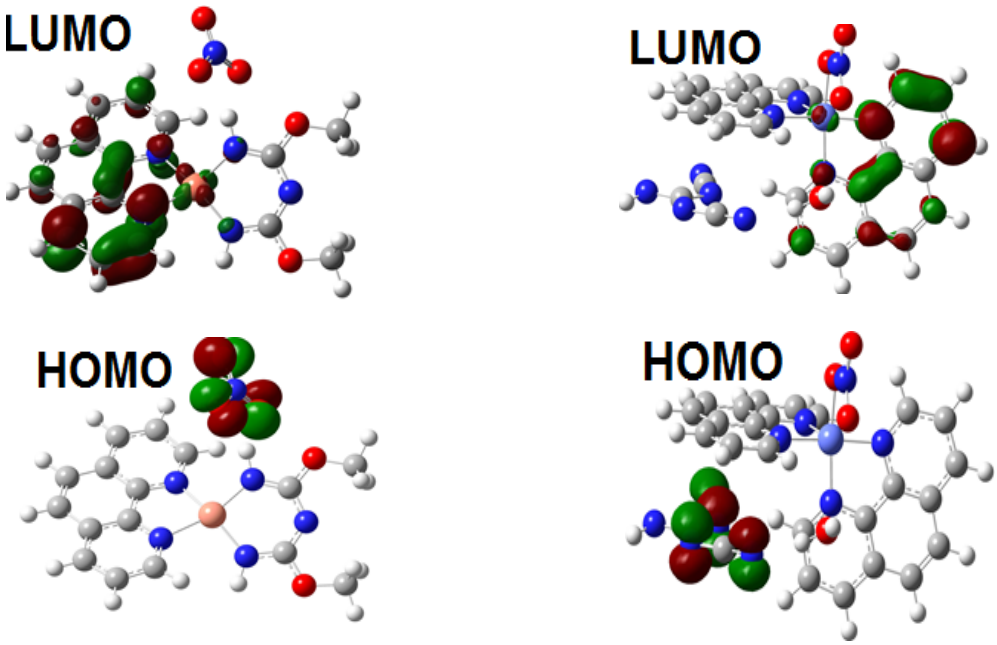

Figure 59: HOMO and LUMO of the complexes **4** (left) and **5** (right)

The energies of the HOMO and LUMO and the gap between the two orbitals for **4** and **5** are presented in Table XXX. The results indicate that **5** is more stable than **4**. This can be explained by the volume of the van der Waals interaction in molecule **5**. Since these are attractive interactions, they stabilize the concerned molecule.

Table XXX: Values of frontier molecular orbital energies (eV)

Complex	HOMO	LUMO	$\Delta E_{(LUMO-HOMO)}$
1	- 5.03	- 2.70	2.33
2	- 5.79	- 2.28	3.51

3.14- Antimicrobial Studies

The potency of the starting materials and the complexes together with the reference antibacterial drugs (amoxicillin, ciprofloxacin, and cloxacillin) and antifungal drug (fluconazole) were evaluated against twenty-three microorganisms comprised of twenty bacteria and three fungi strains. The susceptibility of the bacterial and fungal strains towards these compounds was judged by measuring the size of the growth inhibition diameter (IZ). Compounds, which showed significant activities (IZ > 6 mm), were used for the minimum inhibitory concentration (MIC) test. The MIC values are presented in Table XXXI and summarized in histograms (Fig. 59); (MIC>500 µg/mL poor activity; 250<MIC>125 µg/mL moderate activity; 62.5<MIC>31.25 µg/mL good activity; MIC<31.25 µg/mL very good activity). While the

simple metal salts and the co-ligand dca, were not able to effectively reduce the bacterial and fungal cell proliferation, phen exhibited good inhibitory capability which is in agreement with results obtained from other studies [61, 346].

Complex **1** possesses very good activity against most of the bacteria species with MIC values 15.625 and 31.25 µg/mL, while complexes **2** and **3** are very active against the fungi species with MIC values in the range 7.8–15.6 µg/mL. However, all of these complexes **1**-**3** displayed comparable as well as average antibacterial activities compared to the standard antibacterial (amoxicillin, ciprofloxacin and cloxacillin) but higher antifungal activities as compared to the reference antifungal (fluconazole). Complexes **4** and **5** displayed poor antifungal activities as compared to the reference antifungal (fluconazole) but higher antibacterial activities as compared to the antibiotic (cloxacillin). These activities are comparable to literature reports [76, 347].

Table XXXI: Minimum Inhibitory Concentration (μg/mL) values of the ligands and complexes

Microbes	dca	Phen.	1	2	3	4	5	Amoxicillin	Ciprofloxacin	Cloxacillin	Fluconazole
B1	**>500**	**31.25**	**31.25**	**125**	**250**	**125**	**62.5**	**>32**	**8**	**64**	**/**
B2	**>500**	**7.8125**	**15.625**	**125**	**250**	**125**	**125**	**0.25**	**8**	**4**	**/**
B3	**>500**	**31.25**	**31.25**	**125**	**125**	**62.5**	**62.5**	**>32**	**2**	**64**	**/**
B4	**>500**	**31.25**	**62.5**	**125**	**250**	**62.5**	**6.25**	**0.25**	**1**	**1**	**/**
B5	**>500**	**62.5**	**62.5**	**125**	**250**	**> 500**	**500**	**>32**	**32**	**64**	**/**
B6	**>500**	**31.25**	**31.25**	**125**	**125**	**62.5**	**62.5**	**>32**	**4**	**>64**	**/**
B7	**>500**	**31.25**	**31.25**	**125**	**250**	**250**	**125**	**8**	**16**	**16**	**/**
B8	**>500**	**31.25**	**31.25**	**125**	**250**	**500**	**500**	**>32**	**8**	**32**	**/**
B9	**>500**	**31.25**	**15.625**	**125**	**250**	**> 500**	**250**	**>32**	**4**	**16**	**/**
B10	**>500**	**31.25**	**31.25**	**125**	**250**	**> 500**	**250**	**>32**	**10**	**64**	**/**
B11	**>500**	**31.25**	**31.25**	**125**	**250**	**500**	**500**	**>32**	**4**	**64**	**/**
B12	**>500**	**62.5**	**31.25**	**125**	**250**	**250**	**125**	**16**	**4**	**4**	**/**
B13	**>500**	**62.5**	**31.25**	**250**	**250**	**250**	**125**	**>32**	**4**	**>64**	**/**
B14	**>500**	**62.5**	**31.25**	**125**	**250**	**> 500**	**250**	**>32**	**4**	**4**	**/**
B15	**>500**	**31.25**	**62.5**	**125**	**250**	**125**	**125**	**0.25**	**4**	**8**	**/**
B16	**>500**	**31.25**	**62.5**	**125**	**500**	**125**	**125**	**>32**	**32**	**>64**	**/**
B17	**>500**	**15.625**	**15.625**	**125**	**500**	**500**	**125**	**>32**	**4**	**4**	**/**

Microbes	dca	Phen.	1	2	3	4	5	Amoxicillin	Ciprofloxacin	Cloxacillin	Fluconazole
B18	**>500**	**15.63**	**31.5**	**125**	**250**	**250**	**125**	**0.5**	**4**	**8**	**/**
B19	**>500**	**31.25**	**62.5**	**250**	**500**	**250**	**62.5**	**>32**	**4**	**16**	**/**
B20	**>500**	**15.625**	**15.625**	**250**	**250**	**250**	**250**	**8**	**8**	**8**	**/**
CA	**>500**	**7.8125**	**62.5**	**7.8125**	**15.625**	**> 500**	**> 500**	**/**		**>500**	**32**
CK	**>500**	**15.625**	**62.5**	**7.8125**	**15.625**	**> 500**	**> 500**	**/**		**>500**	**32**
CP	**>500**	**15.625**	**125**	**7.8125**	**15.625**	**> 500**	**> 500**	**/**		**>500**	**32**

Note**:** B1 = *Streptococcus pneumonae* ATCC49619;

B2 = *Staphylococcus aureus* BAA917;

B3 = *Staphylococcus aureus* ATCC43300;

B4 = *Staphylococcus aureus* NR45003;

B5 = *Staphylococcus aureus* NR46003;

B6 = *Staphylococcus aureus* CP7625;

B7 = *Shigella flexineri* NR518;

B8 = *Salmonella enterica* NR4294;

B9 = *Salmonella enterica* NR4311;

B10 = *Salmonella enterica* NR13555;

B11 = *Pseudomonas aeruginosa* NMC592;

B12 = *Klessiella pneumonae* ATCC13883;

B13 = *Klessiella pneumonae* ATCC70603;

B14 = *Klessiella pneumonae* NR41916;

B15 = *Escherishia coli* ATCC25922;

B16 = *Escherishia coli* ATCC35218;

B17 = *Enterococcus fecalis* ATCC51219;

B18 = *Staphylococcus aureus* NR46374;

B19 = *Hemophyllus influenza* ATCC49247;

B20 = *Mycobacterium smegmatis*;

Fungi strains: CK = *Candida krusei*; CP = *Candida parasilosis*; CA = *Candida albicans*

Figure 60: Histogram of MIC against tested microorganism

Complex **1** was the most active and it showed very good activity (MIC 15.625 µg/mL) against the bacteria species *Staphylococcus aureus* BAA917, *Salmonella enterica* NR4311, *Enterococcus fecalis* ATCC51219 and *Mycobacterium smegmatis*. Complex **1** showed good activity (62.5<MIC>31.25 µg/mL) against the bacteria species *Streptococcus pneumonae* ATCC49619, *Staphylococcus aureus* ATCC43300, *Staphylococcus aureus* NR46003, *Salmonella enterica* NR13555, *Pseudomonas aeruginosa* NMC592, *Klessiella pneumonae* ATCC70603, *Klessiella pneumonae* NR41916, *Escherishia coli* ATCC35218 and *Enterococcus fecalis* ATCC51219 as compared to the reference antibacterial (amoxicillin and cloxacillin). The complexes **2** and **3** exhibited very good activity against the fungi species *Candida krusei*, *Candida parasilosis* and *Candida albicans*, as compared to the reference antifungal and but showed poor antibacterial activity comparable to the reference antibiotic. Complexes **4** and **5** possess good activity against (62.5<MIC>31.25 µg/mL) *Staphylococcus aureus* ATCC43300 and B6 = *Staphylococcus aureus* CP7625 as compared to the antibiotic cloxacillin. Complex **5** possesses good activity against *Streptococcus pneumonae* ATCC49619 with MIC value 62.5 µg/mL.

The increased activity of the metal complexes can be explained based on the chelation theory and overtones concept. This indicates that reaction of metal ions with the ligands plays an important role in enhancing its antimicrobial activity. This enhancement of the metal complex activity can also be explained on the basis of chelation theory [48]. Chelation reduces the polarity of the metal atom mainly because of partial sharing of its positive charge with the donor groups and possible π-electron delocalization within the whole chelate ring. Such a chelation also enhances the lipophilic character of the central metal atom, which subsequently favours its permeation through the lipid layers of the cell membrane and the blocking of the metal binding sites on enzymes of microorganism [347]. The overall positive results of the antimicrobial screening against the twenty-three pathogens suggest that the complexes have a broad spectrum of activity and may represent a good candidate as an antimicrobial agent.

CONCLUSION AND PERSPECTIVES

CONCLUSION

Five new complexes $[Mn(Phen)_2(NO_3)_2]$ (**1**), $[Mn(Phen)_2(N_3)_2)]$ (**2**), $[Mn(Phen)_2(dca)_2)]$ (**3**), $[Cu(Phen)(BMCA)]\cdot NO_3$ (**4**); {BMCA = bis(methoxycarbimido)aminato anion and phen=1,10-phenanthroline} and $[Co(phen)_2(NO_3)](dcg^-)]\cdot(H_2O)$ (**5**); (dcg=dicyanoguanidinate anion) were synthesised, characterized and their biological properties were studied. The magnetic moments at room temperature for the Mn(II) complexes were found to be consistent with high spin (d^5) octahedral geometry. The magnetic moment of the $[Cu(Phen)(BMCA)]\cdot NO_3$ complex was found to be 1.75 B.M. which corresponds to one unpaired electron. It was slightly greater than the spin only value of 1.73 B.M for copper(II) that is expected for one unpaired electron. The magnetic moment of $[Co(phen)_2(NO_3)](dcg\text{-})]\cdot(H_2O)$ complex was 3.92 B.M. which is in good agreement with high spin (d^7) octahedral geometry for Co(II). Thermal analyses of the complexes in air indicate that they are stable up to 200 °C. The $[Mn(Phen)_2(NO_3)_2]$ complex; [dinitrato-bis(1,10-phenanthroline-κ^2*N*,*N*')manganese(II)] crystallizes in the orthorhombic crystal system with space group *Pbcn* with four molecules in the unit cell. The $[Mn(Phen)_2(N_3)_2)]$ complex; [diazido-bis(1,10-phen-κ^2N,N′)manganese(II)] crystallizes in the orthorhombic crystal system with space group *Pbcn* with four molecules in the unit cell. The $[Mn(Phen)_2(dca)_2)]$ complex; bis(dicyanamido)bis(1,10-phenanthroline)manganese(II), crystallizes in the monoclinic crystal system with space group $P2_1/c$ with four molecules in the unit cell. Distorted octahedral geometries were confirmed for all the Mn(II) complexes through single-crystal X-ray crystallographic techniques. Cooperation between C–H···O or C–H···N hydrogen bonds between adjacent phen ligands, and π–π stacking interactions stabilize the structures and assemble them into interesting 3D supramolecular structures. The $[Cu(Phen)(BMCA)]\cdot NO_3$ complex; [{bis(methoxycarbimido)aminato-κ^2N,N'}(1,10-phenanthroline-κ^2N,N')copper(II)] crystallizes in the monoclinic crystal system with space group *P21/c* with completely distorted square planar CuN_4 chromophores. The $[Co(phen)_2(NO_3)](dcg\text{-})]\cdot(H_2O)$ complex; [(nitrato-κ^2O,O')(1,10-phenanthroline-κ^2N,N')cobalt(II)] dicyanoguanidinate crystallizes in the monoclinic crystal system with elongated octahedral CoO_2N_4 chromophores. The distorted octahedral of Co(II) ions in the title complex can be explained by Jahn–Teller effect for the d^7 configuration as confirmed by the high spin magnetic moment. Metal-mediated transformations of the dca ligand were observed. The Cu-mediated transformation of dca led to BMCA while that of Co led to dcg. Both reactions are nucleophilic. The packing in the unit cell of both complexes were based on intermolecular hydrogen bonding and π–π stacking interactions extending them to interesting 3D supramolecular structures. The Mn(II) complexes (**1-3)** displayed comparable as well as average antibacterial activities compared to the standard antibacterials (amoxicillin, ciprofloxacin and cloxacillin) but higher antifungal activities as compared to the antifungals (fluconazole). The Cu(II)

and Co(II) complexes (**4** and **5** respectively**)** displayed poor antifungal activities as compared to the standard antifungals (fluconazole) but higher antibacterial activities as compared to the antibiotic (cloxacillin). The $[Mn(Phen)_2(NO_3)_2]$ complex was the most active and it showed very good activity (MIC 15.625 µg/mL) against the bacteria species *Staphylococcus aureus* BAA917, *Salmonella enterica* NR4311, *Enterococcus fecalis* ATCC51219 and *Mycobacterium smegmatis.* The $[Mn(Phen)_2(NO_3)_2]$ complex also showed good activity (62.5<MIC>31.25 µg/mL) against the bacteria species *Streptococcus pneumonae* ATCC49619, *Staphylococcus aureus* ATCC43300, *Staphylococcus aureus* NR46003, *Salmonella enterica* NR13555, *Pseudomonas aeruginosa* NMC592, *Klessiella pneumonae* ATCC70603, *Klessiella pneumonae* NR41916, *Escherishia coli* ATCC35218 and *Enterococcus fecalis* ATCC51219 as compared to the reference antifungal (amoxicillin or cloxacillin). The $[Mn(Phen)_2(N_3)_2)]$ and $[Mn(Phen)_2(dca)_2)]$ complexes exhibited very good activity against the fungi species *Candida krusei*, *Candida parasilosis* and *Candida albicans*, as compared to the reference antifungal but showed poor antibacterial activity compared to the reference antibiotic. The $Cu(Phen)(BMCA)]\cdot NO_3$ and $[Co(phen)_2(NO_3)](dcg^-)]\cdot(H_2O)$ complexes possess good activity against (62.5<MIC>31.25 µg/mL) *Staphylococcus aureus* ATCC43300 and B6 = *Staphylococcus aureus* CP7625 as compared to the antibiotic cloxacillin. The $[Co(phen)_2(NO_3)](dcg-)]\cdot(H_2O)$ complex possesses good activity against *Streptococcus pneumonae* ATCC49619 with MIC value 62.5 µg/mL.

PERSPECTIVES

Though the immediate objectives of this work have been met, we recognise that it is not exhaustive as we envisage to:

- Carry out temperature dependence magnetic susceptibility measurement on the complexes at lower temperature range of 2-300 K.
- Use molecular docking to elucidate the mode of action/inhibition of the complexes in view of understanding the molecular mechanism for their action.
- Determine the toxicity of complexes that are found to be more active than the reference drugs.

This will not only improve the quality of this work but will also serve as directions for further research.

REFERENCES

REFERENCES

1. Chimaine FT, Yufanyi DM, Amah C, Eni DB, Agwara MO: **Synthesis , Crystal Structure , Photoluminescent and Antimicrobial Properties of a Thiocyanato- bridged Copper(II) Coordination Polymer**. *Cogent Chemistry* 2016, **47**:1-14.
2. Tabong CD, Yufanyi DM, Paboudam AG, Nono KN, Eni DB, Agwara MO: **Synthesis, Crystal Structure, and Antimicrobial Properties of [Diaquabis(hexamethylenetetramine) diisothiocyanato-kN] nickel(II) Complex**. *Advances in Chemistry* 2016, **2016**:1-8.
3. Zhang Y, Li J, Nishiura M, Imamoto T: **Structural, Spectral and Thermal Properties of a Polymeric Nickel(II) Complex containing Two-dimensional Network**. *Journal of Molecular Structure* 2000, **520**(1-3):259-263.
4. Yang Y-S, Liu M, Yang Y-P, Jin Q-H, Li Z-F, Xue X-N, Zhang Z-J, Zheng W-J: **Synthesis, structures, luminescence and terahertz time-domain spectroscopy of seven lanthanide complexes with tetrakis (O-isopropyl)methylenediphosphonate and 1,10-phenanthroline**. *Polyhedron* 2015, **93**:66-75.
5. Atamba AM, Agwara MO, Yufanyi DM, Tabong CD, Amah C: **Synthesis, Characterisation and Antimicrobial Properties of some Transition Metal Complexes of 4,4'-Bipyridine**. *International Journal of Current Research in Chemistry and Pharmaceutical Sciences* 2014, **1**(6):101-107.
6. Sutradhar M, Silva MGD, Nesterov DS, Jezierska J, Pombeiro AJL: **1D coordination polymer with octahedral and square-planar nickel(II) centers**. *Inorganic Chemistry Communications* 2013, **29**:82-84.
7. Fang S-M, Ma S-T, Guo L-Q, Zhang Q, Hu M, Zhou L-M, Gao L-J, Liu C-S: **A photoluminescent 3D silver(I) polymer with mixed 2-naphthol-5-carboxylate and hexamethylenetetramine ligands, showing an unusual (3,4)-connected $(6\cdot7\cdot8)_2(4\cdot6\cdot7)_2(4\cdot7\cdot8)_2(7^2\cdot8)_2(6^2\cdot7\cdot8^3)(6^2\cdot7^2\cdot8\cdot10)$ topology**. *Inorganic Chemistry Communications* 2010, **13**(1):139-144.
8. Hazra S, Sarkar B, Naiya S, Drew GBM, Ribas J, Diaz C, Ghosh A: **A self-assembled non-interpenetrating cubic diamondoid coordination polymer of hexamine with linear dicopper spacer: Structural and magnetic studies**. *Inorganic Chemistry Communications* 2011, **14**(12):1860-1863.
9. Terma S, Kompleks D: **Synthesis, Characterization and Thermal Properties of Two Novel Lanthanide 2,2'-Biquinoline-4,4'-Dicarboxylate Complexes**. *Sains Malaysiana* 2011, **40**(9):999-1006.

10. Tanke CE, Ndosiri NB, Mbiangué YA, Bebga G, Nenwa J: **Synthesis, Characterization and X-Ray Structure of a Ba(II)/Ag(I)/Cr(III)-Oxalate Salt with Water-Filled Nanochannels**. *American Journal of Analytical Chemistry* 2016, **7**(1):99-106.
11. Abedi M, Kirschbaum K, Shamkhali AN, Brue CR, Khandar AA: **Synthesis, characterization and crystal structure of dinuclear cobalt(II) macrocyclic complexes, containing thiocyanate and azide groups**. *Polyhedron* 2016, **109**:176-181.
12. Abu-Youssef MA, Mautner FA, Vicente R: **1D and 2D end-to-end azide-bridged cobalt(II) complexes: Syntheses, crystal structures, and magnetic properties**. *Inorganic Chemistry* 2007, **46**(11):4654-4659.
13. Han XY, Ren YT, Zheng YQ: **Syntheses, crystal structures and magnetic properties of two adamantane-1,3-dicarboxylato bridged cobalt(II) phenanthroline complexes**. *Inorganica Chimica Acta* 2010, **363**(2):353–359.
14. Tabrizi L, Chiniforoshan H, McArdle P: **A novel one-dimensional manganese(II) coordination polymer containing both dicyanamide and pyrazinamide ligands: Synthesis, spectroscopic investigations, X-ray studies and evaluation of biological activities**. *Spectrochimica Acta Part A: Molecular and Biomolecular Spectroscopy* 2015, **139**:307-312.
15. Qiu S, Zhu G: **Molecular engineering for synthesizing novel structures of metal-organic frameworks with multifunctional properties**. *Coordination Chemistry Reviews* 2009, **253**(23-24):2891-2911.
16. Batten SR: **Coordination polymers**. *Current Opinion in Solid State & Materials Science* 2001, **5**:107-114.
17. Sotnikova Y, Lukovskaya E, Bobylyova A, Fedorov Y, Novikov V, Peregudov A, Anisimov A, D'Aléo A, Fages F, Fedorova O: **Cation-dependent structural diversity of zinc(II), calcium(II) mono- and binuclear complexes of aryl-imidazo-1,10-phenanthroline derivatives**. *Inorganica Chimica Acta* 2016, **445**:103-109.
18. Manigandan R, Giribabu K, Suresh R, Vijayalakshmi L, Stephen A, Narayanan V: **Cobalt Oxide Nanoparticles: Characterization and its Electrocatalytic Activity towards Nitrobenzene**. *Chemical Science* 2013, **2**(s1):47-50.
19. Liu CS, Chang Z, Wang JJ, Yan LF, Bu XH, Batten SR: **A photoluminescent 3D silver(I) coordination polymer with mixed ligands anthracene-9,10-dicarboxylate and hexamethylenetetramine, showing binodal 4-connected $(4^3.6^3)^2(4^2.6^{2.}8^2)_3$ topology**. *Inorganic Chemistry Communications* 2008, **11**(8):889-892.
20. Zheng SL, Zhang JP, Chen XM, Seik-Weng N: **Effect of synthetic conditions on the structures of silver(I)-hexamethylenetetramine coordination polymers: Crystal**

structures of two three-dimensional frameworks featuring new topological motifs. *Journal of Solid State Chemistry* 2003, **172**(1):45-52.

21. Tabrizi L, Chiniforoshan H, Araújo JP, Lopes AM, Görls H, Plass W, Mohammadnezhad G: **New 3D dicyanamide bridged coordination polymer of Ni(II): Synthesis, crystal structure, magnetic properties and antibacterial assay**. *Inorganica Chimica Acta* 2015, **426**:195-201.
22. Champness NR, Schroder M: **Extended networks formed by coordination polymers in the solid state**. *Current Opinion in Solid State & Materials Science* 1998, **3**(4):419-424.
23. Braga D, Grepioni F: **Organometallic crystal engineering: prospects for a systematic design**. *Coordination Chemistry Reviews* 1999, **183**(1):19-41.
24. Hugas D, Guillaumes L, Duran M, Simon S: **Delocalization indices for non-covalent interaction: Hydrogen and DiHydrogen bond**. *Computational and Theoretical Chemistry* 2012, **998**:113-119.
25. Chahkandi M: **Theoretical investigation of non-covalent interactions and spectroscopic properties of a new mixed-ligand Co(II) complex**. *Journal of Molecular Structure* 2016, **1111**:193-200.
26. Zhu J-L, Li J, Wang M, Jiang G-Q, Jiang G-M: **Crystal structure of aquabis[4-(methylsulfanyl)benzoato-κO](1,10-phenanthroline-κ^2N,N′)copper(II) monohydrate**. *Acta Crystallographica Section E: Crystallographic Communications* 2015, **71**(8):980-982.
27. Frost BJ, Wei-Chih L, Pal K, Kim TH, Derveer DV, Rabinovich D: **Synthesis, structure, and coordination chemistry of OPTA and SPTA with group 12 metals (PTA=1,3,5-triaza-7-phosphaadamantane)**. *Polyhedron* 2010, **29**(11):2373-2380.
28. Wu H, Dong XW, Liu HY, Ma JF, Liu YY, Liu YY, Yang J: **Construction of a series of inorganic-organic hybrid coordination polymers based on hexamethylenetetramine and sulfonate ligands**. *Inorganica Chimica Acta* 2011, **373**(1):19-26.
29. Ji X, Cui L, Xu Y, Liu J: **Non-covalent interactions for synthesis of new graphene based composites**. *Composites Science and Technology* 2015, **106**:25-31.
30. Banerjee S, Choudhury AR, Row TG, Chaudhuri S, Ghosh A: **Three-dimensional supramolecular H-bonding network in the compounds containing hexamethylenetetramine and aquated Ni(II) or Cd(II) salts**. *Polyhedron* 2007, **26**(1):24-32.
31. Dalai S: **Coordination Polymers**. *Journal of Physical Science* 2011, **15**:223-230.

32. Hua M, Zhang S, Pan B, Zhang W, Lu L, Zhang Q: **Heavy metal removal from water/wastewater by nanosized metal oxides: A review**. *Journal of Hazardous Materials* 2012, **211-212**:317-331.

33. Zhu XH, Hang QM: **Microscopical and physical characterization of microwave and microwave-hydrothermal synthesis products**. *Micron* 2013, **44**(1):21-44.

34. Pena-Pereira F, Duarte RM, Duarte AC: **Immobilization strategies and analytical applications for metallic and metal-oxide nanomaterials on surfaces**. *Trends in Analytical Chemistry* 2012, **40**:90-105.

35. Ribas J, Escuer A, Monfort M, Vicente R, Cortes R, Lezama L, Rojo T: **Polynuclear Ni(II) and Mn(II) azido bridging complexes. Structural trends and magnetic behavior**. *Coordination Chemistry Reviews* 1999, **193-195**:1027-1068.

36. Mahmudov KT, Kopylovich MN, Guedes-da-Silva MF, Pombeiro AJ: **Non-covalent interactions in the synthesis of coordination compounds: Recent advances**. *Coordination Chemistry Reviews* 2016:1-19.

37. Weng W, Fang X, Zhang H, Peng H, Lin Y, Chen Y: **Multiresponsive supramolecular gels constructed by orthogonal metal-ligand coordination and hydrogen bonding**. *European Polymer Journal* 2013, **49**(12):4062-4071.

38. Pook N-P, Hentrich P, Gjikaj M: **Crystal structure of bis[tris(1,10-phenanthroline-κ^2N,N′)cobalt(II)] tetranitrate N,N ’-(1,4-phenylenedicarbonyl)diglycine solvate octahydrate**. *Acta Crystallographica Section E: Crystallographic Communications* 2015, **71**(8):910-914.

39. Jin S, Zhang H, Zhao Y, Jin L, Ye X, Liu H, Wang D: **Seven supramolecular frameworks constructed from combination of hydrogen-bonds and other non-covalent associations between organic acids and bis-imidazoles**. *Journal of Molecular Structure* 2015, **1099**:304-316.

40. Su P, Chen Z, Wu W: **An energy decomposition analysis study for intramolecular non-covalent interaction**. *Chemical Physics Letters* 2015, **635**:250-256.

41. Tripuramallu BK: **Mutual interplay of non-covalent interactions in modulating the geometry of organic linkers in their salts**. *Journal of Molecular Structure* 2014, **1071**(1):79-87.

42. Schneider C, Leung E, Brown J, Tollervey D: **The N-terminal PIN domain of the exosome subunit Rrp44 harbors endonuclease activity and tethers Rrp44 to the yeast core exosome**. *Nucleic Acids Research* 2009, **37**(4):1127–1140.

43. Saleh G, Gatti C, Presti LL: **Energetics of non-covalent interactions from electron and energy density distributions**. *Computational and Theoretical Chemistry* 2015, **1053**:53-59.
44. Degagsa B, Faye G, Fernandez N, Faye G, Faye G: **Synthesis, Characterization and Antimicrobial Activity of Hexamethylenetetramine copper(II) Complex**. *Journal of Pharmacy and Pharmaceutical Sciences* 2013, **2**(6):6391-6404.
45. Ndifon PT, Agwara MO, Ndi JN, Yufanyi DM, Paboudam AG, Nyamen LD: **Synthesis, Characterisation and Antimicrobial Activities of Copper(II) and Zinc(II) Complexes of Schiff Bases derived from Amino Acids and 1,10-Phenanthroline Mixed Ligands**. *Research Journal of Chemistry and Environment* 2010, **14**(2):50-54.
46. Akinremi CA, Obaleye JA, Amolegbe SA, Adediji JF, Bamigboye MO: **Biological activities of some Fluoroquinolones-metal complexes,**. *International Journal of Medicine and Biomedical* 2012, **1**(1):24-34.
47. Renfrew AK: **Transition metal complexes with bioactive ligands: mechanisms for selective ligand release and applications for drug delivery**. *Metallomics* 2014:1-12.
48. Chandraleka S, Ramya K, Chandramohan G, Dhanasekaran D, Priyadharshini A, Panneerselvam A: **Antimicrobial mechanism of copper(II) 1,10-phenanthroline and 2,2'-bipyridyl complex on bacterial and fungal pathogens**. *Journal of Saudi Chemical Society* 2014, **18**(6):953-962.
49. Kucková L, Jomová K, Švorcová A, Valko M, Segľa P, Moncoľ J, Kožíšek J: **Synthesis, Crystal Structure, Spectroscopic Properties and Potential Biological Activities of Salicylate–Neocuproine Ternary Copper(II) Complexes**. *Molecules* 2015, **20**:2115 -2137. **Combining**:10486–10496.
50. WHO: **Antimicrobial resistance**. In. Switzerland: Global report on surveillance Geneva; 2014.
51. Tanwar J, Das S, Fatima Z, Hameed S: **Multidrug Resistance: An Emerging Crisis**. *Interdisciplinary Perspectives on Infectious Diseases* 2014, **2014**:1-7.
52. Spellberg B, Guidos R, Gilbert D, Bradley J, Boucher HW, Scheld WM, Bartlett JG, Edwards JJ: **The Epidemic of Antibiotic-Resistant Infections: A Call to Action for the Medical Community from the Infectious Diseases Society of America**. *Clinical Infectious Diseases* 2008, **46**(2):155–164.
53. Beyth N, Houri-Haddad Y, Domb A, Khan W, Hazan R: **Alternative Antimicrobial Approach: Nano-Antimicrobial Materials**. *Journal of Evidence-Based Integrative Medicine* 2015, **2015**:1-16.

54. Kandi V, Kandi S: **Antimicrobial properties of nanomolecules: potential candidates as antibiotics in the era of multi-drug resistance**. *Journal of Epidemiology and Community Health* 2015, **37**:e2015020.

55. Ndosiri NB, Agwara MO, Paboudam AG, Ndifon PT, Yufanyi DM, Amah C: **Synthesis, Characterisation and Antifungal Activities of Mn(II), Co(II), Cu(II) and Zn(II) Mixed-Ligand Complexes containing 1,10-Phenanthroline and 2,2'-Bipyridine**. *Research Journal of Pharmaceutical, Biological and Chemical Sciences* 2013, **4**(1):386-397.

56. Creaven BS, Egan DA, Karcz D, Kavanaugh K, McCann M, Mahon M, Noble A, Thati B, Walsh M: **Synthesis, characterisation and antimicrobial activity of copper(II) and manganese(II) complexes of coumarin-6,7-dioxyacetic acid ($cdoaH_2$) and 4-methylcoumarin-6,7-dioxyacetic acid ($4\text{-}MecdoaH_2$): X-ray crystal structures of $[Cu(cdoa)(phen)_2] \cdot 8.8H_2O$ and $[Cu(4\text{-}Mecdoa)(phen)_2]\cdot 13H_2O$ (phen =1,10-phenanthroline)**. *Journal of Inorganic Biochemistry* 2007, **101**(8):1108–1119.

57. Ndosiri NB, Agwara MO, Ndifon PT, Mohamadou A, Boyom FF: **Synthesis, Characterization, Crystal Structure and Antimicrobial Activities of a Dimeric Copper(I) Chloride- Phenanthroline Complex $\{[Cu(C_{12}H_8N_2)_2Cl].5.5H_2O\}_2n$**. *International Journal of Current Research in Chemistry and Pharmaceutical Sciences* 2015, **2**(6):63-69.

58. Sado DYG, Yufanyi DM, Jagan R, Agwara MO: **Synthesis , characterization and antimicrobial properties of cobalt(II) and cobalt(III) complexes derived from 1,10-phenanthroline with nitrate and azide co-ligands**. *Cogent Chemistry* 2016, **27**(1):1-16.

59. Adelaide OM, James OO: **Antimicrobial , DNA Cleavage and Antitumoral Properties of Some Transition Metal Complexes of 1,10 -Phenanthroline and 2,2 '-Bipyridine: A Review**. *International Journal of Research in Pharmaceutical and Biomedical Sciences* 2013, **4**(4):1160-1171.

60. Lobana TS, Indoria S, Jassal AK, Kaur H, Arora DS, Jasinski JP: **Synthesis, structures, spectroscopy and antimicrobial properties of complexes of copper(II) with salicylaldehyde N-substituted thiosemicarbazones and 2,2'-bipyridine or 1,10-phenanthroline**. *European Journal of Medicinal Chemistry* 2014, **76**:145-154.

61. Sado DYG, Agwara MO, Yufanyi MD, Nenwa J, Jagan R: **Crystal structure and Antimicrobial properties of a Copper(II) complex with 1,10-phenanthroline and azide co-ligand**. *Inorganic and Nano-Metal Chemistry* 2017, **47**(7):618–625.

62. Tabong CD, Yufanyi DM, Eni DB, Agwara MO: **Synthesis , Characterization and Antimicrobial Properties of Some Co(II) Complexes of Hexamethylenetetramine**. *Journal of Chemical and Pharmaceutical Research* 2016, **8**(12):144-151.

63. Refat MS, El-korashy SA, Hussien MA: **Mn(II), Co(II), Fe(III) And Cu(II) Complexes of Antihistaminic ' Fexofenadine ' and Amucolytic ' Carbocysteine ' Drugs : Synthesis , Spectroscopic and Thermal Studies**. 2014, **2**(1):97-107.

64. Khan IM, Ahmad A, Aatif M: **Synthesis, single-crystal characterization, antimicrobial activity and remarkable in vitro DNA interaction of hydrogen-bonded proton-transfer complex of 1,10-phenanthroline with 2,4,6-trinitrophenol**. *Journal of Photochemistry and Photobiology B: Biology* 2011, **105**(1):6-13.

65. Escobar LB, Corrêa CC, Guedes GP, Vaz MG, Greer SM, Hill S, Diniz R, Machado FC: **Two coordination polymers containing the dicyanamide ligand: Synthesis, crystal structures, and HFEPR studies**. *Inorganica Chimica Acta* 2016, **451**:59-64.

66. Yufanyi DM, Agwara MO, Foba-Tendo J, Ketcha JM: **Effect of Decomposition Temperature on the Crystallinity of α-Fe_2O_3 (Hematite) Obtained from an Iron(III)-Hexamethylenetetramine Precursor**. *American Journal of Chemistry* 2015, **5**(1):1-9.

67. Batten SR, Murray KS: **Structure and magnetism of coordination polymers containing dicyanamide and tricyanomethanide**. *Coordination Chemistry Reviews* 2003, **246**(1-2):103-130.

68. Brahma S, Sachin HP, Shivashankar SA, Narasimhamurthy T, Rathore RS: **Adducts of bis-(acetylacetonato)-zinc(II) with 1,10-phenanthroline and 2,2′-bipyridine**. *Acta Crystallographica Section C Crystal Structure Communications* 2008, **64**(3):140-143.

69. Hossain A, Sheikh C, Mahmud SAZ, Alam MA: **Synthesis And Characterization of some Metal Complexes of Zn(II) with 1,10-Phenanthroline And some Amino Acids : Anti-Inflammatory and Analgesic Activities of its Complexes**. *International Journal of Scientific & Technology Research* 2013, **2**(9):233-237.

70. Thornton L, Dixit V, Assad LO, Ribeiro TP, Queiroz DD, Kellett A, Casey A, Colleran J, Pereira MD, Rochford G *et al*: **Water-soluble and photo-stable silver(I) dicarboxylate complexes containing 1,10-phenanthroline ligands: Antimicrobial and anticancer chemotherapeutic potential, DNA interactions and antioxidant activity**. *Journal of Inorganic Biochemistry* 2016, **159**:120-132.

71. Avdeeva VV, Dziova AE, Polyakova IN, Malinina EA, Goeva LV, Kuznetsov NT: **Copper(I), copper(II), and heterovalent copper(I,II) complexes with 1,10-phenanthroline and the closo-decaborate anion**. *Inorganica Chimica Acta* 2015, **430**:74-81.

72. Zoroddu MA, Zanetti S, Pogni R, Basosi R: **An electron spin resonance study and antimicrobial activity of copper(II)-phenanthroline complexes**. *Journal of Inorganic Biochemistry* 1996, **63**(4):291-300.

73. Aljahdali M, El-Sherif AA: **Synthesis, characterization, molecular modeling and biological activity of mixed ligand complexes of Cu(II), Ni(II) and Co(II) based on 1,10-phenanthroline and novel thiosemicarbazone**. *Inorganica Chimica Acta* 2013, **407**:58-68.

74. Agwara MO, Ndifon PT, Ndosiri NB, Paboudam AG, Yufanyi DM, Mohamadou A: **Synthesis, Characterisation and Antimicrobial Activities of Cobalt(II), Copper(II) and Zinc(II) Mixed-Ligand Complexes Containing 1,10-Phenanthroline and 2,2'-Bipyridine**. *Bulletin of the Chemical Society of Ethiopia* 2010, **24**(3):383-389.

75. Colak AT, Oztopcu-Vatan P, Colak F, Akduman D, Kabadere S, Uyar R: **Syntheses, characterization, antimicrobial and cytotoxic activities of pyridine-2,5-dicarboxylate complexes with 1,10-phenanthroline**. *Journal of Trace Elements in Medicine and Biology* 2013, **27**(4):295-301.

76. Coyle B, Kavanagh K, McCann M, Devereux M, Geraghty M: **Mode of anti-fungal activity of 1,10-phenanthroline and its Cu(II), Mn(II) and Ag(I) complexes**. *BioMetals* 2003, **16**(2):321–329.

77. McCann M, Geraghty M, Devereux M, O'Shea D, Mason J, O'Sullivan L: **Insights into the mode of action of the anti-candida activity of 1,10-phenanthroline and its metal chelates**. *Metal Based Drugs* 2000, **7**(4):185-193.

78. Sieranski T, Kruszynski R: **Magnesium sulphate complexes with hexamethylenetetramine and 1,10-phenanthroline: Thermal, structural and spectroscopic properties**. *Journal of Thermal Analysis and Calorimetry* 2012, **109**(1):141-152.

79. Dholariya HR, Patel KS, Patel JC, Patel KD: **Dicoumarol complexes of Cu(II) based on 1,10-phenanthroline: Synthesis, X-ray diffraction studies, thermal behavior and biological evaluation**. *Spectrochimica Acta Part A: Molecular and Biomolecular Spectroscopy* 2013, **108**:319-328.

80. Warad I, Abdoh M, Shivalingegowda N, Lokanath NK, Salghi R, Al-Nuri M, Jodeh S, Radi S, Hammouti B: **Synthesis, spectral, electrochemical, crystal structure studies of two novel di-μ-halo-bis[halo(2,9-dimethyl-4,7-diphenyl-1,10-phenanthroline)cadmium(II)] dimer complexes and their thermolysis to nanometal oxides**. *Journal of Molecular Structure* 2015, **1099**:323-329.

81. Ciesielski A: **Supramolecular nanochemistry: from self-assembly to responsive architectures**. University of Strasbourg; 2010.

82. Sun YM, Dong FY, Wang DQ, Li YT: **Crystal structure, supramolecular self-assembly and interaction with DNA of a mixed ligand manganese(II) complex**. *Journal of the Brazilian Chemical Society* 2011, **22**(6):1089-1095.

83. Srinivasan BR, Sawant JV, Näther C, Bensch W: **Synthesis, spectroscopy and supramolecular structures of two magnesium 4-nitrobenzoate complexes**. *Journal of Chemical Sciences* 2007, **119**(3):243-252.
84. Schneider HJ: **Binding mechanisms in supramolecular complexes**. *Angewandte Chemie International Edition* 2009, **48**(22):3924-3977.
85. Nangia A: **Supramolecular chemistry and crystal engineering**. *Journal of Chemical Sciences* 2009, **122**(3):295-310.
86. Wang Z: **Design of metal-organic framework materials based upon inorganic clusters and polycarboxylates**. University of South Florida; 2006.
87. Han S: **Design and Synthesis of Crystalline and Amorphous Coordination Materials**. Providence, Rhode Island: Brown University; 2009.
88. Melorose J, Perroy R, Careas S: **Synthetic Methods in Organic and Supramolecular Chemistry**. *University of Pittsburgh* 2015.
89. Jacob A, Duncan E: **Explorations in crystal engineering : supramolecular templates , helical assemblies , pharmaceutical reactivity , and applications to radio- imaging**. *University of Iowa* 2017.
90. Khlobystov AN, Blake AJ, Champness NR, Lemenovskii DA, Majouga AG, Zyk NV, Schröder M: **Supramolecular design of one-dimensional coordination polymers based on silver(I) complexes of aromatic nitrogen-donor ligands**. *Coordination Chemistry Reviews* 2001, **222**(1):155-192.
91. Chutia R, Dey SK, Das G: **A supramolecular dual-host based ion-pair induced formation of 1D coordination polymer**. *Crystal Engineering Communication* 2013, **15**(45):9641-9647.
92. Teng C, Xiao H, Cai Q, Tang J, Cai T, Deng Q: **Two supramolecular complexes based on polyoxometalates and Co-EDTA units via covalent connection or non-covalent interaction**. *Journal of Solid State Chemistry* 2016, **243**:146-153.
93. Batten SR, Champness NR, Chen X-M, Garcia-Martinez J, Kitagawa S, Öhrström L, O'Keeffe M, Suh MP, Reedijk J: **Terminology of metal–organic frameworks and coordination polymers (IUPAC Recommendations 2013)**. *Pure and Applied Chemistry* 2013, **85**(8):1715-1724.
94. Batten SR, Champness NR, Chen X-M, Garcia-Martinez J, Kitagawa S, Öhrström L, O'Keeffe M, Suh MP, Reedijk J: **Coordination Polymers, Metal-Organic Frameworks and the Need for Terminology Guidelines**. *crystal engineering communication* 2012, **14**(9):3001-3004.
95. Kumar V, Kundu A, Singh M, Ramanujachary KV, Ramanan A: **Design of non-molecular coordination solids from aqueous solution: [Cu(II)LnX(H_2O)], where X=SO_4, Cl or H_2O**

and L=pyrazole, imidazole or glutamic acid and n=1 or 4. *Journal of Chemical Sciences* 2014, **126**(5):1433-1442.

96. Desiraju GR: **Crystal Engineering: A Holistic View**. *Angewandte Chemie International Edition* 2007, **46**:8342-8356.
97. Prohens R, Puigjaner C: **Crystal Engineering Studies: polymorphs and co-crystals**. *Handbook of instrumental techniques from CCiTUB* 2010:1-9.
98. Desiraju GR: **Crystal engineering: From molecule to crystal**. *Journal of the American Chemical Society* 2013, **135**(27):9952-9967.
99. Naik AD, Dîrtu MM, Railliet AP, Marchand-Brynaert J, Garcia Y: **Coordination polymers and metal organic frameworks derived from 1,2,4-triazole amino acid linkers**. *Polymers (Basel)* 2011, **3**(4):1750-1775.
100. Mohammed SF, Refat MS, El–Metwaly NM: **Synthesis a New Series of Methenamine Complexes with Some Different Metal ions: Spectral, Thermal and Biological Investigations**. *Life Sciences - Journal* 2012, **9**(2):1243-1253.
101. Biradha K, Sarkar M, Rajput L: **Crystal engineering of coordination polymers using 4,4'-bipyridine as a bond between transition metal atoms.** *Chemical communications (Cambridge, England)* 2006, **40**:4169-4179.
102. Rather B, Zaworotko MJ: **A 3D metal-organic network, [Cu2(glutarate)2(4,4A-bipyridine)], that exhibits single-crystal to single-crystal dehydration and rehydration**. *Chemical Communications* 2003, **2**:830-831.
103. Miao XH, Zhu LG: **Supramolecular assembly under the control of the chelating ligand for the MnII/bridging ligands/3-sulfobenzoate system and catalytic properties for the disproportionation of hydrogen peroxide**. *New Journal of Chemistry* 2010, **34**(11):2403-2414.
104. Lemaître VJ: **Non-covalent interactions in biomolecules studied by 17 O NMR and MD simulations**. University of Oxford; 2004.
105. Dhotel A, Chen Z, Delbreilh L, Youssef B, Saiter JM, Tan L: **Molecular motions in functional self-assembled nanostructures**. *International Journal of Molecular Sciences* 2013, **14**(2):2303-2333.
106. Panini P, Chopra D: **Hydrogen Bonded Supramolecular Structures**. 2015, **87**.
107. Dougherty DA: **The cation-π interaction**. *Accounts of Chemical Research* 2013, **46**(4):885-893.

108. Majumder A, Pilet G, Rodriguez MG, Mitra S: **Synthesis and structural characterisation of three dicyanamide complexes with Mn(II), Zn(II) and Cd(II): Supramolecular architectures stabilised by hydrogen bonding**. *Polyhedron* 2006, **25**(13):2550-2558.

109. McGaughey GB, Gagné M, Rappé AK: **π-Stacking interactions: Alive and well in proteins**. *The Journal of Biological Chemistry* 1998, **273**(25):15458-15463.

110. Venkataraman D, Lee S, Moore JS, Zhang P, Hirsch KA, Gardner GB, Covey AC, Prentice CL: **Coordination networks based on multitopic ligands and silver(I) salts: A study of network connectivity and topology as a function of counterion**. *Chemistry of Materials* 1996, **8**(8):2030-2040.

111. Alkorta I, Grabowski SJ: **Non-Covalent Interactions**. *Computational and Theoretical Chemistry* 2009, **998**:1-46.

112. Desiraju GR: **Hydrogen bridges in crystal engineering: Interactions without borders**. *Accounts of Chemical Research* 2002, **35**(7):565-573.

113. Braga D, Grepioni F, Tedesco E: **X−H---π (X = O, N, C) Hydrogen Bonds in Organometallic Crystals**. *Organometallics* 1998, **17**(12):2669-2672.

114. Lindeman SV, Kosynkin D, Kochi JK: **Unusually Short (C−H···π) Hydrogen Bonds for Effective Supramolecular (Aromatic/Aromatic) Organization in Edge-to-Face Motifs**. *Journal of American Chemical Society* 1998, **120**(50):13268-13269.

115. Rozas I, Alkorta I, Elguero J: **Unusual Hydrogen Bonds: H···π Interactions**. *Journal of Physical Chemistry A* 1997, **101**(49):9457-9463.

116. Liu R, Huang M-M, Yao X-X, Li H-H, Yang F-L, Li X-L: **Synthesis, structures and aggregation-induced emissive properties of copper(I) complexes with 1H-imidazo[4,5-f][1,10]phenanthroline derivative and diphosphine as ligands**. *Inorganica Chimica Acta* 2015, **434**:172-180.

117. Jeffrey GA: **An Introduction to Hydrogen Bonding**. In: *Book ReViews*. New York and Oxford: Oxford University Press; 1997: 301-303.

118. Hernández-Paredes J, Carrillo-Torres RC, Hernández-Negrete O, Sotelo-Mundo RR, Glossman-Mitnik D, Esparza-Ponce HE, Alvarez-Ramos ME: **Experimental and theoretical study on the molecular structure, covalent and non-covalent interactions of 2,4-dinitrodiphenylamine: X-ray diffraction and QTAIM approach**. *Journal of Molecular Structure* 2017, **1141**:53-63.

119. Claessens CG, Stoddart JF: **p-p Interactions in Self-Assembly**. *Journal of Physical Organic Chemistry* 1997, **10**(5):254-272.

120. Robin AY, Fromm KM: **Coordination polymer networks with O- and N-donors: What they are, why and how they are made**. *Coordination Chemistry Reviews* 2006, **250**(15-16):2127-2157.

121. Mignon P, Loverix S, Steyaert J, Geerlings P: **Influence of the π-π interaction on the hydrogen bonding capacity of stacked DNA/RNA bases**. *Nucleic Acids Research* 2005, **33**(6):1779-1789.

122. Tamer Ö, Avcı D, Atalay Y, Çoşut B, Zorlu Y, Erkovan M, Yerli Y: **Synthesis, X-ray structure, spectroscopic characterization and nonlinear optical properties of triaqua(1,10-phenanthroline-2,9-dicarboxylato)manganese(II) dihydrate: A combined experimental and theoretical study**. *Journal of Molecular Structure* 2015, **1100**:605-613.

123. Kulandai AM, Shok RF, Vasanthi M, Paulraj A: **Mixed Ligand Complexes of Nickel(II), Copper(II) and Zinc(II) With Nicotinanilide and Thiocyanate**. *International Journal of Life science and Pharma Research* 2013, **3**(2):67-75.

124. Gao Y-G, Wang A: **Crystallographic studies of metal ion -DNA interactions: different binding modes of cobalt(ll), copper(ll) and barium(ll) to N7 of guanines in Z-DNA and a drug-DNA complex**. *Nucleic Acids Research* 1993, **21**(17):4093-4101.

125. Bakir SR: **Synthesis , Spectral Study and Biological Activity of some Metal ions Complexes with Bidentate Ligands**. *Journal of Al Nahrain University* 2012, **15**(3):30-42.

126. Weisany W, Raei Y, Allahverdipoor KH: **Role of Some of Mineral Nutrients in Biological Nitrogen Fixation**. *Bulletin of Environment, Pharmacology and Life Sciences* 2013, **2**(4):77-84.

127. Glusker JP, Katz AK, Bock CW: **Metal Ions in Biological Systems**. *Rigaku Journal* 1999, **16**(2):8-17.

128. Mandlik PR, More MB, Aswar AS: **Synthesis, structural, thermal and biological studies of Cr(III), Mn(III), Fe(III), VO(lV), Zr(lV) and UO_2(VI) Schiff base complexes**. *Indian Journal of Chemistry* 2003, **42**:1064-1067.

129. Patel KS, Patel JC, Dholariya HR, Patel VK, Patel KD: **Synthesis of Cu(II), Ni(II), Co(II), and Mn(II) Complexes with Ciprofloxacin and their Evaluation of Antimicrobial, Antioxidant and Anti-Tubercular Activity**. *Open Journal of Metal* 2012, **2**:49-59.

130. Iakovidis I, Delimaris I, Piperakis SM: **Copper and Its Complexes in Medicine: A Biochemical Approach**. *Molecular Biology International* 2011, **2011**:1-13.

131. Ejelonu BC, Olagboye SA: **Synthesis, Characterization and Antimicrobial Evaluations of Mixed Ligand Complexes of Diphenylamine of Cobalt**. *Research Journal of Pharmaceutical, Biological and Chemical Sciences* 2015, **6**(2):184-190.

132. Onawumi OE, Adeoye IO, Adekunle FO: **Synthesis , characterisation and microbial studies of diperchlorate and its bromide analogue**. *Open Journal of Inorganic Chemistry* 2013, **3**:26-33.

133. Jayaseelan P, Akila E, Rani MU, Rajavel R: **Synthesis, spectral characterization, electrochemical, anti-microbial, DNA binding and cleavage studies of new binuclear Schiff base metal(II) complexes derived from o-hydroxyacetophenone**. *Journal of Saudi Chemical Society* 2016, **20**(6):625-634.

134. Aftab SK: **Studies of the Effect of Transition Metal ion on the Biological Activity of some Novel Organic Compounds**. University of Sargodha; 2010.

135. Wieghardt K: **The Active Sites in Manganese-Containing Metalloproteins and Inorganic Model Complexes**. *Angew Chem Int Ed* 1989, **28**(9):1153-1172.

136. Salomon E, Keren N, Kanteev M, Adir N: **Manganese in Biological Systems: Transport and Function**. In: *PATAI'S Chemistry of Functional Groups.* Edited by Rappoport Z: John Wiley & Sons; 2011.

137. Lee JD: **Concise Inorganic Chemistry**. 1999.

138. Cotton FA, Wilkinson G: **Advanced Inorganic Chemistry**. 1999:1171.

139. Protogeraki C, Andreadou EG, Perdih F, Turel I, Pantazaki AA, Psomas G: **Cobalt(II) complexes with the antimicrobial drug enrofloxacin: Structure, antimicrobial activity, DNA- and albumin-binding**. *European Journal of Medicinal Chemistry* 2014, **86**:189-201.

140. Kurmoo M: **Magnetic metal-organic frameworks**. *Chemical Society Reviews* 2009, **38**(5):1353.

141. Raza MA, Kanwal Z, Riaz S, Naseem S: **Synthesis, characterization and antibacterial properties of nano-sized cobalt particles**. *Advances in Civil, Environmental, and Materials Research (ACEM16)* 2016, **2016**:1-7.

142. Carter MT, Bard AJ: **Voltammetric studies of the interaction of tris(1,10-phenanthroline)cobalt(III) with DNA**. *Journal of the American Chemical Society* 1987, **109**(24):7528-7530.

143. Tabrizi L, McArdle P, Ektefan M, Chiniforoshan H: **Synthesis, crystal structure, spectroscopic and biological properties of mixed ligand complexes of cadmium(II), cobalt(II) and manganese(II) valproate with 1,10-phenanthroline and imidazole**. *Inorganica Chimica Acta* 2016, **439**:138-144.

144. Parada J, Atria AM, Wiese G, Rivas E, Corsini G: **Synthesis , Characterization and Antibacterial Activity of Cobalt(III) Complex With Phenanthroline and Maltose**. *Journal of the Chilean Chemical Society* 2014, **59**(4):2636-2639.

145. Osredkar J: **Copper and Zinc, Biological Role and Significance of Copper/Zinc Imbalance**. *Journal of Clinical Toxicology* 2011, **s3**(01):1-18.

146. Willis MS, Monaghan SA, Miller ML, McKenna RW, Perkins WD, Levinson BS, Bhushan V, Kroft SH: **Zinc-Induced Copper Deficiency: A Report of Three Cases Initially Recognized on Bone Marrow Examination**. *American Journal of Clinical Pathology* 2005, **123**(1):125-131.

147. Konin P, Sajjan C, Ingleshwar NM: **Copper Deficiency leading to Hematological and Neurological Dysfunction caused by Consumption of Zinc-containing Denture Adhesives**. *International Journal of Oral Care and Research* 2017, **5**(1):71-74.

148. Harris ED: **Copper homeostasis: the role of cellular transporters**. *Nutrition Reviews* 2001, **59**(9):281-285.

149. Bonham M, O'Connor JM, Hannigan BM, Strain JJ: **The immune system as a physiological indicator of marginal copper status**. *British Journal of Nutrition* 2002, **87**(05):393-403.

150. Maizes V, Rakel D, Niemiec C: **Integrative medicine and patient-centered care**. *Explore* 2009, **5**(5):277-289.

151. Davis CD: **Low dietary copper increases fecal free radical production, fecal water alkaline phosphatase activity and cytotoxicity in healthy men**. *Journal of Nutrition* 2003, **133**(2):522-527.

152. Christen Y: **Oxidative stress and Alzheimer disease**. *American Journal of Clinical Nutrition* 2000, **71**:621-629.

153. Crayton JW, Walsh WJ: **Elevated serum copper levels in women with a history of post-partum depression**. *Journal of Trace Elements in Medicine and Biology* 2007, **21**(1):17-21.

154. Mahmoud WH, Mohamed GG, El-dessouky MMI: **Synthesis, Characterization and in vitro Biological Activity of Mixed Transition Metal Complexes of Lornoxicam with 1,10-phenanthroline**. *International Journal of Electrochemical Science* 2014, **9**:1415-1438.

155. Silva PP, Guerra W, Silveira JN, Maria A, Ferreira C, Bortolotto T, Fischer FL, Neves A, Pereira-maia EC: **Two New Ternary Complexes of Copper(II) with Tetracycline or Doxycycline and 1,10-Phenanthroline and Their Potential as Antitumoral: Cytotoxicity and DNA Cleavage**. *Inorganic Chemistry* 2011, **50**:6414-6424.

156. Agwara MO, Yufanyi MD, Atamba MA, Ndinteh DT: **Synthesis, characterisation and biological activities of Mn(II), Co(II) and Ni(II) complexes of hexamethylenetetramine**. *Chemical and Pharmaceutical Research* 2011, **3**(3):196-204.

157. Agwara MO, Foba-tendo J, Amah C, Yufanyi DM, Ndosiri NB: **Thermogravimetric and Antimicrobial Properties of some Divalent Metal Complexes of Hexamethylenetetramine**. *Research Journal of Pharmaceutical, Biological and Chemical Sciences* 2012, **3**(3):95-104.

158. Raman N, Mahalakshmi R, Arun T, Packianathan S, Rajkumar R: **Metal based pharmacologically active complexes of Cu(II), Ni(II) and Zn(II): Synthesis, spectral, XRD, antimicrobial screening, DNA interaction and cleavage investigation**. *Journal of Photochemistry and Photobiology B: Biology* 2014, **138**:211-222.

159. Zhang F, Lin QY, Hu WL, Song WJ, Shen ST, Gui P: **Interaction with biomacromolecules and antiproliferative activities of Mn(II), Ni(II), Zn(II) complexes of demethylcantharate and 2,2′-bipyridine**. *Spectrochimica Acta Part A: Molecular and Biomolecular Spectroscopy* 2013, **110**:100-107.

160. Bhattacharyya A, Ghosh BN, Rissanen K, Chattopadhyay S: **Synthesis, characterization and self-assembly of three dicyanamide bridged polynuclear copper(II) complexes with N_2O donor tridentate Schiff bases as blocking ligands**. *Polyhedron* 2016, **117**:138-147.

161. Tang H, Chen Z, Wei L, Miao J, Meng G, He Y, Wu H: **Three cationic iridium(III) complexes with 1,10-phenanthroline or compounds containing 1,10-phenanthroline unit as auxiliary ligands: Synthesis and application in polymer light-emitting diodes**. *Dyes and Pigments* 2016, **131**:340-348.

162. Yesilel OZ, Ucar I, Bulut A, Olmez H, Büyükgüngör O: **Synthesis , Crystal Structure , Spectral and Thermal Characterization of cis -Diaquabis (1,10-phenanthroline) zinc(II) Diorotate Hydrate , cis-$[Zn(H_2O)_2(phen)_2](H_2Or)_2\bullet(H_2O)_{2.125}$**. *Verlag der Zeitschrift fur Naturforschung, Tubingen* 2006, **61b**:147-152.

163. Tang H, Wei L, Meng G, Li Y, Wanga G, Yang F, Wub H, Yang W, Cao Y: **Polymer light-emitting diodes based on cationic iridium(III) complexes with a 1,10-phenanthroline derivative containing a bipolar carbazole–oxadiazole unit as the auxiliary ligand**. *Optical Materials* 2014, **37**:679–687.

164. Tamer Ö, Avcı D, Atalay Y: **A novel Cu(II) Complex of Picolinate and 1,10-Phenanthroline: Preparation, Crystal Structure Determination, Spectroscopic Characterization and Nonlinear Optical Studies**. *Journal of Inorganic and Organometallic Polymers and Materials* 2017, **27**(3):700-713.

165. Zhang C, Janiak C: **Six-coordinated zinc complexes: $[Zn(H_2O)_4(phen)](NO_3)_2\cdot H_2O$ and $[ZnNO_3(H_2O)(bipy)(Him)]NO_3$ (phen=1,10-phenanthroline, bipy=2,2'-bipyridine, and Him=imidazole)**. *Journal of Chemical Crystallography* 2002, **31**(1):29-35.

166. Bottega FC, Oliveira MR, Garcia CV, Menezes DC: **Synthesis, Characterisation and Antifungal Activity of Tris(1,10-Phenanthroline) Iron(II) Bis(N-R-Sulfonyldithiocarbimate)Zincate(II) Fernanda**. *Quim Nov* 2013, **36**(6):803-807.

167. Agwara MO, Ndifon PT, Ndosiri NB, Paboudam AG, Yufanyi DM, Mohamadou A: **Synthesis, Characterisation and Antimicrobial Activities of Cobalt(II), Copper(II) and Zinc(II) Mixed-Ligand Complexes Containing 1,10-Phenanthroline and 2,2'-Bipyridine**. *Bull Chem Soc Ethiop* 2010, **24**(3):383-389.

168. Aljahdali M, El-Sherif AA: **Synthesis, characterization, molecular modeling and biological activity of mixed ligand complexes of Cu(II), Ni(II) and Co(II) based on 1,10-phenanthroline and novel thiosemicarbazone**. *Inorg Chim Acta* 2013, **407**:58-68.

169. Colak AT, Oztopcu-Vatan P, Colak F, Akduman D, Kabadere S, Uyar R: **Syntheses, characterization, antimicrobial and cytotoxic activities of pyridine-2,5-dicarboxylate complexes with 1,10-phenanthroline**. *J Trace Elements in Medicine and Biology* 2013, **27**(4):295-301.

170. Ahmed SK, Khaled S: **Syntheses, spectral characterization, thermal properties and DNA cleavage studies of a series of Co(II), Ni(II) and Cu(II) polypyridine complexes with some new imidazole derivatives of 1,10-phenanthroline**. *Arabian Journal of Chemistry* 2015:1-25.

171. Brandt WW, Gyarfas EC, Dwyer FP: **Chelate Complexes of 1,10-Phenanthroline and Related Compounds**. *Chemical Reviews* 1954, **54**:959-1017.

172. Summers LA: **The Phenanthrolines**. *Advances in Heterocyclic Chemistry* 1978, **22**:1-69.

173. Chelucci G, Addis D, Baldino S: **A new approach to the 1,10-phenanthroline core**. *Tetrahedron Letters* 2007, **48**(19):3359-3362.

174. Adekunle FA: **Ni(II), Cobalt(II), Manganese(II) and Zinc(II) Complexes of 5,6_Dihydro_5,6_Epoxy_1,10_Phenanthroline_ Synthesis and Spectroscopic Studies**. *International Journal of Basic and Applied Sciences* 2013, **13**(3):6-10.

175. Bencini A, Lippolis V: **1,10-Phenanthroline: A versatile building block for the construction of ligands for various purposes**. *Coord Chem Rev* 2010, **254**(17-18):2096-2180.

176. Cogan R: **Synthesis , Characterisation and Anti-Candida Activity of Inorganic and Organic Derivatives of Inorganic and Organic Derivatives of 1,10-Phenanthroline**. Dublin Institute of Technology; 2009.

177. Deegan C, McCann M, Devereux M, Coyle B, Egan DA: **In vitro cancer chemotherapeutic activity of 1,10-phenanthroline (phen), [Ag_2(phen)$_3$(mal)]•2H_2O, [Cu(phen)$_2$(mal)]•2H_2O**

and [Mn(phen)$_2$(mal)]•2H$_2$O (malH$_2$= malonic acid) using human cancer cells. *Cancer Letters* 2007, **247**(2):224–233.

178. Ramírez-Silva MT, Gómez-Hernández M, Pacheco-Hernández ML, AlbertoRojas-Hernández, Galicia L: **Spectroscopy study of 5-amino-1,10-phenanthroline**. *Spectrochimica Acta Part A: Molecular and Biomolecular Spectroscopy* 2004, **60**(4):781-789.
179. Ganeshpandian M, Ramakrishnan S, Palaniandavar M, Suresh E, Riyasdeen A, Akbarsha MA: **Mixed ligand copper(II) complexes of 2,9-dimethyl-1,10-phenanthroline: Tridentate 3N primary ligands determine DNA binding and cleavage and cytotoxicity**. *Journal of Inorganic Biochemistry* 2014, **140**:202–212.
180. Neville NS, Wu MJ, Jones CE, Aldrich-Wright JR: **The antimicrobial efficacy and DNA binding activity of the copper(II) complexes of 3,4,7,8-tetramethyl-1,10-phenanthroline, 4,7-diphenyl-1,10-phenanthroline and 1,2-diaminocyclohexane**. *Journal of Inorganic Biochemistry* 2016, **162**:62-72.
181. İnci D, Aydın R, Yılmaz D, Gençkal HM, Vatan Ö, Çinkılıç N, Zorluc Y: **New water-soluble copper(II) complexes including 4,7-dimethyl-1,10-phenanthroline and l-tyrosine: Synthesis, characterization, DNA interactions and cytotoxicities**. *Spectrochimica Acta Part A: Molecular and Biomolecular Spectroscopy* 2015 **136**(Part B):761-770.
182. Raman N, Mahalakshmi R, Mitu L: **Bio-sensitive activities of coordination compounds containing 1,10-phenanthroline as co-ligand: Synthesis, structural elucidation and DNA binding properties of metal(II) complexes**. *Spectrochimica Acta Part A: Molecular and Biomolecular Spectroscopy* 2014, **131**:355-364.
183. Zhang Z, Zhang L, Ni Z, Kou H: **Syntheses, crystal structures, and magnetic properties of a series of double end-on azido-bridged dinuclear manganese(II) complexes**. *Transition Metal Chemistry* 2014, **39**(5):527-534.
184. Janiak C, Vieth JK: **MOFs, MILs and more: concepts, properties and applications for porous coordination networks (PCNs)**. *New Journal of Chemistry* 2010, **34**(11):2366-2388.
185. Massoud SS, Lemieux MM, Quan LL, Vicente R, Albering JH, Mautner FA: **Dicyanamido-metal(II) complexes. Part 6: 1D polymeric copper(II) complexes bridging by dicyanamide. Effect of copper(II) salt on the nature of the polymeric product**. *Inorganica Chimica Acta* 2012, **388**:71-77.
186. Xu YQ, Luo JH, Yuan DQ, Y. Xu RC, Hong MC: **[Cu(dca)$_2$(en)]$_n$: A two-dimensional copper(II) coordination polymer with both μ$_{1,5}$-dca and pseudo-μ$_{1,3}$-dca bridges**. *Journal of Molecular Structure* 2003, **658**(3):223-228.

187. Mukheljee PS, Konar S, Dalai S, Zangrando E, Chaudhuri NR: **A dinuclear copper(II) complex based on bridging oxalate and single dicyanamide**. *Indian Journal of Chemistry* 2004, **43A**:760-762.

188. Tonzing DS, Batten SR, Murray KS: **1D chain structures of $M(dca)_2(phen)(H_2O)xMeOH$, M=Mn, Fe, Co, Ni, Zn and Cd, dca=dicyanamide, $N(CN)_2^-$, phen=4,7-phenanthroline**. *Journal of Molecular Structure* 2006, **796**(1-3):63-68.

189. Ghoshal D, Mostafa G, Maji TK, Zangrando E, Lu T-H, Ribas J, Chaudhuri NR: **Synthesis, crystal structure and magnetic behavior of three polynuclear complexes: $[Co(pyo)_2(dca)_2]n$, $[Co_3(ac)_4(bpe)_3(dca)_2]n$ and $[\{Co(male)(H_2O)_2\}(H_2O)]n$ [pyo, pyridine-N-oxide; dca, dicyanamide; ac, acetate; bpe, 1,2-bis-(4-pyridyl)ethane and male, maleate]**. *New Journal of Chemistry* 2004, **28**(10):1204-1213.

190. Manna SC, Ghosh AK, Ribas J, Drew MG, Lin CN, Zangrando E, Chaudhuri NR: **Synthesis, crystal structure, magnetic behavior and thermal property of three polynuclear complexes: [M(dca)2(H2O)2]n·(hmt)n [M=Mn(II), Co(II)] and [Co(dca)2(bpds)]n [dca, dicyanamide; hmt, hexamethylenetetramine; bpds, 4,4′-bipyridyl disulfide]**. *Inorganica Chimica Acta* 2006, **359**(5):1395-1403.

191. Shi YJ, Chen XT, Li YZ, Xue Z, You XZ: **$Pb(dca)_2$(dca = dicyanamide): A novel 3D compound with unusual coordination modes of dicyanamide**. *New Journal of Chemistry* 2002, **26**(12):1711-1713.

192. Amah C, Agwara MO, Yufanyi DM, Conde MA, Jagan R, Eyong KO: **Synthesis, Crystal Structure, and Antimicrobial Properties of a Novel 1-D Cobalt Coordination Polymer with Dicyanamide and 2-Aminopyridine**. *International Journal of Inorganic Chemistry* 2015, **2015**:1-9.

193. Manson JL, Brown CM, Huang Q, Schlueter JA, Lancaster T, Blundell SJ, Singleton J, Lynn JW, Pratt FL: **$Mn(dca)_2$(o-phen) {dca = dicyanamide; O-phen = 1,10-phenanthroline}: Long-range magnetic order in a low-dimensional Mn-dca polymer**. *Polyhedron* 2013, **52**:679-688.

194. Carranza J, Sletten J, Lloret F, Julve M: **Structural analysis and magnetic properties of the copper(II) dicyanamide complexes $[Cu_2(dmphen)_2(dca)_4]$, $[Cu(dmphen)(dca)(NO_3)]n$ and $[Cu(4,4'\text{-dmbpy})(H_2O)(dca)_2]$ (dca=dicyanamide; dmphen=2,9-dimethyl-1,10-phenanthroline; 4,4′-dmbpy=4,4′-dimethyl-2,2′-bipy**. *Inorganica Chimica Acta* 2004, **357**(11):3304-3316.

195. Guo W, Escuer A, Tang M, Jiang CH, Du M: **Ligand-to-metal ratio dependent assembly of two distinct 1D and 3D copper(II)-dicyanamide magnetic coordination polymers with a tripyridyltriazole co-tecton**. *Inorganica Chimica Acta* 2013, **403**:142-146.

196. Mal D, Adhikary C, Rentschler E, Miyashita Y, Okamoto K-I, Koner S: **Synthesis, X-ray crystal structure and magnetic study of the 1D {[Cu(N,N-diethyl-1,2-ethanediamine)(μ1,5-dca)(dca)]}n complex**. *Polyhedron* 2007, **26**(3):736-740.

197. Dressick WJ, Deschamps JR, Schmehl RH, Martinez KP, Trammell SA, Goldberg E, Knight DA: **A luminescent 2,2′-bipyridyl tricarbonyl rhenium(I) complex containing a non-bridging dicyanamide ligand**. *Inorganic Chemistry Communications* 2017, **83**:55-58.

198. Mohamadou A, Albada GAv, Kooijman H, Wieczorek B, Spek AL, Reedijk J: **The binding mode of the ambidentate ligand dicyanamide to transition metal ions can be tuned by bisimidazoline ligands with H-bonding donor property at the rear side of the ligand**. *New Journal of Chemistry* 2003, **27**(6):983-988.

199. Triki S, Thetiot F, Galan-Mascaros J-R, Pala JS, Dunbar KR: **New compounds with bridging dicyanamide and bis-chelating 2,2 '-bipyrimidine ligands: syntheses , structural characterisation and magnetic properties of the two-dimensional materials [Fe(dca)(bpym)].H_2O and [Fe(dca)(bpym)(H_2O)$_2$]**. *New Journal of Chemistry* 2001, **25**:954-958.

200. Sen S, Mitra S, Hughes DL, Rosair G, Desplanches C: **Synthesis, crystal structures and magnetic studies of dicyanamide bridged two new 1D copper(II) complexes**. *Inorganica Chimica Acta* 2007, **360**(15):4085-4092.

201. Dong W, Wang Q-L, Liu Z-Q, Liao D-Z, Jiang Z-H, Yan S-P, P. Cheng, " , vol. 22, no. , pp. , 2003: **Syntheses, structures and magnetic properties of 1-D complex {[Ni(μ1,5-dca)(pn)2](ClO4)}n, 2-D complex [Mn(μ1,5-dca)2(phen)]n and 3-D complex [Mn(μ1,5-dca)2L]n (dca=dicyanamide, N(CN)2−; pn=1,3-propane diamine; phen=phenanthroline; L=4,4′-ditriazole metha**. *Polyhedron* 2003, **22**(25-26):3315-3319.

202. Kushch ND, Kazakova AV, Dubrovskii AD, Shilov GV, Buravov LI, Morgunov RB, Kurganova EV, Tanimoto Y, Yagubskii EB: **Molecular magnetic semiconductors formed by cationic and anionic networks: (ET)$_2$Mn[N(CN)$_2$]$_3$ and (ET)$_2$CuMn[N(CN)$_2$]$_4$**. *Journal of Materials Chemistry* 2007, **17**(41):4407–4413.

203. Ferretti V, Bergamini P, Marvelli L, Hushcha Y, Gemmob C, Gambari R, Lampronti I: **Synthesis and characterization of Pt complexes containing dichloroacetate (DCA), designed for dual anticancer action**. *Inorganica Chimica Acta journal* 2017, **2780**:1-9.

204. Ma K, Shi Q, Hu M, Cai X, Huang S: **Two Cd(II) and Ni(II) complexes constructed with dicyanamide and picolinate ligands**. *Inorganica Chimica Acta* 2009, **362**(14):4926-4930.

205. Luo J, Hong M, Weng J, Zhao Y, Cao R: **The complexes with end-to-end dicyanamide bridges: syntheses, characterization and crystal structures of [Cu($\mu_{1,5}$-dca)$_2$(phen)]n and [Cd($\mu_{1,5}$-dca)$_2$(py)$_2$]n (phen=phenanthroline; py=pyridine; dca=dicyanamide, $N(CN)_2^-$)**. *Inorganica Chimica Acta* 2002, **329**:59-65.

206. Ray RK, Bandyopadhyay MK, Kauffman GB: **Metal-mediated addition of alcohols to dicyandiamide**. *Polyhedron* 1989, **8**(6):757-762.

207. Zheng LL, Leng JD, Liu WT, Zhang WX, Lu JX, Tong ML: **Cu^{2+}-mediated nucleophilic addition of different nucleophiles to dicyanamide - synthesis, structures, and magnetic properties of a family of mononuclear, trinuclear, hexanuclear, and polymeric copper(II) complexes**. *European Journal of Inorganic Chemistry* 2008, **4**(29):4616-4624.

208. Kozisek J, Hvastijova M, Kohout J: **Addition of Methanol to Dicyanamide in the Cu(II) Coordination Sphere: Structure of Bis(bis(methoxy- carbimido)atiato)copper(II)**. *Inorganica Chimica Acta* 1990, **168**:157-158.

209. Váhovská L, Potočňák I, Vitushkina S, Walko M: **Low-dimensional compounds containing cyanido groups. Part XXX. Recrystallization of Co(II) complexes with pseudohalogenide ligands leading to CO2 uptake and formation of dicyanoguanidine anion in newly created Co(III) complexes**. *Polyhedron* 2016, **117**:359-366.

210. Abdel-Haleem FM, Rizk MS: **Highly selective thiocyanate optochemical sensor based on manganese(III)-salophen ionophore**. *Materials Science and Engineering: C* 2017, **75**:682-687.

211. Bruce MI, Burgun A, George J, Nicholson BK, Parker CR, Skelton B, Scoleri N, Sumby CJ, Zaitseva NN: **Some reactions of azides with diynyl-bis(phosphine)ruthenium-cyclopentadienyl complexes**. *Journal of Organometallic Chemistry* 2015, **797**:185-193.

212. Dori ZV, Zlolo RF: **The Chemistry of Coordinated Azides**. *Chemical Reviews* 1973, **1972**(4547,):247-254.

213. Tommasino J, Chastanet G, Guennic BL, Robert V, Pilet G: **A 1D coordination polymer built on asymmetric 1,1,3-azide bridge : from unusual topology to magnetic properties and Cu(II)/Cu(I) redox reversibility**. *New Journal of Chemistry* 2012, **36**:2228-2235.

214. Mauro AE, Haddad PS, Zorel HE, Santos RHA, Ananias SR, Martins FR, Tarrasqui LHR: **Mixed pseudohalide complexes of copper(II). Crystal and molecular structure of [Cu(N_3)(NCS)(tmen)]n and of [Cu(N_3)(NCO)(tmen)]$_2$ (tmen = N,N,N′,N′-tetramethylethylenediamine)**. *Transition Metal Chemistry* 2004, **29**:893-899.

215. Shen Z, Zuo J-L, Chinnakali K, Fun H-K, You X-Z: **Diazidobis(1,10-phenanthroline-N,N')-manganese(II)**. *Acta Crystallographica Section C: Crystal Structure Communications* 1999, **c55**:901-903.

216. Lorentzen D, Durairaj L, Pezzulo AA, Nakano Y, Launspach J, Stoltz DA, Zamba G, McCray PB, Zabner J, Welsh MJ *et al*: **Concentration of the antibacterial precursor thiocyanate in cystic fibrosis airway secretions**. *Free Radical Biology and Medicine* 2011, **50**(9):1144-1150.

217. Gao S, Song Y: **Ferromagnetic Ordering in a Two-Dimensional Copper Complex with Dual End-to-End and End-On Azide Bridges**. *Communications* 2000:4-7.

218. Goher AM, Mautner FA, Gatterer K, Abu-Youssef MA, Badr AM, Sodin B, Gspan C: **Four $[Cd(L)_2(N_3)_2]n$ 1D systems with different azide bridging sequences: Synthesis, spectral and structural characterization Mohamed**. *Journal of Molecular Structure* 2008, **876**:199-205.

219. Biswas C, Drew MG, Ruiz E, Estrader M, Diaz C, Ghosh A: **Synthesis, crystal structure and magnetic properties of three unprecedented tri-nuclear and one very rare tetra-nuclear copper(II) Schiff-base complexes supported by mixed azido/phenoxo/nitrato or acetato bridges**. *Dalton Transactions* 2010, **39**(32):7474-7484.

220. Du M, Guo Y-M, Chen S-T, Bu X-H, Batten SR, Ribas J, Kitagawa S: **Preparation of Acentric Porous Coordination Frameworks from an Interpenetrated Diamondoid Array through Anion-Exchange Procedures: Crystal Structures and Properties**. *Inorganic Chemistry* 2004, **43**(4):1287–1293.

221. Papatriantafyllopoulou C, Stamatatos TC, Wernsdorfer W, Teat SJ, Tasiopoulos AJ, Escuer A, Perlepes SP: **Combining Azide, Carboxylate, and 2-Pyridyloximate Ligands in Transition-Metal Chemistry: Ferromagnetic Ni^{II5} Clusters with a Bowtie Skeleton**. *Inorganic Chemistry* 2010, **49**

222. Escuer A, Font-Bardı´ M, Massoud SS, Mautner FA, Pen˜alba E, Solans X, Vicente R: **Three new dinuclear copper(II) complexes with $[Cu(m1,3\text{-}N_3)_2Cu]^{2+}$ and $[Cu(m1,1\text{-}N_3)_2Cu]^{2+}$ asymmetrical cores: syntheses, structures and magnetic behaviour**. *New Journal of Chemistry* 2004, **28**:681-686.

223. Lazari G, Stamatatos TC, Raptopoulou CP, Psycharis V, Pissas M, Perlepes SP, Boudalis AK: **A metamagnetic 2D copper(II)-azide complex with 1D ferromagnetism and a hysteretic spin-flop transition**. *Dalton Transactions* 2009, **17**:3215-3221.

224. Drahoš B, Herchel R, Trávníček Z: **Structural and magnetic properties of heptacoordinated MnIIcomplexes containing a 15-membered pyridine-based macrocycle and halido/pseudohalido axial coligands**. *RSC Advances* 2016, **6**(41):34674-34684.

225. Paboudam AG, Gérard C, Mohamadou A, Agwara MO, Conde MA, Ndifon PT: **Solution Studies on Co(II), Ni(II), Cu(II), and Zn(II) Complexes of Hexamethylenetetramine in Aqueous and Non-Aqueous Solvents**. *International Journal of Inorganic Chemistry* 2014, **2014**:12-16.

226. Das M, Chatterjee S, Chattopadhyay S: **Synthesis and characterization of two new nickel(II) complexes with azide: Formation of a two-dimensional coordination polymer with 63-hcb topology**. *Polyhedron* 2014, **68**:205-211.

227. Shaabani B, Khandar AA, Dusek M, Pojarova M, Mahmoudi F: **Synthesis , crystal structure , antimicrobial activity and electrochemistry study of chromium(III) and copper(II) complexes based on semicarbazone Schiff base and azide ligands**. *Inorganica Chimica Acta* 2013, **394**:563-568.

228. Jena HS, Goswami S, Sanda S, Parshamoni S, Biswas S, Konar S: **A perception of ferro- and antiferromagnetic interactions in a two dimensional Ni(II) heterochiral coordination polymer showing unusual CO_2 uptake behavior**. *Dalton Transactions* 2014, **43**(45):16996-16999.

229. Yolanda R, Hernández-molina M, Sanchiz J, Ruiz-pérez C, Lloret F, Julve M: **Crystal structures and magnetic properties of two- and three-dimensional malonato-bridged manganese(II) complexes**. *Dalton Transactions* 2003, **0**(11):2359-2365.

230. Kim Y, Kwak Y, Lee S: **Synthesis and properties of arylpalladium(II) azido complexes PdAr(N3)(PR3)2. Nucleophilic reactions of the azido ligand with CO and with isocyanides to afford Pd(II) isocyanate, C-tetrazolate and carbodiimide complexes**. *Journal of Organometallic Chemistry* 2000, **603**(2):152-160.

231. Safin DA, Robeyns K, Velde CV, Thijs M, Mitoraj MP, Sagan F, Filinchuk Y: **Azide-rich complexes of cobalt(III) with the rare 5-phenyl-2,2′-bipyridine ligand**. *Inorganica Chimica Acta* 2017, **459**:63-72.

232. Lampropoulos C, Stamatatos TC, Manos MJ, Tasiopoulos AJ, Abboud KA, Christou G: **New Mixed-Valence MnII/III6 Complexes Bearing Oximato and Azido Ligands: Synthesis, and Structural and Magnetic Characterization**. *European Journal of Inorganic Chemistry* 2010, **2010**(15):2244-2253.

233. Singh G, Baranwal BP, Kapoor IP, Kumar D, Singh CP, Fröhlich R: **Some transition metal nitrate complexes with hexamethylenetetramine**. *Journal of Thermal Analysis and Calorimetry* 2008, **91**(3):971-977.

234. Mistri S, García-Granda S, Zangrando E, Manna SC: **Fluorescent bis-chelated-1,10-phenanthroline-azido-copper(II) complex for selective sensing of aniline**. *Polyhedron* 2013, **50**(1):333-338.

235. Fournier É, Lebrun F, Drouin M, Decken A, Harvey PD: **Preparation and Solid-State Characterization of Mixed-Ligand Coordination/Organometallic Oligomers and Polymers of Copper(I) and Silver(I) Using Diphosphine and Mono- and Diisocyanide Ligands**. *Inorganic Chemistry* 2004, **43**(10):3127-3135.

236. Shi W-B, Cui A-L, Kou H-Z: **Assembly of dinuclear copper(II) secondary building units into polymeric complexes: crystal structures and magnetic properties**. *Crystal Engineering Communication* 2014, **16**(34):8027-8034.

237. Borel C, Hakansson M, Ohrstrom L: **Coordination bonds and strong hydrogen bonds giving a framework material based on a 4- and 8-connected net in $[Ca[Co(en)(oxalato)_2]_2]_n$.** *Crystal Engineering Communication* 2006, **8**(9):666-669.

238. Pook N-P, Hentrich P, Gjikaj M: **Crystal structure of bis[tris(1,10-phenanthroline k^2 N,N')cobalt(II)] tetranitrate N,N'-(1,4-phenylenedicarbonyl)diglycine solvate octahydrate**. *Acta Cryst* 2015, **E71**(8):910-914.

239. Sun J, Tong X, Xu H: **Synthesis, structures and properties of Cu and Cd complexes with 1,10-phenanthroline**. *Inorg Chem Commun* 2010, **13**(5):645-648.

240. Dong H-Z, Li M, Li B-Z: **Synthesis and Crystal Structure of Di(thiocyanato-κN)bis(1,10-phenanthroline-5,6-dione-κ^2N,N')- Manganese(II): $[(C_{12}H_6N_2O_2)_2Mn(NCS)_2]_2$**. *Asian Journal of Chemistry* 2010, **22**(6):4950-4952.

241. Yesilel OZ, Olmez H, Yılanc OO, Umeyra H, Aoglu P, Buyukgungor O: **Syntheses, Spectral and Thermal Studies, and Crystal Structure of 1,10-Phenanthroline and Picolinamide Complexes of Cobalt(II) Squarate**. *Verlag der Zeitschrift fur Naturforschung, Tubingen* 2006, **2**:1094-1100.

242. Hu L-X, Zhang B-S: **Aqua(4-bromobenzoato-κO)bis(1,10-phenanthroline-κ^2N,N′)manganese(II) 4-bromobenzoate dihydrate**. *International Union of Crystallography Data* 2016, **1**(5):1-3.

243. Hazari D, Jana SK, Puschmann H, Zangrando E, Dalai S: **Three manganese(II) coordination polymers with mixed donor ligands: synthesis, X-ray structures and luminescence properties**. *Transition Metal Chemistry* 2015, **40**(6):595-604.

244. Čechová D, Martišková A, Moncol J: **Structure of cis-dichlorobis(1,10-phenanthroline)manganese(II) and cis-dichlorobis(2,2´-bipyridine)manganese(II)**. *Acta Chimica Slovaca* 2014, **7**(1):15-19.

245. Saphu W, Chanthee S, Chainok K, Harding DJ, Pakawatchai C: **Trans-Bis(nitrato-O)bis-(1,10-phenanthroline-k^{2}N,N′) manganese(II)**. *Acta Crystallographica Section E: Structure Reports Online* 2012, **68**(8):185–191.

246. Momeni BZ, Haghshenas F, Hadi S: **Synthesis, structural characterization and crystal structure of some dimethyltin complexes containing substituted 1,10-phenanthroline**. *Journal of Molecular Structure* 2017, **1142**:156-167.

247. Janiak C: **Engineering coordination polymers towards applications**. *Dalton Transactions* 2003, **14**:2781-2804.

248. Awad DJ, Conrad F, Koch A, Schilde U, Pöppl A, Strauch P: **1,10-Phenanthroline-dithiolate mixed ligand transition metal complexes. Synthesis, characterization and EPR spectroscopy**. *Inorganica Chimica Acta* 2010, **363**(7):1488-1494.

249. Bubnov M, Skorodumova N, Arapova A, Smirnova N, Bogomyakov A, Samsonov M, Cherkasov V, Abakumov1 G: **New bis-o-semiquinonato cobalt complexes with 1,10-phenanthroline ligands**. *Polyhedron* 2015, **85**:165-171.

250. Sakiyama H, Kato M, Sasaki S, Tasaki M, Asato E, Koikawa M: **Synthesis and magnetic properties of a dinuclear manganese(II) complex with two manganese(II) ions of C2-twisted octahedral geometry**. *Polyhedron* 2016, **111**:32-37.

251. Tetz G, Tetz V: **In vitro antimicrobial activity of a novel compound, Mul-1867, against clinically important bacteria**. *Antimicrobial Resistance and Infection Control* 2015, **4**(1):1-6.

252. Ndifon PT, Agwara MO, Paboudam AG, Yufanyi MD, Foba-Tendo JN, Galindo A, González EÁ: **Synthesis, Characterisation and Crystal Structure of Hexaaquacobalt(II) Dinitrate (Bis)hexamethylenetetramine Tetrahydrate**. *Annales de la Faculté des Sciences, Université de Yaoundé I, série Chimie* 2011, **38**(1):20-29.

253. Kohanski MA, Dwyer DJ, Collins JJ: **How antibiotics kill bacteria: From targets to networks**. *Nature Reviews Microbiology* 2010, **8**(6):423-435.

254. Belland RJ, Morrison SG, Ison C, Huang WM: **Neisseria gonorrhoeae acquires mutations in analogous regions of gyrA and parC in fluoroquinolone□resistant isolates**. *Molecular Microbiology* 1994, **14**(2):371-380.

255. McMurry L, Petrucci RE, Levy SB: **Active efflux of tetracycline encoded by four genetically different tetracycline resistance determinants in Escherichia coli.** *Proceedings of the National Academy of Sciences of the United States of America* 1980, **77**(7):3974-3977.

256. Blanco P, Hernando-Amado S, Reales-Calderon JA, Corona F, Lira F, Alcalde-Rico M, Bernardini A, Sanchez MB, Martinez JL: **Bacterial Multidrug Efflux Pumps: Much More Than Antibiotic Resistance Determinants**. *Microorganisms* 2016, **4**(14):1-19.

257. Croxen MA, Law RJ, Scholz R, Keeney KM, Wlodarska M, Finlay BB: **Recent advances in understanding enteric pathogenic Escherichia coli**. *Clinical Microbiology Reviews* 2013, **26**(4):822-880.

258. Shinde RV, Pawar SK, Mohite RV, Shinde AR, Duggu P: **Study of Nasal Carriage of Staphylococcus aureus with Special Reference to Methicillin Resistance among Nursing Staff**. *Archives of Clinical Microbiology* 2015, **7**(1).

259. Boncompaina CA, Suáreza CA, Morbidoni HR: **Staphylococcus aureus nasal carriage in health care workers: First report from a major public hospital in Argentina**. *Revista Argentina de Microbiología* 2017, **49**(2):125-131.

260. Plata K, Rosato AE, Wegrzyn G: **Staphylococcus aureus as an infectious agent: Overview of biochemistry and molecular genetics of its pathogenicity**. *Acta Biochimica Polonica* 2009, **56**(4):597-612.

261. Madikizela B, Ndhlala AR, Finnie JF, Staden JV: **In vitro antimicrobial activity of extracts from plants used traditionally in South Africa to treat tuberculosis and related symptoms**. *Evidence-Based Complementary and Alternative Medicine* 2011, **6**(9):1-8.

262. Kanungo R: **Antimicrobial resistance: Action by laboratories today for a cure tomorrow**. *Indian Journal of Medical Microbiology* 2011, **29**(3):205.

263. Sangal V, Harbottle H, Mazzoni CJ, Helmuth R, Guerra B, Didelot X, Paglietti B, Rabsch W, Brisse S, Weill Fo-X *et al*: **Evolution and Population Structure of Salmonella enterica Serovar Newport**. *Journal of Bacteriology* 2010, **192**(24):6465–6476.

264. Ajibola O, Mshelia MB, Gulumbe BH, Eze AA: **Typhoid Fever Diagnosis in Endemic Countries: A Clog in the Wheel of Progress?** *Medicina (Kaunas)* 2018, **54**(2):23-.

265. WHO: **Immunization, Vaccines and Biologicals** In: *Vaccines and diseases.* Geneva, Switzerland 2018.

266. Jones G, Steketee RW, Black RE, Bhutta ZA, Morris SS: **How many child deaths can we prevent this year?** *Lancet* 2003, **362**(9377):65-71.

267. WHO: **Diarrhoeal disease**. In. Geneva, Switzerland 2017.

268. Poole K: **Pseudomonas aeruginosa: resistance to the max**. *Frontiers in Microbiology* 2011, **2**(65):1-13.

269. Strateva T, Yordanov D: **Pseudomonas aeruginosa – a phenomenon ofbacterial resistance**. *Journal of Medical Microbiology* 2009, **58**:1133-1148.

270. Theodoratou E, Zhang JS, Kolcic I, Davis AM, Bhopal S, Nair H, Chan KY, Liu L, Johnson H, Rudan I *et al*: **Estimating Pneumonia Deaths of Post-Neonatal Children in Countries of Low or No Death Certification in 2008**. *PLoS ONE* 2011, **6**(9):1-8.

271. Wu P-F, Liu W-L, Hsieh M-H, Hii I-M, Lee Y-L, Lin Y-T, Ho M-W, Liu C-E, Chen Y-H, Wang F-D: **Epidemiology and antifungal susceptibility of candidemia isolates of non-albicans Candida species from cancer patients**. *Emerging Microbes and Infection* 2017, **6**(10):e87.

272. Kidd SE, F H, Tscharke RL, Huynh M, Bartlett KH, Fyfe M, Macdougall L, Boekhout T, Kwon-Chung KJ, Meyer W: **A rare genotype of Cryptococcus gattii caused the cryptococcosis outbreak on Vancouver Island (British Columbia, Canada)**. *Proceedings of the National Academy of Sciences of the United States of America* 2004, **101**(49):17258-17263.

273. Sanglard D: **Emerging Threats in Antifungal-Resistant Fungal Pathogens**. *Frontiers in Medicine (Lausanne)* 2016, **3**:11.

274. Wiederhold NP: **Antifungal resistance: current trends and future strategies to combat**. *Infection and Drug Resistance* 2017, **10**:249-259.

275. Molero G, Díez-Orejas R, Navarro-García F, Monteoliva L, Pla J, Gil C, Sánchez-Pérez M, Nombela C: **Candida albicans: genetics, dimorphism and pathogenicity**. *International Microbiology* 1998, **1**:95-106.

276. Pfaller MA, Jones RN, Doern GV, Sader HS, Messer SA, Houston A, Coffman S, Hollis RJ: **Bloodstream Infections Due to Candida Species: SENTRY Antimicrobial Surveillance Program in North America and Latin America, 1997-1998**. *Antimicrobial Agents and Chemotherapy* 2000, **44**(3):747-751.

277. Singh S, Sobel JD, Bhargava P, Boikov D, Vazquez JA: **Vaginitis due to Candida krusei: epidemiology, clinical aspects, and therapy**. *Clinical Infectious Diseases* 2002, **35**(9):1066-1070.

278. MacGregor RR, Schimmer BM, Steinberg ME: **Results of combined amphotericin B-5-fluorcytosine therapy for prosthetic knee joint infected with Candida parapsilosis**. *ournal of Rheumatology* 1979, **6**(4):451-455.

279. Lin X, Heitman J: **The biology of the Cryptococcus neoformans species complex**. *Annual Review of Microbiology* 2006, **60**:69-105.

280. Goher MA, Mautner FA, Hafez AK, Abu-Youssef MA, Gspan C, Badr AM-A: **Two new polymeric cadmium(II) complexes containing end-to-end bridging azido or thiocyanato ligands with different topologies**. *Polyhedron* 2003, **22**(7):975-979.

281. Dagur P, Chopra D, Prakash AS, Row TG, Hegde MS: **Synthesis, characterization and structure of [Ni(H2O)6]2(Cr2O7)2(hmta)4·2H2O (hmta=hexamethylenetetramine): a novel metal organic-inorganic hybrid**. *Journal of Crystal Growth* 2005, **275**:e2043-e2047.

282. Agwara MO, Ndosiri NB, Mohamadou A, Condé AM: **Synthesis, characterization and antimicrobial evaluation of Mn(II), Co(II), Ni(II), Cu(II), and Zn(II) complexes of pyridine -2- carboxylic acid**. *Research Journal of Pharmaceutical, Biological and Chemical Sciences* 2013, **4**(2):1370-1381.

283. Probetec D: **Recent research in infectious disease drug resistance**. *Drug Resistance Updates* 2007, **10**(6):256-264.

284. Tsipis AC: **DFT flavor of coordination chemistry**. *Coordination Chemistry Reviews* 2014, **272**:1-29.

285. Ciofini I, Daul CA: **DFT calculations of molecular magnetic properties of coordination compounds**. *Coordination Chemistry Reviews* 2003, **238-239** 187-209.

286. Ahuja IS, Singh R, Yadava CL: **Hexamethylenetetramine complexes with manganese(II), cobalt(II), nickel(II), copper(II), zinc(II) and cadmium(II) thiocyanates**. *Spectrochimica Acta Part A: Molecular and Biomolecular Spectroscopy* 1981, **37**(6):407-414.

287. Rai M, Yadav A, Gade A: **Silver nanoparticles as a new generation of antimicrobials**. *Biotechnology Advances* 2009, **27**(1):76-83.

288. Jennifer SJ, Muthiah PT: **Mixed-ligand complexes of Ca(II), Ba(II), Mn(II) and Pd(II) with 1,10-phenanthroline and 5-chloro thiophene 2-carboxylic acid ligands: Role of hybrid carboxylate-water clusters and ligands of crystallisation in building up of supramolecular architectures**. *Inorg Chim Acta* 2014, **414**:170-180.

289. Deegan C, Coyle B, McCann M, Devereux M, Egan DA: **In vitro anti-tumour effect of 1,10-phenanthroline-5,6-dione (phendione), [Cu(phendione)3](ClO4)2•4H2O and [Ag(phendione)2]ClO4using human epithelial cell lines**. *Chemico-Biological Interactions* 2006, **164**(1-2):115-125.

290. Abuskhuna S, Briody J, McCann M, Devereux M, Kavanagh K, Fontecha JB, McKee V: **Synthesis, structure and anti-fungal activity of dimeric Ag(I) complexes containing bis-imidazole ligands**. *Polyhedron* 2004, **23** 1249-1255.

291. Reddy PR, Rajeshwar S, Satyanarayana B: **Synthesis, characterization of new copper (II) Schiff base and 1,10 phenanthroline complexes and study of their bioproperties**. *Journal of Photochemistry and Photobiology B: Biology* 2016, **160**:217-224.

292. Husain A: **Oxidation-Reduction Titrations for Pharmacy Students, 1st Edition.** *Pharmaceutical Analysis* 2017:1-19.

293. García-Martín S, Alario-Franco MA, Ehrenberg H, Rodríguez-Carvajal J, Amador U: **Crystal Structure and Microstructure of Some $La_{2/3-x}Li_{3x}TiO_3$ Oxides: An Example of the Complementary Use of Electron Diffraction and Microscopy and Synchrotron X-ray Diffraction To Study Complex Materials**. *Journal of American Chemical Society* 2004, **126**(11):3587-3596.

294. Bruker: **APEX2 and SAINT Programs for Data Reduction**. In. Madison, Wisconsin, USA: Apex II. p. Bruker AXS Inc.; 2009.

295. Technologies A: **CrysAlisPro Data Collection and Processing Software for Agilent X-ray Diffractometers**. *Technologies UK Ltd, Yarnton, Oxford, UK*, 2014, **44**(0):1-53.

296. Altomare A, Cascarano G, Giacovazzo C, Guagliardi A, Burla MC, Polidori G, Camali M: **SIRPOW92 – a program for automatic solution of crystal structures by direct methods optimized for powder data**. *Journal of Applied Crystallography* 1994, **27**(3):435-436.

297. Linden A, Sheldrick GM: **Chemistry and structure**. *Acta Crystallographica Section C* 2015, **71**(1):1-2.

298. Sheldrick GM: **Serial crystallography with X-ray free-electron laser pulses**. *Acta Crystallographica Section A: Foundations and Advances* 2015, **71**:s1.

299. Macrae CF, Edgington PR, McCabe P, Pidcock E, Shields GP, Taylor R, Towler M, Streek JVd: **Mercury: Visualization and analysis of crystal structures**. *Journal of Applied Crystallography* 2006, **39**(3):453-457.

300. Engel E, Dreizler RM: **Density Functional Theory: An Advanced Course**: Springer; 2011.

301. Becke AD: **Density-functional exchange-energy approximation with correct asymptotic behavior**. *Physical Review A* 1988, **38**(6):3098-3100.

302. Becke AD: **A new mixing of Hartree–Fock and local density□functional theories**. *The Journal of Chemical Physics* 1993, **98**(2):1372-1377.

303. Lee C, Yang W, Parr RG: **Development of the Colle-Salvetti correlation-energy formula into a functional of the electron density**. *Physical Review B* 1988, **37**(2):785-789.

304. Ditchfield R, Hehre WJ, Pople JA: **Self□Consistent Molecular□Orbital Methods. IX. An Extended Gaussian□Type Basis for Molecular□Orbital Studies of Organic Molecules**. *The Journal of Chemical Physics* 1971, **54**(2):724-728.

305. Frisch MJ, Trucks GW, Schlegel HB, Scuseria GE, Robb MA, Cheeseman JR, Montgomery J, J. A., Vreven T, Kudin KN, Burant JC *et al*: **Gaussian 03, Revision A.1**. In. Wallingford, CT: Gaussian, Inc.; 2003.

306. Cramer CJ: **Essentials of Computational Chemistry: Theories and Models**, 2nd edn: Wiley; 2004.

307. Bader RFW: **Atoms in Molecules: A Quantum Theory**. Oxford: Oxford University Press; 1990.

308. Contreras-Garcia J, Yang W, Johnson ER: **Analysis of hydrogen-bond interaction potentials from the electron density: integration of noncovalent interaction regions**. *The journal of physical chemistry A* 2011, **115**(45):12983-12990.

309. Tan SL, Jotani MM, Tiekink ERT: **Utilizing Hirshfeld surface calculations, non-covalent inter-action (NCI) plots and the calculation of inter-action energies in the analysis of molecular packing**. *Acta Crystallogr E Crystallogr Commun* 2019, **75**(Pt 3):308-318.

310. Lu T, Chen F: **Multiwfn: a multifunctional wavefunction analyzer**. *J Comput Chem* 2012, **33**(5):580-592.

311. Berghe DAV, Vlietinck AJ: **Screening for antimicrobila and antiviral agents in K. Hostettmann (ed) Methods in plant biochemistry**. In., vol. 6. London: Academic press; 1991: 47–69.

312. Espinel-Ingroff A, Fothergill A, Ghannoum M, Manavathu E, Ostrosky-Zeichner L, Pfaller MA, Rinaldi MG, Schell W, Walsh TJ: **Quality Control and Reference Guidelines for CLSI Broth Microdilution Method (M38-A Document) for Susceptibility Testing of Anidulafungin against Molds**. *Journal of Clinical Microbiology* 2007, **45**(7):2180-2182.

313. Espinel-Ingroff A: **Comparison of the E-test with the NCCLS M38-P Method for Antifungal Susceptibility Testing of Common and Emerging Pathogenic Filamentous Fungi**. *Journal of Clinical Microbiology* 2001, **39**(4):1360-1367.

314. Kani I, Atlier Ö, Güven K: **Mn(II) complexes with bipyridine, phenanthroline and benzoic acid: Biological and catalase-like activity**. *Journal of Chemical Sciences* 2016, **128**(4):523-536.

315. Ma C, Wang W, Zhu H, Chen C, Liu Q: **Phenanthroline-manganese inclusion complexes of dicarboxylic acid containing extensive hydrogen-bonding interactions**. *Inorganic Chemistry Communications* 2001, **4**(12):730-733.

316. Saravanan C, Mudaliar CG: **Synthesis, characterization and thermal analysis of the copper(II) complexes with 2,2-bipyridyl and 1,10-phenanthroline**. *African Journal of Pure and Applied Chemistry* 2014, **8**(10):162-175.

317. Zierkiewicz W, Privalov T: **A Theoretical Study of the Essential Role of DMSO as a Solvent/Ligand in the $Pd(OAc)_2$/DMSO Catalyst System for Aerobic Oxidation**. *Organometallics* 2005, **24**(24):6019-6028.

318. Mohamed GG, Omar MM, Ibrahim AA: **Preparation, characterization and biological activity of novel metal-NNNN donor Schiff base complexes**. *Spectrochimica Acta Part A: Molecular and Biomolecular Spectroscopy* 2010, **75**(2):678-685.

319. Ndifon PT, Agwara MO, Paboudam AG, Yufanyi DM, Ngoune J, Galindo A, Alvarez E, Mohamadou A: **Synthesis, characterisation and crystal structure of a cobalt(II)-hexamethylenetetramine coordination polymer**. *Transition Metal Chemistry* 2009, **34**(7):745-750.

320. Zheng LL, Zhou CX, Hu S, Zhou AJ: **Structural diversification of coordination assemblies of M(II)-dca - Hydroxylpyridine (dca = Dicyanamide)**. *Polyhedron* 2016, **104**:91-98.

321. Świtlicka-Olszewska A, Palion-Gazda J, Klemens T, Machura B, Vallejo J, Cano J, Lloretb F, Julve M: **Single-ion magnet behaviour in mononuclear and two-dimensional dicyanamide-containing cobalt(II) complexes**. *Dalton Transactions* 2016, **45**(25):10181-10193.

322. Abdel-Kader NS, Mohamed RR: **Synthesis, characterization, and thermal investigation of some transition metal complexes of benzopyran-4-one Schiff base as thermal stabilizers for rigid poly(vinyl chloride) (PVC)**. *Journal of Thermal Analysis and Calorimetry* 2013, **114**(2):603-611.

323. Krishna PM, Reddy KH: **Synthesis, characterization, DNA studies of copper(II) complexes of (2E)-3- phenylprop-2-enal thiosemicarbazones**. *Pharmaceutical Chemistry Journal* 2013, **5**(5):258-269.

324. Kalia SB, Kaushal G, Bharti M: **Magnetic and spectral characterization of new type of 4-methylpiperazine-1-carbodithioate complexes of manganese(II) and manganese(III)**. *IOSR Journal of Applied Chemistry* 2015, **8**(8):26-30.

325. Abdelhak J, Cherni SN, Amami M, Kébir HE, Zid MF, A. Driss, " ., vol. 27, no. 7, pp. , 2014: **Iron(III) and cobalt(III) complexes with oxalate and phenanthroline: Synthesis, crystal structure, spectroscopy properties and magnetic properties**. *Journal of Superconductivity and Novel Magnetism* 2014, **27**(7):1693-1700.

326. Dawood AH, Khalaf R, Salman Z: **Cobalt(II), Nickel(II), and Copper(II) Complexes with Ligands Contain Nitrogen as Donor Atoms type N_3 and Azamacrocylic N_6 , Synthesis and Characterisation.** *National Journal of Chemistry* 2009, **35**:489-505.

327. Konstantinović S, Radovanović B, Cakić I, Vasić V: **Synthesis and characterization of Co(II), Ni(II), Cu(II) and Zn(II) complexes with 3-salicylidenehydrazono-2-indolinone**. *Journal of the Serbian Chemical Society* 2003, **68**((8-9)):641-647.

328. Dawood AH, Kareem ET, Madlool AM: **Binuclear Divalent Complexes of Cobalt, Nickel and Copper with N_2S Ligand Derived from 1,3,4-Thiadiazole-2,5-dithiolate Dipotassium Synthesized via Click Chemistry**. *International Journal of Chemistry* 2012, **4**(6):64-74.

329. Wu D-H, Shi J, Shi Y-J, Jiang G-Q: **Tetrakis(μ-phenoxyacetato-κ^2O:O')-bis[(1,10-phenanthroline-κ^2N,N')- manganese(II)] methanol hemisolvate**. *Acta Crystallographica Section E: Structure Reports Online* 2008, **64**(1):m161-m161.

330. Janiak C: **A critical account on π–π stacking in metal complexes with aromatic nitrogen-containing ligands**. *Journal of the Chemical Society, Dalton Transactions* 2000, **21**:3885-3896.

331. Masárová P, Moncol J: **Crystal structures of $[M(N_3)_2(phen)_2]$ compounds, M = Mn, Co or Cu and phen =1,10-phenanthroline**. *Acta Chimica Slovaca* 2016, **9**(2):152-157.

332. Zhang X, Chen F, Wang W, Chen C, Liu Q: **Aqua(chloroacetato)bis(1,10-phenanthroline-N,N')manganese(II) perchlorate**. *Acta Crystallographica Section E* 2002, **58**(7):m360-m362.

333. Wang ZM, Luo J, Sun BW, Yan CH, Liao CS, Gao S: **cis-Bis(dicyanamido)bis(1,10-phenanthroline)manganese(II) and cis-bis(dicyanamido)bis(1,10-phenanthroline)zinc(II)**. *Acta Crystallographica Section C* 2000, **56**(6):e242-e244.

334. Kozisek J, Hvastijova M, Kohout J: **Addition of Methanol to Dicyanamide in the Cu(II) Coordination Sphere: Structure of Bis(bis(methoxy-carbimido)atiato)copper(II)**. *Inorg Chim Acta* 1990, **168**:157-158.

335. Tong M-L, Wu Y-M, Tong Y-X, Chen X-M, Chang H-C, Kitagawa S: **Rational Design of a Ferromagnetic Trinuclear Copper(II) Complex with a Novel in-situ Synthesised Metalloligand**. *Eur J Inorg Chem* 2003(13):2385-2388.

336. Zheng L-L, Leng J-D, Liu W-T, Zhang W-X, Lu J-X, Tong M-L: **Cu^{2+}-Mediated Nucleophilic Addition of Different Nucleophiles to Dicyanamide - Synthesis, Structures, and Magnetic Properties of a Family of Mononuclear, Trinuclear, Hexanuclear, and Polymeric Copper(II) Complexes**. *European Journal of Inorganic Chemistry* 2008, **2008**(29):4616-4624.

337. Yanick Gaelle DS, Ondoh Agwara M, Yufanyi DM, Nenwa J, Jagan R: **Crystal structure and antimicrobial properties of a copper(II) complex with 1,10-phenanthroline and azide co-ligand**. *Inorganic and Nano-Metal Chemistry* 2017, **47**(4):618-625.

338. Sahin ZS, Sahin O, Daglı Ö, Köse DA: **Diphenic acid/nicotinamide complexes of Co^{II}, Cu^{II} and Zn^{II}. Synthesis and structural investigation**. *Polyhedron* 2016, **117**:214-223.

339. Turner DR, Chesman ASR, Murray KS, Deacon GB, Batten SR: **The chemistry and complexes of small cyano anions**. *Chemical Communications* 2011, **47**(37):10189-10210.

340. Yesilel OZ, Olmez H, Yılanc OO, Aoglu HuP, Buyukgungor O: **Syntheses, Spectral and Thermal Studies, and Crystal Structure of 1,10-Phenanthroline and Picolinamide Complexes of Cobalt(II) Squarate**. *Verlag der Zeitschrift fur Naturforschung, Tubingen* 2003, **2**:1094-1100.

341. Lan T, Fallatah A, Suiter E, Padalkar S: **Size Controlled Copper(I) Oxide Nanoparticles Influence Sensitivity of Glucose Biosensor**. *Sensors* 2017, **17**:1-10.

342. Sawant SS, Bhagwat AD, Mahajan CM: **Novel Facile Technique for Synthesis of Stable Cuprous Oxide (Cu2O) Nanoparticles - an Ageing Effect**. *Journal of Nano- and Electronic Physics* 2016, **8**(1):1-4.

343. Firmansyah DA, Kim T, Kim S, Sullivan K, Zachariah MR, Lee D: **Crystalline Phase Reduction of Cuprous Oxide (Cu_2O) Nanoparticles Accompanied by a Morphology Change during Ethanol-Assisted Spray Pyrolysis**. *Journal of the American Chemical Society* 2009, **25**(12):7063-7071.

344. Grabowski SJ: **Hydrogen bonding strength—measures based on geometric and topological parameters**. *Journal of Physical Organic Chemistry* 2004, **17**(1):18-31.

345. Biswal HS, Shirhatti PR, Wategaonkar S: **O−H···O versus O−H···S Hydrogen Bonding I: Experimental and Computational Studies on the p-Cresol·H2O and p-Cresol·H2S Complexes**. *The Journal of Physical Chemistry A* 2009, **113**(19):5633-5643.

346. Gandra RM, Carron PM, Fernades MF, Ramos LS, Mello JP, Aor AC, McCann M, Devereux M, Santos AL: **Antifungal potential of copper(II), Manganese(II) and silver(I) 1,10-phenanthroline chelates against multidrug-resistant fungal species forming the Candida haemulonii Complex: Impact on the planktonic and biofilm lifestyles**. *Frontiers in Microbiology* 2017, **8**(1257):1-11.

347. Chohan ZH, Munawar A, Supuran CT: **Transition Metal Ion Complexes of Schiff-bases. Synthesis, Characterization and Antibacterial Properties**. *Metal-Based Drugs* 2001, **8**(3):137-143.

APPENDICES

APPENDIX I: SUPPLEMENTARY INFORMATION ON THE CRYSTAL STRUCTURES

1: Supplementary Information for $[Mn(Phen)_2(NO_3)_2]$ Comples

Table XXXII: Atomic coordinates (x 10^4) and equivalent isotropic displacement parameters (A^2 x 10^3). U(eq) is defined as one third of the trace of the orthogonalized Uij tensor.

	x	y	z	U(eq)
C(1)	-1182(3)	-473(4)	6459(2)	62(1)
C(2)	-1277(3)	-1430(4)	5896(2)	73(1)
C(3)	-411(4)	-1761(4)	5485(2)	73(1)
C(4)	566(3)	-1145(4)	5627(2)	58(1)
C(5)	1506(4)	-1443(4)	5213(3)	77(1)
C(6)	2423(3)	-855(4)	5376(3)	75(1)
C(7)	2513(3)	55(4)	5979(2)	62(1)
C(8)	3470(3)	646(4)	6189(3)	78(1)
C(9)	3501(3)	1475(5)	6776(3)	89(2)
C(10)	2555(3)	1792(4)	7160(3)	77(1)
C(11)	1598(2)	394(3)	6399(2)	49(1)
C(12)	599(2)	-217(3)	6213(2)	46(1)
N(1)	-272(2)	123(3)	6618(2)	49(1)
N(2)	1616(2)	1265(3)	6977(2)	58(1)
N(3)	-732(3)	3828(4)	6442(2)	74(1)
O(1)	-1092(4)	3585(8)	7057(3)	194(3)
O(2)	-47(4)	3051(4)	6295(3)	141(2)
O(3)	-1025(3)	4628(4)	6028(3)	153(2)
Mn(1)	0	1777(1)	7500	51(1)

Table XXXIII: Bond lengths [A] and angles [deg]

Bond lengths [A]		angles [deg]	
C(1)-N(1)	1.323(4)	N(1)-C(1)-C(2)	122.9(3)
C(1)-C(2)	1.397(5)	N(1)-C(1)-H(1)	118.6
C(1)-H(1)	0.9300	C(2)-C(1)-H(1)	118.6
C(2)-C(3)	1.350(6)	C(3)-C(2)-C(1)	119.3(3)
C(2)-H(2)	0.9300	C(3)-C(2)-H(2)	120.4
C(3)-C(4)	1.399(5)	C(1)-C(2)-H(2)	120.4
C(3)-H(3)	0.9300	C(2)-C(3)-C(4)	119.8(4)
C(4)-C(12)	1.402(5)	C(2)-C(3)-H(3)	120.1
C(4)-C(5)	1.421(5)	C(4)-C(3)-H(3)	120.1
C(5)-C(6)	1.328(6)	C(3)-C(4)-C(12)	117.4(3)
C(5)-H(5)	0.9300	C(3)-C(4)-C(5)	122.6(4)
C(6)-C(7)	1.417(6)	C(12)-C(4)-C(5)	120.0(3)
C(6)-H(6)	0.9300	C(6)-C(5)-C(4)	120.7(4)
C(7)-C(8)	1.394(6)	C(6)-C(5)-H(5)	119.6
C(7)-C(11)	1.410(5)	C(4)-C(5)-H(5)	119.6
C(8)-C(9)	1.337(7)	C(5)-C(6)-C(7)	121.7(4)
C(8)-H(8)	0.9300	C(5)-C(6)-H(6)	119.1
C(9)-C(10)	1.405(7)	C(7)-C(6)-H(6)	119.1
C(9)-H(9)	0.9300	C(8)-C(7)-C(11)	117.1(4)
C(10)-N(2)	1.335(5)	C(8)-C(7)-C(6)	123.4(4)
C(10)-H(10)	0.9300	C(11)-C(7)-C(6)	119.4(3)
C(11)-N(2)	1.352(4)	C(9)-C(8)-C(7)	120.2(4)
C(11)-C(12)	1.438(4)	C(9)-C(8)-H(8)	119.9
C(12)-N(1)	1.351(4)	C(7)-C(8)-H(8)	119.9
N(1)-Mn(1)	2.319(3)	C(8)-C(9)-C(10)	119.8(4)
N(2)-Mn(1)	2.289(3)	C(8)-C(9)-H(9)	120.1
N(3)-O(3)	1.155(4)	C(10)-C(9)-H(9)	120.1
N(3)-O(2)	1.195(5)	N(2)-C(10)-C(9)	122.4(4)
N(3)-O(1)	1.203(5)	N(2)-C(10)-H(10)	118.8
O(1)-Mn(1)	2.422(6)	C(9)-C(10)-H(10)	118.8
O(2)-Mn(1)	2.495(6)	N(2)-C(11)-C(7)	123.0(3)
Mn(1)-N(2)#1	2.289(3)	N(2)-C(11)-C(12)	118.0(3)
Mn(1)-N(1)#1	2.319(3)	C(7)-C(11)-C(12)	118.9(3)
Mn(1)-O(1)#1	2.422(7)	N(1)-C(12)-C(4)	122.7(3)
Mn(1)-O(2)#1	2.495(6)	N(1)-C(12)-C(11)	118.3(3)
		C(4)-C(12)-C(11)	119.0(3)
		C(1)-N(1)-C(12)	118.0(3)
		C(1)-N(1)-Mn(1)	127.0(2)

C(12)-N(1)-Mn(1)	115.0(2)
C(10)-N(2)-C(11)	117.5(3)
C(10)-N(2)-Mn(1)	126.3(3)
C(11)-N(2)-Mn(1)	116.1(2)
O(3)-N(3)-O(2)	123.8(5)
O(3)-N(3)-O(1)	126.7(6)
O(2)-N(3)-O(1)	109.3(5)
N(3)-O(1)-Mn(1)	103.6(4)
N(3)-O(2)-Mn(1)	100.0(4)
N(2)#1-Mn(1)-N(2)	153.72(15)
N(2)#1-Mn(1)-N(1)#1	72.14(10)
N(2)-Mn(1)-N(1)#1	88.70(10)
N(2)#1-Mn(1)-N(1)	88.70(10)
N(2)-Mn(1)-N(1)	72.14(10)
N(1)#1-Mn(1)-N(1)	87.09(14)
N(2)#1-Mn(1)-O(1)#1	122.84(14)
N(2)-Mn(1)-O(1)#1	78.61(15)
N(1)#1-Mn(1)-O(1)#1	104.40(18)
N(1)-Mn(1)-O(1)#1	148.31(14)
N(2)#1-Mn(1)-O(1)	78.61(15)
N(2)-Mn(1)-O(1)	122.84(14)
N(1)#1-Mn(1)-O(1)	148.31(14)
N(1)-Mn(1)-O(1)	104.40(18)
O(1)#1-Mn(1)-O(1)	81.3(3)
N(2)#1-Mn(1)-O(2)	116.27(14)
N(2)-Mn(1)-O(2)	78.08(14)
N(1)#1-Mn(1)-O(2)	162.70(12)
N(1)-Mn(1)-O(2)	78.33(11)
O(1)#1-Mn(1)-O(2)	84.05(19)
O(1)-Mn(1)-O(2)	46.86(16)
N(2)#1-Mn(1)-O(2)#1	78.08(14)
N(2)-Mn(1)-O(2)#1	116.27(14)
N(1)#1-Mn(1)-O(2)#1	78.33(11)
N(1)-Mn(1)-O(2)#1	162.70(12)
O(1)#1-Mn(1)-O(2)#1	46.86(16)
O(1)-Mn(1)-O(2)#1	84.05(19)
O(2)-Mn(1)-O(2)#1	117.46(19)

Symmetry transformations used to generate equivalent atoms: #1 -x,y,-z+3/2

Table XXXIV: Anisotropic displacement parameters (A^2 x 10^3). The anisotropic displacement factor exponent takes the form: -2 pi^2 [h^2 a*^2 U11 + ... + 2 h k a* b* U12]

	U11	U22	U33	U23	U13	U12
C(1)	50(2)	69(2)	66(2)	-11(2)	3(2)	-11(2)
C(2)	63(2)	78(3)	78(3)	-23(2)	-4(2)	-17(2)
C(3)	79(2)	69(2)	71(3)	-22(2)	-3(2)	-10(2)
C(4)	63(2)	54(2)	56(2)	-2(2)	3(2)	6(2)
C(5)	79(3)	69(2)	82(3)	-13(2)	18(2)	7(2)
C(6)	73(3)	64(2)	89(3)	3(2)	27(2)	17(2)
C(7)	45(2)	60(2)	80(2)	26(2)	7(2)	6(2)
C(8)	51(2)	75(3)	109(4)	30(3)	4(2)	3(2)
C(9)	45(2)	109(4)	112(4)	39(3)	-18(2)	-24(2)
C(10)	63(2)	92(3)	77(3)	7(2)	-17(2)	-26(2)
C(11)	47(2)	47(2)	51(2)	14(1)	0(1)	-1(1)
C(12)	45(2)	47(2)	45(2)	6(1)	-1(1)	0(1)
N(1)	49(1)	52(2)	46(1)	-1(1)	1(1)	-5(1)
N(2)	51(2)	63(2)	59(2)	9(2)	-9(1)	-14(1)
N(3)	61(2)	89(3)	73(2)	23(2)	-15(2)	-18(2)
O(1)	128(4)	333(9)	120(4)	70(5)	26(3)	15(5)
O(2)	175(5)	105(3)	142(4)	-43(3)	-52(3)	45(3)
O(3)	94(3)	151(4)	213(5)	122(4)	-57(3)	-19(2)
Mn(1)	60(1)	48(1)	44(1)	0	-2(1)	0

Table XXXV: Hydrogen coordinates (x 10^4) and isotropic displacement parameters (A^2 x 10^3).

	x	y	z	U(eq)
H(1)	-1786	-245	6735	74
H(2)	-1929	-1834	5805	87
H(3)	-463	-2397	5109	88
H(5)	1478	-2056	4823	92
H(6)	3022	-1046	5086	91
H(8)	4090	464	5920	94
H(9)	4145	1840	6929	106
H(10)	2585	2390	7558	93

Table XXXVI: Torsion angles [deg].

N(1)-C(1)-C(2)-C(3)	-0.8(7)
C(1)-C(2)-C(3)-C(4)	-0.1(7)
C(2)-C(3)-C(4)-C(12)	1.4(6)
C(2)-C(3)-C(4)-C(5)	-179.6(4)
C(3)-C(4)-C(5)-C(6)	-178.6(4)
C(12)-C(4)-C(5)-C(6)	0.3(6)
C(4)-C(5)-C(6)-C(7)	2.0(7)
C(5)-C(6)-C(7)-C(8)	177.0(4)
C(5)-C(6)-C(7)-C(11)	-2.8(6)
C(11)-C(7)-C(8)-C(9)	1.3(6)
C(6)-C(7)-C(8)-C(9)	-178.5(4)
C(7)-C(8)-C(9)-C(10)	-2.7(7)
C(8)-C(9)-C(10)-N(2)	2.0(7)
C(8)-C(7)-C(11)-N(2)	0.9(5)
C(6)-C(7)-C(11)-N(2)	-179.2(3)
C(8)-C(7)-C(11)-C(12)	-178.6(3)
C(6)-C(7)-C(11)-C(12)	1.3(5)
C(3)-C(4)-C(12)-N(1)	-2.2(5)
C(5)-C(4)-C(12)-N(1)	178.9(3)
C(3)-C(4)-C(12)-C(11)	177.2(3)
C(5)-C(4)-C(12)-C(11)	-1.8(5)
N(2)-C(11)-C(12)-N(1)	0.8(4)
C(7)-C(11)-C(12)-N(1)	-179.7(3)
N(2)-C(11)-C(12)-C(4)	-178.6(3)
C(7)-C(11)-C(12)-C(4)	0.9(5)
C(2)-C(1)-N(1)-C(12)	0.1(5)
C(2)-C(1)-N(1)-Mn(1)	177.5(3)
C(4)-C(12)-N(1)-C(1)	1.4(5)
C(11)-C(12)-N(1)-C(1)	-177.9(3)
C(4)-C(12)-N(1)-Mn(1)	-176.3(2)
C(11)-C(12)-N(1)-Mn(1)	4.3(3)
C(9)-C(10)-N(2)-C(11)	0.3(6)
C(9)-C(10)-N(2)-Mn(1)	-176.0(3)
C(7)-C(11)-N(2)-C(10)	-1.7(5)
C(12)-C(11)-N(2)-C(10)	177.8(3)
C(7)-C(11)-N(2)-Mn(1)	174.9(2)
C(12)-C(11)-N(2)-Mn(1)	-5.6(4)
O(3)-N(3)-O(1)-Mn(1)	179.6(4)
O(2)-N(3)-O(1)-Mn(1)	3.8(5)
O(3)-N(3)-O(2)-Mn(1)	-179.6(4)
O(1)-N(3)-O(2)-Mn(1)	-3.6(5)

Symmetry transformations used to generate equivalent atoms:
#1 -x,y,-z+3/2

2: Supplementary Information for [Mn(Phen)$_2$(N$_3$)$_2$] Complex

Table XXXVII: Fractional atomic coordinates and isotropic or equivalent isotropic displacement parameters (Å2)

	x	*y*	*z*	U_{iso}*/U_{eq}
Mn1	0.5000	0.19559 (11)	0.7500	0.0462 (4)
N1	0.4944 (3)	0.0209 (4)	0.6562 (2)	0.0494 (10)
N2	0.6594 (3)	0.1433 (5)	0.7160 (3)	0.0510 (11)
N3	0.5386 (4)	0.3406 (7)	0.8396 (4)	0.099 (2)
C11	0.6708 (4)	0.0438 (5)	0.6599 (3)	0.0499 (13)
N4	0.5953 (4)	0.4041 (6)	0.8712 (3)	0.0688 (14)
C12	0.5836 (4)	−0.0203 (5)	0.6279 (3)	0.0474 (12)
C7	0.7654 (4)	0.0028 (6)	0.6335 (4)	0.0644 (16)
C10	0.7405 (4)	0.1985 (6)	0.7477 (4)	0.0616 (14)
H10	0.7329	0.2657	0.7865	0.074*
C1	0.4128 (4)	−0.0373 (7)	0.6274 (3)	0.0656 (16)
H1	0.3508	−0.0079	0.6456	0.079*
C4	0.5932 (5)	−0.1225 (7)	0.5701 (3)	0.0668 (17)
C6	0.7715 (6)	−0.1000 (8)	0.5739 (4)	0.088 (2)
H6	0.8340	−0.1274	0.5558	0.106*
C8	0.8483 (4)	0.0642 (7)	0.6691 (5)	0.081 (2)
H8	0.9123	0.0383	0.6536	0.098*
C2	0.4168 (6)	−0.1415 (8)	0.5704 (4)	0.088 (2)
H2	0.3583	−0.1821	0.5521	0.106*
C5	0.6905 (6)	−0.1584 (8)	0.5432 (4)	0.086 (2)
H5	0.6975	−0.2240	0.5034	0.104*
C9	0.8363 (4)	0.1605 (7)	0.7256 (5)	0.080 (2)
H9	0.8915	0.2011	0.7495	0.096*
C3	0.5059 (6)	−0.1831 (7)	0.5420 (4)	0.088 (2)
H3	0.5091	−0.2521	0.5038	0.106*
N5	0.6523 (8)	0.4665 (12)	0.9015 (5)	0.184 (5)

Table XXXVIII: Atomic displacement parameters (Å2)

	U^{11}	U^{22}	U^{33}	U^{12}	U^{13}	U^{23}
Mn1	0.0383 (6)	0.0451 (7)	0.0553 (7)	0.000	0.0008 (5)	0.000
N1	0.054 (2)	0.055 (3)	0.040 (2)	−0.008 (2)	0.001 (2)	−0.0005 (19)
N2	0.042 (2)	0.052 (3)	0.058 (3)	−0.002 (2)	0.003 (2)	0.006 (2)
N3	0.074 (4)	0.092 (5)	0.132 (6)	0.001 (3)	−0.011 (4)	−0.054 (4)
C11	0.050 (3)	0.045 (3)	0.054 (3)	0.006 (2)	0.011 (2)	0.015 (3)
N4	0.070 (3)	0.071 (4)	0.066 (3)	−0.009 (3)	−0.014 (3)	−0.002 (3)
C12	0.057 (3)	0.047 (3)	0.038 (3)	0.004 (2)	0.011 (2)	0.006 (2)
C7	0.061 (4)	0.055 (4)	0.077 (4)	0.016 (3)	0.023 (3)	0.015 (3)
C10	0.043 (3)	0.067 (4)	0.075 (3)	−0.004 (3)	−0.002 (3)	0.000 (3)
C1	0.064 (4)	0.080 (5)	0.053 (3)	−0.014 (3)	0.000 (3)	−0.014 (3)
C4	0.084 (4)	0.062 (4)	0.055 (4)	0.002 (3)	0.012 (3)	−0.005 (3)
C6	0.090 (5)	0.077 (5)	0.098 (5)	0.022 (4)	0.045 (4)	0.002 (4)
C8	0.046 (3)	0.074 (5)	0.124 (6)	0.019 (3)	0.020 (4)	0.023 (5)
C2	0.092 (5)	0.101 (6)	0.071 (5)	−0.026 (5)	−0.006 (4)	−0.026 (4)
C5	0.107 (6)	0.077 (5)	0.075 (5)	0.012 (4)	0.034 (4)	−0.013 (4)
C9	0.042 (3)	0.080 (5)	0.118 (6)	0.003 (3)	−0.002 (3)	0.010 (4)
C3	0.116 (6)	0.084 (5)	0.064 (4)	−0.008 (5)	0.005 (4)	−0.031 (4)
N5	0.214 (10)	0.209 (11)	0.129 (7)	−0.097 (9)	−0.045 (7)	−0.026 (7)

Table XXXIX: Bond lengths [A]

Mn1—N3	2.130 (6)	C7—C6	1.419 (9)
Mn1—N3i	2.130 (6)	C10—C9	1.386 (8)
Mn1—N2i	2.268 (4)	C10—H10	0.93
Mn1—N2	2.268 (4)	C1—C2	1.397 (9)
Mn1—N1i	2.320 (4)	C1—H1	0.93
Mn1—N1	2.320 (4)	C4—C3	1.391 (9)
N1—C1	1.323 (6)	C4—C5	1.425 (9)
N1—C12	1.347 (6)	C6—C5	1.329 (10)
N2—C10	1.325 (7)	C6—H6	0.93
N2—C11	1.360 (7)	C8—C9	1.345 (10)
N3—N4	1.114 (7)	C8—H8	0.93
C11—C7	1.401 (7)	C2—C3	1.348 (10)
C11—C12	1.430 (7)	C2—H2	0.93
N4—N5	1.100 (9)	C5—H5	0.93
C12—C4	1.397 (8)	C9—H9	0.93

Table XL: Bond angles [deg]

N3—Mn1—N3i	97.9 (4)	C8—C7—C6	124.0 (6)
N3—Mn1—N2i	101.1 (2)	C11—C7—C6	118.5 (6)
N3i—Mn1—N2i	95.7 (2)	N2—C10—C9	122.9 (6)
N3—Mn1—N2	95.7 (2)	N2—C10—H10	118.5
N3i—Mn1—N2	101.1 (2)	C9—C10—H10	118.5
N2i—Mn1—N2	154.3 (2)	N1—C1—C2	122.0 (6)
N3—Mn1—N1i	88.8 (2)	N1—C1—H1	119
N3i—Mn1—N1i	167.17 (19)	C2—C1—H1	119
N2i—Mn1—N1i	72.16 (16)	C3—C4—C12	117.4 (6)
N2—Mn1—N1i	89.03 (15)	C3—C4—C5	123.8 (6)
N3—Mn1—N1	167.17 (19)	C12—C4—C5	118.8 (6)
N3i—Mn1—N1	88.8 (2)	C5—C6—C7	122.0 (6)
N2i—Mn1—N1	89.03 (15)	C5—C6—H6	119
N2—Mn1—N1	72.16 (16)	C7—C6—H6	119
N1i—Mn1—N1	86.8 (2)	C9—C8—C7	120.4 (6)
C1—N1—C12	118.4 (5)	C9—C8—H8	119.8
C1—N1—Mn1	126.0 (4)	C7—C8—H8	119.8
C12—N1—Mn1	115.5 (3)	C3—C2—C1	119.8 (6)
C10—N2—C11	118.4 (5)	C3—C2—H2	120.1
C10—N2—Mn1	125.4 (4)	C1—C2—H2	120.1
C11—N2—Mn1	116.2 (3)	C6—C5—C4	121.2 (6)
N4—N3—Mn1	150.6 (6)	C6—C5—H5	119.4
N2—C11—C7	121.7 (5)	C4—C5—H5	119.4
N2—C11—C12	118.6 (4)	C8—C9—C10	119.1 (6)
C7—C11—C12	119.7 (5)	C8—C9—H9	120.4
N5—N4—N3	178.8 (9)	C10—C9—H9	120.4
N1—C12—C4	122.7 (5)	C2—C3—C4	119.7 (6)
N1—C12—C11	117.5 (5)	C2—C3—H3	120.1

C4—C12—C11	119.8 (5)	C4—C3—H3	120.1
C8—C7—C11	117.5 (6)		

Table XLI: Torsion angles [deg].

C10—N2—C11—C7	−2.2 (7)	Mn1—N1—C1—C2	179.5 (5)
Mn1—N2—C11—C7	179.6 (4)	N1—C12—C4—C3	−0.4 (9)
C10—N2—C11—C12	177.4 (5)	C11—C12—C4—C3	178.9 (6)
Mn1—N2—C11—C12	−0.8 (6)	N1—C12—C4—C5	179.4 (5)
C1—N1—C12—C4	−0.7 (8)	C11—C12—C4—C5	−1.3 (8)
Mn1—N1—C12—C4	−178.8 (4)	C8—C7—C6—C5	178.1 (7)
C1—N1—C12—C11	−180.0 (5)	C11—C7—C6—C5	−0.4 (10)
Mn1—N1—C12—C11	1.9 (6)	C11—C7—C8—C9	−1.1 (9)
N2—C11—C12—N1	−0.8 (7)	C6—C7—C8—C9	−179.6 (6)
C7—C11—C12—N1	178.8 (5)	N1—C1—C2—C3	−1.5 (11)
N2—C11—C12—C4	179.9 (5)	C7—C6—C5—C4	−1.5 (12)
C7—C11—C12—C4	−0.5 (8)	C3—C4—C5—C6	−177.9 (7)
N2—C11—C7—C8	2.4 (8)	C12—C4—C5—C6	2.3 (11)
C12—C11—C7—C8	−177.2 (5)	C7—C8—C9—C10	−0.3 (10)
N2—C11—C7—C6	−179.0 (5)	N2—C10—C9—C8	0.5 (10)
C12—C11—C7—C6	1.4 (8)	C1—C2—C3—C4	0.4 (12)
C11—N2—C10—C9	0.8 (8)	C12—C4—C3—C2	0.5 (10)
Mn1—N2—C10—C9	178.7 (5)	C5—C4—C3—C2	−179.3 (7)
C12—N1—C1—C2	1.6 (9)		

Table XLII: Hydrogen-bond geometry (Å, º)

D—H···*A*	*D*—H	H···*A*	*D*···*A*	*D*—H···*A*
C10—H10···N4	0.93	2.69	3.481 (8)	143
C10—H10···N4	0.93	2.69	3.481 (8)	143

Symmetry code: (i) −*x*+1, *y*, −*z*+3/2

3: Supplementary Information for [Mn(Phen)$_2$(dca)$_2$] Complex

Table XLIII: Atomic coordinates (x 10^4) and equivalent isotropic displacement parameters (Å^{2}x 10^3) for ke07. U(eq) is defined as one third of the trace of the orthogonalized U^{ij} tensor.

	x	y	z	U(eq)
Mn(1)	7115(1)	7184(1)	4885(1)	19(1)
N(1)	8941(1)	6283(1)	5453(1)	20(1)
N(2)	8584(1)	7148(1)	4063(1)	22(1)
N(3)	6020(1)	8457(1)	4330(1)	22(1)
N(4)	8452(1)	8418(1)	5464(1)	21(1)
N(5)	5708(2)	6293(1)	4093(1)	32(1)
N(6)	5000(2)	5088(2)	3128(1)	54(1)
N(7)	2647(2)	4532(1)	2481(1)	35(1)
N(8)	6182(2)	7084(1)	5866(1)	30(1)
N(9)	5228(2)	7481(1)	6977(1)	39(1)
N(10)	2761(2)	7499(2)	7040(1)	47(1)
C(1)	9102(2)	5845(1)	6129(1)	24(1)
C(2)	10360(2)	5436(1)	6521(1)	31(1)
C(3)	11492(2)	5486(1)	6205(1)	33(1)
C(4)	11362(2)	5926(1)	5482(1)	26(1)
C(5)	10056(2)	6313(1)	5123(1)	20(1)
C(6)	9857(2)	6764(1)	4379(1)	20(1)
C(7)	10959(2)	6789(1)	4002(1)	27(1)
C(8)	10689(2)	7200(1)	3255(1)	36(1)
C(9)	9396(2)	7565(1)	2938(1)	38(1)
C(10)	8370(2)	7533(1)	3363(1)	30(1)
C(11)	12484(2)	6002(1)	5097(1)	35(1)
C(12)	12291(2)	6407(1)	4393(1)	36(1)
C(13)	4835(2)	8472(1)	3772(1)	28(1)
C(14)	4178(2)	9283(2)	3457(1)	34(1)
C(15)	4765(2)	10098(1)	3728(1)	33(1)
C(16)	6024(2)	10113(1)	4318(1)	28(1)
C(17)	6618(2)	9268(1)	4603(1)	22(1)
C(18)	7910(2)	9248(1)	5207(1)	22(1)
C(19)	8552(2)	10074(1)	5503(1)	27(1)
C(20)	9813(2)	10023(1)	6093(1)	31(1)
C(21)	10355(2)	9186(1)	6348(1)	30(1)
C(22)	9647(2)	8403(1)	6017(1)	25(1)
C(23)	6709(2)	10938(1)	4634(1)	35(1)
C(24)	7917(2)	10920(1)	5198(1)	34(1)
C(25)	5286(2)	5740(1)	3630(1)	28(1)
C(26)	3719(2)	4831(1)	2804(1)	27(1)
C(27)	5666(2)	7253(1)	6370(1)	24(1)
C(28)	3891(2)	7472(1)	6973(1)	30(1)

Table XLIV: Bond lengths [Å] and angles [°].

Bond lengths [Å]		Bond angles [°]	
Mn(1)-N(5)	2.1505(16)	N(5)-Mn(1)-N(8)	98.21(6)
Mn(1)-N(8)	2.1552(15)	N(5)-Mn(1)-N(3)	93.37(6)
Mn(1)-N(3)	2.2549(14)	N(8)-Mn(1)-N(3)	98.65(5)
Mn(1)-N(1)	2.2593(14)	N(5)-Mn(1)-N(1)	104.32(6)
Mn(1)-N(2)	2.2897(13)	N(8)-Mn(1)-N(1)	93.31(5)
Mn(1)-N(4)	2.3214(14)	N(3)-Mn(1)-N(1)	157.00(5)
N(1)-C(1)	1.328(2)	N(5)-Mn(1)-N(2)	89.05(6)
N(1)-C(5)	1.366(2)	N(8)-Mn(1)-N(2)	165.68(5)
N(2)-C(10)	1.324(2)	N(3)-Mn(1)-N(2)	93.19(5)
N(2)-C(6)	1.364(2)	N(1)-Mn(1)-N(2)	72.87(5)
N(3)-C(13)	1.328(2)	N(5)-Mn(1)-N(4)	164.65(6)
N(3)-C(17)	1.361(2)	N(8)-Mn(1)-N(4)	90.62(6)
N(4)-C(22)	1.331(2)	N(3)-Mn(1)-N(4)	72.81(5)
N(4)-C(18)	1.360(2)	N(1)-Mn(1)-N(4)	87.57(5)
N(5)-C(25)	1.152(2)	N(2)-Mn(1)-N(4)	85.19(5)
N(6)-C(25)	1.286(3)	C(1)-N(1)-C(5)	117.89(15)
N(6)-C(26)	1.307(3)	C(1)-N(1)-Mn(1)	125.75(11)
N(7)-C(26)	1.156(2)	C(5)-N(1)-Mn(1)	115.56(11)
N(8)-C(27)	1.155(2)	C(10)-N(2)-C(6)	118.27(15)
N(9)-C(27)	1.294(2)	C(10)-N(2)-Mn(1)	126.81(12)
N(9)-C(28)	1.318(2)	C(6)-N(2)-Mn(1)	114.56(10)
N(10)-C(28)	1.151(2)	C(13)-N(3)-C(17)	118.20(15)
C(1)-C(2)	1.397(3)	C(13)-N(3)-Mn(1)	124.99(13)
C(2)-C(3)	1.368(3)	C(17)-N(3)-Mn(1)	116.80(11)
C(3)-C(4)	1.405(3)	C(22)-N(4)-C(18)	117.58(15)
C(4)-C(5)	1.406(2)	C(22)-N(4)-Mn(1)	127.78(12)
C(4)-C(11)	1.440(3)	C(18)-N(4)-Mn(1)	114.62(11)
C(5)-C(6)	1.438(2)	C(25)-N(5)-Mn(1)	161.68(14)
C(6)-C(7)	1.409(2)	C(25)-N(6)-C(26)	122.57(18)
C(7)-C(8)	1.411(3)	C(27)-N(8)-Mn(1)	163.57(15)
C(7)-C(12)	1.438(3)	C(27)-N(9)-C(28)	122.18(17)
C(8)-C(9)	1.369(3)	N(1)-C(1)-C(2)	122.92(17)
C(9)-C(10)	1.402(3)	C(3)-C(2)-C(1)	119.46(17)
C(11)-C(12)	1.344(3)	C(2)-C(3)-C(4)	119.55(17)
C(13)-C(14)	1.402(3)	C(3)-C(4)-C(5)	117.37(16)
C(14)-C(15)	1.362(3)	C(3)-C(4)-C(11)	123.70(17)
C(15)-C(16)	1.409(3)	C(5)-C(4)-C(11)	118.93(17)
C(16)-C(17)	1.408(2)	N(1)-C(5)-C(4)	122.77(16)
C(16)-C(23)	1.430(3)	N(1)-C(5)-C(6)	117.38(14)
C(17)-C(18)	1.444(2)	C(4)-C(5)-C(6)	119.85(15)
C(18)-C(19)	1.407(2)	N(2)-C(6)-C(7)	122.56(16)
C(19)-C(20)	1.412(3)	N(2)-C(6)-C(5)	117.75(14)
C(19)-C(24)	1.432(3)	C(7)-C(6)-C(5)	119.69(16)
C(20)-C(21)	1.369(3)	C(6)-C(7)-C(8)	117.47(17)

C(21)-C(22)	1.394(2)	C(6)-C(7)-C(12)	118.96(17)
C(23)-C(24)	1.350(3)	C(8)-C(7)-C(12)	123.56(17)
		C(9)-C(8)-C(7)	119.24(17)
		C(8)-C(9)-C(10)	119.57(18)
		N(2)-C(10)-C(9)	122.84(19)
		C(12)-C(11)-C(4)	121.26(18)
		C(11)-C(12)-C(7)	121.21(17)
		N(3)-C(13)-C(14)	122.84(18)
		C(15)-C(14)-C(13)	119.43(17)
		C(14)-C(15)-C(16)	119.52(17)
		C(17)-C(16)-C(15)	117.53(17)
		C(17)-C(16)-C(23)	119.39(17)
		C(15)-C(16)-C(23)	123.08(17)
		N(3)-C(17)-C(16)	122.48(16)
		N(3)-C(17)-C(18)	117.91(15)
		C(16)-C(17)-C(18)	119.61(16)
		N(4)-C(18)-C(19)	122.87(16)
		N(4)-C(18)-C(17)	117.82(15)
		C(19)-C(18)-C(17)	119.31(15)
		C(18)-C(19)-C(20)	117.46(16)
		C(18)-C(19)-C(24)	119.44(17)
		C(20)-C(19)-C(24)	123.10(17)
		C(21)-C(20)-C(19)	119.36(17)
		C(20)-C(21)-C(22)	119.13(17)
		N(4)-C(22)-C(21)	123.60(17)
		C(24)-C(23)-C(16)	121.06(17)
		C(23)-C(24)-C(19)	121.19(18)
		N(5)-C(25)-N(6)	171.7(2)
		N(7)-C(26)-N(6)	172.9(2)
		N(8)-C(27)-N(9)	173.4(2)
		N(10)-C(28)-N(9)	173.4(2)

Symmetry transformations used to generate equivalent atoms:

Table XLV: Anisotropic displacement parameters ($Å^2 x\ 10^3$). The anisotropic displacement factor exponent takes the form: $-2\pi^2[\ h^2\ a^{*2}U^{11} + ...\ + 2\ h\ k\ a^*\ b^*\ U^{12}\ ]$

	U^{11}	U^{22}	U^{33}	U^{23}	U^{13}	U^{12}
Mn(1)	16(1)	23(1)	20(1)	-1(1)	6(1)	2(1)
N(1)	19(1)	19(1)	22(1)	-2(1)	7(1)	0(1)
N(2)	23(1)	24(1)	20(1)	0(1)	9(1)	-1(1)
N(3)	20(1)	28(1)	20(1)	1(1)	6(1)	4(1)
N(4)	22(1)	22(1)	20(1)	0(1)	6(1)	2(1)
N(5)	21(1)	37(1)	38(1)	-11(1)	6(1)	-3(1)
N(6)	24(1)	70(1)	64(1)	-42(1)	5(1)	2(1)
N(7)	32(1)	36(1)	33(1)	2(1)	1(1)	-5(1)
N(8)	25(1)	40(1)	29(1)	4(1)	13(1)	5(1)
N(9)	30(1)	64(1)	24(1)	-4(1)	10(1)	9(1)
N(10)	41(1)	68(1)	39(1)	9(1)	24(1)	16(1)
C(1)	28(1)	24(1)	23(1)	-2(1)	8(1)	0(1)
C(2)	36(1)	28(1)	26(1)	3(1)	3(1)	6(1)
C(3)	26(1)	31(1)	36(1)	-2(1)	-2(1)	9(1)
C(4)	20(1)	23(1)	34(1)	-7(1)	4(1)	1(1)
C(5)	18(1)	17(1)	25(1)	-5(1)	7(1)	-1(1)
C(6)	20(1)	18(1)	24(1)	-6(1)	10(1)	-3(1)
C(7)	28(1)	23(1)	38(1)	-8(1)	21(1)	-5(1)
C(8)	46(1)	32(1)	40(1)	-5(1)	31(1)	-7(1)
C(9)	55(1)	38(1)	28(1)	4(1)	24(1)	-1(1)
C(10)	36(1)	34(1)	22(1)	2(1)	10(1)	1(1)
C(11)	19(1)	34(1)	54(1)	-4(1)	12(1)	4(1)
C(12)	26(1)	32(1)	58(1)	-7(1)	27(1)	-2(1)
C(13)	24(1)	37(1)	23(1)	1(1)	5(1)	4(1)
C(14)	28(1)	46(1)	25(1)	8(1)	4(1)	11(1)
C(15)	38(1)	35(1)	27(1)	10(1)	11(1)	16(1)
C(16)	35(1)	29(1)	22(1)	5(1)	15(1)	10(1)
C(17)	25(1)	25(1)	19(1)	2(1)	11(1)	4(1)
C(18)	26(1)	23(1)	19(1)	0(1)	10(1)	3(1)
C(19)	34(1)	23(1)	26(1)	-2(1)	14(1)	-1(1)
C(20)	35(1)	28(1)	31(1)	-9(1)	10(1)	-8(1)
C(21)	28(1)	33(1)	26(1)	-6(1)	2(1)	-3(1)
C(22)	24(1)	27(1)	24(1)	-2(1)	4(1)	1(1)
C(23)	53(1)	24(1)	32(1)	6(1)	19(1)	11(1)
C(24)	49(1)	21(1)	34(1)	-2(1)	15(1)	-1(1)
C(25)	16(1)	37(1)	30(1)	-4(1)	5(1)	3(1)
C(26)	27(1)	30(1)	24(1)	1(1)	6(1)	6(1)
C(27)	19(1)	30(1)	24(1)	5(1)	5(1)	5(1)
C(28)	36(1)	37(1)	21(1)	6(1)	14(1)	11(1)

4: Supplementary Information for [Cu(phen)(BMCA)](NO_3) Complex

Table XLVI: Atomic coordinates (x 10^4) and equivalent isotropic displacement parameters (pm^2x 10^{-1}). U(eq) is defined as one third of the trace of the orthogonalized U^{ij} tensor.

	x	y	z	U(eq)
Cu(1)	7456(1)	7585(1)	5064(1)	20(1)
O(1)	9220(3)	9926(2)	6311(1)	22(1)
O(2)	5745(3)	9887(2)	3748(1)	21(1)
O(3)	856(4)	7079(2)	2550(2)	40(1)
O(4)	3855(4)	7382(2)	2975(2)	42(1)
O(5)	2424(6)	7762(2)	1780(2)	53(1)
O(3F)	2260(60)	7220(30)	3150(20)	58(13)
O(4F)	4200(40)	7890(20)	2577(17)	29(9)
O(5F)	1180(50)	7680(20)	1952(18)	30(9)
N(1)	7580(4)	6531(2)	4316(1)	19(1)
N(2)	7311(4)	6563(2)	5835(1)	19(1)
N(3)	8526(4)	8507(2)	5811(2)	21(1)
N(4)	6395(4)	8483(2)	4294(2)	21(1)
N(5)	7498(4)	9836(2)	5028(1)	18(1)
N(6)	2399(5)	7420(3)	2436(2)	21(1)
N(6F)	2530(40)	7610(20)	2535(18)	21(1)
C(1)	7558(4)	5696(2)	4681(2)	19(1)
C(2)	7379(4)	5715(2)	5504(2)	18(1)
C(3)	7065(5)	6608(3)	6589(2)	25(1)
C(4)	6921(5)	5820(3)	7044(2)	26(1)
C(5)	7065(5)	4975(3)	6719(2)	26(1)
C(6)	7293(5)	4889(2)	5916(2)	21(1)
C(7)	7437(5)	4038(2)	5515(2)	25(1)
C(8)	7623(5)	4023(2)	4742(2)	24(1)
C(9)	7701(4)	4860(2)	4299(2)	21(1)
C(10)	7904(5)	4901(2)	3486(2)	24(1)
C(11)	7974(5)	5740(3)	3135(2)	25(1)
C(12)	7801(5)	6544(2)	3560(2)	22(1)
C(13)	8966(6)	10911(3)	6227(2)	25(1)
C(14)	8373(5)	9392(2)	5688(2)	19(1)
C(15)	6587(5)	9373(2)	4388(2)	18(1)
C(16)	6060(6)	10868(2)	3793(2)	23(1)

Table XLVII: Bond lengths [pm] and angles [°]

Bond lengths [pm]		Bond angles [°]	
Cu(1)-N(4)	189.1(3)	N(4)-Cu(1)-N(3)	91.52(11)
Cu(1)-N(3)	189.3(3)	N(4)-Cu(1)-N(2)	154.32(13)
Cu(1)-N(2)	199.4(3)	N(3)-Cu(1)-N(2)	98.62(11)
Cu(1)-N(1)	200.3(3)	N(4)-Cu(1)-N(1)	98.48(11)
O(1)-C(14)	135.1(3)	N(3)-Cu(1)-N(1)	154.57(12)
O(1)-C(13)	144.3(4)	N(2)-Cu(1)-N(1)	82.28(10)
O(2)-C(15)	135.4(3)	C(14)-O(1)-C(13)	117.6(3)
O(2)-C(16)	143.9(4)	C(15)-O(2)-C(16)	117.6(2)
O(3)-N(6)	124.6(4)	C(12)-N(1)-C(1)	118.0(3)
O(4)-N(6)	123.2(4)	C(12)-N(1)-Cu(1)	129.4(2)
O(5)-N(6)	122.5(4)	C(1)-N(1)-Cu(1)	112.4(2)
O(3F)-N(6F)	123(2)	C(3)-N(2)-C(2)	117.8(3)
O(4F)-N(6F)	123(2)	C(3)-N(2)-Cu(1)	129.2(2)
O(5F)-N(6F)	123(2)	C(2)-N(2)-Cu(1)	112.9(2)
N(1)-C(12)	132.5(4)	C(14)-N(3)-Cu(1)	125.4(2)
N(1)-C(1)	136.2(4)	C(14)-N(3)-H(1N3)	112(3)
N(2)-C(3)	133.1(4)	Cu(1)-N(3)-H(1N3)	123(3)
N(2)-C(2)	135.8(4)	C(15)-N(4)-Cu(1)	125.4(2)
N(3)-C(14)	130.3(4)	C(15)-N(4)-H(1N4)	113(3)
N(3)-H(1N3)	72(3)	Cu(1)-N(4)-H(1N4)	121(3)
N(4)-C(15)	130.5(4)	C(15)-N(5)-C(14)	120.8(3)
N(4)-H(1N4)	78(3)	O(5)-N(6)-O(4)	122.2(4)
N(5)-C(15)	132.9(4)	O(5)-N(6)-O(3)	118.5(4)
N(5)-C(14)	133.2(4)	O(4)-N(6)-O(3)	119.3(4)
C(1)-C(9)	138.9(4)	O(3F)-N(6F)-O(5F)	119(3)
C(1)-C(2)	143.1(4)	O(3F)-N(6F)-O(4F)	114(3)
C(2)-C(6)	139.5(4)	O(5F)-N(6F)-O(4F)	126(3)
C(3)-C(4)	139.5(5)	N(1)-C(1)-C(9)	123.6(3)
C(3)-H(3)	96(3)	N(1)-C(1)-C(2)	116.2(3)
C(4)-C(5)	135.6(5)	C(9)-C(1)-C(2)	120.2(3)
C(4)-H(4)	95(3)	N(2)-C(2)-C(6)	124.1(3)
C(5)-C(6)	141.2(5)	N(2)-C(2)-C(1)	116.1(3)
C(5)-H(5)	87(3)	C(6)-C(2)-C(1)	119.8(3)
C(6)-C(7)	142.5(5)	N(2)-C(3)-C(4)	122.2(3)
C(7)-C(8)	134.8(5)	N(2)-C(3)-H(3)	119(2)
C(7)-H(7)	95(4)	C(4)-C(3)-H(3)	118(2)
C(8)-C(9)	143.6(5)	C(5)-C(4)-C(3)	119.6(3)
C(8)-H(8)	87(3)	C(5)-C(4)-H(4)	121(2)
C(9)-C(10)	142.1(5)	C(3)-C(4)-H(4)	120(2)
C(10)-C(11)	136.1(5)	C(4)-C(5)-C(6)	120.4(3)
C(10)-H(10)	95(3)	C(4)-C(5)-H(5)	120(2)
C(11)-C(12)	139.0(5)	C(6)-C(5)-H(5)	120(2)
C(11)-H(11)	85(3)	C(2)-C(6)-C(5)	115.8(3)
C(12)-H(12)	96(3)	C(2)-C(6)-C(7)	119.3(3)

C(13)-H(13A)	97(3)	C(5)-C(6)-C(7)	124.9(3)
C(13)-H(13B)	96(4)	C(8)-C(7)-C(6)	120.8(3)
C(13)-H(13C)	100(3)	C(8)-C(7)-H(7)	124(2)
C(16)-H(16A)	97(3)	C(6)-C(7)-H(7)	115(2)
C(16)-H(16B)	102(3)	C(7)-C(8)-C(9)	121.3(3)
C(16)-H(16C)	91(3)	C(7)-C(8)-H(8)	124(2)
		C(9)-C(8)-H(8)	115(2)
		C(1)-C(9)-C(10)	116.8(3)
		C(1)-C(9)-C(8)	118.6(3)
		C(10)-C(9)-C(8)	124.6(3)
		C(11)-C(10)-C(9)	118.9(3)
		C(11)-C(10)-H(10)	123(2)
		C(9)-C(10)-H(10)	118(2)
		C(10)-C(11)-C(12)	120.4(3)
		C(10)-C(11)-H(11)	124(2)
		C(12)-C(11)-H(11)	116(2)
		N(1)-C(12)-C(11)	122.2(3)
		N(1)-C(12)-H(12)	117.7(18)
		C(11)-C(12)-H(12)	120.1(18)
		O(1)-C(13)-H(13A)	111(2)
		O(1)-C(13)-H(13B)	112(2)
		H(13A)-C(13)-H(13B)	117(3)
		O(1)-C(13)-H(13C)	105.7(19)
		H(13A)-C(13)-H(13C)	105(3)
		H(13B)-C(13)-H(13C)	106(3)
		N(3)-C(14)-N(5)	128.4(3)
		N(3)-C(14)-O(1)	115.5(3)
		N(5)-C(14)-O(1)	116.1(3)
		N(4)-C(15)-N(5)	128.4(3)
		N(4)-C(15)-O(2)	115.3(3)
		N(5)-C(15)-O(2)	116.2(3)
		O(2)-C(16)-H(16A)	105.0(16)
		O(2)-C(16)-H(16B)	112.6(19)
		H(16A)-C(16)-H(16B)	109(2)
		O(2)-C(16)-H(16C)	110(2)
		H(16A)-C(16)-H(16C)	110(3)
		H(16B)-C(16)-H(16C)	110(3)

Symmetry transformations used to generate equivalent atoms:

Table XLVIII: Anisotropic displacement parameters ($pm^2 x\ 10^{-1}$). The anisotropic displacement factor exponent takes the form: $-2\pi^2[\ h^2 a^{*2} U^{11} + ... + 2\ h\ k\ a^*\ b^*\ U^{12}\ ]$

	U^{11}	U^{22}	U^{33}	U^{23}	U^{13}	U^{12}
Cu(1)	22(1)	20(1)	17(1)	1(1)	3(1)	1(1)
O(1)	23(1)	23(1)	18(1)	-2(1)	-1(1)	0(1)
O(2)	26(1)	18(1)	18(1)	2(1)	1(1)	3(1)
O(3)	29(2)	43(2)	50(2)	-3(1)	11(1)	-7(1)
O(4)	33(2)	36(2)	46(2)	-7(2)	-16(1)	2(2)
O(5)	99(3)	33(2)	31(2)	14(1)	21(2)	-1(2)
N(1)	17(2)	22(2)	18(1)	5(1)	3(1)	4(1)
N(2)	20(2)	19(2)	18(1)	-1(1)	2(1)	-4(1)
N(3)	18(2)	24(2)	18(1)	1(1)	-3(1)	-1(1)
N(4)	22(2)	23(2)	15(1)	-3(1)	0(1)	1(1)
N(5)	16(1)	19(1)	19(1)	-1(1)	3(1)	1(1)
N(6)	31(2)	13(2)	21(1)	-1(1)	6(1)	0(1)
N(6F)	31(2)	13(2)	21(1)	-1(1)	6(1)	0(1)
C(1)	13(2)	22(2)	20(2)	-1(1)	0(1)	2(1)
C(2)	11(2)	22(2)	20(2)	0(1)	0(1)	1(1)
C(3)	28(2)	29(2)	19(2)	-3(1)	3(1)	-4(2)
C(4)	28(2)	33(2)	16(2)	1(1)	5(1)	-5(2)
C(5)	21(2)	31(2)	26(2)	10(2)	3(1)	-2(2)
C(6)	15(2)	21(2)	27(2)	3(1)	2(1)	-1(1)
C(7)	20(2)	19(2)	36(2)	7(2)	4(2)	0(2)
C(8)	18(2)	18(2)	35(2)	-3(1)	6(2)	1(2)
C(9)	12(2)	26(2)	25(2)	-1(1)	2(1)	-1(1)
C(10)	19(2)	24(2)	28(2)	-7(2)	2(1)	1(2)
C(11)	22(2)	34(2)	19(2)	1(2)	6(1)	-1(2)
C(12)	23(2)	24(2)	21(2)	2(1)	5(1)	3(2)
C(13)	26(2)	21(2)	28(2)	-5(1)	5(2)	0(2)
C(14)	13(2)	25(2)	18(2)	-4(1)	4(1)	0(1)
C(15)	15(2)	22(2)	18(2)	1(1)	5(1)	2(1)
C(16)	22(2)	19(2)	26(2)	5(1)	2(2)	3(2)

Table XLIX: Hydrogen coordinates (x 10^4) and isotropic displacement parameters (pm^2x 10^{-1}).

	x	y	z	U(eq)
H(1N3)	9050(50)	8400(20)	6212(19)	26(11)
H(1N4)	5830(50)	8340(20)	3871(19)	30(11)
H(3)	6970(50)	7200(20)	6831(19)	28(10)
H(4)	6700(50)	5880(20)	7575(19)	26(9)
H(5)	7000(50)	4480(20)	7006(18)	18(9)
H(7)	7370(50)	3500(30)	5830(20)	41(11)
H(8)	7780(50)	3520(20)	4482(19)	28(10)
H(10)	7960(50)	4340(20)	3206(19)	29(10)
H(11)	8060(50)	5810(20)	2650(18)	20(9)
H(12)	7840(40)	7140(20)	3309(16)	12(8)
H(13A)	9610(50)	11150(20)	5812(19)	25(9)
H(13B)	7640(50)	11090(20)	6190(20)	34(11)
H(13C)	9700(50)	11180(20)	6740(20)	31(10)
H(16A)	5310(40)	11108(19)	3295(16)	7(7)
H(16B)	5580(50)	11160(20)	4260(18)	27(9)
H(16C)	7330(50)	11000(20)	3824(17)	12(8)

Table L: Hydrogen bonds [pm and °].

D-H...A	d(D-H)	d(H...A)	d(D...A)	<(DHA)
N(3)-H(1N3)...O(3)#1	72(3)	247(3)	319.5(4)	176(4)
N(4)-H(1N4)...O(4)	78(3)	231(3)	302.8(4)	154(4)

Symmetry transformations used to generate equivalent atoms: #1 x+1,-y+3/2,z+1/2

5: Supplementary Information for $[Co(phen)_2(NO_3)](dcg^-)\cdot(H_2O)$ Complex

Table LI: Atomic coordinates (x 10^4) and equivalent isotropic displacement parameters (pm^2x 10^{-1}). U(eq) is defined as one third of the trace of the orthogonalized U^{ij} tensor.

	x	y	z	U(eq)
Co(1)	2874(1)	2153(1)	4407(1)	15(1)
O(1)	2050(3)	1118(2)	4379(3)	18(1)
O(2)	3683(3)	1108(2)	4427(3)	20(1)
O(3)	2859(4)	-218(1)	4427(4)	29(1)
O(4)	5809(4)	1504(3)	3204(4)	67(1)
N(1)	1788(3)	3052(3)	4280(3)	17(1)
N(2)	2647(4)	2221(3)	2856(3)	18(1)
N(3)	3956(3)	3058(3)	4563(3)	16(1)
N(4)	3098(3)	2183(2)	5951(3)	15(1)
N(5)	2863(5)	597(2)	4411(4)	29(1)
N(6)	5376(3)	2911(3)	1618(3)	37(1)
N(7)	4197(3)	3743(2)	259(2)	24(1)
N(8)	3509(3)	4429(3)	1639(3)	21(1)
N(9)	2362(4)	5495(3)	2344(3)	28(1)
N(10)	2874(3)	4715(3)	-174(4)	28(1)
C(1)	1443(4)	3278(3)	3225(4)	18(1)
C(2)	1906(4)	2813(3)	2465(4)	17(1)
C(3)	3115(4)	1761(3)	2177(4)	21(1)
C(4)	2847(5)	1874(4)	1059(4)	26(1)
C(5)	2092(4)	2471(4)	659(4)	26(1)
C(6)	1600(4)	2968(4)	1354(4)	22(1)
C(7)	798(4)	3603(4)	1049(4)	25(1)
C(8)	360(4)	4037(3)	1783(4)	26(1)
C(9)	675(4)	3903(3)	2918(4)	22(1)
C(10)	228(4)	4311(4)	3734(4)	26(1)
C(11)	558(5)	4063(3)	4767(4)	26(1)
C(12)	1334(4)	3433(3)	5032(4)	20(1)
C(13)	4292(4)	3267(3)	5602(3)	15(1)
C(14)	3816(4)	2794(3)	6368(4)	17(1)
C(15)	2649(4)	1702(3)	6620(4)	21(1)
C(16)	2896(4)	1815(4)	7737(4)	22(1)
C(17)	3612(4)	2427(4)	8159(4)	22(1)
C(18)	4114(4)	2940(3)	7456(4)	17(1)
C(19)	4905(4)	3579(3)	7803(4)	21(1)
C(20)	5360(4)	4036(3)	7074(4)	22(1)
C(21)	5072(4)	3888(3)	5946(4)	18(1)
C(22)	5509(4)	4308(3)	5144(4)	21(1)
C(23)	5183(4)	4088(3)	4085(4)	23(1)
C(24)	4392(4)	3459(3)	3825(4)	21(1)
C(25)	4812(3)	3315(3)	1030(3)	28(1)
C(26)	3523(3)	4295(2)	593(3)	20(1)
C(27)	2887(5)	4990(4)	1962(5)	20(1)

Table LII: Bond lengths [pm] and angles [°].

Bond lengths [pm]		Bond angles [°]	
Co(1)-O(1)	188.8(4)	O(1)-Co(1)-O(2)	69.67(8)
Co(1)-O(2)	189.0(4)	O(1)-Co(1)-N(4)	91.74(16)
Co(1)-N(4)	192.7(4)	O(2)-Co(1)-N(4)	90.78(15)
Co(1)-N(2)	193.7(4)	O(1)-Co(1)-N(2)	91.76(16)
Co(1)-N(1)	195.6(5)	O(2)-Co(1)-N(2)	92.87(17)
Co(1)-N(3)	195.7(4)	N(4)-Co(1)-N(2)	175.65(9)
Co(1)-N(5)	232.0(3)	O(1)-Co(1)-N(1)	98.15(17)
O(1)-N(5)	132.4(6)	O(2)-Co(1)-N(1)	167.32(17)
O(2)-N(5)	132.6(6)	N(4)-Co(1)-N(1)	93.18(17)
O(3)-N(5)	121.6(3)	N(2)-Co(1)-N(1)	83.75(18)
O(4)-H(1O4)	96(4)	O(1)-Co(1)-N(3)	168.13(17)
O(4)-H(2O4)	95(4)	O(2)-Co(1)-N(3)	99.26(17)
O(4)-H(3O4)	95(4)	N(4)-Co(1)-N(3)	83.93(17)
N(1)-C(12)	133.5(6)	N(2)-Co(1)-N(3)	93.13(17)
N(1)-C(1)	137.9(6)	N(1)-Co(1)-N(3)	93.13(8)
N(2)-C(3)	133.1(6)	O(1)-Co(1)-N(5)	34.81(18)
N(2)-C(2)	135.3(7)	O(2)-Co(1)-N(5)	34.87(18)
N(3)-C(24)	132.0(6)	N(4)-Co(1)-N(5)	91.24(17)
N(3)-C(13)	135.3(6)	N(2)-Co(1)-N(5)	93.12(18)
N(4)-C(15)	132.3(6)	N(1)-Co(1)-N(5)	132.9(2)
N(4)-C(14)	136.0(6)	N(3)-Co(1)-N(5)	134.0(2)
N(6)-C(25)	113.7(6)	N(5)-O(1)-Co(1)	90.7(2)
N(7)-C(25)	132.7(5)	N(5)-O(2)-Co(1)	90.6(3)
N(7)-C(26)	133.5(5)	H(1O4)-O(4)-H(2O4)	93(6)
N(8)-C(27)	128.9(8)	H(1O4)-O(4)-H(3O4)	84(8)
N(8)-C(26)	134.1(5)	H(2O4)-O(4)-H(3O4)	112(10)
N(9)-C(27)	118.2(8)	C(12)-N(1)-C(1)	117.9(5)
N(10)-C(26)	134.2(5)	C(12)-N(1)-Co(1)	130.3(3)
N(10)-H(1N)	81(6)	C(1)-N(1)-Co(1)	111.7(3)
N(10)-H(2N)	83(5)	C(3)-N(2)-C(2)	119.3(5)
C(1)-C(9)	138.8(7)	C(3)-N(2)-Co(1)	128.0(4)
C(1)-C(2)	140.7(7)	C(2)-N(2)-Co(1)	112.7(4)
C(2)-C(6)	141.6(7)	C(24)-N(3)-C(13)	118.1(4)
C(3)-C(4)	141.0(7)	C(24)-N(3)-Co(1)	129.9(3)
C(3)-H(3)	95.00	C(13)-N(3)-Co(1)	112.0(3)
C(4)-C(5)	137.3(8)	C(15)-N(4)-C(14)	118.4(5)
C(4)-H(4)	95.00	C(15)-N(4)-Co(1)	128.7(4)
C(5)-C(6)	139.1(8)	C(14)-N(4)-Co(1)	112.9(4)
C(5)-H(5)	95.00	O(3)-N(5)-O(1)	125.5(6)
C(6)-C(7)	143.0(8)	O(3)-N(5)-O(2)	125.4(6)
C(7)-C(8)	134.1(8)	O(1)-N(5)-O(2)	109.0(2)
C(7)-H(7)	95.00	O(3)-N(5)-Co(1)	179.2(5)
C(8)-C(9)	144.1(8)	O(1)-N(5)-Co(1)	54.48(18)
C(8)-H(8)	95.00	O(2)-N(5)-Co(1)	54.54(18)

C(9)-C(10)	141.0(7)	C(25)-N(7)-C(26)	115.3(3)
C(10)-C(11)	135.8(8)	C(27)-N(8)-C(26)	121.6(4)
C(10)-H(10)	95.00	C(26)-N(10)-H(1N)	119(4)
C(11)-C(12)	139.4(7)	C(26)-N(10)-H(2N)	120(3)
C(11)-H(11)	95.00	H(1N)-N(10)-H(2N)	119(6)
C(12)-H(12)	95.00	N(1)-C(1)-C(9)	123.2(5)
C(13)-C(21)	140.4(7)	N(1)-C(1)-C(2)	115.3(5)
C(13)-C(14)	142.7(7)	C(9)-C(1)-C(2)	121.5(4)
C(14)-C(18)	138.5(7)	N(2)-C(2)-C(1)	116.4(4)
C(15)-C(16)	140.7(7)	N(2)-C(2)-C(6)	122.8(5)
C(15)-H(15)	95.00	C(1)-C(2)-C(6)	120.8(5)
C(16)-C(17)	136.1(8)	N(2)-C(3)-C(4)	121.2(5)
C(16)-H(16)	95.00	N(2)-C(3)-H(3)	119.4
C(17)-C(18)	142.1(7)	C(4)-C(3)-H(3)	119.4
C(17)-H(17)	95.00	C(5)-C(4)-C(3)	119.6(5)
C(18)-C(19)	143.2(7)	C(5)-C(4)-H(4)	120.2
C(19)-C(20)	136.5(7)	C(3)-C(4)-H(4)	120.2
C(19)-H(19)	95.00	C(4)-C(5)-C(6)	120.2(5)
C(20)-C(21)	143.2(7)	C(4)-C(5)-H(5)	119.9
C(20)-H(20)	95.00	C(6)-C(5)-H(5)	119.9
C(21)-C(22)	139.6(7)	C(5)-C(6)-C(2)	116.9(5)
C(22)-C(23)	137.7(7)	C(5)-C(6)-C(7)	126.1(5)
C(22)-H(22)	95.00	C(2)-C(6)-C(7)	117.0(5)
C(23)-C(24)	140.6(7)	C(8)-C(7)-C(6)	121.5(5)
C(23)-H(23)	95.00	C(8)-C(7)-H(7)	119.3
C(24)-H(24)	95.00	C(6)-C(7)-H(7)	119.3
		C(7)-C(8)-C(9)	122.3(5)
		C(7)-C(8)-H(8)	118.8
		C(9)-C(8)-H(8)	118.8
		C(1)-C(9)-C(10)	117.5(5)
		C(1)-C(9)-C(8)	116.8(5)
		C(10)-C(9)-C(8)	125.5(5)
		C(11)-C(10)-C(9)	118.6(5)
		C(11)-C(10)-H(10)	120.7
		C(9)-C(10)-H(10)	120.7
		C(10)-C(11)-C(12)	121.5(5)
		C(10)-C(11)-H(11)	119.2
		C(12)-C(11)-H(11)	119.2
		N(1)-C(12)-C(11)	121.2(5)
		N(1)-C(12)-H(12)	119.4
		C(11)-C(12)-H(12)	119.4
		N(3)-C(13)-C(21)	124.1(4)
		N(3)-C(13)-C(14)	115.7(4)
		C(21)-C(13)-C(14)	120.2(4)
		N(4)-C(14)-C(18)	123.9(5)
		N(4)-C(14)-C(13)	115.4(5)

	C(18)-C(14)-C(13)	120.7(5)
	N(4)-C(15)-C(16)	121.5(5)
	N(4)-C(15)-H(15)	119.3
	C(16)-C(15)-H(15)	119.3
	C(17)-C(16)-C(15)	120.4(5)
	C(17)-C(16)-H(16)	119.8
	C(15)-C(16)-H(16)	119.8
	C(16)-C(17)-C(18)	119.0(4)
	C(16)-C(17)-H(17)	120.5
	C(18)-C(17)-H(17)	120.5
	C(14)-C(18)-C(17)	116.8(5)
	C(14)-C(18)-C(19)	119.0(5)
	C(17)-C(18)-C(19)	124.2(5)
	C(20)-C(19)-C(18)	120.6(4)
	C(20)-C(19)-H(19)	119.7
	C(18)-C(19)-H(19)	119.7
	C(19)-C(20)-C(21)	121.4(5)
	C(19)-C(20)-H(20)	119.3
	C(21)-C(20)-H(20)	119.3
	C(22)-C(21)-C(13)	116.4(4)
	C(22)-C(21)-C(20)	125.4(5)
	C(13)-C(21)-C(20)	118.2(4)
	C(23)-C(22)-C(21)	119.8(5)
	C(23)-C(22)-H(22)	120.1
	C(21)-C(22)-H(22)	120.1
	C(22)-C(23)-C(24)	119.3(5)
	C(22)-C(23)-H(23)	120.3
	C(24)-C(23)-H(23)	120.3
	N(3)-C(24)-C(23)	122.3(5)
	N(3)-C(24)-H(24)	118.9
	C(23)-C(24)-H(24)	118.9
	N(6)-C(25)-N(7)	173.8(4)
	N(7)-C(26)-N(8)	121.5(3)
	N(7)-C(26)-N(10)	116.3(3)
	N(8)-C(26)-N(10)	122.1(4)
	N(9)-C(27)-N(8)	174.4(7)

Symmetry transformations used to generate equivalent atoms:

Table LIII: Anisotropic displacement parameters ($pm^2 x\ 10^{-1}$). The anisotropic displacement factor exponent takes the form: $-2\pi^2[\ h^2 a^{*2} U^{11} + ... + 2\ h\ k\ a^*\ b^*\ U^{12}\ ]$

	U11	U22	U33	U23	U13	U12
Co(1)	16(1)	16(1)	13(1)	0(1)	2(1)	0(1)
O(1)	15(2)	20(2)	21(2)	-1(1)	4(1)	-4(1)
O(2)	21(2)	18(2)	19(2)	0(1)	1(1)	-1(1)
O(3)	37(1)	16(1)	35(1)	-4(2)	10(1)	4(2)
O(4)	68(3)	73(3)	70(3)	28(2)	39(3)	34(2)
N(1)	18(2)	16(2)	17(2)	0(2)	2(2)	-1(2)
N(2)	22(2)	21(2)	11(2)	-1(1)	4(2)	0(2)
N(3)	19(2)	16(2)	13(2)	0(1)	4(2)	0(2)
N(4)	11(2)	14(2)	20(2)	-1(1)	0(2)	1(1)
N(5)	33(1)	32(1)	24(1)	-9(2)	5(1)	-16(3)
N(6)	32(2)	47(2)	33(2)	5(2)	11(2)	14(2)
N(7)	27(2)	27(1)	18(1)	0(1)	6(1)	1(1)
N(8)	27(2)	22(2)	15(1)	-3(1)	4(1)	-4(1)
N(9)	28(2)	34(2)	24(2)	-2(2)	6(2)	-2(2)
N(10)	33(2)	34(2)	15(1)	0(1)	2(1)	5(1)
C(1)	18(3)	16(2)	20(2)	2(2)	2(2)	-5(2)
C(2)	16(2)	16(2)	16(2)	2(2)	-4(2)	-4(2)
C(3)	22(3)	19(2)	22(2)	-4(2)	3(2)	2(2)
C(4)	35(3)	27(3)	19(2)	-7(2)	8(2)	-9(2)
C(5)	28(3)	31(3)	16(2)	6(2)	-3(2)	-12(2)
C(6)	18(3)	28(3)	17(2)	3(2)	-1(2)	-10(2)
C(7)	21(3)	26(3)	24(2)	10(2)	-6(2)	-6(2)
C(8)	16(3)	23(3)	37(3)	9(2)	2(2)	-5(2)
C(9)	16(3)	18(2)	30(3)	6(2)	-1(2)	-4(2)
C(10)	19(2)	20(2)	40(3)	-4(2)	7(2)	2(2)
C(11)	27(3)	24(3)	28(3)	-2(2)	9(2)	2(2)
C(12)	21(3)	19(2)	21(2)	-5(2)	6(2)	-4(2)
C(13)	15(2)	15(2)	16(2)	-1(2)	1(2)	1(2)
C(14)	17(2)	16(2)	19(2)	2(2)	7(2)	3(2)
C(15)	25(3)	24(2)	17(2)	1(2)	7(2)	1(2)
C(16)	26(3)	23(2)	18(2)	3(2)	7(2)	-1(2)
C(17)	28(3)	25(2)	14(2)	7(2)	6(2)	5(2)
C(18)	20(2)	15(2)	16(2)	-1(2)	0(2)	3(2)
C(19)	22(3)	22(2)	18(2)	-3(2)	1(2)	5(2)
C(20)	23(3)	21(2)	18(2)	-8(2)	-3(2)	-1(2)
C(21)	18(3)	15(2)	21(2)	-1(2)	4(2)	0(2)
C(22)	19(2)	18(2)	27(2)	-5(2)	2(2)	-1(2)
C(23)	20(3)	21(3)	29(3)	4(2)	8(2)	0(2)
C(24)	24(3)	22(2)	18(2)	0(2)	4(2)	-1(2)
C(25)	31(2)	30(2)	25(2)	-2(2)	14(2)	0(2)
C(26)	23(2)	21(1)	18(1)	-1(1)	4(1)	-4(1)
C(27)	22(1)	23(1)	14(1)	1(1)	1(1)	-6(1)

Table LIV: Hydrogen coordinates (x 10^4) and isotropic displacement parameters (pm^2x 10^{-1}).

	x	y	z	U(eq)
H(3)	3639	1348	2450	25
H(4)	3187	1539	585	32
H(5)	1905	2546	-94	31
H(7)	570	3720	310	29
H(8)	-178	4448	1547	31
H(10)	-292	4750	3565	31
H(11)	252	4326	5321	31
H(12)	1544	3273	5762	24
H(15)	2149	1271	6339	26
H(16)	2562	1461	8200	26
H(17)	3772	2510	8913	26
H(19)	5115	3685	8548	25
H(20)	5879	4461	7321	26
H(22)	6029	4745	5329	26
H(23)	5489	4358	3537	27
H(24)	4163	3319	3092	25
H(1N)	2910(50)	4620(30)	-800(50)	30(16)
H(2N)	2360(40)	4970(30)	-20(40)	37(13)
H(1O4)	5470(30)	1190(30)	2590(30)	30
H(2O4)	6460(40)	1290(50)	3120(70)	30
H(3O4)	5620(110)	2030(60)	2780(100)	30

Table LV: Hydrogen bonds [pm and °].

D-H...A	d(D-H)	d(H...A)	d(D...A)	<(DHA)
O(4)-H(3O4)...N(6)	95(4)	196(6)	289.5(6)	165(13)
O(4)-H(2O4)...N(9)#1	95(4)	204(5)	290.5(6)	151(7)
N(10)-H(1N)...N(9)#2	81(6)	235(6)	311.6(6)	158(6)
N(10)-H(1N)...C(27)#2	81(6)	289(6)	365.1(8)	158(5)
N(10)-H(2N)...C(11)#2	83(5)	277(5)	356.4(7)	161(4)
N(10)-H(2N)...C(12)#2	83(5)	275(5)	347.1(6)	147(4)

Symmetry transformations used to generate equivalent atoms: #1 x+1/2,y-1/2,z #2 x,-y+1,z-1/2

APPENDIX II

PUBLICATION FROM THE WORK

Chemical Papers (2020) 74:3003–3016
https://doi.org/10.1007/s11696-020-01109-1

ORIGINAL PAPER

Synthesis, characterization and thermal properties of 1,10-phenanthroline mixed-ligand complexes of cobalt(II) and copper(II): metal-mediated transformations of the dicyanamide ion

Donatus B. Eni[1] · Divine M. Yufanyi[2] · Jean H. Nono[2] · Che D. Tabong[3] · Moise O. Agwara[1]

Received: 12 November 2019 / Accepted: 17 February 2020 / Published online: 20 March 2020

Abstract
The reaction of 1,10-phenanthroline and dicyanamide ligands with Cu(II) and Co(II) nitrates afforded the complexes [Cu(phen)(BMCA)](NO_3)] (**1**) and [Co(phen)$_2$(NO_3)](dcg-)·(H_2O) (**2**). The dicyanamide anion was transformed in **1** and **2** to bis(methoxycarbimido)aminato (BMCA) and dicyanoguanidinate (dcg) anions, respectively. The complexes were characterized by elemental analysis, infrared spectroscopy and ultraviolet–visible spectroscopy, magnetic susceptibility measurement and X-ray crystallography. Both complexes crystallize in the monoclinic crystal system, and the structures are stabilized by extended hydrogen bonding networks as well as aromatic π–π stacking interactions. The thermal and antimicrobial properties of the complexes have also been evaluated. Density functional theory calculations were also performed in order to gain insights into the molecular interactions in the synthesized compounds and to predict some of their electronic properties.

Keywords Antimicrobial properties · Dicyanamide · Metal(II) · 1,10-Phenanthroline · X-ray crystal structures

Introduction

Scientific interest in the fundamental chemistry of 1,10-phenanthroline (phen) and its metal complexes is sustained due to their interesting catalytic, redox, photochemical, chemosensing (Alreja and Kaur 2016) and biological properties (Creaven et al. 2007; Bencini and Lippolis 2010; Chandraleka et al. 2014; Ganeshpandian et al. 2014; Gaëlle et al. 2016; Ng et al. 2016; Yanick Gaelle et al. 2016; Momeni et al. 2017). Diimine ligands, such as phen and 2,2′-bipyridine, have been employed in the design and synthesis of metal complexes, for the development of new functional materials with intriguing structures and potential applications (Amani et al. 2007). Phen is an efficient chelating N-donor ligand which forms stable complexes in solution with transition metal ions. This chelating, bidentate, rigid and planar ligand has been used in reactions with transition metal ions, resulting in complexes which display diverse structures and properties (Bencini and Lippolis 2010; Nord 1985; Sammes and Yahioglu 1994). The σ-donation, complemented by the π-acceptor ability in 1,10-phen, gives the formed complexes greater stability (Janiak 2000; Pook et al. 2015). Amongst these complexes, those of Co(II) and Cu(II) are of particular interest for their chemosensing, therapeutic and biological properties (Gaëlle et al. 2016; Abu Ali et al. 2017; McCarron et al. 2018; Şahin et al. 2016; Dağlı et al. 2019). For example, the $[Cu(phen)_2]^{2+}$ complex ion showed antitumor activity in the inhibition of DNA or RNA polymerase (Deegan et al. 2006, 2007; Mahmoud et al. 2014). Likewise, the complexes [Cu(en)(phen)$_2$]·2Br_2(phen)·8H_2O and [Cu(en)(phen)$_2$](ClO_4)$_2$ have exhibited antimicrobial

Electronic supplementary material The online version of this article (https://doi.org/10.1007/s11696-020-01109-1) contains supplementary material, which is available to authorized users.

✉ Divine M. Yufanyi
dyufanyi@yahoo.com

✉ Moise O. Agwara
agwara29@yahoo.com

[1] Department of Inorganic Chemistry, University of Yaounde I, P.O. Box 812, Yaounde, Cameroon

[2] Department of Chemistry, Faculty of Science, The University of Bamenda, P.O. Box 39, Bambili, Bamenda, Cameroon

[3] Department of Chemistry, Higher Teachers' Training College Bambili, The University of Bamenda, Bamenda, Cameroon

activities comparable to that of the standard drug used for *Staphylococcus aureus*, *Escherichia coli*, *Pseudomonas aeruginosa*, *Streptoccocus pyogeneous*, *Candida albicans* and *Aspergillus niger* (Onawumi et al. 2013). While cobalt is a component of vitamin B12 complex that is useful in the prevention of anaemia and the production of erythrocytes, its complexes are of interest due to their therapeutic and biological applications (Mishra et al. 2008). Furthermore, Cu^{2+}, the third most abundant metal in the human body, plays an important role in various biological processes (Fraústo da Silva and Williams 1991).

Although the synthesis and structural characterization of many metal complexes of phen have been reported to date, the design and synthesis of new phen metal complexes using different synthetic methods or by varying the reactants and synthetic conditions are currently under investigation. In this context, the N-donor co-ligand dicyanamide (dca), which shows a variety of coordination modes and is versatile in the formation of multi-dimensional coordination polymers, has been explored (Bencini and Lippolis 2010; Dong et al. 2003; Carranza et al. 2004; Tonzing et al. 2006; Manson et al. 2013).

There are literature reports of metal-mediated nucleophilic additions of different nucleophiles to dicyanamide in complexes (Zheng et al. 2008). Zn^{2+} and Cu^{2+} ions are known to catalyse, in situ, the addition of 2 mol of methanol to dicyanamide to form bis(methoxycarbimido)-amine, $HN{=}C(OCH_3)NH{\cdot}(OCH_3)C{=}NH$ (BMCA) (Zheng et al. 2008; Ray et al. 1989; Kozisek et al. 1990). In the presence of Co^{2+}, the dcg counter ion is thought to result from the reaction of two dicyanamide anions. Váhovská et al. (2016) obtained the complex $[Co(bpy)_2CO_3](dcg)$ when $[Co(bpy)_2(dca)_2]$ was the recrystallized from methanol. Recently, we have embarked on the study of phen metal complexes in the presence of N-donor pseudo-halide co-ligands (Gaëlle et al. 2016; Yanick Gaelle et al. 2016; Ndosiri et al. 2013). Considering the diverse applications of cobalt and copper mixed-ligand complexes, exploring the good biological properties of these metals and phen as well as the structure-directing properties and transformation reactions of dca, we report herein the synthesis and structure elucidation of the complexes $[Cu(phen)(BMCA)](NO_3)]$ (1) and $[Co(phen)_2(NO_3)](dcg^-){\cdot}(H_2O)$ (2).

Experimental

Materials

All the chemicals were of reagent grade and were used as such without further purification. All the used solvents were dried and distilled according to standard methods.

Synthesis of the complexes

Synthesis of $[Cu(Phen)(BMCA)]{\cdot}NO_3$ (1) At room temperature, a solution of $Cu(NO_3)_2{\cdot}3H_2O$ (0.241 g, 1 mmol) in methanol (25 mL) was added dropwise to a solution of 1,10-phenanthroline (0.396 g, 2 mmol) in methanol (25 mL) with constant stirring and the reaction mixture was refluxed at 85 °C for an hour. A solution of sodium dicyanamide (0.36 g, 4 mmol) in 10 mL water/methanol (1:4 v/v) was added dropwise to the reaction mixture, and it was further refluxed for 3 h. The dark green precipitate formed was filtered, washed with methanol and dried over silica gel in a desiccator. The volume of the filtrate was reduced to ca. 10 mL. Violet-pink crystals of **1** (327 mg, 75%) were obtained from this filtrate at 25 °C.

Synthesis of $[Co(phen)_2(NO_3)](dcg^-){\cdot}(H_2O)$ (2) At room temperature, a solution of $Co(NO_3)_2{\cdot}6H_2O$ (0.29 g, 1.0 mmol) in methanol (25 mL) was added dropwise to a solution of 1,10-phenanthroline (0.396 g, 2 mmol) in methanol (25 mL) with constant stirring and the reaction mixture was refluxed at 85 °C for an hour. A solution of sodium dicyanamide (0.36 g, 4 mmol) in 10 mL water/methanol (1:4 v/v) was added dropwise to the reaction mixture, and it was further refluxed for 3 h. The dark orange precipitate formed was filtered, washed with methanol and dried over silica gel in a desiccator. The volume of the filtrate was reduced to ca. 10 mL. At 25 °C, **2** was obtained as dark orange crystals (533 mg, 80%).

Characterization

Elemental analyses for C, H and N were performed on a FLASH 2000 Organic Elemental Analyser. The melting point/decomposition temperatures of the complexes were obtained using the STUART Scientific Melting Point SMP1 Device with maximum temperature at 360 °C. IR spectra/KBr pellets were prepared in a nitrogen-filled glovebox, and the spectra were recorded on a PerkinElmer System 2000 FTIR spectrometer in the range 350–4000 cm^{-1}. Thermogravimetric (TG) and differential thermal analyses (DTA) data were obtained using a NETZSCH STA449F1 thermoanalyser in a dynamic argon atmosphere (heating rate 10 °C·min^{-1}, flow rate 25 mL/min, aluminium oxide crucible, mass 25 mg and temperature range from room temperature up to 900 °C). Room-temperature magnetic susceptibility measurements of the complexes were determined using the Gouy method with mercury tetrathiocyanocobalt(II) as calibrant on a Stanton Instruments Limited (Model A49). Powder XRD measurements were performed with a Stoe-StadiP powder diffractometer with a CuKα (1.540598 Å) X-ray source (0.5°/step and 30 s/step (2 repetitions)); tube power: 40 kV/40 mA; scan mode: Debye–Scherrer using

a borosilicate glass capillary as sample holder during the measurement.

Data collection and structural refinement

X-ray data were collected with a GEMINI CCD diffractometer (Rigaku Inc.), λ(Mo-Kα) = 0.71073 Å, T = 130(2) K, ω-scan rotation. Data reduction was performed with CrysAlis Pro including the program SCALE3 ABSPACK for empirical absorption correction (CrysAlisPro 2013). All structures were solved by dual-space methods with SHELXT-20xy (Sheldrick 2015). Structure refinement was done with SHELXL-2018 (Sheldrick 2015) by using full-matrix least-square routines against F2. Hydrogen atoms for (**1**) and NH and OH for (**2**) were located on difference Fourier maps calculated at the final stage of the structure refinement. The remaining hydrogen atoms of (**2**) were calculated on idealized positions using the riding model. The pictures were generated with the program Mercury (Macrae et al. 2006). CCDC 1958341 (**1**) and CCDC 1958342 (**2**) contain the supplementary crystallographic data for this paper. These data can be obtained free of charge via www.ccdc.cam.ac.uk/data_request/cif (or from the Cambridge Crystallographic Data Centre, 12 Union Road, Cambridge CB2 1EZ, UK; fax: (+44)1223-336-033; or deposit@ccdc.cam.uk).

Theoretical studies

Calculations were performed on the complexes to gain further insights into the molecular interactions in the synthesized compounds and to predict some of their electronic properties. The calculations were performed using the DFT method, and the exchange–correlation functional (Engel and Dreizler 2011) was approximated by the Becke three-parameter exchange functionals (Becke 1988, 1993) and the Lee–Yang–Parr correlation functional (Lee et al. 1988). The molecular orbitals of the studied molecules were described by a Pople double-split valence orbitals basis set 6-31G (Ditchfield et al. 1971) as implemented in the Gaussian 03, Revision A1 package (Montgomery J 2003). This basis set has been polarized for all atoms to improve the flexibility of molecular orbitals (Cramer 2004). The geometries obtained from the crystal structures were used as the starting point for the optimization. The optimized geometries were subjected to frequency calculations to verify whether they represent energy minima. The non-covalent interactions (NCIs) such as hydrogen bond and van der Waals interactions were described by two theories based on the electron distribution in the molecular system: the Bader and collaborators approach known as quantum theory of atom in molecules (QTAIM) (Bader 1990) and the Contreras-Garcia and collaborators approach referred to as non-covalent interactions index (Contreras-Garcia et al. 2011; Tan et al. 2019). The Multiwfn software (Lu and Chen 2012) was used for this purpose.

Antimicrobial tests

The antimicrobial tests were carried out in the Applied Microbiology and Molecular Pharmacology Laboratory (LMP) of the University of Yaoundé I, Cameroon. The tests were done on twenty-three pathogenic microorganisms; twenty bacterial strains: B1 = *Streptococcus pneumoniae* ATCC49619, B2 = *Staphylococcus aureus* BAA917, B3 = *Staphylococcus aureus* ATCC43300, B4 = *Staphylococcus aureus* NR45003, B5 = *Staphylococcus aureus* NR46003, B6 = *Staphylococcus aureus* CP7625, B7 = *Shigella flexineri* NR518, B8 = *Salmonella enterica* NR4294, B9 = *Salmonella enterica* NR4311, B10 = *Salmonella enterica* NR13555, B11 = *Pseudomonas aeruginosa* NMC592, B12 = *Klebsiella pneumoniae* ATCC13883, B13 = *Klebsiella pneumoniae* ATCC70603, B14 = *Klebsiella pneumoniae* NR41916, B15 = *Escherichia coli* ATCC25922, B16 = *Escherichia coli* ATCC35218, B17 = *Enterococcus faecalis* ATCC51219, B18 = *Staphylococcus aureus* NR46374, B19 = *Hemophyllus influenza* ATCC49247, B20 = *Mycobacterium smegmatis* and three yeasts: *Candida krusei*, *Candida parasilosis* and *Candida albicans*, obtained from Centre Pasteur Yaoundé, Cameroon. The selected microorganisms represent the causative agents for diseases that are prevalent in our environment. The microbial isolates were maintained on agar slant at 4 °C in the laboratory. The strains were subcultured on the fresh appropriate agar plate in incubators 18 h prior to any antimicrobial test.

Sensitivity test

The ligands, metal salts and the complexes were diluted in sterilized distilled water at 100 mg/mL, and 1 mg of each test compound was placed on a sterilized filter paper disc and allowed to dry. The reference antibiotics (RB) amoxicillin, ciprofloxacin and cloxacillin and the reference antifungal (RF) drug fluconazole were also prepared in the same manner, and 10 µg was placed on a sterilized filter paper disc and dried, prior to testing.

Diffusion tests

In vitro antimicrobial activity of the ligand, metal salts and complexes were evaluated using the disc-diffusion method as previously reported (Gaëlle et al. 2016). Three replicas were performed for each sample, and mean values of the growth inhibition zone were calculated. Compounds with a zone of inhibition IZ < 7 mm were considered to be inactive,

those in the range $7 < IZ < 20$ mm as active and those with $IZ > 20$ mm, very active.

The minimum inhibitory concentration of the complexes

The minimum inhibitory concentration (MIC) was determined according to National Committee for Clinical Laboratory Standards (NCCLS) M38, a microdilution method using (12 × 8 wells) microtitre plates, as previously reported (Gaëlle et al. 2016). The lowest concentration inhibiting the growth of microorganisms was considered as the minimum inhibitory concentration (MIC).

Results and discussion

Synthesis of the complexes

The complexes [Cu(phen)(BMCA)](NO_3) (**1**) and [$Co(phen)_2(NO_3)$](dcg^-)·(H_2O) (**2**) obtained were crystalline, air-stable and non-hygroscopic as compared to the starting materials. They could also be reproducibly prepared in high yields (> 70%) (Table S1, ESI). Complex **1** had a sharp melting point (202 ± 2 °C) while **2** changed in colour upon heating from dark orange to brown and then melted at 296 ± 2 °C. The change in colour of **2** with an increase in temperature could be attributed to the change in crystal structure geometry from octahedral to tetrahedral as the nitrate ion and water of crystallization are lost (Ma et al. 2001; Kani et al. 2016). The molar conductivity (Ω^{-1} cm^2 mol^{-1}) values of the complexes in DMSO, at room temperature, indicate that both complexes are 1:1 electrolytes (Mohamed et al. 2010).

The complexes [Cu(phen)(BMCA)](NO_3) (**1**), BMCA = bis(methoxycarbimido)aminato anion and [$Co(phen)_2(NO_3)$](dcg^-)·(H_2O) (**2**) were obtained in stoichiometric reactions (1:2:2) of the metal(II) salt, 1,10-phenanthroline and dicyanamide, in a methanol/H_2O mixture at 85 °C. A transformation of the dicyanamide anion to bis(methoxycarbimido)aminate anion (BMCA) or dicyanoguanidinate anion (dcg) was observed during the reaction (Scheme 1). These metal-promoted transformations proceed through a nucleophilic attack of the nitrile groups of dca on methanol (case of BMCA), or on another dicyanamide (case of dcg), as previously reported (Zheng et al. 2008; Ray et al. 1989; Kozisek et al. 1990). The BMCA ligand is isoelectronic with acetyl acetonate (Turner et al. 2011).

These transformation reactions are a function of the reaction temperature, the transition metal ion used, and the molar ratio of dca^-/nucleophile on the product (Zheng et al. 2008).

Crystal structure of [Cu(phen)(BMCA)]·NO_3 (1)

Complex **1** crystallizes in the monoclinic crystal system with space group C2/c with four molecules in the unit cell. The molecular structure and atom-labelling scheme used in the corresponding tables of the crystal structure [{bis(methoxycarbimido)aminato-κ^2N,N′} (1,10-phenanthroline-κ^2N,N′)copper(II)] nitrate and [Cu(phen)(BMCA)]·NO_3 is shown in Fig. 1. The selected bond lengths and bond angles are presented in Table 1. The asymmetric unit consists of one Cu(II) cation, one

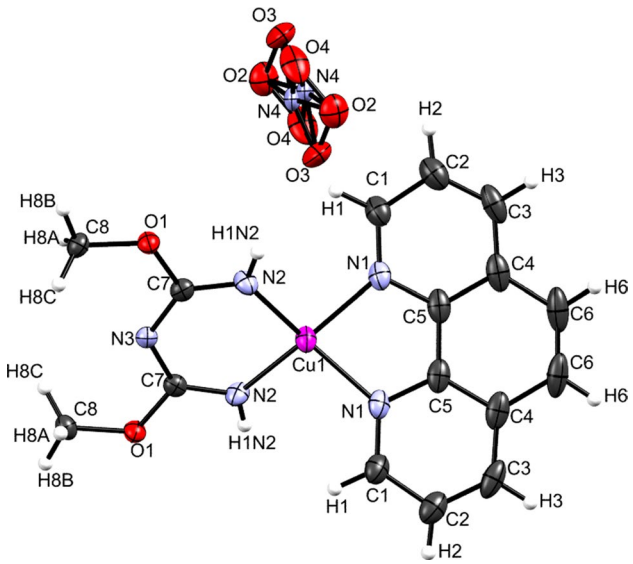

Fig. 1 Molecular structure and atom-labelling scheme for **1** with ellipsoids drawn at 50% probability level

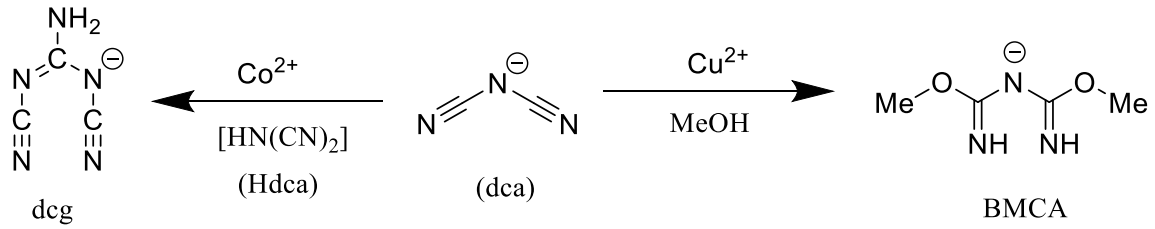

Scheme 1 Transformation of dca to BMCA and dcg

Table 1 The selected bond lengths (Å) and bond angles (°) of **1**

Bond length (Å)		Bond angle (°)	
Cu(1)–N(2)	189.2(2)	N(2)–Cu(1)–N(2)#1	91.66(13)
Cu(1)–N(2)#1	189.2(2)	N(2)–Cu(1)–N(1)	154.36(9)
Cu(1)–N(1)	199.8(2)	N(2)#1–Cu(1)–N(1)	98.50(9)
Cu(1)–N(1)#1	199.8(2)	N(2)–Cu(1)–N(1)#1	98.50(9)
O(1)–C(7)	135.3(3)	N(2)#1–Cu(1)–N(1)#1	154.36(9)
O(1)–C(8)	144.1(3)	N(1)–Cu(1)–N(1)#1	82.30(13)
O(2)–N(4)	123.7(2)		
O(3)–N(4)	123.7(2)		
N(2)–C(7)	130.5(3)		
N(3)–C(7)	132.9(3)		

bis(methoxycarbimido)aminato (BMCA) anion, one phen molecule, and one nitrate counter anion. BMCA and the phen ligand are coordinating at Cu in a planar fashion, but both planes are not coplanar. Least squares planes for these two units are shifted by an angle of 36.55(3)°. The Cu–N_{phen} bond distances are 1.998(2) Å which are comparable to those reported in the literature (Yanick Gaelle et al. 2016; Zheng et al. 2008; Kozisek et al. 1990; Váhovská et al. 2016; Tong et al. 2003). The Cu−N_{BMCA} bond lengths fall in the range 1.892(2)–1.998(2) Å but are quite shorter compared to those of related complexes (1.928(3)−1.932(3) Å) (Zheng et al. 2008; Kozisek et al. 1990; Váhovská et al. 2016; Tong et al. 2003). Cu(1), BMCA and phen are located on a twofold axis. It forms two metallocycles: a six-membered ring with the BMCA anion and a five-membered ring with the phen molecule. The two CH_3O groups of the BMCA ligand are in *syn*–*syn* conformation in the complex. Parallel π-stacking interactions, between adjacent phen ligands, stabilize the structure and assemble complex 1 into an interesting 3D structure (Şahin et al. 2016; Dağlı et al. 2019) (CCDC 1958341 at www.ccdc.cam.ac.uk/data_request/cif).

Crystal structures of [{Co(phen)$_2$(NO$_3$)}(dcg$^-$)]·(H$_2$O) (2)

Complex **2** crystallizes in the monoclinic crystal system, space group Cc, with four molecules in the unit cell. The molecular structure and atom-labelling scheme used in the corresponding tables of the crystal structure [(nitrato-κ^{2}O,O′)(1,10-phenanthroline-κ^{2}N,N′)cobalt(II)] dicyanoguanidinate; [{Co(Phen)$_2$(NO$_3$)}(dcg)]·H$_2$O is shown in Fig. 2. The crystallographic data and structure refinement parameters of the complex are presented in Table 2. The selected bond lengths and bond angles are presented in Table 3, while the H-bond parameters are given in Table S2 (ESI).

The asymmetric unit consists of one Co(II) cation, one nitrate anion, two phen molecules, one lattice water molecule and one dicyanoguanidinate counter anion. As illustrated in Fig. 6, the Co atom is chelated by two oxygen atoms from one nitrate anion and also coordinated to four N atoms from two phen ligands to complete a distorted octahedral environment with a CoO_2N_4 chromophore. The Co–O bond lengths vary from 1.888(4) Å to 1.890(4) Å, while the Co–N bond distances fall in the range of 1.927(4)–1.957(4) Å. The deviation of the bond angles O(1)–Co(1)–O(2)–O(2)–Co(1)–N(3) (69.67(8)–99.26(17)°) and O(2)–Co(1)–N(1)–N(4)–Co(1)–N(2) (167.32(17)–175.65(9)°) (Table 4) from the ideal values (90°, 180°) for a regular octahedron indicates that the coordination polyhedron of Co(II) ions is highly distorted octahedron. These angles, as well as Co–N and Co–O bond lengths, are quite similar to those of related complexes (Gaëlle et al. 2016; Şahin et al. 2016; Dağlı et al. 2019; Váhovská et al. 2016; Han et al. 2010). The distortion is also thought to result from the high-spin 3d^7 ion of cobalt(II) which gives a $^4F_{9/2}$ ground term in octahedral ligand fields (Han et al. 2010). This distortion is also a consequence of the rigidity of the ligands. All ligands are coordinating in a chelate fashion.

Parallel π stacking interactions between phen ligands and numerous N–H···N, C–H···N and C–H···O hydrogen bonds extend the structure into a three-dimensional network (CCDC 1958342 (**2**) at www.ccdc.cam.ac.uk/data_request/cif).

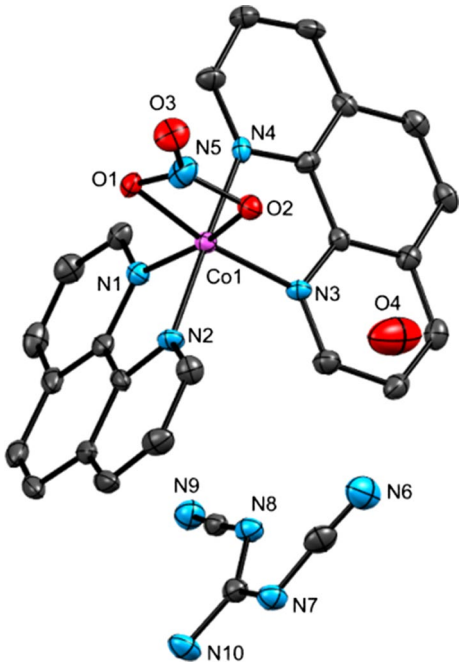

Fig. 2 Molecular structure and atom-labelling scheme for **2** with ellipsoids drawn at 50% probability level. H atoms are omitted for clarity

Table 2 Crystallographic data for the complexes **1** and **2**

Complex	**1**	**2**
Chemical formula	$C_{16}H_{16}CuN_5O_2^{+}\cdot NO_3^{-}$	$C_{27}H_{20}CoN_{10}O_4$
M_r	435.89	607.46
Crystal system, space group	Monoclinic, C2/c	Monoclinic, Cc
Temperature (K)	130(2)	130(2)
a, *b*, *c* (Å)	17.0517(12), 14.5051(5), 7.0537(3)	13.2779(3), 14.9105(3), 12.6468(3)
β (°)	102.252(4)	99.501(2)
V (Å^3)	1705.17(12)	2469.47(10)
Z	4	4
μ (mm^{-1})	1.33	0.755
Crystal size (mm)	0.20×0.10×0.01	0.35×0.30×0.20
T_{min}, T_{max}	0.993, 1.000	0.9759, 1.0000
No. of measured, independent and observed [$I > 2\sigma(I)$] reflections	8594, 2366, 1861	14,308, 6751, 1244
R_{int}	0.051	0.0253
$(\sin\theta/\lambda)_{max}$ (Å^{-1})	0.712	0.0392
$R[F^2 > 2\sigma(F^2)]$, $wR(F^2)$, S	0.047, 0.087, 1.04	0.0470, 0.0941, 1.029
No. of reflections	2366	6751
No. of parameters	178	400
No. of restraints	7	6
H-atom treatment	All H-atom parameters refined	H-atom parameters constrained
$\Delta\rho$max, $\Delta\rho$min (*e* Å^{-3})	0.35, −0.43	0.475, −0.755

Table 3 Selected bond lengths (Å) and bond angles (°) of **2**

Bond length (Å)		Bond angle (°)	
Co(1)–O(1)	1.888(4)	O(1)–Co(1)–O(2)	69.67(8)
Co(1)–O(2)	1.890(4)	O(1)–Co(1)–N(4)	91.74(16)
Co(1)–N(4)	1.927(4)	O(2)–Co(1)–N(4)	90.78(15)
Co(1)–N(2)	1.937(4)	O(1)–Co(1)–N(2)	91.76(16)
Co(1)–N(1)	1.956(5)	O(2)–Co(1)–N(2)	92.87(17)
Co(1)–N(3)	1.957(4)	N(4)–Co(1)–N(2)	175.65(9)
Co(1)–N(5)	2.320(3)	O(1)–Co(1)–N(1)	98.15(17)
O(1)–N(5)	1.324(6)	O(2)–Co(1)–N(1)	167.32(17)
O(2)–N(5)	1.326(6)	N(4)–Co(1)–N(1)	93.18(17)
O(3)–N(5)	1.216(3)	N(2)–Co(1)–N(1)	83.75(18)
O(4)–H(1O4)	0.96(4)	O(1)–Co(1)–N(3)	168.13(17)
O(4)–H(2O4)	0.95(4)	O(2)–Co(1)–N(3)	99.26(17)
O(4)–H(3O4)	0.95(4)	N(4)–Co(1)–N(3)	83.93(17)

Table 4 Selected IR absorption bands (cm^{-1}) of the ligands and their metal complexes

Bond	dca	Phen	**1**	**2**
ν(C=N)		1586 s	1600 vs	1666 vs
ν(C=C)		1501 vs	1520 s	1514 vs
ν(C≡N)	2285 vs		2140 s	2147 vs
	2229 s			2178 s
	2173 vs			
ν(N–H)			3275 vs	3196 m
$\nu(NH_2)$				3492 vs
				3440 vs
ν(N–O)			1751	1758
ν(C–O)			1046 vs	
			1085vs	
γ(C–H) sp^2 stretch		3057 s	3064 s	3196 m
			3017 s	3064 s
γ(C–H) *sp*3 stretch			2958 s	
ν(M–N)			512 m	551 s

br Broad, *s* strong, *vs* very strong, *m* medium, *w* weak

N,N'-dicyanoguanidine (dcg) is present in **2** as a counter anion. The molar conductance ($\Lambda_M = 82.5$ O^{-1} cm^2 mol^{-1}) of **2**, measured at room temperature in DMSO, indicates that it is a 1:1 electrolyte (Yesilel et al. 2006). *N,N'*-dicyanoguanidinate anion results from the nucleophilic reaction of two dicyanamide anions, with the subsequent elimination of the cyano group (Scheme 2, ESI). However, the mechanism of the elimination of the cyano group leading to the dcg anion is unclear. Dicyanoguanidine (both in its neutral and anionic form) has been characterized in the literature (Váhovská et al. 2016).

Infrared spectroscopy

The most relevant absorption bands in the IR spectra of the ligands and the complexes (Figure S2, ESI) are summarized in Table 4. The absorption bands at 1586 and 1501 cm^{-1} assigned to ν(C=N) and ν(C=C) stretching vibrations, respectively, of 1,10-phen are shifted in the complexes to 1600 and 1520 cm^{-1} for 1 and 1666 and 1514 cm^{-1} for **2**, respectively. These shifts indicate the participation of the C=N of 1,10-phen in bonding (Gaëlle et al. 2016; Yanick Gaelle et al. 2016). The vibrational bands at 3050–3075 cm^{-1} are assigned to C^2_{sp}–H stretching vibrations of phen (Parada et al. 2014). The appearance of the ν(N−H) at 3275 cm^{-1} in 1 is an indication of the transformation of dca ligand (Kozisek et al. 1990). The appearance of the $\nu(C^3_{sp}–H)$ stretching and ν(C–O) alkoxy vibrations at 2958 cm^{-1} and 1085 cm^{-1}, respectively, indicates the addition of methanol to dca (Kozisek et al. 1990). Characteristic nitrile bands (C≡N) due to dicyanamide expected at 2173 and 2229 cm^{-1} were not observed in the spectrum; instead, characteristic C–O–CH_3 stretch at about 1200 cm^{-1} and a C–H symmetrical deformation vibration at about 1400 cm^{-1} were observed (Ray et al. 1989).

In **2**, the band at 2147 cm^{-1} and the shoulder at 2178 cm^{-1} are the characteristic bands of dicyanoguanidinate (dcg) anion assigned to ν(C≡N) vibrations which are observed in the spectrum of dcg anion at 2138 and 2160 cm^{-1} (Váhovská et al. 2016). The twin bands at 3440 and 3492 cm^{-1} assigned to the $\nu(NH_2)$ and the band at 3196 cm^{-1} assigned to the ν(N–H) both from the amino group of dcg anion indicate that the lone pairs on these N atoms are not involved in bonding. This suggests that the *N,N′*-dicyanoguanidine ($(H_2N)C(NCN)_2$) anion is present as a counter ion in **2** (Váhovská et al. 2016). The new band at 1758 cm^{-1} is assigned to the ν(N–O) vibration for the nitrato ligand (Váhovská et al. 2016; Ndifon et al. 2009). The broad and diffuse band at 3500 cm^{-1} is assigned to ν(O–H) vibration of a lattice water molecule. The new bands at 512 cm^{-1} for 1 and 551 cm^{-1} for **2** can be attributed to ν(M–N) stretching while the new band observed in the low-frequency region at 445 cm^{-1} for **2** may be attributed to ν(M–O) vibration (Abdel-Kader and Mohamed 2013).

Electronic absorption spectra

The significant electronic absorption bands in the spectra of the complexes (Figs. S3 and S4, ESI) are summarized in Table 5.

The UV–visible spectrum of **1** (Fig. S3) displays a broad peak in the UV region at $\lambda = 270–379$ nm (37,037–26,385 cm^{-1}) due to the ligand field ($\pi \rightarrow \pi^*$ and $n \rightarrow \pi^*$) and charge transfer ($d - \pi^*$) transitions. The *d–d* transitions appear in the visible region at $\lambda = 437$ nm (22,883 cm^{-1}) attributed to the transition $^2T_2 \rightarrow {}^2E$, corresponding to a tetrahedral geometry around the copper ion (Dawood et al. 2012).

Table 5 Significant absorption bands in the spectra of the complexes

Complex	Wavelength (nm)	Wavenumber (cm^{-1})	Band assignment
1	297	33,670	$\pi \rightarrow \pi^*$
	314	31,847	$\pi \rightarrow \pi^*$
	326	30,675	$n \rightarrow \pi^*$
	437	22,883	$^2T_2 \rightarrow {}^2E$
2	271	36,900	$\pi \rightarrow \pi^*$
	297	33,670	$\pi \rightarrow \pi^*$
	314	31,847	$\pi \rightarrow \pi^*$
	325	30,769	$\pi \rightarrow \pi^*$
	346	28,901	$\pi \rightarrow \pi^*$
	361	27,700	$\pi \rightarrow \pi^*$
	379	26,385	$n \rightarrow \pi$
	501	19,960	$^4T_{1g} \rightarrow {}^4T_{2g}$

The UV–Vis spectrum of the **2** (Fig. S4) shows broad peaks at $\lambda = 270–361$ nm (37,037–27,700 cm^{-1}) which were attributed to intra-ligand ($\pi \rightarrow \pi^*$ and $n \rightarrow \pi^*$) transitions of the coordinated phen groups due to the ligand field and charge transfer ($d \rightarrow \pi^*$) transitions (Abdelhak et al. 2014). The visible region contains peaks at $\lambda = 501$ nm (19,960 cm^{-1}) due to the *d–d* transition $^4T_{1g} \rightarrow {}^4T_{2g}$, suggesting a distorted octahedral geometry around the cobalt(II) (Dawood et al. 2012; Abdelhak et al. 2014).

Magnetic susceptibility measurement

The magnetic moments are summarized in Table S3. The room-temperature magnetic moments of **1** and **2** are 1.75 B.M and 3.92 B.M., respectively. These values correspond to one unpaired electron for **1** (Krishna and Reddy 2013; Saravanan and Mudaliar 2014) and a high-spin (d^7) octahedral geometry for **2** (Abdel-Kader and Mohamed 2013).

Thermal analysis

The thermal properties of complexes **1** and **2** were studied by simultaneous TG/DTA/MS analyses in the temperature range 30–800 °C under an argon atmosphere. In **1** (Fig. 3), the TG curve displays the first endothermic oxidation at DTA = 252 °C with weight loss: 43.25% (190–340 °C, calc. 44.07%) attributed to the release of the BMCA, {bis(methoxycarbimido)aminato}, and the nitrate ions in the form of gases. The last stage (340–700 °C) is due to the complete endothermic decomposition of the remaining components, $Cu(phen)^{2+}$ complex ion. The residue was analysed

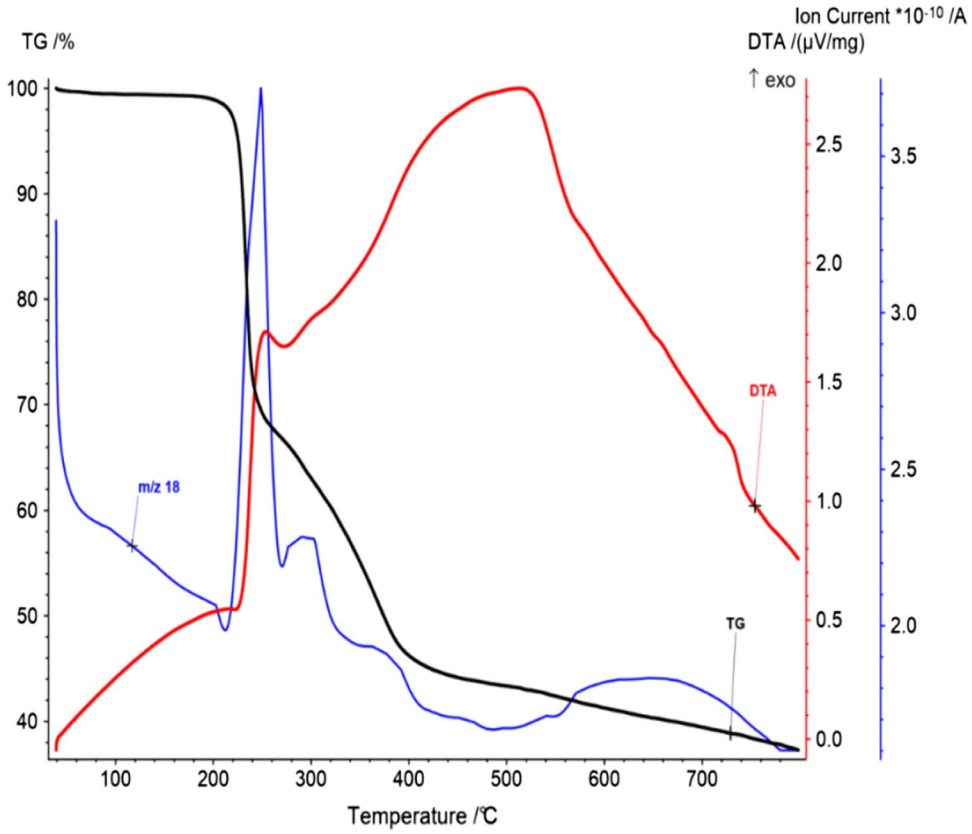

Fig. 3 TG-DTA curves of [Cu(Phen)(BMCA)]·NO_3 (**1**)

by PXRD (Onawumi et al. 2013; Yesilel et al. 2006; Lan et al. 2017).

The TG curve of **2** (Fig. 4) displays the first exothermic DTA peak at 218 °C with weight loss: 12.76% (120–235 °C, calc. 13.17%) attributed to the release of the lattice water molecule and the nitrato ligand. The last step from 235 to 700 °C, with an endothermic DTA peak at 470 °C, is due to the complete decomposition of $[Co(phen)_2(dcg^-)]^+$ complex ion. A black powder remains as final decomposition product.

The PXRD pattern of the residue of **1** (Fig. 5) indicates that the residue is crystalline and a mixture of two phases. The residue has a well-defined diffraction pattern and matched well with the powder diffraction patterns of [04-0836] Cu and Cu_2O [05–0667] (Lan et al. 2017).

Calculations

The optimized geometries of **1** and **2** (Fig. S5) were obtained at the DFT-B3LYP/6-31G(d,p) level of theory. The calculated and experimental bond lengths for **1** and **2** are presented in Table S4. The results show that the deviation of calculated M–N (M=Co(II), Cu(II)), N–O and C–X (X=C, N and O) bond lengths is in the range 0.004–0.028 Å, except for O2–N5 where it is 0.079 Å. In the case of C–H bond lengths, the deviation is in the range 0.075–0.14 Å. The most important deviation 0.494 Å was obtained for the Co–O2 bond of **2**. The linear correlation between experimental and calculated bond lengths gave a regression coefficient of 0.979 and a standard deviation of 0.05 for **1** and 0.977 with 0.06 standard deviation for **2**. These results show that there is a good agreement between experimental and calculated geometries and thereby indicate that the used level of theory is adequate to describe the properties of the concerned molecules.

Non-covalent interactions have been described using NCI index plot since it is able to reveal very weak interactions and to distinguish between attractive and repulsive interactions as well as strong and weak NCI (Contreras-Garcia et al. 2011; Tan et al. 2019). This plot (Fig. 6) represents the distribution of the electron density in the region of weak density (less than 0.05 a.u.). The inspection of the NCI isosurface of molecule **1** indicates the presence of a moderate hydrogen bond between O3 and H-N4 (1.872 Å/161.1°) and a weak hydrogen bond between O4 and H11-C11 (2.035 Å/140.2°). Also, it reveals the presence of an attractive weak interaction (green surface) between O2 and C11. The QTAIM analysis of the molecular graph of this molecule (Fig. S6) shows the existence of bond critical point (BCP) for these three interactions, and some of the parameters of these BCPs are presented in Table 6. The values of the energy of these two interactions, their electron density, ρ (between 0.002 and 0.04 a.u.), and Laplacian of electron density, $\nabla^2\rho$ (between

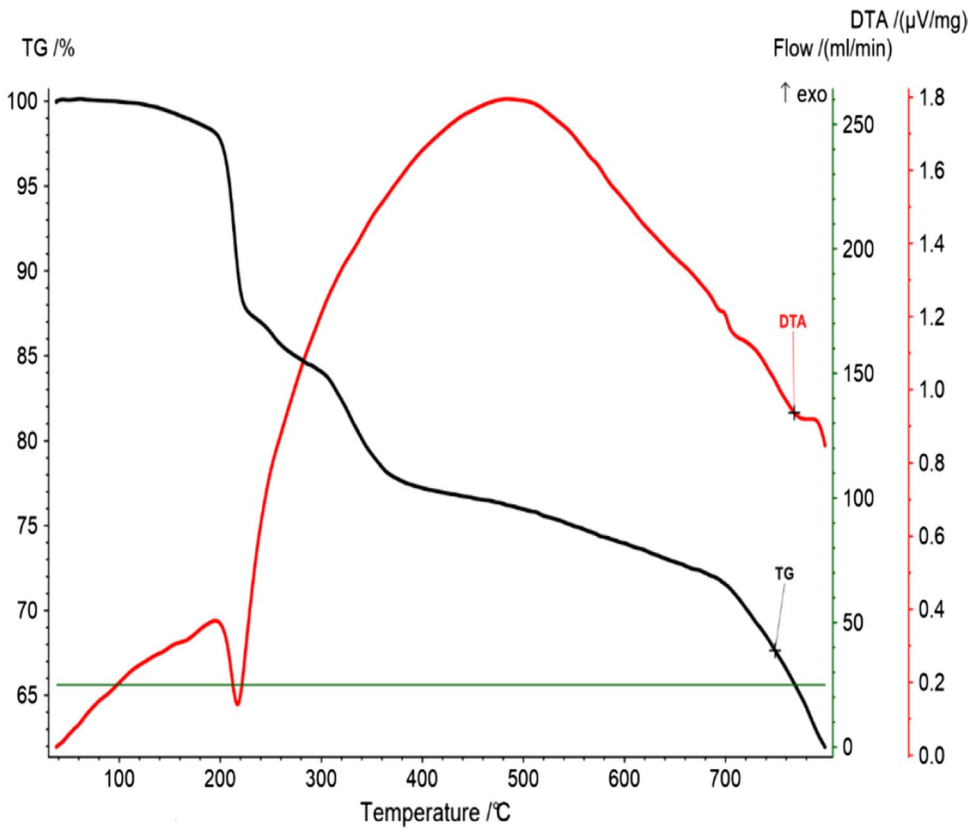

Fig. 4 TG-DTA curves of [{Co(phen)$_2$(NO$_3$)}(dcg-)]·(H$_2$O) (**2**)

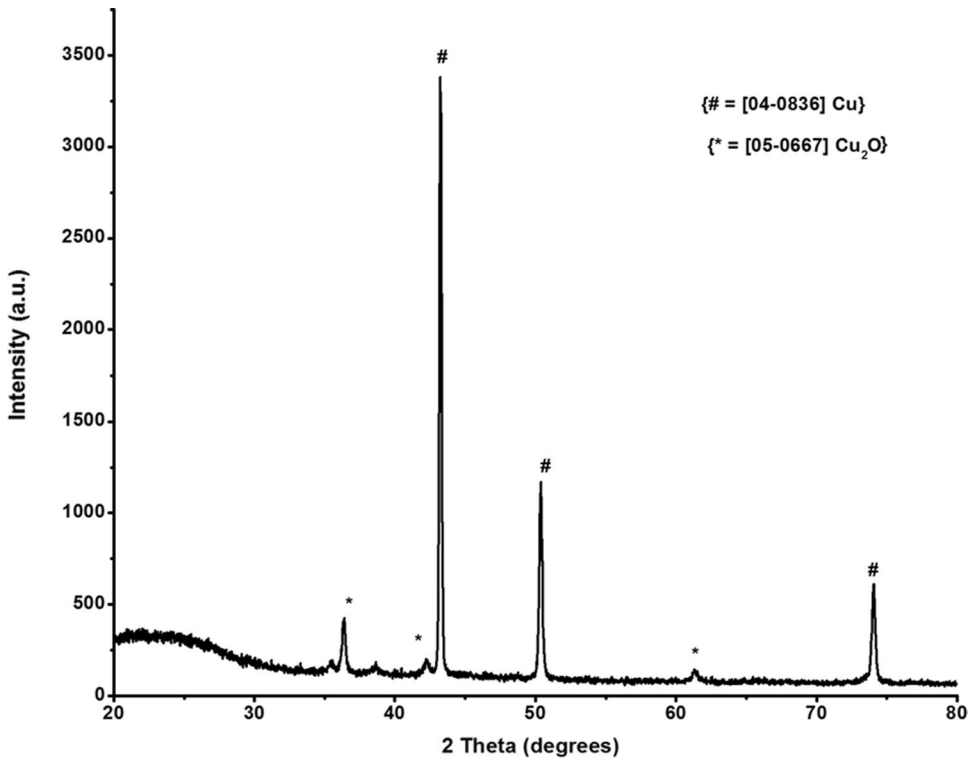

Fig. 5 PXRD pattern of the residue of **1**

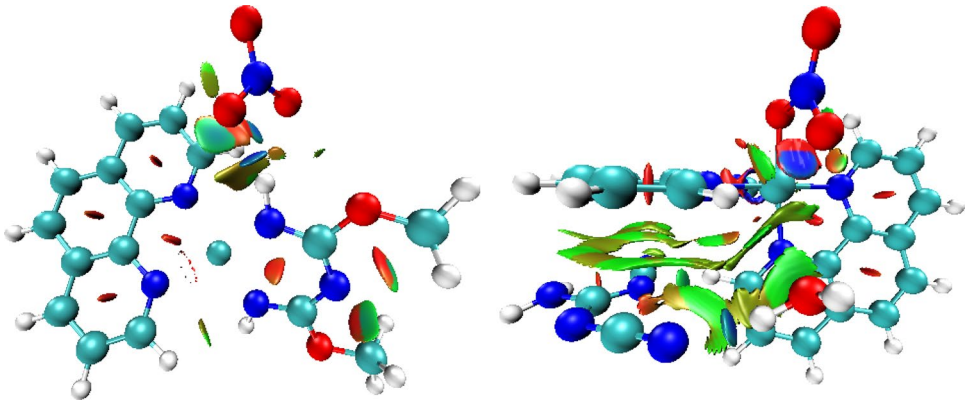

Fig. 6 Plot of NCI isosurface for molecules of **1** (left) and **2** (right). The blue region of these plots represents the strong attractive interactions (hydrogen bond), the green region indicates weak attractive interactions (van der Waals interactions and dispersing hydrogen bond), and the red region indicates the strong repulsion interactions (steric effects)

0.024 and 0.139 a.u.) (Grabowski 2004; Biswal et al. 2009), confirm their hydrogen bond character and that O3—H–N4 is stronger than O4—H11–C11.

The NCI plot of **2** (Fig. 6) indicates the presence of two hydrogen bonds N6—H–OH, (1.916/165.1°) and N8—H24-C24 (2282 Å/142,6°), but the latter is very weak compared to the former. This plot also exhibits a very large green surface indicating the existence of many van der Waals interactions in this complex. These van der Waals interactions are mostly found between the counter ion dca, the water molecule and the ligands. The QTAIM analysis of **2** reveals the presence of a BCP between N6—H–OH, and N8—H24–C24 and many others between the counter ion and the ligand.

The values of the most relevant vibrational bands found in complexes **1** and **2** calculated at DFT-B3LYP/6-31G(d,p) level of theory are also presented in Table S5. The Gauss View 5.0.8 molecular visualization program (Montgomery J 2003) was used to assign the calculated harmonic vibrational frequency bands. The theoretical values of the frequencies were scaled by a factor of 0.977 to reduce the basis set and method limitations to reproduce experimental vibrational frequencies. The theoretical spectrum of molecule **1** shows two absorption bands in the high-frequency region (above 3000 cm^{-1}) assigned to the vibration of the two N–H bonds of dca. The lowest value 3189 cm^{-1} corresponds to the vibration of the N–H which is involved in N–H—O3 hydrogen bond. This value is lower than the experimental value probably because of the overestimation of the energy of N–H—O3 hydrogen bond by the level of theory as observed during geometry analysis. For the same reason, the calculated vibration frequency of N–O bond is also lower than the experimental value. The two bands observed in the region above 3000 cm^{-1} in the spectrum of molecule **2** correspond to the symmetric (3514 cm^{-1}) and asymmetric (3655 cm^{-1}) N–H stretch. The harmonic frequency vibrations of C=N and N–O bonds obtained for molecule **2** are lower than the experimental values while the value of C—N is significantly higher. However, for most vibration frequencies of molecule **1**, there is a good agreement with experimental values. The shapes (drawn with Gauss View graphical interface software) and the distribution of the HOMO and LUMO of the complexes are shown in Fig. 7.

Table 6 Electron density $\rho(r)$ (a.u.), Laplacian of electron density $\nabla^2\rho(r)$ (a.u.), potential energy density $V^{®}$ (a.u.) and bond energy E_{HB} (kJ/mol) at the BCP of hydrogen bonds in the molecules

		$\rho(r)$	$\nabla^2\rho(r)$	$V^{®}$	E_{HB}
1	O3–H–N4	0.03204	0.08784	−0.02388	−31
	O4–H–C12	0.02468	0.07328	−0.01944	−26
2	CH–N	0.01660	0.04691	−0.01083	−14
	HOH–N	0.02846	0.08199	−0.01936	−25
	O2–NO–Co	0.03548	0.13473	−0.04393	−58

The HOMO of the two complexes is localized on the counter ions with mainly π-type orbitals. From the orbital composition analysis by Hirshfeld method, the oxygen of nitrate anion of **1** contributes up to 78% of the HOMO, and in the case of **2**, the HOMO is composed of 78% of the atoms N6, N7, N8 and N9 and 16% C25, C26 and C27. The LUMO of **1** is localized on phen and copper atom, and the Hirshfeld orbital composition analysis reveals that this orbital is composed of 12% of π*-type orbitals of the N5, 15% of d* orbital of Cu and 60% of π*-type of carbon atoms of phen. However, the main contributors are C1 to C5. The π*-type orbital of N4 contributes only 4% to the LUMO of **1**. The LUMO of **2** is also delocalized on the surface of phen and the π*-type orbital of carbon of phen involved, contributing about 75% of this LUMO. The π*-type orbitals of N3 and N4 contribute 4 and 14%, respectively, which is practically the same in 1. The contribution of d*-type orbitals of Co(II) ion to the LUMO of 2 is insignificant (3%). The distribution obtained by the isosurface is in agreement with the Hirshfeld orbital analysis composition.

The energies of the HOMO and LUMO and the gap between the two orbitals for **1** and **2** are presented in Table 7. The results indicate that **2** is more stable than **1**. This can be explained by the volume of the van der Waals interaction

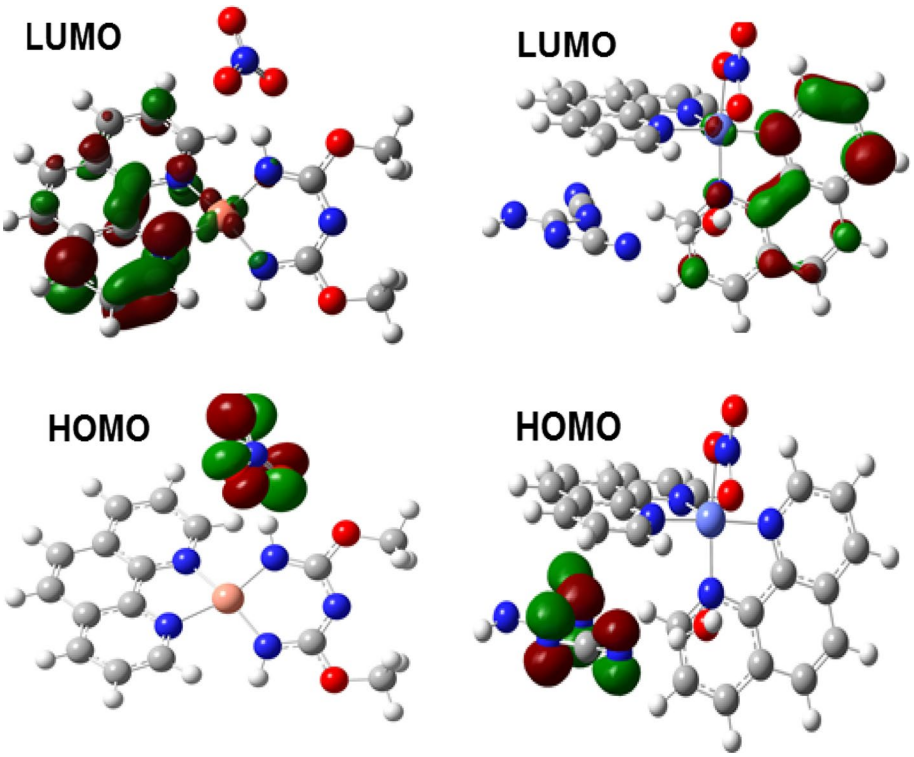

Fig. 7 HOMO and LUMO of the complexes **1** (left) and **2** (right)

Table 7 Values of frontier molecular orbital energies (eV)

Complex	HOMO	LUMO	$\Delta E_{(\text{LUMO–HOMO})}$
1	−5.03	−2.70	2.33
2	−5.79	−2.28	3.51

in molecule **2**. Since these are attractive interactions, they stabilize the concerned molecule.

Antimicrobial studies

The potency of the starting materials and the complexes together with the reference antibacterial drugs (amoxicillin, ciprofloxacin and cloxacillin) and antifungal drug (fluconazole and cloxacillin) were evaluated against twenty-three microorganisms comprised of twenty bacteria and three fungi strains. The susceptibility of the bacterial and fungal strains towards these compounds was judged by measuring the size of the growth inhibition diameter (IZ). Compounds, which showed significant activities (IZ > 6 mm), were used for the minimum inhibitory concentration (MIC) test. The MIC values (Table S6) are summarized in histograms (Fig. S7). While the simple metal salts and the co-ligand dca were not able to effectively reduce the bacterial and fungal cell proliferation, phen exhibited good inhibitory capability which is in agreement with results obtained from other studies (Yanick Gaelle et al. 2016; Gandra et al. 2017).

Complexes **1** and **2** possess good activity against B3 = *Staphylococcus aureus* ATCC43300; B4 = *Staphylococcus aureus* NR45003; and B6 = *Staphylococcus aureus* CP7625 with MIC value 62.5 µg/mL as compared to the antibiotic cloxacillin. Complex **2** possesses good activity against B1 = Streptococcus pneumoniae ATCC49619 and B19 = Hemophyllus influenza ATCC49247 with MIC value 62.5 µg/mL. However, the complexes displayed poor antifungal activities as compared to the standard antifungals (fluconazole, cloxacillin) but higher antibacterial activities as compared to the antibiotic (cloxacillin). These activities are comparable to literature reports (Gandra et al. 2017; Coyle et al. 2003).

Conclusions

Two complexes $[Cu(Phen)(BMCA)]\cdot NO_3$ (**1**); {BMCA = bis(methoxycarbimido)aminato anion and phen = 1,10-phenanthroline} and $[\{Co(phen)_2(NO_3)\}(dcg^-)]\cdot(H_2O)$ (**2**); (dcg = dicyanoguanidinate anion) have been synthesized. The room-temperature magnetic moments of the complexes are 1.75 B.M. and 3.92 B.M., respectively, for **1** and **2**, which corresponds to one unpaired electron and possibly tetrahedral geometry for **1** and high-spin (d7) octahedral geometry for **2**. The dicyanamide was transformed through a nucleophilic attack by methanol. The distorted octahedral geometry of Co(II) ions in complex **2** can be

explained by Jahn–Teller effect for the d^7 configuration as confirmed by the high-spin magnetic moment. The N,N'-dicyanoguanidinate (dcg) present as a counter anion originated from the reaction of two dicyanamide anions with a subsequent elimination of the cyano group. The packing in the unit cell of both complexes was based on intermolecular hydrogen bonding and π−π stacking interactions extending them to interesting 3D structures. Complexes **1** and **2** showed good activity against B3 = *S. aureus* ATCC43300; B4 = *S. aureus* NR45003; and B6 = *S. aureus* CP7625 with MIC value 62.5 µg/mL as compared to the antibiotic cloxacillin. Complex **2** demonstrated good activity against B1 = *S. pneumoniae* ATCC49619 and B19 = *H. influenza* ATCC49247 with MIC value 62.5 µg/mL. However, the complexes displayed poor antifungal activities as compared to the standard antifungals (fluconazole, cloxacillin) but higher antibacterial activities as compared to the antibiotic (cloxacillin).

Acknowledgements The authors are grateful to Dr. Peter Lönnecke of the Institute of Inorganic Chemistry, Faculty of Chemistry and Mineralogy, Universität Leipzig, Germany, for assistance with single-crystal X-ray measurements.

Compliance with ethical standards

Conflict of interest On behalf of all authors, the corresponding author states that there is no conflict of interest.

References

Abdelhak J, Namouchi Cherni S, Amami M, El Kébir H, Zid MF, Driss A (2014) Iron(III) and Cobalt(III) complexes with oxalate and phenanthroline: synthesis, crystal structure, spectroscopy properties and magnetic properties. J Supercond Novel Magn 27:1693–1700. https://doi.org/10.1007/s10948-014-2479-2

Abdel-Kader NS, Mohamed RR (2013) Synthesis, characterization, and thermal investigation of some transition metal complexes of benzopyran-4-one Schiff base as thermal stabilizers for rigid poly(vinyl chloride) (PVC). J Therm Anal Calorim 114:603–611. https://doi.org/10.1007/s10973-013-3006-6

Abu Ali H, Abu Shamma A, Kamel S (2017) New mixed ligand cobalt(II/III) complexes based on the drug sodium valproate and bioactive nitrogen-donor ligands. Synthesis, structure and biological properties. J Mol Struct 1142:40–47. https://doi.org/10.1016/j.molstruc.2017.04.048

Alreja P, Kaur N (2016) Recent advances in 1,10-phenanthroline ligands for chemosensing of cations and anions. RSC Adv 6:23169–23217. https://doi.org/10.1039/c6ra00150e

Amani V, Safari N, Khavasi HR, Mirzaei P (2007) Iron(III) mixed-ligand complexes: synthesis, characterization and crystal structure determination of iron(III) hetero-ligand complexes containing 1,10-phenanthroline, 2,2′-bipyridine, chloride and dimethyl sulfoxide, [Fe(phen)Cl_3(DMSO)] and [Fe(bipy)Cl_3(DMSO)]. Polyhedron 26:4908–4914. https://doi.org/10.1016/j.poly.2007.06.038

Bader RFW (1990) Atoms in molecules: a quantum theory. Oxford University Press, Oxford

Becke AD (1988) Density-functional exchange-energy approximation with correct asymptotic behavior. Phys Rev A 38:3098–3100. https://doi.org/10.1103/PhysRevA.38.3098

Becke AD (1993) A new mixing of Hartree-Fock and local density-functional theories. J Chem Phys 98:1372–1377. https://doi.org/10.1063/1.464304

Bencini A, Lippolis V (2010) 1,10-Phenanthroline: a versatile building block for the construction of ligands for various purposes. Coord Chem Rev 254:2096–2180. https://doi.org/10.1016/j.crr.2010.04.008

Biswal HS, Shirhatti PR, Wategaonkar S (2009) O–H···O versus O–H···S hydrogen bonding I: experimental and computational studies on the p-Cresol·H_2O and p-Cresol·H_2S complexes. J Phys Chem A 113:5633–5643. https://doi.org/10.1021/jp9009355

Carranza J, Sletten J, Lloret F, Julve M (2004) Structural analysis and magnetic properties of the copper(II) dicyanamide complexes [Cu_2(dmphen)$_2$(dca)$_4$], [Cu(dmphen)(dca)(NO_3)]$_n$ and [Cu(4,4′-dmbpy)(H_2O)(dca)$_2$] (dca = dicyanamide; dmphen = 2,9-dimethyl-1,10-phenanthroline; 4,4′-dmbpy = 4,4′-dimethyl-2,2′-bipy. Inorg Chim Acta 357:3304–3316. https://doi.org/10.1016/j.ica.2004.01.044

Chandraleka S, Ramya K, Chandramohan G, Dhanasekaran D, Priyadharshini A, Panneerselvam A (2014) Antimicrobial mechanism of copper (II) 1,10-phenanthroline and 2,2′-bipyridyl complex on bacterial and fungal pathogens. J Saudi Chem Soc 18:953–962. https://doi.org/10.1016/j.jscs.2011.11.020

Contreras-Garcia J, Yang W, Johnson ER (2011) Analysis of hydrogen-bond interaction potentials from the electron density: integration of noncovalent interaction regions. J Phys Chem A 115:12983–12990. https://doi.org/10.1021/jp204278k

Coyle B, Kavanagh K, McCann M, Devereux M, Geraghty M (2003) Mode of anti-fungal activity of 1,10-phenanthroline and its Cu(II), Mn(II) and Ag(I) complexes. Biometals 16:321–329. https://doi.org/10.1023/A:1020695923788

Cramer CJ (2004) Essentials of computational chemistry: theories and models. Wiley, Hoboken

Creaven BS, Egan DA, Karcz D, Kavanaugh K, McCann M, Mahon M, Noble A, Thati B, Walsh M (2007) Synthesis, characterisation and antimicrobial activity of copper(II) and manganese(II) complexes of coumarin-6,7-dioxyacetic acid (cdoaH_2) and 4-methylcoumarin-6,7-dioxyacetic acid (4-MecdoaH_2): X-ray crystal structures of [Cu(cdoa)(phen)$_2$]$_8$.8H_2O and [Cu. J Inorg Biochem 101:1108–1119. https://doi.org/10.1016/j.jinorgbio.2007.04.010

CrysAlisPro (2013) Data collection and processing software package, Rigaku Oxford Diffraction

Dağlı Ö, Köse DA, İçten O, Avcı GA, Şahin O (2019) The mixed ligand complexes of Co(II), Ni(II), Cu(II) and Zn(II) with coumarilic acid/1,10-phenanthroline. J Therm Anal Calorim 136:1467–1480. https://doi.org/10.1007/s10973-018-7773-y

Dawood AH, Kareem ET, Madlool AM (2012) Binuclear divalent complexes of cobalt, nickel and copper with N_2S ligand derived from 1,3,4-Thiadiazole-2,5-dithiolate dipotassium synthesized via click chemistry. Int J Chem 4:64–74. https://doi.org/10.5539/ijc.v4n6p64

Deegan C, Coyle B, McCann M, Devereux M, Egan DA (2006) In vitro anti-tumour effect of 1,10-phenanthroline-5,6-dione (phendione), [Cu(phendione)$_3$](ClO_4)$_2$•4H_2O and [Ag(phendione)$_2$]ClO_4 using human epithelial cell lines. Chem Biol Interact 164:115–125. https://doi.org/10.1016/j.cbi.2006.08.025

Deegan C, McCann M, Devereux M, Coyle B, Egan DA (2007) In vitro cancer chemotherapeutic activity of 1,10-phenanthroline (phen), [Ag_2(phen)$_3$(mal)]•2H_2O, [Cu(phen)$_2$(mal)]•2H_2O and [Mn(phen)$_2$(mal)]•2H_2O (malH_2 = malonic acid) using human cancer cells. Cancer Lett 247:224–233. https://doi.org/10.1016/j.canlet.2006.04.006

Ditchfield R, Hehre WJ, Pople JA (1971) Self-consistent molecular-orbital methods. IX. An extended Gaussian-type basis for molecular-orbital studies of organic molecules. J Chem Phys 54:724–728. https://doi.org/10.1063/1.1674902

Dong W, Wang Q-L, Liu Z-Q, Liao D-Z, Jiang Z-H, Yan S-P, Cheng P (2003) Syntheses, structures and magnetic properties of 1-D complex $\{[Ni(\mu\text{-}1,5\text{-}dca)(phen)_2](ClO_4)\}_n$, 2-D complex $[Mn(\mu\text{-}1,5\text{-}dca)_2(phen)]_n$ and 3-D complex $[Mn(\mu\text{-}1,5\text{-}dca)_2L]_n$ (dca = dicyanamide, $N(CN)_2^-$; pn = 1,3-propane diamine; phen = phenanthroline; L = 4,4′-ditriazole metha. Polyhedron 22:3315–3319. https://doi.org/10.1016/S0277-5387(03)00476-5

Engel E, Dreizler RM (2011) Density functional theory: an advanced course. Springer, Berlin

Fraústo da Silva JJR, Williams RJP (eds) (1991) The biological chemistry of the elements. Clarendon Press, Oxford

Frisch MJ, Trucks GW, Schlegel HB, Scuseria GE, Robb MA, Cheeseman JR, Montgomery JA, Vreven T, Kudin KN, Burant JC, Millam JM, Iyengar SS, Tomasi J, Barone V, Mennucci B, Cossi M, Scalmani G, Rega N, Petersson GA, Nakatsuji H, Hada M, Ehara M, Toyota K, Fukuda R, Hasegawa J, Ishida M, Nakajima T, Honda Y, Kitao O, Nakai H, Klene M, Li X, Knox JE, Hratchian HP, Cross JB, Bakken V, Adamo C, Jaramillo J, Gomperts R, Stratmann RE, Yazyev O, Austin AJ, Cammi R, Pomelli C, Ochterski JW, Ayala PY, Morokuma K, Voth GA, Salvador P, Dannenberg JJ, Zakrzewski VG, Dapprich S, Daniels AD, Strain MC, Farkas O, Malick DK, Rabuck AD, Raghavachari K, Foresman JB, Ortiz JV, Cui Q, Baboul AG, Clifford S, Cioslowski J, Stefanov BB, Liu G, Liashenko A, Piskorz P, Komaromi I, Martin RL, Fox DJ, Keith T, Al-Laham MA, Peng CY, Nanayakkara A, Challacombe M, Gill PMW, Johnson B, Chen W, Wong MW, Gonzalez C, Pople JA (2003) Gaussian 03, Revision A.1. Gaussian, Inc., Wallingford

Gaëlle DSY, Yufanyi DM, Jagan R, Agwara MO (2016) Synthesis, characterization and antimicrobial properties of cobalt(II) and cobalt(III) complexes derived from 1,10-phenanthroline with nitrate and azide co-ligands. Cogent Chem 2:1253201. https://doi.org/10.1080/23312009.2016.1253201

Gandra RM, Mc Carron P, Fernandes MF, Ramos LS, Mello TP, Aor AC, Branquinha MH, McCann M, Devereux M, Santos ALS (2017) Antifungal potential of copper(II), manganese(II) and silver(I) 1,10-phenanthroline chelates against multidrug-resistant fungal species forming the candida haemulonii complex: impact on the planktonic and biofilm lifestyles. Front Microbiol 8:1257. https://doi.org/10.3389/fmicb.2017.01257

Ganeshpandian M, Ramakrishnan S, Palaniandavar M, Suresh E, Riyasdeen A, Akbarsha MA (2014) Mixed ligand copper(II) complexes of 2,9-dimethyl-1,10-phenanthroline: tridentate 3N primary ligands determine DNA binding and cleavage and cytotoxicity. J Inorg Biochem 140:202–212. https://doi.org/10.1016/j.jinorgbio.2014.07.021

Grabowski SJ (2004) Hydrogen bonding strength—measures based on geometric and topological parameters. J Phys Org Chem 17:18–31. https://doi.org/10.1002/poc.685

Han X-Y, Ren Y-T, Zheng Y-Q (2010) Syntheses, crystal structures and magnetic properties of two adamantane-1,3-dicarboxylato bridged cobalt(II) phenanthroline complexes. Inorg Chim Acta 363:353–359. https://doi.org/10.1016/j.ica.2009.10.023

Janiak C (2000) A critical account on π–π stacking in metal complexes with aromatic nitrogen-containing ligands. J Chem Soc Dalton Trans. https://doi.org/10.1039/b003010o

Kani I, Atlier Ö, GÜVen K (2016) Mn(II) complexes with bipyridine, phenanthroline and benzoic acid: biological and catalase-like activity. J Chem Sci 128:523–536. https://doi.org/10.1007/s12039-016-1050-z

Kozisek J, Hvastijova M, Kohout J (1990) Addition of methanol to dicyanamide in the Cu(II) coordination sphere: structure of Bis(bis(methoxy-carbimido)atiato)copper(II). Inorg Chim Acta 168:157–158. https://doi.org/10.1016/S0020-1693(00)80934-2

Krishna PM, Reddy KH (2013) Synthesis, characterization, DNA studies of copper(II) complexes of (2E)-3- phenylprop-2-enal thiosemicarbazones. Pharm Chem J 5:258–269

Lan T, Fallatah A, Suiter E, Padalkar S (2017) Size controlled copper (I) oxide nanoparticles influence sensitivity of glucose biosensor. Sensors (Basel) 17:1–10. https://doi.org/10.3390/s17091944

Lee C, Yang W, Parr RG (1988) Development of the Colle-Salvetti correlation-energy formula into a functional of the electron density. Phys Rev B 37:785–789. https://doi.org/10.1103/PhysRevB.37.785

Lu T, Chen F (2012) Multiwfn: a multifunctional wavefunction analyzer. J Comput Chem 33:580–592. https://doi.org/10.1002/jcc.22885

Ma CB, Wang WG, Zhu HP, Chen CN, Liu QT (2001) Phenanthroline-manganese inclusion complexes of dicarboxylic acid containing extensive hydrogen-bonding interactions. Inorg Chem Commun 4:730–733. https://doi.org/10.1016/S1387-7003(01)00312-4

Macrae CF, Edgington PR, McCabe P, Pidcock E, Shields GP, Taylor R, Towler M, van de Streek J (2006) Mercury: visualization and analysis of crystal structures. J Appl Crystallogr 39:453–457. https://doi.org/10.1107/s002188980600731x

Mahmoud WH, Mohamed GG, El-Dessouky MMI (2014) Synthesis, characterization and in vitro biological activity of mixed transition metal complexes of lornoxicam with 1,10-phenanthroline. Int J Electrochem Sc 9:1415–1438

Manson JL, Brown CM, Huang Q, Schlueter JA, Lancaster T, Blundell SJ, Singleton J, Lynn JW, Pratt FL (2013) $Mn(dca)_2$(o-phen) {dca = dicyanamide; O-phen = 1,10-phenanthroline}: long-range magnetic order in a low-dimensional Mn-dca polymer. Polyhedron 52:679–688. https://doi.org/10.1016/j.poly.2012.07.087

McCarron P, McCann M, Devereux M, Kavanagh K, Skerry C, Karakousis PC, Aor AC, Mello TP, Santos ALS, Campos DL, Pavan FR (2018) Unprecedented in vitro antitubercular activitiy of manganese(II) complexes containing 1,10-phenanthroline and dicarboxylate ligands: increased activity, superior selectivity, and lower toxicity in comparison to their copper(II) analogs. Front Microbiol 9:1432. https://doi.org/10.3389/fmicb.2018.01432

Mishra A, Kaushik NK, Verma AK, Gupta R (2008) Synthesis, characterization and antibacterial activity of cobalt(III) complexes with pyridine-amide ligands. Eur J Med Chem 43:2189–2196. https://doi.org/10.1016/j.ejmech.2007.08.015

Mohamed GG, Omar MM, Ibrahim AA (2010) Preparation, characterization and biological activity of novel metal-NNNN donor Schiff base complexes. Spectrochim Acta A Mol Biomol Spectrosc 75:678–685. https://doi.org/10.1016/j.saa.2009.11.039

Momeni BZ, Haghshenas F, Hadi S (2017) Synthesis, structural characterization and crystal structure of some dimethyltin complexes containing substituted 1,10-phenanthroline. J Mol Struct 1142:156–167. https://doi.org/10.1016/j.molstruc.2017.04.042

Ndifon PT, Agwara MO, Paboudam AG, Yufanyi DM, Ngoune J, Galindo A, Álvarez E, Mohamadou A (2009) Synthesis, characterisation and crystal structure of a cobalt(II)-hexamethylenetetramine coordination polymer. Transit Met Chem 34:745–750. https://doi.org/10.1007/s11243-009-9257-1

Ndosiri NB, Agwara MO, Paboudam AG, Ndifon PT, Yufanyi DM, Amah C (2013) Synthesis, characterisation and antifungal activities of Mn(II), Co(II), Cu(II) and Zn(II) mixed-ligand complexes containing 1,10-Phenanthroline and 2,2′-Bipyridine. Res J. Pharm Biol Chem Sci 4:386–397

Ng NS, Wu MJ, Jones CE, Aldrich-Wright JR (2016) The antimicrobial efficacy and DNA binding activity of the copper(II) complexes of 3,4,7,8-tetramethyl-1,10-phenanthroline, 4,7-diphenyl-1,10-phenanthroline and 1,2-diaminocyclohexane. J Inorg Biochem 162:62–72. https://doi.org/10.1016/j.jinorgbio.2016.06.006

Nord G (1985) Some properties of 2,2′-bipyridine, 1,10-phenanthroline and their metal complexes. Comments Inorg Chem 4:193–212. https://doi.org/10.1080/02603598508072261

Onawumi OE, Adeoye IO, Adekunle FO (2013) Synthesis, characterisation and microbial studies of [bis(1,10-phenanthroline) (ethylenediamine) copper(II)] diperchlorate and its bromide analogue. Open J. Inorg Chem 1:26–33. https://doi.org/10.4236/ojic.2013.31004

Parada J, Atria ANAM, Wiese G, Rivas E, Corsini G (2014) Synthesis, Characterization and Antibacterial Activity of Cobalt(III) Complex with Phenanthroline and Maltose. J Chil Chem Soc 59:2636–2639. https://doi.org/10.4067/s0717-97072014000400002

Pook NP, Hentrich P, Gjikaj M (2015) Crystal structure of bis-[tris-(1,10-phenanthroline-kappa(^{2}) N,N′)cobalt(II)] tetra-nitrate N,N′-(1,4-phenyl-enedicarbon-yl)diglycine solvate octa-hydrate. Acta Crystallogr E Crystallogr Commun 71:910–914. https://doi.org/10.1107/s2056989015013006

Ray RK, Bandyopadhyay MK, Kauffman GB (1989) Metal-mediated addition of alcohols to dicyandiamide. Polyhedron 8:757–762. https://doi.org/10.1016/S0277-5387(00)83844-9

Şahin ZS, Şahin O, Dağlı Ö, Köse DA (2016) Diphenic acid/nicotinamide complexes of Co^{II}, Cu^{II} and Zn^{II}. Synthesis and Structural Investigation. Polyhedron 117:214–223. https://doi.org/10.1016/j.poly.2016.05.051

Sammes PG, Yahioglu G (1994) 1,10-Phenanthroline—a versatile ligand. Chem Soc Rev 23:327–334. https://doi.org/10.1039/cs9942300327

Saravanan C, Mudaliar CG (2014) Synthesis, characterization and thermal analysis of the copper(II) complexes with 2,2-bipyridyl and 1,10-phenanthroline. Afr. J Pure Appl. Chem 8:162–175. https://doi.org/10.5897/AJPAC2014.0592

Sheldrick GM (2015) SHELXT-20xy. Acta Crystallogr A 71:3–8

Tan SL, Jotani MM, Tiekink ERT (2019) Utilizing Hirshfeld surface calculations, non-covalent inter-action (NCI) plots and the calculation of interaction energies in the analysis of molecular packing. Acta Crystallogr E Crystallogr Commun 75:308–318. https://doi.org/10.1107/S2056989019001129

Tong M-L, Wu Y-M, Tong Y-X, Chen X-M, Chang H-C, Kitagawa S (2003) Rational Design of a ferromagnetic trinuclear copper(II) complex with a novel in situ synthesised metalloligand. Eur J Inorg Chem. https://doi.org/10.1002/ejic.200300197

Tonzing DS, Batten SR, Murray KS (2006) 1D chain structures of $M(dca)_2(phen)(H_2O)$.MeOH, M = Mn, Fe Co, Ni, Zn and Cd, dca = dicyanamide, $N(CN)_2^-$, phen = 4,7-phenanthroline. J Mol Struct 796:63–68. https://doi.org/10.1016/j.molstruc.2006.03.033

Turner DR, Chesman AS, Murray KS, Deacon GB, Batten SR (2011) The chemistry and complexes of small cyano anions. Chem Commun (Camb) 47:10189–10210. https://doi.org/10.1039/c1cc11909e

Váhovská L, Potočňák I, Vitushkina S, Walko M (2016) Low-dimensional compounds containing cyanido groups. Part XXX. Recrystallization of Co(II) complexes with pseudohalogenide ligands leading to CO2 uptake and formation of dicyanoguanidine anion in newly created Co(III) complexes. Polyhedron 117:359–366. https://doi.org/10.1016/j.poly.2016.06.007

Yanick Gaelle DS, Ondoh Agwara M, Yufanyi DM, Nenwa J, Jagan R (2016) Crystal structure and antimicrobial properties of a copper(II) complex with 1,10-phenanthroline and azide co-ligand. Inorg Nano-Metal Chem 47:618–625. https://doi.org/10.1080/15533174.2016.1212220

Yesilel OZ, Ucar I, Bulut A, Olmez H, Büyükgüngör O (2006a) Synthesis, crystal structure, spectral and thermal characterization of cis -Diaquabis (1,10-phenanthroline) zinc(II) Diorotate Hydrate, cis-$[Zn(H_2O)_2(phen)_2](H_2O)_2{\cdot}(H_2O)_{2.125}$. Verlag der Zeitschrift fur Naturforschung, Tubingen 61:147–152. https://doi.org/10.1515/znb-2006-0205

Yesilel OZ, Olmez H, Yılanc OO, Aoglu HP, Buyukgungor O (2006b) Syntheses, spectral and thermal studies, and crystal structure of 1,10-phenanthroline and picolinamide complexes of cobalt(II) squarate. Verlag der Zeitschrift fur Naturforschung, Tubingen 61b:1094–1100. https://doi.org/10.1515/znb-2006-0907

Zheng L-L, Leng J-D, Liu W-T, Zhang W-X, Lu J-X, Tong M-L (2008) Cu^{2+}-mediated nucleophilic addition of different nucleophiles to dicyanamide—synthesis, structures, and magnetic properties of a family of mononuclear, trinuclear, hexanuclear, and polymeric copper(II) complexes. Eur J Inorg Chem 2008:4616–4624. https://doi.org/10.1002/ejic.200800486

International Journal of Chemistry; Vol. 10, No. 4; 2018
ISSN 1916-9698 E-ISSN 1916-9701
Published by Canadian Center of Science and Education

Synthesis, Crystal Structures, Thermal and Antimicrobial Properties of Mn(II) Complexes of 1,10-Phenanthroline With Some Co-Ligands

Donatus Bekindaka Eni[1], Divine Mbom Yufanyi[2], Che Dieudonne Tabong[3], Rajamony Jagan[4], Moise Ondoh Agwara[4]

[1]Department of Inorganic Chemistry, University of Yaounde I, P.O. Box 812 Yaounde, Cameroon

[2]Department of Chemistry, Faculty of Science, The University of Bamenda, P.O. Box 39 Bambili, Cameroon

[3]Department of Chemistry, Higher Teachers' Training College Bambili, The University of Bamenda, Cameroon

[4]Sophisticated Analytical Instruments Facility, Indian Institute of Technology, Chennai-600036, Madras, India

Correspondence: Moise Ondoh Agwara, Department of Inorganic Chemistry, University of Yaounde I, P.O. Box 812 Yaounde, Cameroon. Tel: (+237) 679 87 52 45 E-mail: agwara29@yahoo.com

Received: November 9, 2018 Accepted: November 27, 2018 Online Published: November 28, 2018

doi:10.5539/ijc.v10n4p155 URL: https://doi.org/10.5539/ijc.v10n4p155

Abstract

The complexes of Manganese(II) with 1,10-phenanthroline using the nitrate, azide and dicyanamide as co-ligands have been synthesized and characterized by elemental analysis, infrared spectroscopy, thermal analysis and room temperature magnetic susceptibility measurements. The magnetic moments of the complexes are consistent with high spin (d^5) octahedral geometry. Single-crystal X-ray analysis confirmed the complexes to be $[Mn(Phen)_2(NO_3)_2]$ (**1**), $[Mn(Phen)_2(N_3)_2)]$ (**2**), and $[Mn(Phen)_2(dca)_2)]$ (**3**). Complexes **1** and **2** crystallize in an orthorhombic crystal system with space group *Pbcn* while complex **3** crystallizes in the monoclinic crystal system with space group $P2_1/c$. The complexes have been screened for in vitro antibacterial and antifungal activities by the disc diffusion method. The minimum inhibitory concentration values indicate that the complexes showed greater activity against the fungi strains tested compared to that of the reference antifungal.

Keywords: antimicrobial properties, azide; dicyanamide, manganese(II), 1,10-phenanthroline, X-ray crystal structure

1. Introduction

Recently, there has been sustained interest in the coordination chemistry of 1,10-phenanthroline (Bencini and Lippolis 2010). Its unique physical and chemical properties coupled with its coordination ability, makes it suitable for various applications. For example, these complexes have potential technological applications due to their ability to absorb strongly in the the ultraviolet spectral region, emit bright light alongside their good electro- and photoactive properties (Bencini and Lippolis 2010). 1,10-Phenanthroline (phen) is also a biologically important ligand which, together with some of its metal complexes, has been shown to be effective against various strains of microorganisms (McCann, Geraghty et al. 2000, Agwara, Ndifon et al. 2010, Aljahdali and El-Sherif 2013, Colak, Oztopcu-Vatan et al. 2013).) This rigid, planar framework and versatile polypyridine nitrogen donor ligand 1,10-Phenanthroline (phen), has been extensively studied for its coordination ability (scheme 1) and stability in biochemical processes. Due to the chelating nature of phenanthroline and substituted phenanthroline ligands in metal complexes, they control the supramolecular assemblies formed through chelation of the metal center (Bencini and Lippolis 2010).

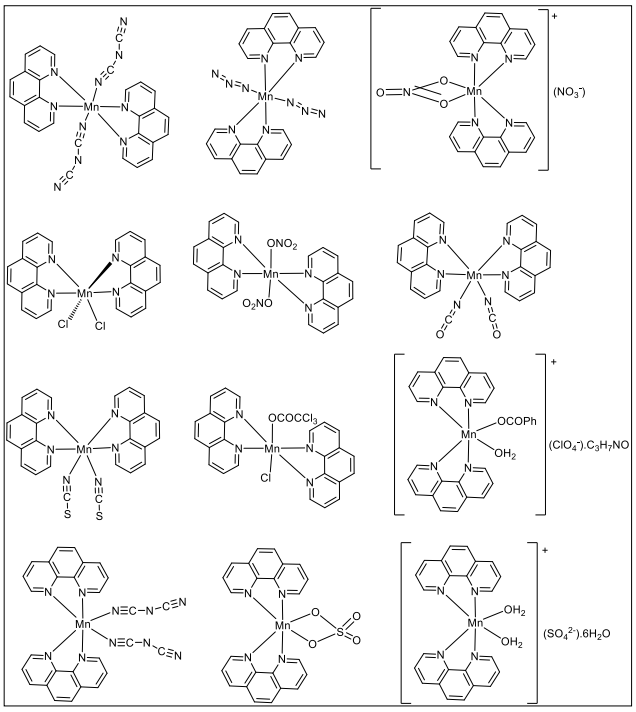

Scheme 1. Some complexes of Mn-Phen found in the literature

The potential of mixed ligand complexes with 1,10-phen as models for biological systems, such as binding of small molecules to DNA, has attracted scientific interest (Jennifer and Muthiah 2014). Interest is also focused on the the ability of 1,10-phen to use its extended π-system to form non-covalent π-interactions, which mimic various biological processes (Jennifer and Muthiah 2014, Pook, Hentrich et al. 2015). The use of mixed ligands having different donor atoms to synthesise complexes, can lead to changes in their physical and chemical properties. Metal complexes of these heterocyclic aromatic ring systems are electron-deficient and can undergo π-π stacking interactions as π-acceptors (Pook, Hentrich et al. 2015). Though hydrogen bonding still remains the most reliable and widely used means of enforcing molecular recognition, an interplay of weak intermolecular interactions (offset π stacking and C-H···π interactions) also determines the self-assembly of these molecules into 3D networks (Sun, Tong et al. 2010).

Manganese is an essential trace element and plays an important role in several physiological processes as a constituent or activator of some enzymes. Mn(II) ion has a $3d^5$ outer electronic configuration, with no crystal-field stabilisation energy in its high-spin complexes. No electronic restraints are expected in these high-spin structures. The most common structures of Mn(II) are therefore those that minimise steric repulsion (octahedral and tetrahedral), some other coordinate (five-coordinate and seven-coordinate) complexes are known in biological systems. Interest in the coordination chemistry of Mn(II) compounds has increased due to their significant role as redox sites in biological systems such as pyruvate carboxylase, oxaloacetate decarboxylase, superoxide dismutases and diamine oxidases (Wieghardt 1989).

The azide anion exhibits different coordination modes with transition metal ions, leading to a wide variety of fascinating structures (discrete molecules to 3-D arrays) (Chen, Jiang et al. 2009, Lazari, Stamatatos et al. 2009). The coordination modes (Scheme 2a) range from monodentate to bridging bi-, tri- and tetra-dentate (Batten and Murray 2003, Lazari, Stamatatos et al. 2009, Adhikary and Koner 2010).

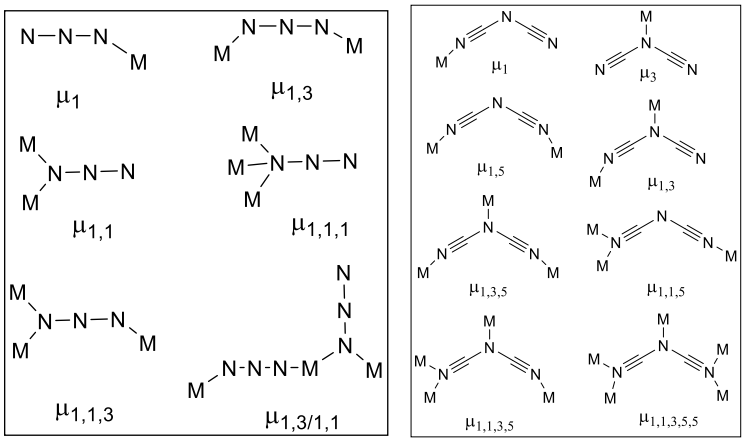

(a) (b)

Scheme 2. Bonding modes of (a) azide and (b) dicyanamide

The dicyanamide anion shows a variety of different coordination modes (scheme 2b) which include the terminal and the bridging (Batten and Murray 2003, Mohamadou, van Albada et al. 2003, Sun, Tong et al. 2010).

The nitrate anion in complexes can be a bidentate, bridging, or monodentate ligand or it is as an ionic species. The bonding type is probably a function of the nature and number of other ligands present (Yanick Gaelle, Ondoh Agwara et al. 2017).

One of our research interests is the systematic study of transition metal complexes containing heterocyclic N-donor ligands and other co-ligands (Agwara, Ndifon et al. 2010, Amah, Ondoh et al. 2015, Ga ëlle, Yufanyi et al. 2016, Tabong, Yufanyi et al. 2016). The emergence of drug-resistant bacterial and fungal strains has become a public health concern (WHO 2014). This increasing resistance of microbes to antibacterial and antifungal drugs has necessitated the search for new compounds to target these pathogenic microbes (Spellberg, Guidos et al. 2008). Strategies to develop antimicrobial agents to fight against these resistant pathogens include the research and development of new antimicrobial agents (Weinstein and Fridkin 2003, Spellberg, Guidos et al. 2008, Beyth, Houri-Haddad et al. 2015). The modification of biologically active ligands through coordination to metal ions is a possible route for the development of new active agents.

In view of the varied applications of manganese mixed ligand complexes and exploring the good biological and chelating ability of phenanthroline as well as the versatile bonding modes of dca^-, N_3^- and NO_3^-, we report herein the synthesis and structure elucidation of three manganese(II) complexes of 1,10-phen and co-ligands. Strong hydrogen bonds and π···π interactions play important roles in the formation of the 3D structures. The effects of the co-ligands on the biological activities of the complexes towards some resistant pathogens, evaluated using *in vitro* assays, are also presented.

2. Method

All the chemicals were of reagent grade and were used as such without further purification. All solvents used were dried and distilled according to standard methods.

2.1 Synthesis of the Complexes

2.1.1 Synthesis of $[Mn(Phen)_2(NO_3)_2]$ (**1**)

A 25 mL methanol solution of $Mn(NO_3)_2{\cdot}4H_2O$ (0.251 g, 1 mmol) was added drop wise to a 25 mL methanol solution of 1,10-phenanthroline (0.396 g, 2 mmol) with constant stirring and refluxed at 85 ℃ for 4 h. The light yellow precipitate obtained was washed with ethanol and the filtrate preserved for crystal growth. Yellow crystals, suitable for single crystal X-ray diffraction, were obtained from the filtrate after two days. The crystals were washed with acetone and then dried *in vacuo*. *Yield: 75%; anal. Calc.(Found) for* $C_{24}H_{16}N_6O_6Mn$*; C:53.45(51.88); H:2.99(2.50); N:15.58(15.57).*

2.1.2 Synthesis of $[Mn(Phen)_2(N_3)_2]$ (**2**)

A 25 mL methanol solution of $Mn(NO_3)_2{\cdot}4H_2O$ (0.251 g, 1 mmol) was added, drop wise to a 25 mL methanol solution of 1,10-phenanthroline (0.396 g, 2 mmol) with constant stirring and refluxed at 85 ℃ for 1 h. After an hour, a 10 mL water/methanol (1:4 v/v) solution of sodium azide (0.13 g, 2 mmol) was added drop wise to the mixture and it was further refluxed for 3 h. The intense yellow precipitate obtained was washed with ethanol. Yellow crystals, suitable for

single crystal X-ray diffraction, were obtained from the filtrate after one day. The crystals were washed with acetone and then dried *in vacuo*. *Yield: 80%; anal. Calc.(Found) for $C_{24}H_{16}MnN_{10}$; C:57.72(56.65); H:3.23(3.03); N:28.05(29.01).*

2.1.3 Synthesis of $[Mn(Phen)_2(dca)_2]$ (**3**)

To a 25 mL methanol solution of $Mn(NO_3)_2{\cdot}4H_2O$ (0.251 g, 1 mmol) was added, drop wise a 25 mL methanol solution of 1,10-phenanthroline (0.396 g, 2 mmol) with constant stirring and refluxed at 85 ℃ for 1 h. After an hour, a 10 mL water/methanol (1:4 v/v) solution of sodium dicyanamide (0.18 g, 2 mmol) was added drop wise to the mixture and it was further refluxed for 3 h. The yellow precipitate obtained was washed with ethanol. Light yellow crystals, suitable for single crystal X-ray diffraction, were obtained from the filtrate after one day. The crystals were washed with acetone and then dried *in vacuo*. *Yield: 85%; anal. Calc.(Found) for $C_{24}H_{16}MnN_{10}$; C:61.43(62.29); H:2.95(2.33); N:25.59(25.92).*

2.2 Characterisation

Elemental analyses (C, H, N) of the complexes was carried out on a FLASH 2000 Organic Elemental Analyzer. The melting point/decomposition temperatures of the complexes were obtained using the STUART Scientific Melting Point SMP1 Device with maximum temperature at 360 ^{o}C. The FT-IR spectra of the complexes and ligands were recorded from 4000-400 cm^{-1} on a PerkinElmer Spectrum Two universal attenuated total reflectance Fourier transform infrared (UATR-FT-IR) spectrometer. Thermogravimetric (TG) and differential thermal analysis (DTA) curves were obtained using a NETZSCH STA449F1 thermoanalyzer in a dynamic argon atmosphere (heating rate 10 ℃ min^{-1}, flow rate 25 mL/min, aluminium oxide crucible, mass 20 mg, and temperature range from room temperature up to 900 ℃). Room temperature magnetic susceptibility measurements of the complexes were determined using the Gouy method with mercury tetrathiocyanocobalt(II) as calibrant on a Stanton Instruments Limited (Model A49).

2.3 Magnetic Susceptibility Measurement

Magnetic susceptibility measurements are widely used in studying the magnetic properties of transition metal complexes. The magnetic properties are due to the presence of unpaired electrons in the partially filled d-orbital in the outer shell of these elements. These magnetic measurements give information on the electronic state of the metal ion in the complexes. The magnetic measurements were performed at a temperature range of 5-300 K using a Sherwood Scientific magnetic susceptibility balance. The magnetic data of the samples were obtained by taking the difference in mass between an empty sample tube and the sample tube filled with sample which is in the form of a reasonable fine and uniform powder. The diamagnetic corrections for the samples were estimated using Pascal's constant and the magnetic data were corrected for diamagnetic contributions using sample holder.

The mass susceptibility, χ_g, is calculated using the equation:

$$\chi_g = \frac{C_{Bal}\, l(R-R_o)}{10^9 m} \quad (1)$$

Where l = sample length (cm); m = sample mass (g), R = reading for tube plus sample, R_o = empty tube reading, C_{Bal} = balance calibration constant.

2.4 Single crystal X-ray Data Collection and Structural Refinement

All intensity data were collected on Bruker AXS Kappa APEX II single crystal CCD Diffractometer, equipped with graphite-monochromated MoKα radiation (λ = 0.71073 Å). Data reduction and absorption corrections were performed by APEX2, SAINT-plus and SADABS program (Bruker 2004). The structure was solved by direct methods and the refinement of all non-hydrogen atoms was performed with SHELX97 (Sheldrick 1997). H-atoms were mainly calculated on idealised positions. Structure figures were generated with ORTEP (Farrugia 1997). CCDC 1485344 (**1**), CCDC 1417782 (**2**) and CCDC 1485343 (**3**) contain the supplementary crystallographic data for this paper. These data can be obtained free of charge via www.ccdc.cam.ac.uk/conts/retrieving.html (or from the Cambridge Crystallographic Data Centre, 12 Union Road, Cambridge CB2 1EZ, UK; fax: (+44)1223-336-033; or deposit@ccdc.cam.uk).

2.5 Antimicrobial Tests

The antimicrobial tests were carried out in the Applied Microbiology and Molecular Pharmacology Laboratory (LMP) of the University of Yaoundé I, Cameroon. The tests were done on twenty four pathogenic micro-organisms; twenty bacterial strains: B1=*Streptococcus pneumonae* ATCC49619, B2=*Staphylococcus aureus* BAA917, B3=*Staphylococcus aureus* ATCC43300, B4=*Staphylococcus aureus* NR45003, B5=*Staphylococcus aureus* NR46003, B6=*Staphylococcus aureus* CP7625, B7=*Shigella flexineri* NR518, B8=*Salmonella enterica* NR4294, B9=*Salmonella enterica* NR4311, B10=*Salmonella enterica* NR13555, B11=*Pseudomonas aeruginosa* NMC592, B12=*Klessiella pneumonae* ATCC13883, B13=*Klessiella pneumonae* ATCC70603, B14=*Klessiella pneumonae* NR41916, B15=*Escherishia* coli

ATCC25922, B16=Escherishia coli ATCC35218, B17=Enterococcus fecalis ATCC51219, B18=*Staphylococcus aureus* NR46374, B19=*Hemophyllus influenza* ATCC49247, B20 = *Mycobacterium smegmatis* and four yeasts: *Candida krusei*, *Candida parasilosis*, *Candida albicans*, *Cryptococcus neoformans* obtained from Centre Pasteur Yaoundé, Cameroon. The selected microorganisms represent the causative agents for diseases that are prevalent in our environment. The microbial isolates were maintained on agar slant at 4 ℃ in the laboratory. The strains were sub-cultured on fresh appropriate agar plate in incubators 18 hours prior to any antimicrobial test. Amoxicillin, ciprofloxacin and cloxacillin were used as reference antibiotics (RB) while fluconazole was the reference antifungal (RF).

2.5.1 Diffusion Tests

In vitro antimicrobial activity of the ligand, metal salts and complexes were evaluated using the disc-diffusion method as previously described (Gaëlle, Yufanyi et al. 2016, Yanick Gaelle, Ondoh Agwara et al. 2017). The antimicrobial tests were carried out as described by Berghe and Vlietinck (Berghe and Vlietinck 1991). Three replicas were performed for each sample and mean values of the growth inhibition zone were calculated. Compounds with a zone of inhibition IZ <7 mm were considered to be inactive, those in the range 7 < IZ < 20 mm as active and those with IZ > 20 mm, very active.

2.5.2 Minimum Inhibitory Concentration of the Complexes

The Minimum Inhibitory Concentration (MIC) was determined according to National Committee for Clinical Laboratory Standards (NCCLS) M38, a microdilution method using (12 x 8 wells) microtitre plates, as previously described (Sidjui, Toghueo et al. 2016).

3. Results and Discussion

Complexes 1-3 were obtained relatively quickly without solvent evaporation. All the complexes are crystalline, coloured and air-stable can be reproducibly prepared in high yields (>70 %). Their physicochemical properties are summarized in Table 1.

Table 1. Physical data of the complexes

Complex	Nature	Colour	Yield (%)	Melting point (^{o}C)	Molar conductivity ($\Omega^{-1}cm^{2}mol^{-1}$)
$[Mn(Phen)_2(NO_3)_2]$ (**1**)	Crystals	Yellow	75	356	41.36
$[Mn(Phen)_2(N_3)_2)]$ (**2**)	Crystals	Intense yellow	80	/	23.04
$[Mn(Phen)_2(dca)_2)]$ (**3**)	Crystals	Yellow	85	290	15.7

Complex **1** melted at (356 ± 2 ℃) while the melting point of the $[Mn(Phen)_2(N_3)_2)]$ complex could not be determined due to the explosive nature of the azide. Complex **3** changed in colour upon heating from yellow to dark orange and then melted at (290 ± 2 ℃). This change in colour is attributed to change in crystal structural geometry from octahedral to tetrahedral as the dca molecules are lost (Allan, Brown et al. 1970, Nagase, Yokobayashi et al. 1976, McCann, Geraghty et al. 2000, Colak, Oztopcu-Vatan et al. 2013). The low molar conductivity values of 41.36 Ωcm^{-2} mol^{-1}, 23.04 Ωcm^{-2} mol^{-1} and 15.7 Ωcm^{-2} mol^{-1} in water, for **1**, **2** and **3**, respectively, indicates the molecular nature of the complexes.

3.1 X-ray Crystal Structure

The crystallographic data and structure refinement parameters of complexes **1**-**3** are presented in Table 2.

Table 2. Crystal data and structure refinement parameters for complexes **1**-**3**

Complex	**1**	**2**	**3**
Chemical formula	$C_{24}H_{16}MnN_6O_6$	$C_{24}H_{16}MnN_{10}$	$C_{28}H_{16}MnN_{10}$
Crystal system, space group	Orthorhombic, *Pbcn*	Orthorhombic, *Pbcn*	Monoclinic, $P2_1/c$
Temperature (K)	296	296	150
a, *b*, *c* (Å)	12.5477 (14), 10.1607 (10), 17.695 (2)	13.395 (2), 9.6457 (14), 16.979 (3)	9.8716 (8), 14.6636 (8), 17.6165 (11)
β (°)			104.364 (3)
V (Å^3)	2256.0 (4)	2193.8 (6)	2470.3 (3)
Z	4	4	4
Radiation type	Mo *K*α	Mo *K*α	Mo *K*α
μ (mm^{-1})	0.64	0.64	0.57
Crystal size (mm)	0.30 × 0.25 × 0.25	0.25 × 0.25 × 0.20	0.17 × 0.16 × 0.13
T_{min}, T_{max}	0.831, 0.856	0.861, 0.941	0.847, 0.867
No. of measured, independent and observed [$I > 2\sigma(I)$] reflections	12206, 2957, 1774	22275, 2029, 1349	54213, 6160, 4835
R_{int}	0.026	0.041	0.056
$(\sin\theta/\lambda)_{max}$ (Å^{-1})	0.703	0.606	0.668
$R[F^2 > 2\sigma(F^2)]$, $wR(F^2)$, *S*	0.058, 0.187, 1.02	0.077, 0.179, 1.17	0.036, 0.085, 1.06
No. of reflections	2957	2029	6160
No. of parameters	168	159	352
No. of restraints	0	0	0
H-atom treatment	H-atom parameters constrained	H-atom parameters constrained	H-atom parameters constrained
$\Delta\rho_{max}$, $\Delta\rho_{min}$ (e Å^{-3})	0.67, −0.55	0.71, −0.52	0.37, −0.39

3.1.1 Crystal Structure of $[Mn(Phen)_2(NO_3)_2]$ (**1**)

Complex **1** crystallizes in the orthorhombic crystal system with space group *Pbcn* with four molecules in the unit cell. The ORTEP representation of the crystal structure is shown in Figure 1 and the packing diagram in Figure 2. Selected bond lengths and angles are presented in Table 3 while the H-bond parameters are given in Table 4. The asymmetric unit of complex **1** consists of one phenanthroline molecule, one nitrate ion and one Mn(II) ion and the other half of the asymmetric unit is generated by inversion symmetry. The Mn(II) ion is coordinated by four N atoms from two chelating phen ligands and two O atoms from two nitrate ions giving a MnN_4O_2 coordination sphere with a distorted octahedral geometry. Three phen N atoms [N(1)-Mn(1) 2.319(3) Å, N(2)-Mn(1) 2.289(3) Å, Mn(1)-N(2)#1 2.289(3) Å] and one nitrate O atom [O(1)-Mn(1) 2.422(6) Å] form the equatorial plane, whereas symmetry related fourth phen N atom [Mn(1)-N(1)#1 2.319(3)] and the second nitrate ion [Mn(1)-O(1)#1 2.422(7)] are in apical positions. The N(2)-Mn(1)-N(1)#1 bond angle of 88.70(10)° indicates that the N(2)–Mn(1) and Mn(1)–N(1)#1 bonds are in different planes, almost perpendicular to each other. The 5-membered chelating rings of Mn(II) and N atoms of phen exhibit a near perfect plane; the N2−C11–C12–N1 torsion angle is 0.84(4) ° for complex **1**. The Mn–N bond lengths are in the range 2.289(3)–2.319(3) Å, which are similar to values reported in the literature (Ma, Wang et al. 2001, Kani, Atlier et

al. 2016). The N(2)-Mn(1)-N(1) chelating angle is 72.14(10) °. The bond lengths in the phenanthroline ring range from 1.328(6)–1.438(4) Å in C–C and from 1.323(4)–1.352(4) Å in C–N and this is similar to literature reported values for phenanthroline complexes (Ma, Wang et al. 2001, Kani, Atlier et al. 2016).

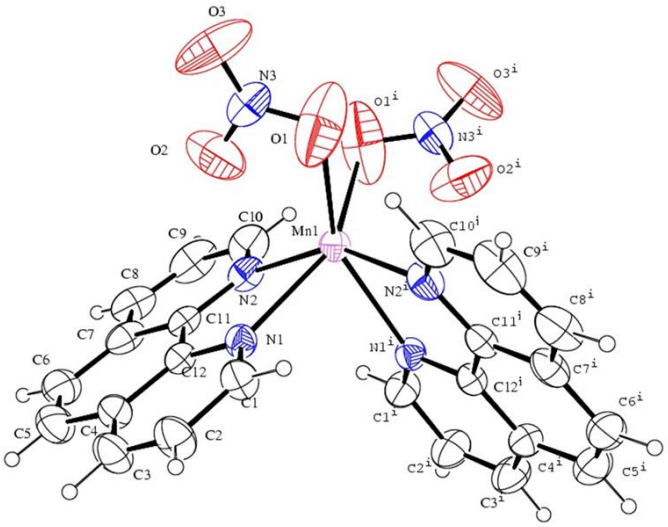

Figure 1. ORTEP view of the crystal structure of [dinitrato-bis(1,10-phenanthroline-κ^2N,N')manganese(II) (**1**)

The packing in the unit cell is based on intermolecular hydrogen bonding and π–π stacking interactions. Cooperation between extensive series of C–H ··O hydrogen bonds (Čechová, Martišková et al. 2014, Hu and Zhang 2016) (Table 4) and face-to-face π–π [C9–C4 3.369(6) Å; symmetry code -1/2+x,-1/2+y,3/2-z] stacking interactions (Janiak 2000), between adjacent phen ligands, stabilize the structure and assemble complex **1** into an interesting 3D supramolecular structure. It is noteworthy to mention that a polymorph of **1** is known (Saphu, Chanthee et al. 2012). The comparative crystal data of the complexes are presented in Table 5.

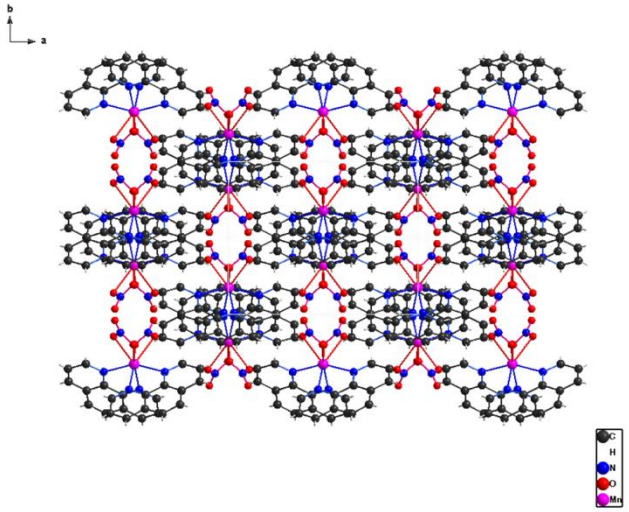

Figure 2. Packing diagram of **1** seen along the crystallographic c-axis

Table 3. Selected bond lengths and bond angles for complex **1**

Bond	Length (Å)	Bond	Angle (°)
N(1)-Mn(1)	2.319(3)	O(3)-N(3)-O(2)	123.8(5)
N(2)-Mn(1)	2.289(3)	O(3)-N(3)-O(1)	126.7(6)
N(3)-O(3)	1.155(4)	O(2)-N(3)-O(1)	109.3(5)
N(3)-O(2)	1.195(5)	N(3)-O(1)-Mn(1)	103.6(4)
N(3)-O(1)	1.203(5)	N(3)-O(2)-Mn(1)	100.0(4)
O(1)-Mn(1)	2.422(6)	N(2)#1-Mn(1)-N(2)	153.72(15)
O(2)-Mn(1)	2.495(6)	N(2)#1-Mn(1)-N(1)#1	72.14(10)
Mn(1)-N(2)#1	2.289(3)	N(2)-Mn(1)-N(1)#1	88.70(10)
Mn(1)-N(1)#1	2.319(3)	N(2)#1-Mn(1)-N(1)	88.70(10)
Mn(1)-O(1)#1	2.422(7)	N(2)-Mn(1)-N(1)	72.14(10)
Mn(1)-O(2)#1	2.495(6)	N(1)#1-Mn(1)-N(1)	87.09(14)
C(10)-H(10)	0.9300	N(2)#1-Mn(1)-O(1)#1	122.84(14)
C(11)-N(2)	1.352(4)	N(2)-Mn(1)-O(1)#1	78.61(15)
C(11)-C(12)	1.438(4)	N(1)#1-Mn(1)-O(1)#1	104.40(18)
C(12)-N(1)	1.351(4)	N(1)-Mn(1)-O(1)#1	148.31(14)
C(5)-C(6)	1.328(6)	N(2)#1-Mn(1)-O(1)	78.61(15)

Table 4. Hydrogen-bond geometry (Å, °) for (**1**)

D–H···*A*	*D*–H	H ···*A*	*D* ···*A*	*D*–H···*A*
C10–H10···O1^{i}	0.93	2.34	2.935 (8)	122
C3–H3···O2^{ii}	0.93	2.65	3.460(6)	144.1
C6–H6···O3^{iii}	0.931	2.719	3.394(7)	130.1
C6–H6···O3^{iv}	0.931	2.579	3.381(5)	144.5

Symmetry code: (i) −x, y, −z+3/2; (ii) -x,-y,1-z ; (iii) -1/2+x,1/2-y,1-z ; (iv) -1/2+x,-1/2+y,3/2-z

Table 5. Comparative crystal data of **1** with that of a known polymorph

Complex	**1** (this work)	$[Mn(NO_3)_2(C_{12}H_8N_2)_2]$ (Saphu, Chanthee et al. 2012)
Chemical formula	$C_{24}H_{16}MnN_6O_6$	$C_{24}H_{16}MnN_6O_6$
M_r	539.37	539.37
Crystal system, space group	Orthorhombic, *Pbcn*	Monoclinic, C2/c
Temperature (K)	296	298
a	12.5477 (14)	11.6191 (6)
b	10.1607 (10)	15.1164 (8)
c (Å)	17.695 (2)	13.4526 (7)
β (°)	90	105.387 (1)
V (Å^3)	2256.0 (4)	2278.1 (2)
Z	4	4

3.1.2 Crystal Structure of $[Mn(Phen)_2(N_3)_2)]$ (**2**)

Complex **2** crystallizes in the orthorhombic crystal system with space group *Pbcn* with four molecules in the unit cell. The ORTEP representation of the crystal structure is shown in Figure 3 and the packing diagram in Figure 4. Selected bond lengths and angles are presented in Table 6 while the H-bond parameters are given in Table 7. The asymmetric unit consists of one molecule of phen, one azide anion, one Mn(II) ion and the other half of the asymmetric unit is generated by inversion symmetry. Chemically, each Mn atom is six-coordinate with four N atoms of two phen molecules [Mn1–N1 2.320(4) Å, Mn1–N1i 2.320(4) Å, Mn1–N2 2.268(4) Å, Mn1–N2i 2.268(4) Å] and two terminal N

atoms from two azide anions [Mn1–N3 2.130(6) Å, Mn1–N3i 2.130(6) Å] giving a distorted octahedral geometry around the Mn atom with MnN6 chromophore. The azido ligands have a cis configuration in the structure. This observation is similar to literature reports of the same structure obtained by different synthetic methods but with slightly different crystal parameters (Shen, Zuo et al. 1999, Mas árov á and Moncol 2016).

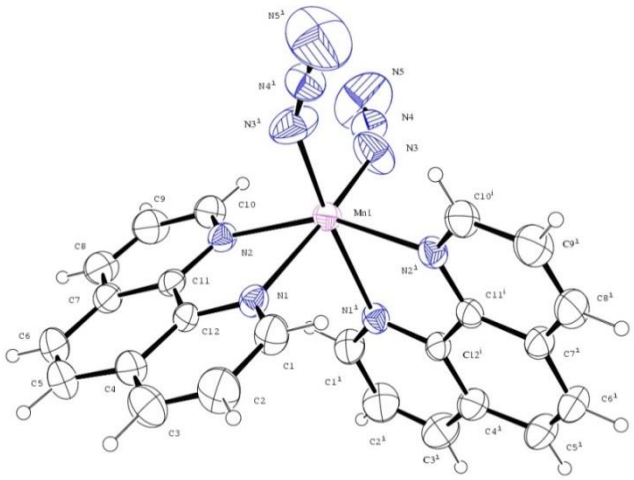

Figure 3. ORTEP view of crystal structure of [diazido-bis(1,10-phenanthroline-κ^2N,N')manganese(II) (**2**)

Table 6. Selected bond lengths and angles for **2**

Bond	Length (Å)	Bond	Angle (°)
Mn1–N3	2.130 (6)	N3–Mn1–N3^i	97.9 (4)
Mn1–N3^i	2.130 (6)	N3–Mn1–N2^i	101.1 (2)
Mn1–N2^i	2.268 (4)	N3i–Mn1–N2^i	95.7 (2)
Mn1–N2	2.268 (4)	N3–Mn1–N2	95.7 (2)
Mn1–N1^i	2.320 (4)	N3i–Mn1–N2	101.1 (2)
Mn1–N1	2.320 (4)	N2i–Mn1–N2	154.3 (2)
N1–C1	1.323 (6)	N3–Mn1–N1^i	88.8 (2)
C4–C5	1.425 (9)	N3i–Mn1–N1^i	167.17 (19)
N1–C12	1.347 (6)	N2i–Mn1–N1^i	72.16 (16)
C6–C5	1.329 (10)	N2–Mn1–N1^i	89.03 (15)
N2–C10	1.325 (7)	N3–Mn1–N1	167.17 (19)
		N1i–Mn1–N1	86.8 (2)
		N5–N4–N3	178.8 (9)

The axial positions are occupied by the N3^i from one azide and N1^i from a phen molecule [N3^i–Mn1–N1^i 167.17(19) °] while the equatorial plane is formed by the coordinating atoms N1, N2 from one phen molecule, N2^i from the second phen molecule and N3 from an azide ion. The bond angles in the equatorial plane deviate noticeably from the ideal value of 90 °, with two larger, 101.1(2) ° for N3–Mn1–N2^i, 95.7(2)° for N3–Mn1–N2 and two smaller angles of 89.03(15) ° for N2^i–Mn1–N1 and 72.16(16)° for N2–Mn1–N1. This deviation in bond angles coupled with the observation that the Mn–$N_{(azide)}$ bonds are slightly shorter than the Mn-$N_{(phen)}$ bonds indicate a highly distorted square-planar arrangement in the equatorial plane. There are two long Mn-$N_{(phen)}$ bonds [Mn1–N1 2.320(4) Å] and two short ones [Mn1–N2 2.268(4) Å]. Each of the phen ligands forms a five-membered chelate ring with Mn. They are almost planar [torsion angle N2–C11–C12–N1 is −0.8(7)°] and are oriented in two different molecular planes (Shen, Zuo et al. 1999, Zhang, Chen et al. 2002, Čechová, Martišková et al. 2014). The N5–N4–N3 bond angle of 178.8 (9)° indicates that the azide anion is almost linear. The C8–H8···N3 H-bonds between the nitrogen atom of an azide ion and

one phenanthroline ligand coupled with π–π stacking interactions between the phen ring systems are observed and consolidate an extensive three-dimensional supramolecular network.

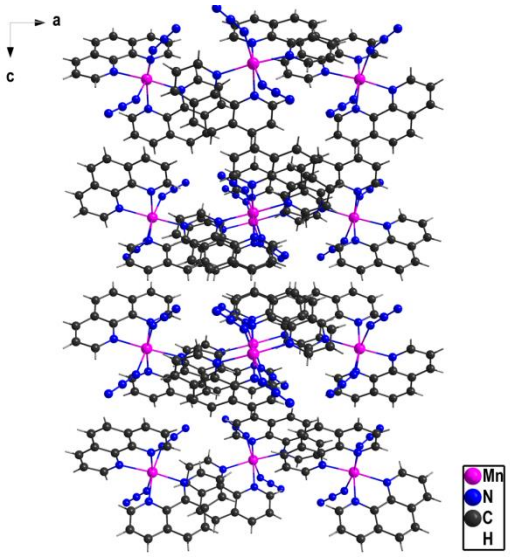

Figure 4. Packing diagram of **2** seen along the crystallographic b-axis showing

Table 7. Hydrogen-bond geometry for **2** (Å, ٩)

D–H···*A*	*D*–H	H ··*A*	*D* ··*A*	*D*–H···*A*
C8–H8···N3	0.931	2.552	3.342(8)	143

3.1.3 Crystal Structure Of $[Mn(Phen)_2(dca)_2]$ (**3**)

Complex **3**, bis(dicyanamido)bis(1,10-phenanthroline)manganese(II), crystallizes in the monoclinic crystal system with space group $P2_1/c$ with four molecules in the unit cell. The ORTEP view of the crystal structure together with the atom numbering scheme used in the corresponding tables are shown in Figure 5 and the crystal packing diagram seen along the crystallographic *b*-axes is shown in Figure 6. Selected bond lengths and angles are presented in Table 8 while the H-bond parameters are given in Table 9.

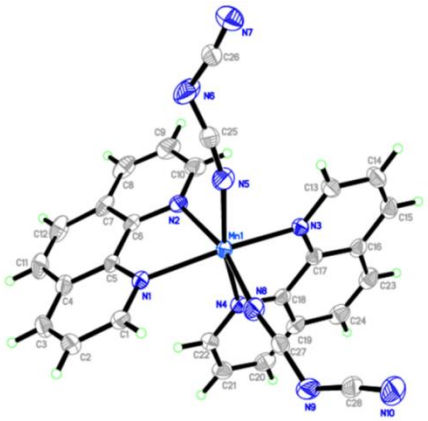

Figure 5. ORTEP view of crystal structure of **3**

The asymmetric unit consists of two 1,10-phenanthroline molecules, two monodentate non-bridging dicyanamido anions, and one Mn(II) ion. A similar structure with slightly different parameters, obtained by a 1:1:1 reaction of $Mn(OAc)_2{\cdot}4H_2O$, Na(dca), and o-phen in an ethanol/water mixture, has been reported (Wang, Luo et al. 2000). Chemically, each manganese atom is six-coordinate; bonded to four N-atoms of two phen molecules [Mn1–N1 2.2593(14) Å, Mn1–N2 2.2897(13) Å, Mn1–N3 2.2549(14) Å, Mn1–N4 2.3214(14) Å] and two terminal N-atoms from

two dicyanamide anions [Mn1–N5 2.1505(16) Å, Mn1–N8 2.1552(15) Å] giving a distorted octahedral geometry around the Mn atom with MnN_6 chromophore. The axial positions are occupied by the N2 atom of one phen ring and the N8 atom of one azide ion [N(8)–Mn(1)–N(2) 165.68(5)°] while the equatorial plane is formed by the coordinating atoms N1, N3, N4 from two different phen molecules and N5 from the another dicyanamide anion. The Mn–N(phen) [2.2549(14)–2.3214(14) Å] and the Mn–N(dca) [2.1505(16)–2.1552(15) Å] are in agreement with values reported in the literature (Wang, Luo et al. 2000, Manson, Brown et al. 2013). The longer Mn-N(phen) bonds [Mn(1) –N(2) 2.2897(13), Mn(1)–N(4) 2.3214(14)] are trans to each other [N(2)–Mn(1)–N(4) 85.19(5)°]. The N(5)–Mn(1)–N(8) bond angle of 98.21(6)2(6)° indicates that the Mn1–N5 and N8–Mn1 bonds are in two different molecular planes almost perpendicular to each other. The dicyanamido anions do not coordinate linearly [N8–C27–N9 173.4(2)°, N5–C25–N6 171.7(2)°] to the metal centre as observed in other Mn-dca complexes (Wang, Luo et al. 2000, Manson, Brown et al. 2013). The two phen ligands which form five-membered chelate rings with Mn are oriented in two different molecular planes.

Table 8. Selected Bond lengths (Å) and angles (°) for **3**

Bond	Length (Å)	Bond	Angle (°)
Mn(1)–N(5)	2.1505(16)	N(5) –Mn(1) –N(8)	98.21(6)
Mn(1) –N(8)	2.1552(15)	N(5) –Mn(1) –N(3)	93.37(6)
Mn(1) –N(3)	2.2549(14)	N(8) –Mn(1) –N(3)	98.65(5)
Mn(1) –N(1)	2.2593(14)	N(5) –Mn(1) –N(1)	104.32(6)
Mn(1) –N(2)	2.2897(13)	N(8) –Mn(1) –N(1)	93.31(5)
Mn(1) –N(4)	2.3214(14)	N(3) –Mn(1) –N(1)	157.00(5)
N(3) –C(13)	1.328(2)	N(5) –Mn(1) –N(2)	89.05(6)
N(3) –C(17)	1.361(2)	N(8) –Mn(1) –N(2)	165.68(5)
N(4) –C(22)	1.331(2)	N(3) –Mn(1) –N(2)	93.19(5)
N(4) –C(18)	1.360(2)	N(1) –Mn(1) –N(2)	72.87(5)
N(5) –C(25)	1.152(2)	N(5) –Mn(1) –N(4)	164.65(6)
N(6) –C(25)	1.286(3)	N(8) –Mn(1) –N(4)	90.62(6)
N(6) –C(26)	1.307(3)	N(3) –Mn(1) –N(4)	72.81(5)
N(7) –C(26)	1.156(2)	N(1) –Mn(1) –N(4)	87.57(5)
N(8) –C(27)	1.155(2)	N(2) –Mn(1) –N(4)	85.19(5)
N(9) –C(27)	1.294(2)	C(1) –N(1) –Mn(1)	125.75(11)
N(9) –C(28)	1.318(2)	C(5) –N(1) –Mn(1)	115.56(11)
N(10) –C(28)	1.151(2)	C(27) –N(8) –Mn(1)	163.57(15)

The packing in the unit cell is based on intermolecular hydrogen bonding and π–π stacking interactions. Cooperation between π–π stacking interactions of phen rings of adjacent molecules and an extensive series of weak $C–H\cdots N_{(dca)}$ hydrogen bonds (Table 9) between neighbouring molecules further stabilize the structure and form an extended three-dimensional network (Manson, Brown et al. 2013).

Table 9. Hydrogen-bond geometry for **3** (Å, º)

D–H···*A*	*D*–H	H ···*A*	*D* ···*A*	*D*–H···*A*
C1–H1···N7^{i}	0.95	2.516	3.372	150
C3–H3···N6^{ii}	0.951	2.567	3.473	159.6
C20–H20···N7^{iii}	0.95	2.708	3.292	120.4
C21–H21···N7^{iv}	0.95	2.567	3.224	126.5
C10–H10···N9^{v}	0.95	2.657	3.439	140
C8–H8···N10^{vi}	0.951	2.406	3.336	165.8
C12–H12···N5^{vii}	0.949	2.662	3.546	155.1

i)1-x,1-y,1-z; ii) 2-x,1-y,1-z; iii) -1+x,1.5-y,-1/2+z; iv) -1+x,1.5-y,-1/2+z; v) x,1.5-y,-1/2+z; vi) -1+x,1.5-y,1/2+z ; vii) -1+x,y,z

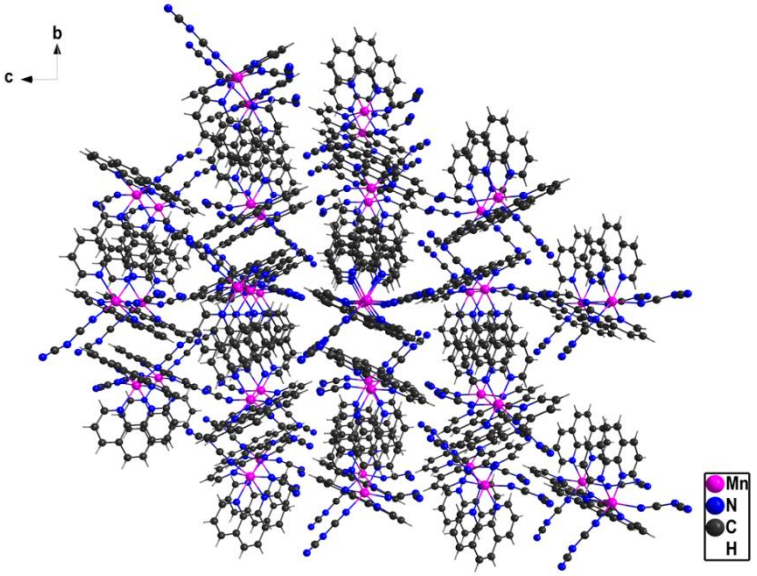

Figure 6. Packing diagram of **3** seen along the crystallographic a-axis

3.2 Magnetic Susceptibility

The magnetic moments of the Mn(II) complexes (Table 10) **1**, **2** and **3** are 5.86, 5.83 and 5.92 B.M., respectively. These values are consistent with high spin (d^5) octahedral geometry.

Table 10. Magnetic moments of the complexes

Compound	Mass susceptibility (χ_g) x10^{-6}	Molar susceptibility (χ_m) x10^{-6}	Susceptibility of ligand (χ_L) x10^{-6}	χ_A	Magnetic moment (μ_{eff}) B.M.
$[Mn(Phen)_2(NO_3)_2]$ (**1**)	23.33	13868.00	-293.80	14162.60	5.86
$[Mn(Phen)_2(N_3)_2]$ (**2**)	27.48	13725.90	-282.02	14007.80	5.83
$[Mn(Phen)_2(dca)_2]$ (**3**)	25.79	14117.30	-310.20	14427.50	5.92

3.3 IR Spectroscopy

The relevant absorption bands in the IR spectra of the ligands and the complexes are summarized in Table 11. In the spectrum of the phen ligand, the absorption bands at 1586 and 1501 cm^{-1} assigned to $\nu_{(C=N)}$ and $\nu_{(C=C)}$ stretching vibrations, respectively, are shifted in the complexes to 1580 cm^{-1} and 1521cm^{-1} for **1**, 1513 cm^{-1} and 1413 cm^{-1} for **2**, 1580 cm^{-1} and 1515 cm^{-1} for **3**, respectively. These shifts indicate the participation of the C=N of phen in bonding (Yanick Gaelle, Ondoh Agwara et al. 2017). The strong absorption band at 2229 cm^{-1} in the spectrum of dca ligand, assigned to the $\nu_{(C\equiv N)}$ is shifted

to 2209 cm^{-1} in **3**. The strong absorption band at 2105 cm^{-1} in the spectrum of the azide ligand, assigned to the asymmetric stretching vibration $\nu_{(N3)}$ of the azide is shifted to 2040 cm^{-1} in **2**, indicating terminal coordination of the azide to the metal ion (Yanick Gaelle, Ondoh Agwara et al. 2017). The new bands at 550, 551 and 557 cm^{-1} in the complexes indicate the presence of Mn-N bonding between the metal and the nitrogen atoms of phen, dca and the azide.

Table 11. Selected IR absorption bands (cm^{-1}) of the ligands and their metal complexes

Compound	$\nu_{(C=N)}$	$\nu_{(C-N)}$	$\nu_{(C=C)}$	$\nu_{(C\equiv N)}$	$\nu_{(N=N=N)}$	$\nu_{(M-N)}$	$\nu_{(N-O)}$	$\nu_{(Mn-O)}$
N_3					2105vs			
dca		1338s		2229s				
Phen	1587s		1501vs					
$[Mn(Phen)_2(dca)_2]$	1580s		1515vs	2209s		557m		
$[Mn(Phen)_2(N_3)_2]$	1513s		1514s		2040vs	551m		
$[Mn(Phen)_2(NO_3)_2]$	1580		1521			550	1305	1750

Br=broad, s=strong, vs=very strong, m=medium, w=weak.

3.4 Thermal Analysis

The thermal decomposition behaviour of compounds **1** and **3** have been investigated by DTA-TG under an inert atmosphere at a heating rate of 10 ℃ min^{-1} from 30 ℃ to 900 ℃. The TG curve of complex **1** (Fig. 7) shows that it is stable up to 300 ℃. The first and major decomposition step is from 300 to 370 ℃ with a mass loss of 48.61% is attributed to the decomposition of one phenanthroline ring and one nitrate into some solid and a mixture of gaseous products. This step corresponds to a sharp and exothermic DTA peak at 370 °C. The second and third stages from 380–720 °C and 730–900 °C are weak mass loss processes considered to be further decomposition of the second nitrate with mass loss of 10.38% (calculated 11.49%). These two stages correspond to two exothermic peaks, one broad and one shallow in the DTA curve with peak temperatures 480 ℃ and 880 ℃, respectively. The residual mass (41%) is probably composed of Mn and nitrogen in a carbon residue.

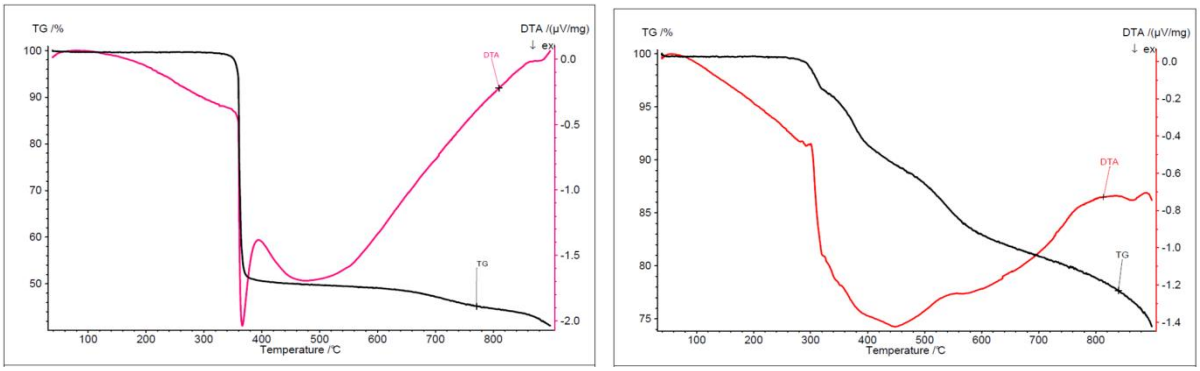

(a) (b)

Figure 7. TG-DTA Curves of (a) **1** and (b)**3**

The TG curve of complex **3** (Figure 7) shows that it stable up to 320 ℃. The first decomposition step is endothermic, as shown on the DTA curve, followed by a series of decomposition steps from 330 to 600 ℃ with a cumulative mass loss of 17.10%. This is attributed to partial decomposition of the solid. This corresponds to a broad exothermic peak in the DTA centred at 450 ℃. The last decomposition step from 600 to 900 ℃ is another weak mass loss step 8.56%, considered to be further decomposition of the product. The residual mass is 74.34% indicating high carbon content.

3.5 Antimicrobial Studies

The starting materials, the complexes, the reference antibiotic (amoxicillin, ciprofloxacin) and antifungal agents (fluconazole, Cloxacillin) were evaluated against some selected microbial pathogens (twenty bacteria and four fungi strains). The susceptibility of the bacteria and fungi strains towards these compounds was judged by measuring the growth

inhibition diameter. The diameter of the zone of inhibition (IZ, mm) was used to compare the antimicrobial activity of the test compound with that of the reference antibiotic and antifungal. Compounds which showed significant activities (IZ > 6 mm) were used for the minimum inhibitory concentration (MIC) test. The MIC values are presented in histograms (Fig. 9 and 10); (MIC>500 μg/mL poor activity; 250<MIC>125 μg/mL moderate activity; 62.5<MIC>31.25 μg/mL good activity; MIC<31.25 μg/mL very good activity). While the simple metal salt $Mn(NO_3)_2$ and the co-ligands N_3^- and dca, were not able to effectively reduce the bacterial and fungal cell proliferation, 1,10-phen exhibited good inhibitory capability which is in agreement with results obtained from other studies (Gandra, Mc Carron et al. 2017, Yanick Gaelle, Ondoh Agwara et al. 2017). Complex 1 possesses very good activity against most of the bacteria species with MIC values 15.625 and 31.25 μg/mL, while complexes 2 and 3 are very active against the fungi species with MIC values in the range 7.8–15.6 μg/mL. However, all of these complexes displayed comparable as well as poor antibacterial activities compared to the standard antibacterials (amoxicillin, ciprofloxacin) but higher antifungal activities as compared to the antifungals (fluconazole, Cloxacillin). These activities are comparable to literature reports (Coyle, Kavanagh et al. 2003, Gandra, Mc Carron et al. 2017). Complex 1 was the most active and it showed very good activity (MIC 15.625 μg/mL) against the bacteria species *Staphylococcus aureus* BAA917, *Salmonella enterica* NR4311, *Enterococcus fecalis* ATCC51219 and *Mycobacterium smegmatis*. The complexes exhibited very good activity against the fungi species *Candida krusei*, *Candida parasilosis* and *Candida albicans*, as compared to the reference antifungal and also showed good antibacterial activity comparable to the reference antibiotic. For example, the $[Mn(Phen)_2(NO_3)_2)]$ complex (**1**) showed greater activity against streptococcus pneumonae compared to the ligands, the metal salt and the reference antibiotic demonstrating that the chelates are much superior antimicrobial agents. The most active compound (**1**) showed very good activity (MIC 15.625 μg/mL) against the bacteria species *Staphylococcus aureus* BAA917, *Salmonella enterica* NR4311, *Enterococcus fecalis* ATCC51219 and *Mycobacterium smegmatis*.

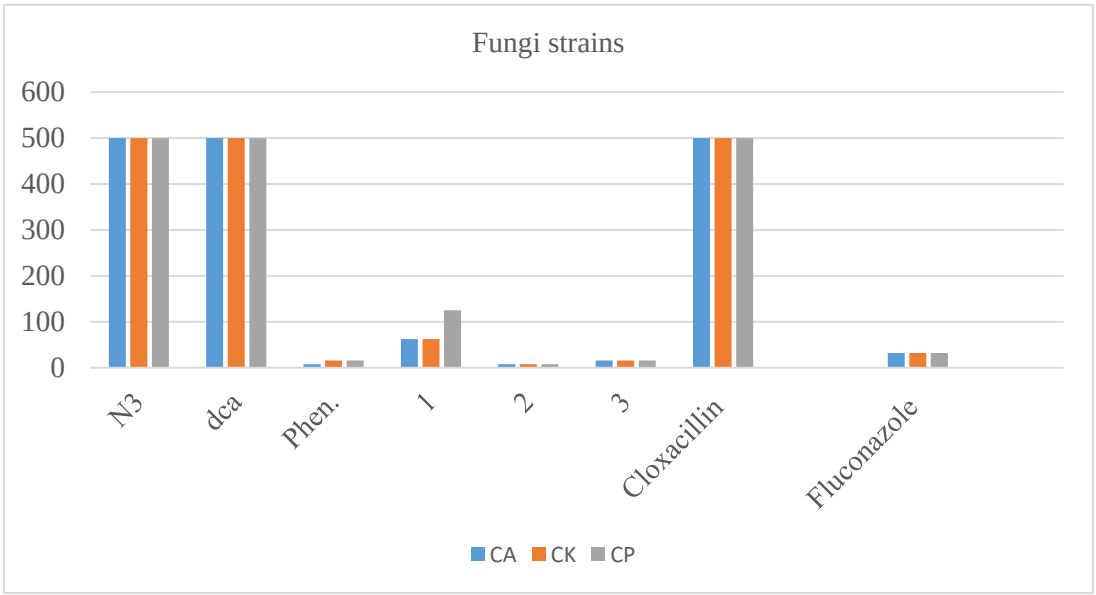

Figure 8. Histogram of MIC against yeast species

Figure 9. Histogram of MIC against bacteria species

The increased activity of the metal complexes can be explained based on the chelation theory and overtones concept.

This indicates that reaction of metal ions with the ligands plays an important role in enhancing its antimicrobial activity. This enhancement of the metal complex activity can also be explained on the basis of chelation theory. Chelation reduces the polarity of the metal atom mainly because of partial sharing of its positive charge with the donor groups and possible π-electron delocalization within the whole chelate ring. Such a chelation also enhances the lipophilic character of the central metal atom, which subsequently favours its permeation through the lipid layers of the cell membrane and the blocking of the metal binding sites on enzymes of microorganism (Chohan, Munawar et al. 2001). The overall positive results of the antimicrobial screening against the twenty-three pathogens suggest that the complexes have a broad spectrum of activity and may represent a good candidate as an antimicrobial agent.

4. Conclusion

Manganese(II) complexes $[Mn(Phen)_2(NO_3)_2]$ (**1**), $[Mn(Phen)_2(N_3)_2)]$ (**2**), and $[Mn(Phen)_2(dca)_2)]$ (**3**) have been synthesized. Distorted octahedral geometries were confirmed through single-crystal X-ray crystallographic techniques. Cooperation between C–H ··O or C–H ··N hydrogen bonds between adjacent phen ligands, and π–π stacking interactions stabilize the structures and assemble them into interesting 3D supramolecular structures. The magnetic moments of the Mn(II) complexes were found to be consistent with high spin (d^5) octahedral geometry. Thermal analyses of the complexes **1** and **3** under inert conditions indicate that they are stable up to 300 ℃. A high residual (> 40%) indicates high carbon content in the residue. The complexes exhibited poor antibacterial activities as compared to standard antibacterials (amoxicillin, ciprofloxacin) but very good activity against the fungi species *Candida krusei*, *Candida parasilosis* and *Candida albicans*, as compared to the reference antifungals (fluconazole, Cloxacillin). This high antifungal activity indicates the potential of the complexes as alternative antifungal agents to fluconazole. However, additional and profound *in vitro* antimicrobial studies mainly in relation to the elucidation of the mechanism of growth of inhibition and toxicity of the complex is on-going.

Competing Interests

The authors declare that there is no conflict of interests regarding the publication of this paper.

Acknowledgments

The authors acknowledge Dr. Kevin Klausmeyer, Department of Chemistry and Biochemistry Baylor University, USA for assistance with one of the crystal structures.

References

Adhikary, C., & Koner, S. (2010). Structural and magnetic studies on copper(II) azido complexes. *Coord. Chem. Rev.*, *254*(23-24), 2933-2958. http://dx.doi.org/10.1016/j.ccr.2010.06.001.

Agwara, M. O., Ndifon, P. T., Ndosiri, N. B., Paboudam, A. G., Yufanyi, D. M., & Mohamadou, A. (2010). Synthesis, Characterisation and Antimicrobial Activities of Cobalt(II), Copper(II) and Zinc(II) Mixed-Ligand Complexes Containing 1,10-Phenanthroline and 2,2'-Bipyridine. *Bull. Chem. Soc. Ethiop.*, *24*(3), 383-389.

Aljahdali, M., & El-Sherif, A. A. (2013). Synthesis, characterization, molecular modeling and biological activity of mixed ligand complexes of Cu(II), Ni(II) and Co(II) based on 1,10-phenanthroline and novel thiosemicarbazone. *Inorg. Chim. Acta, 407*, 58-68. http://dx.doi.org/10.1016/j.ica.2013.06.040.

Allan, J. R., Brown D. H., & Lappin, M. (1970). Transition Metal Halide Complexes of Hexamethylenetetramine. *J. Inorg. Nucl. Chem., 32*, 2287-2292.

Amah, C., Ondoh, A. M., Yufanyi, D. M., & Gaelle, D. S. Y. (2015). Synthesis, Crystal Structure and Antimicrobial Properties of an Anhydrous Copper(II) Complex of Pyridine-2-Carboxylic Acid *Inter. J. Chem., 7*(1), 10-20. http://dx.doi.org/10.5539/ijc.v7n1p10.

Batten, S. R., & Murray, K. S. (2003). Structure and magnetism of coordination polymers containing dicyanamide and tricyanomethanide. *Coord. Chem. Rev., 246*(1-2), 103-130. 10.1016/S0010-8545(03)00119-X.

Bencini, A., & Lippolis, V. (2010). 1,10-Phenanthroline: A versatile building block for the construction of ligands for various purposes. *Coord. Chem. Rev., 254*(17-18), 2096-2180. http://dx.doi.org/10.1016/j.ccr.2010.04.008.

Berghe, D. V., & Vlietinck, A. (1991). Screening methods for antibacterial and antiviral agents from higher plants Methods in plant biochemistry: Volume 6. Assays for bioactivity. K. Hostettmann. London, Academic Press Ltd.: xi + 360 pp.

Beyth, N., Houri-Haddad, Y., Domb, A., Khan, W., & Hazan, R. (2015). Alternative Antimicrobial Approach: Nano-Antimicrobial Materials. *J. Evid. Based Complementary Altern. Med.* 2015: *16*. https://doi.org/10.1155/2015/246012.

Bruker (2004). APEX2, SAINT-Plus and XPREP. Madison, Wisconsin, USA., Bruker AXS Inc.

Čechová, D., Martišková, A., & Moncol, J. (2014). Structure of cis-dichlorobis(1,10-phenanthroline)manganese(II) and cis-dichlorobis(2,2´-bipyridine)manganese(II). *Acta Chim. Slovaca, 7*(1), 15. https://doi.org/10.2478/acs-2014-0003.

Chen, Z. L., Jiang, C. F., Yan, W. H., Liang, F. P., & Batten, S. R. (2009). Three-Dimensional Metal Azide Coordination Polymers with Amino Carboxylate Coligands, Synthesis, Structure, and Magnetic Properties. *Inorg. Chem., 48*, 4674-4684. http://dx.doi.org/10.1021/ic802026n.

Chohan, Z. H., Munawar, A., & Supuran, C. T. (2001). Transition Metal Ion Complexes of Schiff-bases. Synthesis, Characterization and Antibacterial Properties. *Metal-Based Drugs, 8*(3), 137-143. https://dx.doi.org/10.1155/mbd.2001.137.

Colak, A. T., Oztopcu-Vatan, P,. Colak, F., Akduman, D., Kabadere, S., & Uyar, R. (2013). Syntheses, characterization, antimicrobial and cytotoxic activities of pyridine-2,5-dicarboxylate complexes with 1,10-phenanthroline. *J. Trace Elements in Medicine and Biology, 27*(4), 295-301. https://dx.doi.org/10.1016/j.jtemb.2013.04.005.

Coyle, B., Kavanagh, K., McCann, M., Devereux, M., & Geraghty, M. (2003). Mode of anti-fungal activity of 1,10-phenanthroline and its Cu(II), Mn(II) and Ag(I) complexes. *Biometals 16*(2), 321-329. https://dx.doi.org/10.1023/a:1020695923788.

Farrugia, L. (1997). ORTEP-3 for Windows - a version of ORTEP-III with a Graphical User Interface (GUI). *J. Appl. Crystallog., 30*(5 Part 1), 565. https://dx.doi.org 10.1107/S0021889897003117.

Gaëlle, D. S. Y., Yufanyi, D. M., Jagan, R., & Agwara, M. O. (2016). Synthesis, characterisation and antimicrobial properties of cobalt(II) and cobalt(III) complexes derived from 1,10-phenanthroline with nitrate and azide co-ligands. *Cogent Chem., 2*, 1253201. https://dx.doi.org/10.1080/23312009.2016.1253201.

Gandra, R. M., Mc Carron, P., Fernandes, M. F., Ramos, L. S., Mello, T. P., Aor, A. C., … Santos, A. L. S. (2017). Antifungal Potential of Copper(II), Manganese(II) and Silver(I) 1,10-Phenanthroline Chelates Against Multidrug-Resistant Fungal Species Forming the Candida haemulonii Complex: Impact on the Planktonic and Biofilm Lifestyles. *Frontiers in Microbiology, 8*(1257). https://dx.doi.org/10.3389/fmicb.2017.01257.

Hu, L. X., & Zhang, B. S. (2016). Aqua(4-bromobenzoato-kO)bis(1,10-phenanthroline-k^{2}N,N')manganese(II) 4-bromobenzoate dihydrate. *IUCrData, 1*(5), x160833. https://dx.doi.org/10.1107/S2414314616008336.

Janiak, C. (2000). A critical account on π–π stacking in metal complexes with aromatic nitrogen-containing ligands. *J. Chem. Soc., Dalton Trans.*, (21), 3885-3896. https://dx.doi.org/10.1039/B003010O.

Jennifer, S. J., & Muthiah, P. T. (2014). Mixed-ligand complexes of Ca(II), Ba(II), Mn(II) and Pd(II) with 1,10-phenanthroline and 5-chloro thiophene 2-carboxylic acid ligands: Role of hybrid carboxylate-water clusters and ligands of crystallisation in building up of supramolecular architectures. *Inorg. Chim. Acta, 414*, 170-180. https://dx.doi.org/10.1016/j.ica.2014.01.053.

Kani, I., Atlier, Ö., & Güven, K. (2016). Mn(II) complexes with bipyridine, phenanthroline and benzoic acid: Biological and catalase-like activity. *J. Chem. Sci., 128*(4), 523-536. https://dx.doi.org/10.1007/s12039-016-1050-z.

Lazari, G., Stamatatos, T. C., Raptopoulou, C. P., Psycharis, V., Pissas, M., Perlepes, S. P., & Boudalis, A. K. (2009). A metamagnetic 2D copper(II)-azide complex with 1D ferromagnetism and a hysteretic spin-flop transition. *Dalton Trans.*: 3215-3221. https://dx.doi.org/10.1039/b823423j.

Ma, C., Wang, W., Zhu, H., Chen, C., & Liu, Q. (2001). Phenanthroline–manganese inclusion complexes of dicarboxylic acid containing extensive hydrogen-bonding interactions. *Inorg. Chem. Commun. 4*(12), 730-733. https://doi.org/10.1016/S1387-7003(01)00312-4.

Manson, J. L., Brown, C. M., Huang, Q., Schlueter, J. A., Lancaster, T., Blundell, S. J. … Pratt, F. L. (2013). Mn(dca)$_2$(o-phen) {dca=dicyanamide; o-phen=1,10-phenanthroline}: Long-range magnetic order in a low-dimensional Mn-dca polymer. *Polyhedron, 52*, 679-688. https://doi.org/10.1016/j.poly.2012.07.087.

Masárová, P., & Moncol, J. (2016). Crystal structures of [M(N$_3$)$_2$(phen)$_2$] compounds, M = Mn, Co or Cu and phen = 1,10-phenanthroline. *Acta Chim. Slovaca, 9*(2), 152. https://doi.org/10.1515/acs-2016-0026.

McCann, M., Geraghty, M., Devereux, M., O'Shea, D., Mason, J., & O'Sullivan, L. (2000). Insights into the mode of action of the anti-candida activity of 1,10-phenanthroline and its metal chelates. *Metal Based Drugs, 7*(4), 185-193.

Mohamadou, A., van Albada, G. A., Kooijman, H., Wieczorek, B., Spek, A. L., & Reedijk, J. (2003). The binding mode

of the ambidentate ligand dicyanamide to transition metal ions can be tuned by bisimidazoline ligands with H-bonding donor property at the rear side of the ligand. *New J. Chem., 27*(6), 983-988. https://dx.doi.org/10.1039/B212059C

Nagase, K., Yokobayashi, H., & Sone, K. (1976). Color and Structural Changes of Bis(hexamethylenetetramine)cobalt(II) and Nickel(II) Complexes in the Course of Thermal Dehydration in the Solid State. *Bulletin of the Chemical Society of Japan, 49*(6), 1563-1567.

Pook, N. P., Hentrich, P., & Gjikaj, M. (2015). Crystal structure of bis[tris(1,10-phenanthroline k^2 N,N')cobalt(II)] tetranitrate N,N'-(1,4-phenylenedicarbonyl)diglycine solvate octahydrate. *Acta Cryst. E, 71*(8), 910-914. https://dx.doi.org/10.1107/S2056989015013006.

Saphu, W., Chanthee, S., Chainok, K., Harding, D. J., & Pakawatchai, C. (2012). trans-Bis(nitrato-kO)bis(1,10-phenanthroline-k^2N,N')manganese(II). *Acta Cryst. E 68*(8), m1026. https://dx.doi.org/10.1107/S1600536812029364.

Sheldrick, G. M. (1997). S{HELX}97. {P}rograms for crystal structure analysis.

Shen, Z., Zuo, J. L., Chinnakali, K., Fun, H. K., & You, X. Z. (1999). Diazidobis(1,10-phenanthroline-N,N')manganese(II). *Acta Cryst. C, 55*(6), 901-903. https://dx.doi.org/10.1107/S010827019900181X.

Sidjui, L. S., Toghueo, R. M. K., Zeuko`o, E. M., Mbouna, C. D. J., Leddet, V. M., Herbette, G., … Folefoc, G. N. (2016). Antibacterial Activity of the Crude Extracts, Fractions and Compounds from the Stem Barks of *Jacaranda mimosifolia* and *Kigelia africana* (*Bignoniaceae*). *Pharmacologia, 7*(1), 22-31. https://dx.doi.org/10.5567/pharmacologia.2016.22.31

Spellberg, B., Guidos, R., Gilbert, D., Bradley, J., Boucher, H. W., Scheld, W. M., … Edwards, A. The Infectious Diseases Society of (2008). The Epidemic of Antibiotic-Resistant Infections: A Call to Action for the Medical Community from the Infectious Diseases Society of America. *Clinical Infectious Diseases, 46*(2), 155-164. https://dx.doi.org/10.1086/524891

Sun, J., Tong, X., & Xu, H. (2010). Synthesis, structures and properties of Cu and Cd complexes with 1,10-phenanthroline. *Inorg. Chem. Commun. 13*(5), 645-648. https://dx.doi.org/10.1016/j.inoche.2010.03.009.

Tabong, C. D., Yufanyi, D. M., Paboudam, A. G., Nono, K. N., Eni, D. B., & Agwara, M. O. (2016). Synthesis, Crystal Structure, and Antimicrobial Properties of [Diaquabis(hexamethylenetetramine)diisothiocyanato-kN]nickel(II) Complex. *Advances in Chemistry* 2016, Article ID 5049718: *8* pages. https://dx.doi.org/10.1155/2016/5049718.

Wang, Z. M., Luo, J., Sun, B. W., Yan, C. H., Liao, C. S., & Gao, S. (2000). cis-Bis(dicyanamido)bis(1,10-phenanthroline)manganese(II) and cis-bis(dicyanamido)bis(1,10-phenanthroline)zinc(II). *Acta Cryst. C 56*(6), e242-e244. https://dx.doi.org/10.1107/S0108270100006132.

Weinstein, R. A., & Fridkin, S. K. (2003). Routine Cycling of Antimicrobial Agents as an Infection-Control Measure. *Clinical Infectious Diseases, 36*(11), 1438-1444. https://dx.doi.org/10.1086/375082.

WHO (2014). Antimicrobial resistance. Global report on surveillance Geneva, Switzerland.

Wieghardt, K. (1989). The Active Sites in Manganese-Containing Metalloproteins and Inorganic Model Complexes. *Angew. Chem. Int. Ed., 28*(9), 1153-1172. https://dx.doi.org/10.1002/anie.198911531.

Yanick, G. D. S., Ondoh, A. M., Yufanyi, D. M., Nenwa, J., & Jagan, R. (2017). Crystal structure and antimicrobial properties of a copper(II) complex with 1,10-phenanthroline and azide co-ligand. *Inorg. and Nano-Metal Chem., 47*(4), 618-625. https://dx.doi.org/10.1080/15533174.2016.1212220

Zhang, X., Chen, F., Wang, W., Chen, C., & Liu, Q. (2002). Aqua(chloroacetato)bis(1,10-phenanthroline-N,N')manganese(II) perchlorate. *Acta Cryst. E 58*(7), m360-m362. https://dx.doi.org/10.1107/S1600536802010899

APPENDIX III

OTHER PUBLICATIONS

Available online www.jocpr.com

Journal of Chemical and Pharmaceutical Research, 2016, 8(12):144-151

Research Article

ISSN : 0975-7384
CODEN(USA) : JCPRC5

Synthesis, Characterization and Antimicrobial Properties of Some Co (II) Complexes of Hexamethylenetetramine

Che Dieudonne Tabong[1], Divine Mbom Yufanyi[2], Donatus Bekindaka Eni[1] and Moise Ondoh Agwara[1*]

[1]Department of Inorganic Chemistry, Faculty of Science, University of Yaoundé I, Yaoundé, Cameroon
[2]Department of Chemistry, Faculty of Science, The University of Bamenda, Bamenda, Cameroon

---

ABSTRACT

Four Co(II) complexes of hexamethylenetetramine (HMTA), $[Co(HMTA)_2(NO_3)_2(H_2O)_2]$, $[Co(HMTA)(SCN)_2(H_2O)_3]$, $[Co_2(HMTA)(N_3)_3(H_2O)_5]$ and $[Co(HMTA)(DCA)_2(H_2O)]$. H_2O have been synthesized and were characterized by physico-chemical and spectroscopic methods. The results suggest that these complexes are octahedral, stable in air and non-hygroscopic as opposed to the starting metal salt. The ligands, metal salt and the complexes were also evaluated for their antimicrobial activities in vitro against seven pathogens.

Keywords: Cobalt (II); Hexamethylenetetramine; thiocyanate; azide; dicyanamide; Antimicrobial

---

INTRODUCTION

Transition metal complexes of N-donor ligands are of interest due to their applications in biology, pharmacology, magnetism, etc. Among these ligands is hexamethylenetetramine (HMTA), a potential tetradentate ligand or hydrogen bond acceptor suitable in self-assembly systems. HMTA is a commercially available organic molecule which possesses three fused rings in the chair conformation similar to the cage-like structure of adamantine [1]. It is a cheap, eco-friendly and readily available for reactions with many hydrated salts. It forms molecular complexes, with varied coordination patterns ranging from monodentate [2], bridging [3, 4], non-chelating to hydrogen-bonded frameworks [5-7], inducing the formation of one-, two- and three-dimensional framework structures. Biologically, HMTA has found applications as a cosmetic biocide in eye make-up preparation, preservative in lotions and creams and antiseptic agent for the treatment of urinary tract infections [8, 9]. Recently, interest in HMTA has increased due to the enhanced thermodynamic and kinetic stability of its metal complexes, and their application in various activities such as anticancer, antitubercular, antibiotic, antimicrobial and antifungal agent [10, 11].

Cobalt is an essential metal element widely distributed in the biological systems. It is a component of vitamin B_{12} complex that is useful in the prevention of anaemia and the production of erythrocytes. Interest in cobalt complexes has also increased due to their therapeutic and biological applications [12].

Among the inorganic anions serving as co-ligands, thiocyanate SCN^- (an ambidentate ligand) is very important due to its great tendency to combine with a variety of metal ions, forming either thiocyanato (M-SCN) or isothiocyanato (M-NCS) complexes and also bridges metal ions. The nature of these complexes depends on the inter-play between the metal ion, the counter ion and HMTA [13].

The nitrate anion can function as a bidentate, bridging or monodentate ligand or as an ionic species in different complexes. The bonding type is probably a function of the nature and number of other ligands present.[14, 15]

The azide anion, N_3^-, is a versatile ligand which can bind to metal ions in several coordination modes: terminal mode via one nitrogen donor, as a bridge ($\mu_{1,1}$) via one nitrogen donor, and in the $\mu_{1,3}$ way via both of the peripheral nitrogen donor atoms.[16] The azide anion coordinated to transition metals has been intensively studied for diverse applications.[17, 18]

In order to fight against antimicrobial resistance, our research team has recently focused on the synthesis and antimicrobial screening of some transition metal complexes of the ligands hexamethylenetetramine [19], pyridine [20], pyridine-2-carboxylic acid [21], 2-aminopyridine [22] and 1,10-phenanthroline.[23, 24] The upsurge of resistant pathogens impedes the effective prevention and treatment of an ever-increasing variety of infections caused by bacteria, parasites, viruses and fungi [25]. This increasing resistance of microbes to antibacterial and antifungal drugs has necessitated the search for new compounds to target pathogenic microbes [25, 26]. Several efforts have been made to develop antimicrobial agents to fight against these resistant pathogens amongst which are the protection of the efficacy and appropriate use of existing drugs as well as research and development of new antimicrobial agents that are not affected by the currently known, predicted, or unknown mechanisms of resistance [27-29]. The incorporation of metals into antibacterial molecules is expected to enhance the bactericidal or fungicidal properties of these drugs.

In view of the varied applications of cobalt complexes and exploring the good biological properties of cobalt and HMTA as well as the structure-directing properties of SCN^-, NO_3^- and N_3^-, we report herein the synthesis and structure elucidation of cobalt(II) complexes of HMTA, SCN^-, N_3^- and NO_3^-. The effects of the co-ligands on the biological activities of the complexes towards some resistant pathogens, evaluated using in vitro assays, are also presented.

EXPERIMENTAL

Materials

$Co(NO_3)_2{\cdot}6H_2O$, hexamethylenetetramine, ammonium thiocyanate and sodium azide were obtained from Sigma Aldrich. The chemicals were of analytical grade and were used without further purification. Methanol was obtained from Reidel-De Haen (Germany). All solvents used were distilled according to standard methods.

Methods

Generally, the complexes were prepared by the reaction of the metal salt, $Co(NO_3)_2.6H_2O$ with the ligands at room temperature.

Synthesis of $[Co(HMTA)_2(NO_3)_2(H_2O)_2]$

$Co(NO_3)_2{\cdot}6H_2O$ (0.528 g; 1 mmol) in 20 mL methanol was added drop wise into a solution of HMTA (0.28 g; 2 mmol) in 20 mL methanol while stirring. The mixture was then stirred for 4 hours and the pink precipitate formed was filtered, washed with diethylether and dried in vacuum over silica gel. Light pink crystals were obtained from the filtrate, at room temperature, after three weeks.

Synthesis of $[Co(HMTA)(SCN)_2(H_2O)_3]$

$Co(NO_3)_2{\cdot}6H_2O$ (0.291 g; 1 mmol) in 15 mL methanol was added drop wise into a solution of HMTA (0.560 g; 2 mmol) in 15 mL methanol while stirring. The solution was stirred for 1 hour at room temperature. Ammonium thiocyanate (0.156 g; 2 mmol) in 10 ml methanol was added into the solution and the mixture was further stirred for 3 hours. The precipitate formed was filtered, washed with diethylether and dried in vacuum over silica. Light pink crystals were obtained from the filtrate, at room temperature, after two weeks.

Synthesis of $[Co(HMTA)(DCA)_2(H_2O){\cdot}H_2O]$

$Co(NO_3)_2{\cdot}6H_2O$ (0.291 g; 1 mmol) in 15 mL methanol was added drop wise into a solution of HMTA (0.560 g; 2 mmol) in 15 mL methanol while stirring. The solution was stirred for 1 hour at room temperature. Sodium dicyanamide (0.36 g; 2 mmol) in 10 ml methanol was added into the solution and the mixture was further stirred for 3 hours. The precipitate formed was filtered, washed with diethylether and dried in vacuum over silica. Purple crystals were obtained from the filtrate, at room temperature, three weeks.

Synthesis of $[Co_2(HMTA)(N_3)_3(H_2O)_5]$

$Co(NO_3)_2{\cdot}6H_2O$ (0.291 g; 1 mmol) in 15 mL methanol was added into a solution of HMTA (0.560 g; 2 mmol) in 15 mL methanol while stirring and the solution was stirred for 1 hour at room temperature. Sodium azide (0.260 g; 2 mmol) in 10 ml H_2O/methanol (1:5 v/v) was added into the solution. The mixture was further stirred for 3 hours and the precipitate formed was filtered, washed with diethylether and dried in vacuum over silica gel. Light pink crystals were obtained from the filtrate, at room temperature, after two weeks.

Characterization

Microanalyses for carbon, hydrogen and nitrogen in the compounds were carried out on a Flash 2000 Thermo Scientific analyser. The infrared spectra was recorded on a Bruker ALPHA-P spectrophotometer directly on a small sample of the complex in the range of 400 - 4000 cm^{-1}, while the UV-visible spectrum of an aqueous solution of the complex was recorded using a Bruker HACH DR3900 UV-Visible spectrophotometer at room

temperature. Melting point/decomposition temperatures of the complexes were obtained using a STUART Scientific Melting Point SMP1 device with maximum temperature at 360^{o}C. Conductivity of the complexes was measured in distilled water using the HACH HQ14d Instrument at room temperature.

Antimicrobial Tests

The *in vitro* antimicrobial tests were carried out in the Laboratory of Phytobiochemical and Medicinal Plant Study, University of Yaoundé I, Cameroon. Four strains of bacteria (*Salmonella enterica*, *Shigella flexineri*, *Escherichia coli* and *Staphylococcus aureus*) and three strains of fungi (*Candida albicans*, *Candida parapsilosis* and *Candida krusei*) were used for this study. All the species were derived from stock cultures obtained from the Medical Bacteriology Laboratory of Centre Pasteur Yaoundé, Cameroon. Reference antibacterial drug chloramphenicol and reference antifungal drug fluconazole were evaluated for their antibacterial and antifungal activities and their results were compared to those of the free ligands and the complex. The disc diffusion method, using Muller Hinton Agar, from the protocol described by the National Committee for Clinical Laboratory Standard (NCCLS, 2004) was used for preliminary screening.

Mueller-Hinton agar was prepared from a commercially available dehydrated base according to the manufacturer's instructions. Several colonies of each microorganism was collected and suspended in saline (0.9% NaCl). Then, the turbidity of the test suspension was standardized to match that of a 0.5 McFarland standard (corresponds to approximately 1.5 x 10^8 CFU/mL for bacteria or 1 x 10^6 to 5 x 10^6 cells/mL for yeast). Each compound or reference was accurately weighed and dissolved in the appropriate diluents (DMSO at 10%, Methanol at 10% or distilled water) to yield the required concentration (2 mg/mL for compound or 1 mg/mL for reference drug), using sterile glassware. Whatman filter paper No. 1 was used to prepare discs approximately 6 mm in diameter, which were packed up with aluminum paper and sterilized by autoclaving. Then, 25 µL of stock solutions of compound or positive control were delivered to each disc, leading to 50 µg of compound or 25 µg of reference drug.

The dried surface of a Müeller-Hinton agar plate was inoculated by flooding over the entire sterile agar surface with 500 µL of inoculum suspensions. The lid was left ajar for 3 to 5 minutes to allow for any excess surface moisture to be absorbed before applying the drug impregnated discs. Discs containing the compounds or antimicrobial agents were applied within 15 minutes of inoculating the MHA plate. Six discs per petri dish were plated. The plates were inverted and placed in an incubator set to 35°C. After 24 hours (for bacteria) and 48 hours (for yeasts) of incubation, each plate was examined. The disc diameter and the diameter of the zones of complete inhibition (as judged by the unaided eye) were measured. Zones were measured to the nearest whole millimetre, using sliding callipers, which was held on the back of the inverted petri plate. Three replicas were performed for each sample and mean values of the growth inhibition zone (IZ) were calculated. Compounds were considered active when the IZ was greater than 6 mm.

Minimum Inhibitory Concentration

The microbroth dilution method was used to determine the minimum inhibitory concentration (MIC) of the compounds and the reference antibiotic on a given microorganism. A polystyrene tray containing 80 wells is filled with small volumes of serial two-fold dilutions of the complex and reference antibiotics. The inoculum suspension and standardization is done according to McFarland standard. The bacterial inoculum is then inoculated into the wells and incubated at 37°C overnight while the fungi is incubated for 48 hours. The lowest concentration of antibiotic that completely inhibits visual growth of bacteria (no turbidity) is recorded as MIC.

The MBC and MFC were determined by transferring 25 µL aliquots of the clear wells into 100 µL of freshly prepared Muller Hinton Broth medium and incubating at 35 °C for 24 hour. MBC is the lowest concentration of test sample which did not produce turbidity as above, indicating no microbial growth. All tests were performed in triplicates.

RESULTS AND DISCUSSION

Synthesis of the complexes

The reaction of $Co(NO_3)_2.6H_2O$ and HMTA with thiocyanate, nitrate, azide or dicyanamide in methanol yielded four complexes whose physicochemical properties are summarised in Table 1. The complexes which are coloured and air stable were obtained in good yields (>65 %). Complexes 1 and 2 had sharp melting points (148ºC and 174°C, respectively) indicating their purity while the complex 3 decomposes at 210°C. Complexes 1 and 2 underwent colour changes at 85°C to brown and 95°C to purple, respectively. Complex 3 changed color from purple to brown at 224°C but remained stable up to 360°C (maximum limit of device). Complex 4 also changed color from light pink to brown at 195°C and decomposed at 224°C. The molar conductivity values of the complexes in water were in the range 16 to 41 $\Omega cm^{-2}mol^{-1}$ indicating that the complexes are non-electrolytes and are molecular.

Table 1: Physical and Analytical Data of the Complexes

Complexes	Colour	Melting Point/oC	Conductivity (Ωcm-2mol-1)	%yield	Elemental Analyses % Found (% Calc.)			
					%C	%H	%N	%Co
Co(HMTA)2(NO3)2(H2O)2 (1)	Pink	148	37.5	72	28.73	5.82	27.56	11.63
					-28.86	-5.65	-28.05	-11.8
Co(HMTA)(SCN)2(H2O)3 (2)	Pink	174	27.3	65	24.9	5.1	21.73	15.42
					-25.7	-4.85	-22.47	-15.21
[Co2(HMTA)(N3)3(H2O)5] (3)	Purple	210 (decompose)	41.5	81	15.19	4.18	39.83	24.12
					-15.2	-4.68	-38.4	-24.22
[Co(HMTA)(DCA)2(H2O)].H2O (4)	Light pink	>360	16.6	94	32.62	4.21	38.18	15.95
					-32.71	-4.39	-38.14	-16.05

Infrared Spectroscopy

The relevant vibrational frequencies of hexamethylenetetramine and the complexes are presented in Table 2.The broad hypsochromic bands at 3435-3390 cm^{-1} observed in all the complexes has been assigned to the υ_s(O-H) vibration. In the complexes, the signals of υ_s(O-H) are blue shifted to 3500-3700 cm^{-1}, become sharper and can be differentiated due to the effect of oxygen donation to the Co^{2+} which weakens the O-H bonds. The υ_s and υ_{as} vibrations of the methylene groups of HMTA appear between 3003 and 2887 cm^{-1}. These symmetric and asymmetric stretching bands overlap with the ν_s(O-H) in complex 2. In the IR spectra of complexes 2, 3 and 4 very strong, characteristic peaks originating from the azide N=N [24, 30], thiocyanate [31] and dicyanamide C=N bond [32] stretching vibrations were observed at 2107 cm^{-1}, 2130 cm^{-1} and 2207 cm^{-1}, respectively. Also, in complex 2, weak symmetric vibrations were observed at 787 cm^{-1} corresponding to C-S stretching vibrations of thiocyanate.

The coordination of water molecules to the cobalt ion results in the appearance of a vibrational band at 697-702 cm^{-1} and assigned to υ[(M-H_2O)] [20, 33]. A single band for the complex 1, 2 and 3 at 1675 cm^{-1}, 1664 cm^{-1} and 1625 cm^{-1}, respectively indicates that all the water molecules are crystallographically equivalent [34, 35]. The spectrum of complex 4 showed two bands at 1673 and 1606 cm^{-1} assigned to νH_2O. This is an indication that there are two types of crystallographically non-equivalent water molecules (coordinated and non-coordinated water molecules) [35-38].

Table 2: Relevant IR (cm^{-1}) bands of HMTA and the metal complexes

HMTA	1	2	3	4	Assignment
-	3501br	3390vbr	3414br	3435br	ν(OH) (coordinated water)
-				3248	ν(OH) (lattice water)
2955		3002s	3003m	2971s	ν(CH_2)
		2971s	2966w,	2887w	
-		, 2073vs,	-	-	CN (of SCN)
		-	2130vs	-	CN of DCA
-		-	-	2207vs	N=N=N stretching
-	1780		1738w		Co-NO_3
-	1675	1664	1625w	1673	HOH bend (*ν*M-H_2O)
				1606	HOH bend (lattice water)
1457	1475	1465	1458	**1462**	ν(CH_2) scissor (HMTA)
1370	1349	1382	1362	1366	ν(CH_2) wag (HMTA)
			1301		*ν*N-O (nitro)
1236	1240	1252	1238	1240	ν(CH_2) rock (HMTA)
	1227	1201	1224		
1000	1002	1031vs	1014	1027	ν(CN) stretch (HMTA)
812	819	827	802	808	ν(CN) stretch (HMTA)
		787	774	778	
		755			C-S of SCN
6,70,690	682	697	700s	,705s	H_2O
		6,73,655	660	678	N-C-N bend (HMTA)
			624		N=N=N
	504	515	516s	526	M-O stretch
		478,	495w, 458	475w	M-N stretch*

The band at 1236cm^{-1}, assigned to the $\nu(CH_2)$ rocking vibration of the free HMTA ligand is observed at 1238-1252cm^{-1} in all the complexes. This band is observed at 1240 cm^{-1} in complex **4** and split into 1240 and 1227 cm^{-1}; 1252 and 1201 cm^{-1} ; and 1238 and 1224 cm^{-1} in complexes **1**, **2** and **3**, respectively, suggesting that HMTA is coordinated to the cobalt ion [34, 39]. The C-N stretching vibration of HMTA which normally appears at 1000 cm^{-1} in the free ligand are red shifted to 1002-1031 cm^{-1} in all the complexes while the C-N peak at 812 cm^{-1} is blue shifted to 802 and 808 cm^{-1} in **3** and **4** while it is red shifted to 819 and 827 cm^{-1} in **1** and **2**, respectively.

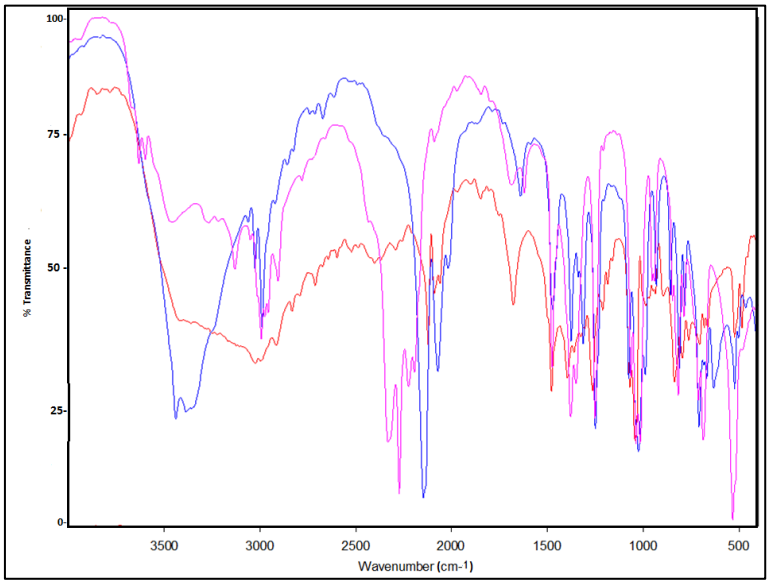

Figure 1: IR Spectra complexes 1 (orange), 2 (red), 3 (blue) and 4 (pink)

UV–Vis Spectroscopy

The electronic spectral data of the complexes in water are presented in Table 3. The electronic absorption spectra reveal two bands each for the complexes (1 – 4). These bands have been assigned to $^4T_{1g}(F) \rightarrow {}^4T_{1g}(P)$ and $^4T_{1g}(F) \rightarrow {}^4A_{2g}$ transitions respectively. Similar bands have been reported in literature suggesting an octahedral geometry around the cobalt(II) ion [38].

Table 3: Electronic Spectral data of the complexes

Complex	ν_{max} (cm^{-1})	Band Assignement
1	20,790	$^4T_{1g}(F) \rightarrow {}^4T_{1g}(P)$
	19,608	$^4T_{1g}(F) \rightarrow {}^4A_{2g}$
2	20,833	$^4T_{1g}(F) \rightarrow {}^4T_{1g}(P)$
	19,646	$^4T_{1g}(F) \rightarrow {}^4A_{2g}$
3	19,231	$^4T_{1g}(F) \rightarrow {}^4T_{1g}(P)$
	19,157	$^4T_{1g}(F) \rightarrow {}^4A_{2g}$
4	21,322	$^4T_{1g}(F) \rightarrow {}^4T_{1g}(P)$
	19,685	$^4T_{1g}(F) \rightarrow {}^4A_{2g}$

Antimicrobial Tests

The metal salt, ligands, metal complexes and the reference antibiotic and reference antifungal drugs were tested for antimicrobial activity in vitro against four bacteria and three fungi strains. The susceptibility of the bacteria and fungi strains towards the compounds was judged by measuring the diameter of the growth inhibition zone. The results are summarized in Table 4 and presented in Figure 2.

Table 4: Inhibition Zone (diameter in mm) of compounds against bacteria and fungi

Compounds	Bacteria				Fungi		
	A_1	A_2	A_3	A_4	B_1	B_2	B_3
NH_4SCN	6±0.0	6±0.0	0	6±0.0	0	6±0.0	0
NaN_3	0	7±0.0	17±1.4	9.5±0.7	0	6±0.0	0
DCA	6	6	6	9	7.5	8	6
HMTA	0	0	0	9±1.4	0	8.5±0.7	30±0.0
$Co(NO_3)_2.6H_2O$	9.5±0.7	0	6±0.0	6.5±0.7	0	6±0.0	0
1	8±0.0	7±0.0	6±0.0	10±0.0	0	6±0.0	0
2	8.5±0.7	9±0.0	7.5±0.7	11.5±0.7	10.5±0.7	7.5±0.7	6.5±0.7
3	10±0.0	12.5±0.7	6±0.0	15.5±0.7	0	6±0.0	0
4	9±1.4	10±1.4	18±0.0	10±0.0	12±1.4	8.5±0.7	11.5±0.7
RA	22±0.0	20±0.0	19±1.4	20±0.0	/	/	/
RB	/	/	/	/	30±0.0	32±0.0	22±0.0

A_1= *Staphylococcus aureus*, A_2 = *Salmonella enterica*, A_3 = *Shigella flexineri*, A_4 = *Escherichia coli*, B_1 = *Candida albicans*, B_2=*Candida parapsilosis*, B_3=*Candida krusei*, RA=Reference Antibacterial (Chloramphenicol), RB = Reference Antifungal (Fluconazole), / = not tested

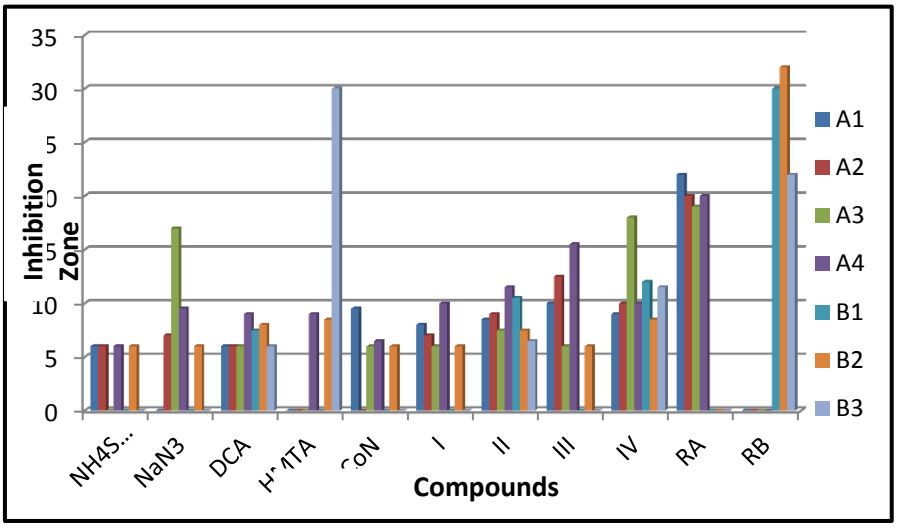

Figure 2: Inhibition zone of ligands, metal salt and complexes against microorganisms

The active compounds **1**, **2**, **3** and **4** were further evaluated in order to confirm their activity by measuring their Minimal Inhibitory Concentrations (MIC). The results are presented in Table 5.

Table 5: Minimal Inhibitory Concentrations (mg/ml) of the complexes 1, 2, 3 and 4

Complexes	Bacteria				Fungi		
	A_1	A_2	A_3	A_4	B_1	B_2	B_3
1	0.62±0.00	1.25±0.00	0.62±0.00	1.25±0.00	0.62±0.00	0.62±0.00	1.25±0.00
2	1.25±0.00	1.25±0.00	1.25±0.00	1.25±0.00	0.62±0.00	0.625±0.00	0.31±0.00
3	0.62±0.00	0.62±0.00	0.62±0.00	1.25±0.00	0.31±0.00	0.31±0.00	0.31±0.00
4	0.62±0.00	0.62±0.00	0.62±0.00	1.25±0.00	0.31±0.00	0.62±0.00	0.62±0.00
RA	0.078±0.00	0.019±0.00	0.008±0.00	0.014±0.007	/	/	/
RB	/	/	/	/	0.016±0.00	0.032±0.00	0.032±0.00

The ligand (HMTA) was found to be active only on one *(Escherichia coli)* of the bacteria strains. Dicyanoamide (DCA) showed mild activity against all the bacteria. The ligands NH_4SCN and NaN_3, each showed low activity against three of the bacteria strains and no activity against *Shigella flexineri and Staphylococcus aureus*,

respectively. All the metal complexes tested, showed some activity against bacteria. This increase in activity on coordination could be explained on the basis of Overton's concept and chelation theory [40-42]. According to Overton's concept of cell permeability, the lipid membranes that surround the cell favors the passage of only lipid-soluble material and lipid-solubility is an important factor that controls antimicrobial activity. On coordination, the polarity of the metal ion is reduced due to overlap of the ligand orbital and partial sharing of the positive charge of the metal ion with the ligand's donor atoms so that, there is electron delocalization within the whole chelate ring. This may increase the lipophilic character of the metal complex, enabling it to permeate the lipid membrane of the bacteria and thus killing them more effectively. Also, factors such as solubility, different dipole moments and cell permeability mechanisms may be influenced by the presence of the different anions and this affects the mechanism of permeation through the lipid layer of the organisms killing more of them effectively [35, 43].

All the test compounds were active against the fungus *Candida parapsilosis*. The fungi *Candida albicans* and *Candida krusei* were inhibited by complexes **1**, **3** and all the ligands except DCA. Complexes **2** and **4** showed good activity against all the fungi strains. This shows an increase in antifungal activity upon introduction of the thiocyanate and dicyanamide ions into the coordination sphere. The most active complexes are **2** and **4**. The tested compounds are arranged in increasing order of activity as follows: **4** > **2** > **3** > **1** > DCA> $Co(NO_3)_2.6H_2O$ > NaN_3 > NH_4SCN.

CONCLUSION

Four mixed ligand Co(II) complexes with HMTA and nitrate, thiocyanate, azide or dicyanamide co-ligands have been reported. The complexes are octahedral. The results of the preliminary antimicrobial screening against four pathogenic bacteria and three fungi species indicates that complexes **2** and **4** are very active and could be further screened in vitro against a wide range of pathogens. The complexes have activities higher than that of the metal salt and ligands towards the microorganisms. The most sensitive strains are the bacteria species *Escherichia coli* and *Shigella flexineri.* Complexes **2** and **4** showed broad range activity against all the bacteria and fungi strains. Both complexes (**2** and **4**) may represent good candidates as antimicrobial agents. However, additional and profound *in vitro* antimicrobial studies mainly in relation to elucidation of the mechanism of growth inhibition and toxicity of the complexes are necessary.

ACKNOWLEDGEMENT

AMO and DMY acknowledge the Government of Cameroon for financial support through the Fonds d'Appuis à la Recherche. The authors thank the Laboratory of Phytobiochemical and Medicinal Plant Study, University of Yaounde I for the antimicrobial tests.

CONFLICT OF INTERESTS

The authors declare that there is no conflict of interests regarding the publication of this paper.

REFERENCES

[1] AM Kirillov. *Coord Chem Rev*, **2011**, 255(15–16), 1603-1622.
[2] MK Ammar; T Jouini and A Driss; *Chem Cryst*, **2000**, 30(4265).
[3] A Ray; J Chakraborty; B Samanta; S Thakurta; C Marschner; MS El Fallah; S Mitra. *Inorg Chim Acta*, **2008,** 361(7), 1850-1860.
[4] Y Chen; Y-L Wang; S-M Ying; S-L Cai. *Acta Crystallogr*, **2007**, E63(11), m2751.
[5] A Trzesowska; R Kruszynski. *Trans Met Chem*, **2007**, 32(625 - 633).
[6] X-L Li; Z-S Lu; D-Z Niu. *Acta Crystallogr*, **2007,** E63(11), m2640.
[7] D Pritesh; C Deepak; AS Prakash; R Guru; MS Hegde. *J Cryst Growth*, **2004,** 275(e2043), 1-2.
[8] MO Agwara; DM Yufanyi; JN Foba-Tendo; MA Atamba; DT Ndinteh. *J Chem Pharm Res*, **2011,** 3(3), 196-204.
[9] L S Miall; Mackenzie. *A Dictionary of Chemistry, Longmans*, **1956**.
[10] MO Agwara; PT Ndifon; MK Ndikontar. *Bull. Chem Soc Ethiopia*, **2004,** 18(2), 143-148.
[11] KS Prasad; LS Kumar; HD Revanasiddappa; B Vijay; B Jayalakshmi. *Aston j*, **2011** CSJ-12
[12] A Mishra; NK Kaushik; AK Verma; R Gupta. *Eur J Med Chem* **2008**, 43(10), 2189 - 2196.
[13] MO Agwara; PT Ndifon; MK Ndikontar. *Bull. Chem. Soc. Ethiopia*, **2004,** 18(2), 143-148.
[14] IV Morozov; VN Serezhkin; SI Troyanov. *Russ Chem B*+, **2009,** 58(12), 2407-2417.

[15] GRA Wyllie; OQ Munro; CE Schulz; WR Scheidt. *Polyhedron*, **2007,** 26(16), 4664-4672.
[16] MAS Goher; FA Mautner. *Polyhedron* **1995**, 14(11), 1439-1446.
[17] G Lazari; TC Stamatatos; CP Raptopoulou; V Psycharis; M Pissas; SP Perlepes; AK Boudalis. *Dalton Trans*, **2009,** 3215-3221.
[18] Z-L Chen; C-F Jiang; W-H Yan; F-P Liang; SR Batten. *Inorg Chem*, **2009**, 48, 4674-4684.
[19] CD Tabong; DM Yufanyi; AG Paboudam; KN Nono; DB Eni; MO Agwara. *Adv Chem*, **2016,** Volume 2016.
[20] FT Chimaine; DM Yufanyi; ACB Yuoh; DB Eni; MO Agwara. *Cogent Chem*, **2016,** 2, 1253905.
[21] C Amah; AM Ondoh; DM Yufanyi; DSY Gaelle. *Int J Chem*, **2015,** 7(1), 10-20.
[22] ACB Yuoh; MO Agwara; DM Yufanyi; MA Conde; R Jagan; KO Eyon. *Int J Inorg Chem*, **2015**, Article ID 106838, 8 pages.
[23] DYG Sado; MO Agwara; MD Yufanyi; J Nenwa; R Jagan. *Inorg Nano-Met Chem*, **2017**, 1-8.
[24] DSY Gaëlle; DM Yufanyi; R Jagan; MO Agwara. *Cogent Chem*, **2016,** 2, 1253201.
[25] WHO, Geneva, Switzerland, **2014**.
[26] J Tanwar, S Das, Z Fatima and S Hameed, Interdisciplinary Perspectives on Infectious Diseases, **2014,** 2014, Article ID 541340.
[27] B Spellberg; R Guidos; D Gilbert; J Bradley; HW Boucher; WM Scheld; JG Bartlett; J Edwards; the Infectious Diseases Society of *Clin Infect Dis*, **2008**, 46(2), 155-164.
[28] N Beyth; Y Houri-Haddad; A Domb; W Khan; R Hazan. Evidence Based Complementary and Alternative Medicine. **2015**, 2015, Article ID 246012.
[29] V Kandi; S Kandi. *Epidemio Health*, **2015,** 37, Article ID, e2015020
[30] SS Massoud; FA Mautner; M Abu-Youssef; NM Shuaib. *Polyhedron*, **1999,** 18(1), 2287-2291.
[31] E Czubacka, R Kruszynski and T Sieranski, Struct Chem, **2012**, 23(2), 451-459.
[32] S Triki, F Thetiot, J-R Galan-Mascaros, JS Pala and KR Dunbar, *RSC Adv*, **2001**, 25, 954 - 958.
[33] E Czubacka; R Kruszynski; T Sieranski. *J Struct Chem*, **2012**, 23(2), 451–459.
[34] PT Ndifon; MO Agwara; AG Paboudam; DM Yufanyi; J Ngoune; A Galindo; E Alvarez; A Mohamadou. *Transition Met Chem*, **2009**, 34, 745-750.
[35] MO Agwara; MD Yufanyi; JN Foba-Tendo; MA Atamba; DT Ndinteh, *J Chem Pharm Res*, **2011**, 3(3), 196-204.
[36] TG Balicheva; IV Pologikh; DI Kovachev; AJ Statelova. *Russ. J Inorg Chem*, **1975,** 20, 87 - 90.
[37] TG Balicheva; IV Pologikh, *Russ J Inorg Chem*, **1975,** 20(12), 1769-1773.
[38] MO Agwara; JN Foba-Tendo; A Colette; DM Yufanyi; NB Ndosiri. *Res J Pharm, Biol Chem Sci*, **2012,** 3(3), 95.
[39] CD Tabong; AM Ondoh; DM Yufanyi; J Foba. *J Mater Sci Res*, **2015**, 4(4), 70-81.
[40] ZH Chohan; KM Khan; CT Supuran; *Appl Organomet Chem*, **2004,** 18(7), 305-310.
[41] R Shakru; NJP Subhashini; SK Kumar; Shivaraj. *J Chem Pharm Res* **2010**, 2(1), 38-46.
[42] PT Ndifon; MO Agwara; NJ Ngu; DM Yufanyi; PG Awawou; LD Nyamen. *Res J Chem Env*, **2010,** 14(2), 50-54.
[43] ZH Chohan; H Pervez; A Rauf; CT Supuran. *Met Based Drugs*, **2002**, 8(5), 263–267.

cogent chemistry

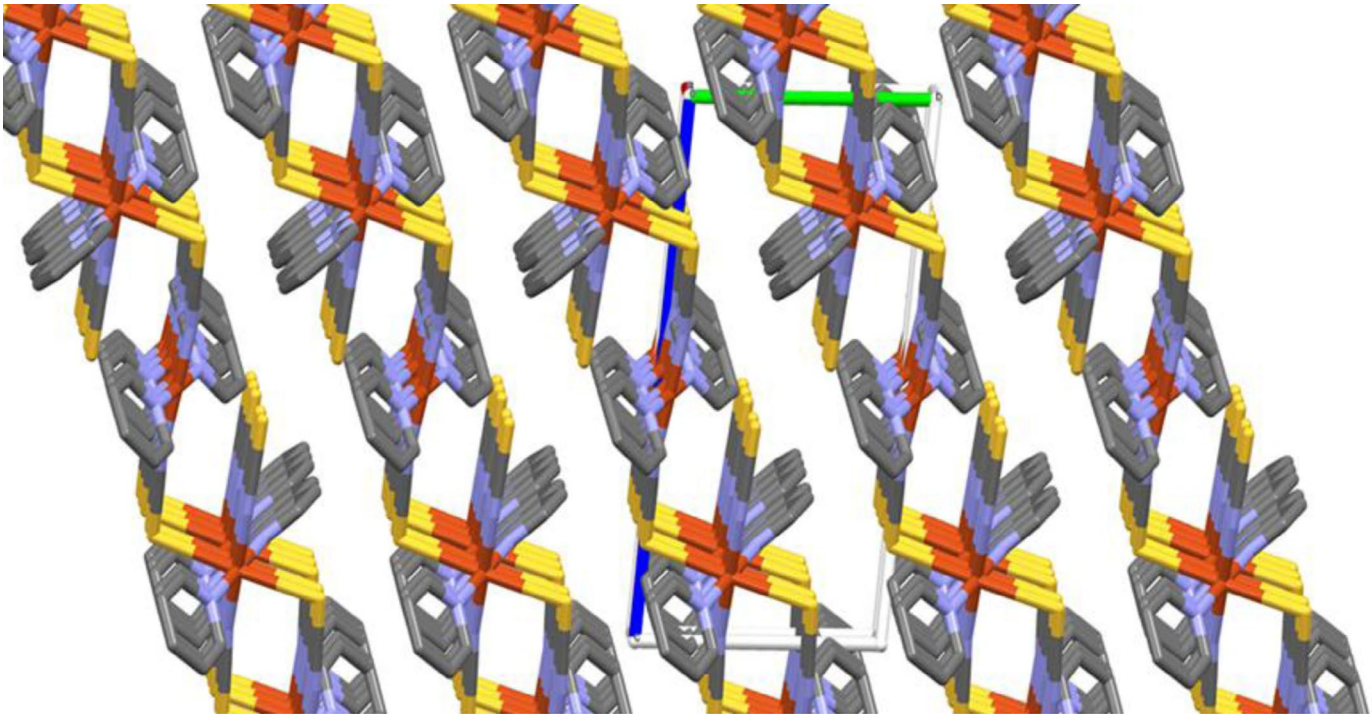

INORGANIC CHEMISTRY | RESEARCH ARTICLE

Synthesis, crystal structure, photoluminescent and antimicrobial properties of a thiocyanato-bridged copper(II) coordination polymer

Feudjio Tsague Chimaine, Divine Mbom Yufanyi, Amah Colette Benedicta Yuoh, Donatus Bekindaka Eni and Moise Ondoh Agwara

Cogent Chemistry (2016), 2: 1253905

cogent oa

cogent chemistry

INORGANIC CHEMISTRY | RESEARCH ARTICLE

Synthesis, crystal structure, photoluminescent and antimicrobial properties of a thiocyanato-bridged copper(II) coordination polymer

Feudjio Tsague Chimaine[1], Divine Mbom Yufanyi[2], Amah Colette Benedicta Yuoh[1], Donatus Bekindaka Eni[1] and Moise Ondoh Agwara[1]*

Received: 22 September 2016
Accepted: 18 October 2016
First Published: 31 October 2016

*Corresponding author: Moise Ondoh Agwara, Department of Inorganic Chemistry, University of Yaounde I, P.O. Box 812 Yaounde, Yaounde, Cameroon
E-mail: agwara29@yahoo.com

Reviewing editor:
J. Derek Woollins, University of St. Andrews, UK

Additional information is available at the end of the article

Abstract: A Cu(II) 1D polymer with mixed ligands (SCN^- and pyridine) has been synthesized and characterized by elemental analyses, IR, UV–visible and TG-DTA analytical techniques. The crystal structure was determined by single-crystal X-ray diffraction analyses. The complex crystallizes in the triclinic crystal system with space group $P\bar{1}$ with one formula unit. Each Cu(II) atom is six coordinate with two N atoms of two pyridine molecules, two N atoms and two S-atoms from bridging SCN anions giving a distorted octahedral geometry with a CuS_2N_4 chromophore. The spectroscopic, photoluminescent and the antimicrobial activities of the synthesized complex were investigated.

Subjects: Applied & Industrial Chemistry; Inorganic Chemistry; Materials Chemistry

Keywords: crystal structure; copper(II); photoluminescence; antimicrobial properties; thiocyanate

1. Introduction

Research interest in coordination polymers has increased recently not only as a result of their fascinating topologies and intriguing frameworks but also due to their potential applications in gas storage, separation, biosensing, luminescence, magnetism, conductivity, nanoparticles, antimicrobial

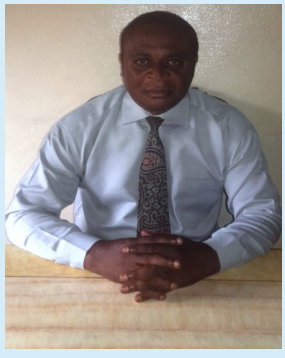

Moise Ondoh Agwara

ABOUT THE AUTHOR

Moise Ondoh Agwara is Associate Professor of Chemistry at the Department of Inorganic Chemistry, University of Yaounde I in Cameroon. He obtained a PhD in chemistry from the University of Ibadan, Nigeria in 1986. Research activities within his research group are focused on the development of the chemistry of transition metal complexes with heterocyclic N-, O- and N,O-donor ligands and some co-ligands. Such interest derives from the fascinating structural chemistry of the complexes obtained, their interesting physico-chemical properties and their diverse applications such as antimicrobials, in photoluminescence and as precursors for the development of nanostructured functional materials.

PUBLIC INTEREST STATEMENT

Interest in coordination polymers has increased because of their fascinating structures and potential applications in gas storage, separation, biosensing, luminescence, magnetism, conductivity, nanoparticles, antimicrobial activity and catalysis. Self-assembly of these coordination polymers through a mixed ligand strategy has progressively become an effective approach, which is expected to generate frameworks with more diverse structures and properties. The focus of this paper is the synthesis and determination of the structure and properties (thermal and photoluminescent) of a Cu(II)-pyridine thiocyanate coordination polymer. The complex exhibited photoluminescent properties in the solid state at room temperature because of charge transfer from ligand to the metal. The results of the preliminary antimicrobial screening against four pathogenic bacteria and four fungi species indicate that the complex is most active against *Salmonella typhi*.

activity and catalysis (Batten, Harris, Murray, & Smith, 2002; Eddaoudi et al., 2001; Etaiw & El-bendary, 2013; Henninger, Jeremias, Kummer, & Janiak, 2012; Janiak, 2003; Rowsell & Yaghi, 2004; Zaworotko, 2001). The topology and dimensionality of these frameworks is dependent on the rational choice of the metal ion and the ligands. Weak intermolecular interactions such as hydrogen bonding and π–π stacking interactions may also play an important role on the overall arrangement and influence the properties (Baca et al., 2008; Batten et al., 2002; Prins, Reinhoudt, & Timmerman, 2001; Whitesides & Boncheva, 2002). Furthermore, synthesis conditions (synthetic methods, reaction temperature, metal/ligand ratio, pH value and the types of solvents) can also greatly influence the crystal structure and its dimensionality (Etaiw & El-bendary, 2013).

The design and synthesis of one-dimensional coordination polymers is important since they can be used as examples for developing theoretical models of the exchange interaction in extended lattices (Demir, Yilmaz, Sariboga, Buyukgungor, & Mrozinski, 2010). Choice of organic ligands and metal ions is of great importance in the construction of these polymeric structures. Transition metals show rich diversity of oxidation states, coordination numbers and geometries, and their complexes and solid-state compounds possess an array of interesting redox, magnetic, optical, electrical and catalytic properties (Chattopadhyay et al., 2012; Chattopadhyay, Drew, Diaz, & Ghosh, 2007; Demir et al., 2010; Hong, 2008; Hu, Li, Wang, Du, & Guo, 2009).

Among several ligands employed, SCN^- is a highly versatile ambidentate ligand with two different donor atoms, which can coordinate through terminal modes or bridging modes: end-to-end (μ-1,3-NCS) and end-on (μ-1,1-NCS, μ-1,1-SCN) fashions via the nitrogen and sulphur atoms to generate coordination networks as well as interlink the one- or two-dimensional molecules into frameworks via non-covalent interactions (Li, Liang, & Tian, 2011; Shen & Feng, 2002). The rational design and construction of thiocyanato-brigded coordination polymers has been explored due to their fascinating topologies and remarkable properties (Bai, Shang, Dang, Sun, & Gao, 2009; Banerjee, Drew, & Ghosh, 2003; Chattopadhyay et al., 2007, 2012; Das et al., 2012; Hong, 2008; Li et al., 2011; Shi et al., 2005; You & Zhu, 2005; Yue et al., 2008). The thiocyanate group plays a key role in stabilizing a variety of transition metal centres and determining the structure of polymeric transition-metal complexes (Das et al., 2012). Recently, a large number of thiocyanato-bridged coordination polymers with intriguing topologies and fascinating properties have been reported (Bai et al., 2009; Banerjee et al., 2003; Chattopadhyay et al., 2007, 2012; Das et al., 2012; Li et al., 2011; Neumann, Jess, & Näther, 2014; Shen & Feng, 2002; Shi et al., 2005; You & Zhu, 2005; Yue et al., 2008). Among these are the thiocyanato-bridged copper(II) coordination polymers with N-donor auxiliary ligands (Das et al., 2012; Hong, 2008; Shen & Feng, 2002; Shi et al., 2005).

However, controlled synthesis of coordination polymers with preferred structures is still a challenge. Self-assembly of these coordination polymers through a mixed ligand strategy has progressively become an effective approach, which is expected to generate frameworks with more diverse structural motifs (Du, Li, Liu, & Fang, 2013; Shirdel, Marandi, Jalilzadeh, Huber, & Pfitzner, 2015; Yang & Sun, 2013). Auxiliary ligands such as N-donor heterocyclic ligands play a significant role in many biological systems, being a component of several vitamins and drugs (Dhaveethu & Ramachandramoothy, 2013). Nitrogen-containing heterocycles have been found to possess diverse pharmacological activities (Forood, Flatt, Chassaing, & Katritzky, 2002). Among this group of heterocycles are pyridine and its derivatives. Taking advantage of the coordination ability and properties of copper, pyridine and SCN, herein we report the synthesis, crystal structure and the luminescent properties of a thiocyanate-bridged copper(II) coordination polymer with pyridine. In addition, the *in vitro* antimicrobial activity of the complex against selected micro-organisms is reported.

2. Experimental

All chemicals and solvents were obtained from commercial sources and were used as received.

2.1. Synthesis of the complex

A 40 mL dry methanolic solution of $CuCl_2{\cdot}2H_2O$ (5.1144 g; 30 mmol) was poured into a three-neck round bottom flask under nitrogen atmosphere. To this solution was added drop wise, while stirring, a dry methanolic solution of a mixture of NH_4SCN (4.5672 g; 60 mmol) and pyridine (9.617 mL; 120 mmol). Upon addition of the mixed ligand solution into the dark green solution in the round bottom flask, a light green precipitate was formed. The mixture was refluxed for 3 h under nitrogen atmosphere at 30°C. The light green precipitate was filtered, washed with dry methanol, air dried and weighed. The powder was recrystallized by the diffusion method. It was dissolved in DMSO in a small vial and placed in a bigger vial containing DMF (in which it is insoluble). Shiny blue crystals, in good yield (92%), were afforded within 48 h.

2.2. Characterization techniques

The melting point was recorded using a Stuart SMP10 system. Conductivity measurement was carried out in distilled water using a HANNA multimeter H19811-5; pH/°C/EC/TDS meter at room temperature. Elemental analysis (C, H, N, S, Cu) was carried out on a Perkin-Elmer automated model 2400 series II CHNS/M analyser. The infrared spectrum was recorded using a Thermo Scientific Nicolet iS5 instrument directly on a small sample of the complex in the range of 400–4,000 cm^{-1}. The UV–vis spectrum of a DMSO solution of the complex was recorded using a Varian, Cary 50 UV–vis spectrophotometer at room temperature. Photoluminescence studies were carried out using a Perkin-Elmer, LS55 Luminescence Spectrometer, while thermal studies were carried out using the TGA/DSC 1 (STAR System) instrument. The TGA analyses were conducted between 30 and 600°C under nitrogen atmosphere at a flow rate of 10 mL min^{-1} and a temperature ramp of 10°C min^{-1}.

2.3. Single-crystal X-ray structure determination

Intensity data for the compound were collected using a Bruker AXS Kappa APEX II single crystal CCD diffractometer, equipped with graphite-monochromated CuKα radiation (λ = 1.5418 Å) at room temperature. The selected crystal for the diffraction experiment had a dimension of 0.21 × 0.12 × 0.06 mm^3. The structure was solved by direct methods and refined by full-matrix least squares (Sheldrick, 1997) on F^2. The non-hydrogen atoms were refined anisotropically. H atoms were included in calculated positions with C–H lengths of 0.95(CH), 0.99(CH_2) and 0.98(CH_3) Å; U_{iso}(H) values were fixed at 1.2U_{eq}(C) except for CH_3 where it was 1.5U_{eq}(C). They were assigned isotopic thermal parameters and allowed to ride on their parent carbon atoms. All calculations were carried out using the SHELXTL package (Bruker, 2001).

2.4. Antimicrobial tests

The antimicrobial tests were carried out in the laboratory of Phytobiochemical and Medicinal Plant Study, University of Yaounde I. The tests were done on eight pathogenic micro-organisms, 4 yeasts, *Candida albicans ATCC P37039, C. albicans 194B, Candida glabrata 44B* and *Cryptococcus neoformans* and 4 bacterial strains, Gram-positive *Staphylococcus aureus CIP 7625 and Gram-negatives, Pseudomonas aeruginosa CIP 76110, Salmonella typhi* and *Escherichia coli ATCC25922* obtained from Centre Pasteur, Yaounde, Cameroon. Reference antibacterial drug chloramphenicol and antifungal drug nystatin were evaluated for their antibacterial and antifungal activities and their results were compared with those of the free ligands and the complex. The disc diffusion method, using Muller Hinton Agar, from the protocol described by the National Committee for Clinical Laboratory Standard was used for preliminary screening. Mueller-Hinton agar was prepared from a commercially available dehydrated base according to the manufacturer's instructions. Several colonies of each micro-organism were collected and suspended in saline (0.9% NaCl). Then, the turbidity of the test suspension was standardized to match that of a 0.5 McFarland standard (corresponds to approximately 1.5 × 10^8 CFU/mL for bacteria or 1 × 10^6 to 5 × 10^6 cells/mL for yeast). Each compound or reference was accurately weighed and dissolved in the appropriate diluents (DMSO at 10%, methanol at 10%, or distilled water) to yield the required concentration (2 mg mL^{-1} for compound or 1 mg mL for reference drug), using sterile glassware.

Whatman filter paper number 1 was used to prepare discs approximately 6 mm in diameter, which were packed up with aluminium paper and sterilized by autoclaving. Then, 25 µL of stock solutions of compound or positive control was delivered to each disc, leading to 50 µg of compound or 25 µg of reference drug. The dried surface of a Muller-Hinton agar plate was inoculated by flooding over the entire sterile agar surface with 500 µL of inoculum suspensions. The lid was left ajar for 3 to 5 min to allow for any excess surface moisture to be absorbed before applying the drug-impregnated discs. Discs containing the compounds or antimicrobial agents were applied within 15 min of inoculating the MHA plate. Six discs per Petri dish were plated. The plates were inverted and placed in an incubator set to 35°C. After 18 h (for bacteria) and 24 h (for yeasts) of incubation, each plate was examined. The diameters of the zones of complete inhibition (as judged by the unaided eye) were measured, including the diameter of the disc. Zones were measured to the nearest whole millimetre, using sliding callipers, which were held on the back of the inverted Petri plate. All experiments were carried out in duplicate. The compound was considered active against a microbe if the inhibition zone was 6 mm and above.

3. Results and discussion

3.1. Synthesis of the complex

The title complex was green in colour and air stable, with a sharp melting point (186°C) indicating its purity. The molar conductivity value of 60 Ωcm^{-2} mol^{-1} for the complex in water indicates that it is a nonelectrolyte. The complex was obtained in good yield (92%). The physicochemical properties of the title complex are summarized in Table 1.

3.2. X-ray crystal structure

The ORTEP representation of the asymmetric unit of $[Cu(py)_2(SCN)_2]_n$ is shown in Figure 1, the unit cell structure in Figure 2, while the 1-D polymeric chain structure together with the atomic numbering

Table 1. Physical data of the complexes

Complex	Nature	Colour	Yield (%)	Melting point (°C)	Molar conductivity ($\Omega^{-1}cm^2$ mol^{-1})	Elemental analyses: %found (%calc.)			
						%C	%H	%N	%Cu
$[Cu(py)_2(SCN)_2]_n$	Crystals	Green	92	186	60	40.88	3.36	16.27	19.18
						(42.65)	(2.98)	(16.58)	(18.81)

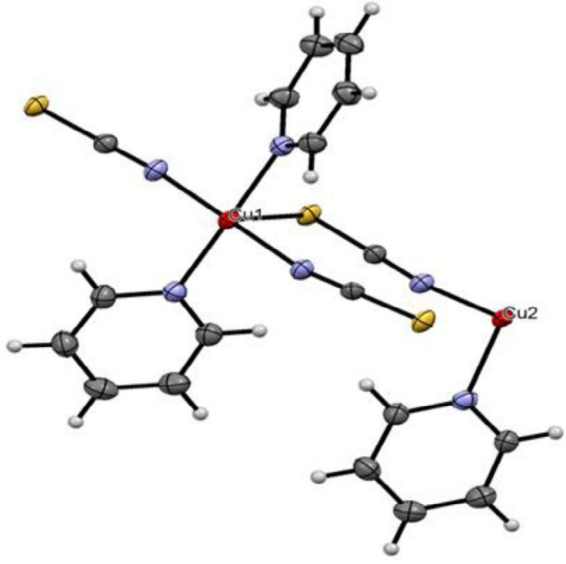

Figure 1. Asymmetric unit of the complex.

Figure 2. Unit cell diagram of the complex.

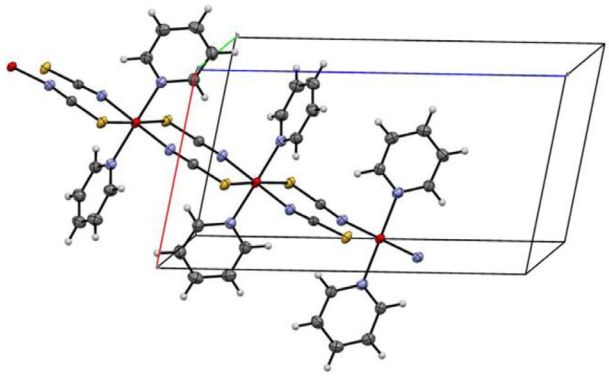

Figure 3. 1D polymeric structure of the complex with atom numbering scheme.

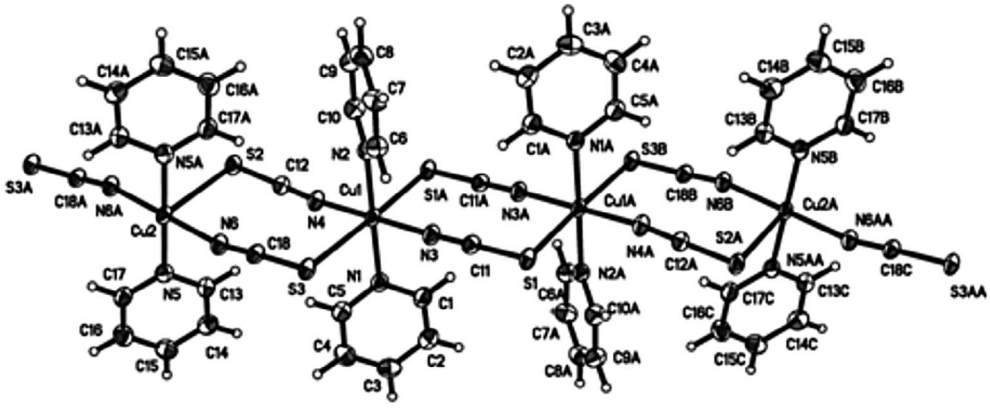

Figure 4. Packing diagram of complex showing 1-D chains parallel to the bc plane.

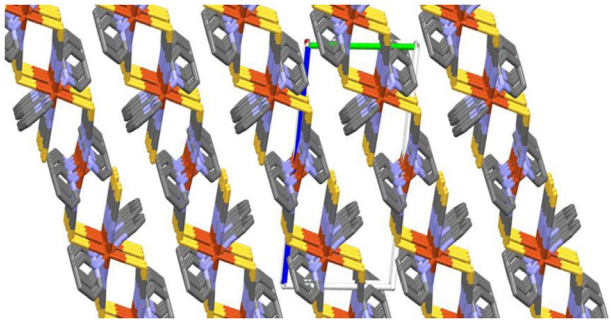

scheme of the complex is shown in Figure 3. The crystal packing diagram of $[Cu(py)_2(SCN)_2]_n$ is shown in Figure 4. The crystal data and structure refinement are presented in Table 2, while the selected bond lengths and bond angles are shown in Table 3.

Table 2. Crystal data and structure refinement for $[Cu(Py)_2(SCN)_2]_n$

Crystal data	
Chemical formula	$C_{36}H_{30}Cu_3N_{12}S_6$
M_r	1,013.70
Crystal system, space group	Triclinic, $P\bar{1}$
Temperature (K)	100 (2)
a, *b*, *c* (Å)	8.5381 (6), 8.6690 (8), 15.5456 (9)
α, β, γ (°)	93.367 (6), 96.385 (5), 114.746 (8)
V (Å^3)	1,031.40 (13)
Z	1
Radiation type	Cu *K*α
μ (mm^{-1})	5.00
Crystal size (mm)	0.21 × 0.12 × 0.06
Crystal colour	Block blue
Data collection	
Diffractometer	Bruker *APEX*-II CCD diffractometer
Absorption correction	Multi-scan
T_{min}, T_{max}	0.781, 1.000
No. of measured, independent and observed [$I > 2\sigma(I)$] reflections	7,998, 3,899, 2,981
R_{int}	0.038
$(\sin \theta/\lambda)_{max}$ (Å^{-1})	0.626
Refinement	
$R[F^2 > 2\sigma(F^2)]$, $wR(F^2)$, *S*	0.048, 0.154, 1.07
No. of reflections	3,899
No. of parameters	259
No. of restraints	0
H-atom treatment	H-atom parameters constrained
$\Delta\rho_{max}$, $\Delta\rho_{min}$ (e Å^{-3})	1.07, −0.98

Notes: Computer programs: *CrysAlis PRO*, Agilent Technologies, Version 1.171.36.20 (release 27-06-2012 CrysAlis171 .NET).

The title compound is a one-dimensional thiocyanato-bridged polymeric structure. The complex crystallizes in the triclinic crystal system with space group $P\bar{1}$ and its asymmetric unit (Figure 1) consists of two crystallographically independent copper(II) atoms, of which one (Cu1) is located on a general position whereas the second (Cu2) is located on a crystallographic inversion centre. The structure is polymorphic to $[Cu(Py)_2(SCN)_2]_n$ (Chen, Bai, & Qu, 2005) and iso-structural with $[Ni(NCS)_2(pyridine)_2]_n$ (Neumann et al., 2014) found in the literature. There is one molecule in the triclinic unit cell as opposed to three in the previous report (Chen et al., 2005).

The crystal structure shows that Cu(II) is coordinated by four thiocyanate anions (μ-1,3) and two pyridine ligands adopting a slightly distorted octahedral coordination environment (CuS_2N_4). The Cu-N(pyridine) axial bonds are of length (Cu(1)-N(1) 2.045(3) Å, Cu(1)-N(2) 2.051(3) Å, Cu(2)-N(6)#1 1.943(3) Å, Cu(2)-N(5)#1 2.038(3) Å), while the equatorial Cu-N(thiocyanate) bonds (Cu(1)-N(3) 1.944(3) Å, Cu(1)-N(4) 1.951(3) Å). These bond lengths are similar to those found in the literature (Chen et al., 2005; Wohlert, Wriedt, Jess, & Nather, 2011). The Cu-S bonds (Cu1-S3 2.984(1) Å, Cu1-S1 2.923(1) Å, Cu2-S2 3.009 Å) are also close to reported values (Chen et al., 2005). Adjacent Cu centres are bridged by two SCN^- ions resulting in a 1D polymeric chain structure extending along the crystallographic c-axis (Figure 4). The Cu1-Cu1 and Cu2-Cu2 distances within the chains are 8.669 Å while that of Cu1-Cu2 is 5.616 Å. In the equatorial plane, the SCN^- ion is almost linear as evidenced by the bond angles N(3)-C(11)-S(1) 179.0(3)° and N(4)-C(12)-S(2) 179.4(4)°. The pyridine molecules are

Table 3. Selected bond lengths (Å) and angles (°) for $[Cu(Py)_2(SCN)_2]_n$

Cu(1)-N(3)	1.944(3)	N(3)-Cu(1)-N(4)	179.74(11)
Cu(1)-N(4)	1.951(3)	N(3)-Cu(1)-N(1)	88.72(12)
Cu(1)-N(1)	2.045(3)	N(4)-Cu(1)-N(1)	91.16(12)
Cu(1)-N(2)	2.051(3)	N(3)-Cu(1)-N(2)	89.66(12)
N(1)-C(5)	1.327(5)	N(4)-Cu(1)-N(2)	90.45(11)
N(1)-C(1)	1.347(4)	N(1)-Cu(1)-N(2)	178.06(11)
N(2)-C(10)	1.337(5)	N(3)-C(11)-S(1)	179.0(3)
N(2)-C(6)	1.344(4)	N(4)-C(12)-S(2)	179.4(4)
N(3)-C(11)	1.164(5)	N(6)-Cu(2)-N(6)#1	179.999(1)
N(4)-C(12)	1.164(5)	N(6)-Cu(2)-N(5)#1	89.64(11)
Cu(2)-N(6)	1.943(3)	N(6)#1-Cu(2)-N(5)#1	90.36(11)
Cu(2)-N(6)#1	1.943(3)	N(6)-Cu(2)-N(5)	90.36(11)
Cu(2)-N(5)#1	2.038(3)	N(6)#1-Cu(2)-N(5)	89.64(11)
Cu(2)-N(5)	2.038(3)	N(5)#1-Cu(2)-N(5)	180.0
N(5)-C(17)	1.337(4)	C(17)-N(5)-C(13)	118.3(3)
N(5)-C(13)	1.346(4)	C(17)-N(5)-Cu(2)	121.7(2)
N(6)-C(18)	1.167(5)		

almost linearly arranged on the axial plane as confirmed by the bond angle N(1)-Cu(1)-N(2) (178.06°). These results are similar to those reported in literature (Małecki, Machura, Świtlicka, Gron, & Bałanda, 2011). The SCN^- and pyridine ligands are in different planes at right angles to each other as evidenced by the bond angles N(3)-Cu(1)-N(2) 89.66(12) and N(6)-Cu(2)-N(5) (90.36°). Selected crystal data of a polymorph of the complex are compared with crystal data of the title complex in Table 3. The title complex differs structurally from that in the literature (Chen et al., 2005) in terms of molecular weight, unit cell parameters and the number of atoms in a unit cell. The methods of syntheses of these complexes also differ.

Adjacent 1-D chains are further connected to form a 2-D supramolecular layer parallel to the bc plane by alternating S1...S3, S2...S2 (3.567(1) Å) and S3...S1 (3.541(1) Å) interactions as shown in Figure 5. This is similar to literature reports (Lu, Liu, Zhang, Wang, & Niu, 2010). The two-dimensional layers are further connected by off-set π–π stacking of pyridine rings, C–H...S and C–H...C interactions (Table 4) to form a three-dimensional supramolecular structure as shown in Figure 6 (Gerlach et al., 2015; Laachir, Bentiss, Guesmi, Saadi, & El Ammari, 2016; Trivedi, Pandey, & Rath, 2009). These

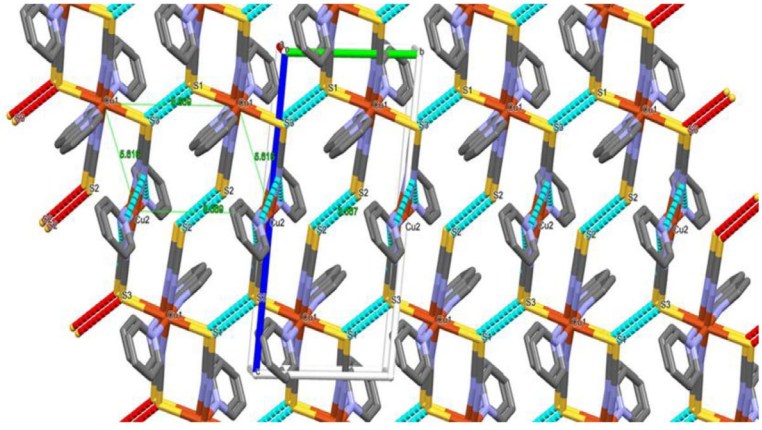

Figure 5. Part of the crystal structure showing the formation, through S...S contacts, of the two dimensional supramolecular sheet extending in the bc plane.

Table 4. Comparative crystal data of the complexes

Parameter	$[Cu_3(py)_6(SCN)_6]_n$ [this work]	$[Cu(py)_2(SCN)_2]_n$ [33]
Empirical formula	$C_{36}H_{30}Cu_3N_{12}S_6$	$C_{12}H_{10}CuN_4S_2$
Formula weight	1,013.70	337.90
Colour	Block blue	Block blue
Crystal system	Triclinic	Triclinic
Space group	$P\bar{1}$	$P\bar{1}$
Unit cell dimensions		
a	8.5381(6) Å	8.528(2) Å
b	8.6690(8) Å	9.128(1) Å
c	15.5456(9) Å	15.371(1) Å
α	93.367(6)°	91.737(1)°
β	96.385(5)°	97.043(1)°
γ	114.746(8)°	115.639(1)°
Unit cell volume, *V*	1,031.40(13) $Å^3$	1,065.9(3) $Å^3$
Calc. density	1.632 mg m^{-3}	1.579 mg m^{-3}
Z	1	3

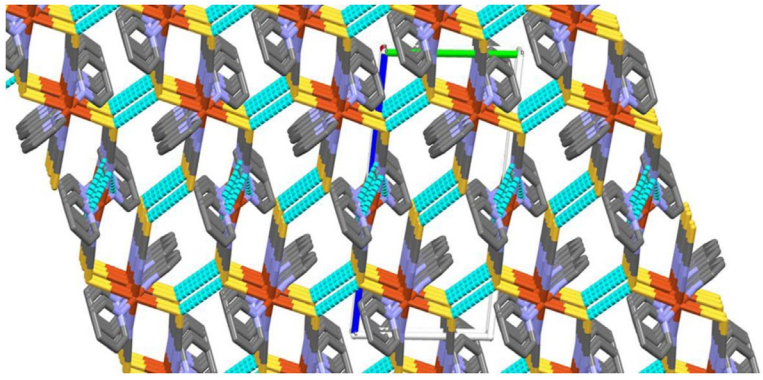

Figure 6. View of the 3D supramolecular layers of the complex down the *a*-axis via π–π and C–H...S interactions.

interactions, though weak compared to the metal–nitrogen and metal–sulphur coordination bonds, are crucial in the self-assembly of the 3D supramolecular structure.

3.3. IR spectroscopy

In the spectrum of the pyridine ligand as well as that of the complex, the absorption bands at 1,442 cm^{-1} are assigned to the aryl C–H stretching vibrations. The $\nu_{C=N}$ stretching modes of the pyridine ring shifted from 1,595 to 1,604 cm^{-1} in the spectrum of the complex, indicating its participation in bonding. The $\nu_{C\equiv N}$ asymmetric stretching vibrations of the thiocyanate have shifted from 2,063 to 2,087 cm^{-1} in the spectrum of the complex, indicating it has taken part in bonding (Kabesova & Gazo, 1980). The ν_{SC} vibration frequency of the isothiocyanato ligand appears at 746 cm^{-1} on the SCN^- spectrum and shifts to 753 cm^{-1} on the spectrum of the complex, indicating NCS-M coordination in the complex (Kabesova & Gazo, 1980). These bands indicate the coordination of SCN^- in a bridging mode (Shen & Feng, 2002), which is confirmed by the crystal structure of the complex. The strong, well-resolved and sharp absorption bands found in the region of 1,495–1,000 cm^{-1} in the spectrum of the complex are assigned to the coordinated pyridine ring (Das et al., 2012). The ν_{Cu-NPy} stretching mode is present at about 549 cm^{-1}.

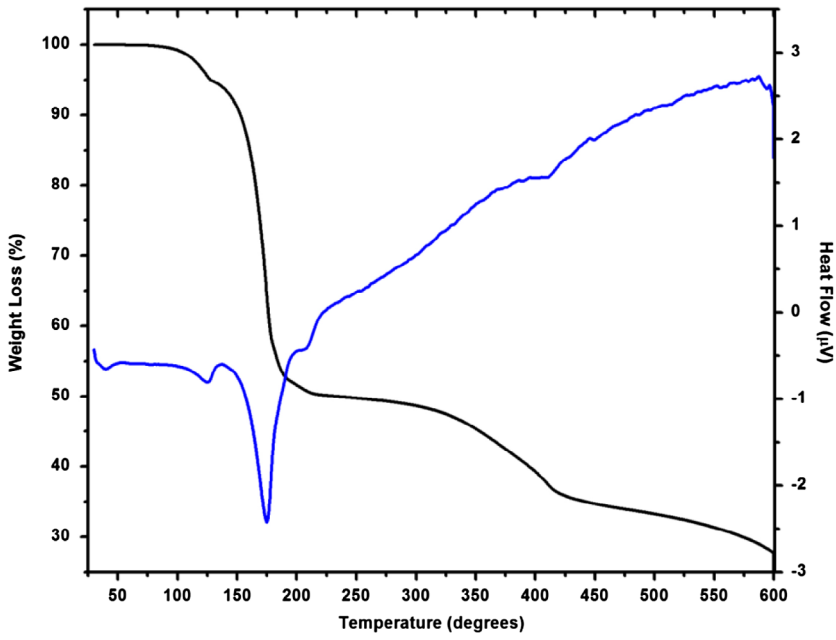

Figure 7. TG/DTA plots of the complex.

3.4. UV–Vis spectroscopy

The electronic absorption spectrum of the complex shows a single broad band centred at 15,625 cm^{-1} (640 nm). This d-d transition band in the Cu(II) ion has been assigned to $^2E_g \rightarrow {}^2T_{2g}$ transition (Kurdziel, Głowiak, Materazzi, & Jezierska, 2003; Rapheal, Manoj, & Kurup, 2007; Reddy, Nethaji, & Chakravarty, 2002). The observed band is consistent with an octahedral geometry for Cu(II) complexes as confirmed by the single X-ray crystal structure. This value is smaller than that of $Cu(en)_2(SCN)_2$ (19,047 cm^{-1}; 525 nm) and $Cu(en)_2[Cd(SCN)_3]_2$ (18,248 cm^{-1}; 548 nm) (Shen & Feng, 2002) with analogous CuN_4S_2 chromophores. This shift in band position indicates some distortion from the perfect octahedral symmetry of Cu(II) (Bai et al., 2008).

3.5. Thermal analysis

In order to establish the thermal stability of the title complex, TG/DTA analyses were carried out in the temperature range of 30–600°C. The thermal decomposition thermogram (Figure 7) shows that the complex decomposes in several steps resulting in different phases of $[Cu_3(Py)_6(SCN)_6]_n$ as temperature was increased. The first weight loss of 5.62% from 80 to 120°C is probably due to the loss of adsorbed water molecules from the atmosphere. The second degradation step in the range of 130–220°C with mass loss of 43.92% is attributed to the loss of six pyridine molecules (calculated 46.76%). The sharp exothermic DTA peak at 170°C indicates that this is the major decomposition temperature. The third degradation step in the range of 260–460°C with weight loss of 14.92% is due to the loss of three SCN^- anions (calculated 17.16%). In the last decomposition step from 510 to 590°C with mass loss of 8.48% is attributed to the loss of one SCN^- and CN^- (calculated 8.29%). A stable mass is reached at 600°C. The residual mass 27.96% (calculated 28.56%) is probably due to CuS. The measured mass loss for each stage is in good agreement with the calculated values.

3.6. Photoluminescence studies

The fluorescence emission spectra of the ligand and the complex are shown in Figure 8. The results show that the ligand pyridine and the complex exhibit only one emission peak each at 23,923 cm^{-1} (418 nm) and 24,509 cm^{-1} (408 nm), respectively, when excited at 33,333 cm^{-1} (300 nm). For the ligand, the peak at 23,923 cm^{-1} is attributed to $n \rightarrow \pi^*$ transition. The red shift of 10 nm in the spectrum of the complex indicates charge transfer from ligand to the metal (PyN→Cu) (Etaiw & Abdou, 2016; Rapheal et al., 2007).

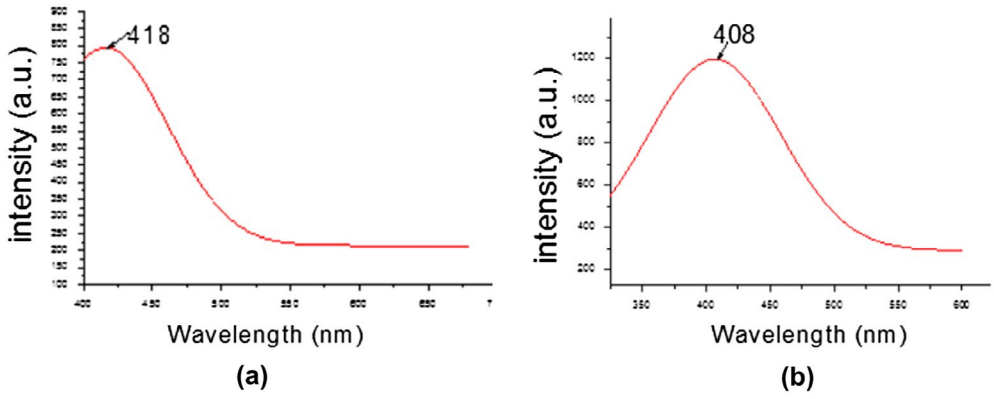

Figure 8. Photoluminescent emission spectra of (a) pyridine and (b) CuPySCN complex.

Table 5. Diameters of inhibition zones of compounds against microorganisms

Compounds	A	B	C	D	E	F	G	H
$CuCl_2.2H_2O$	0.0	7.0	6.0	7.0	6.0	9.0	10.0	9.0
SCN^-	6.0	8.0	6.0	11.5	9.0	6.0	6.0	6.0
Pyridine	6.0	7.5	3.0	3.0	6.5	6.0	6.0	6.0
$[Cu_3(py)_6(SCN)_6]_n$	6.0	9.0	9.0	7.5	6.0	10.5	10.5	9.0
Chloramphenicol	7.5	14.5	6.0	10.5	12.0	11.5	10.0	14.0
Nystatin	6.0	7.0	6.0	9.5	6.0	6.0	6.0	10.5

Notes: A = *C. albicans ATCC P37039;* B = *C. albicans 194B*; C = *C. glabrata 44B*; D = *C. neoformans*; E = *E. coli*; F = *P. aeruginosa*; G = *S. typhi*; H = *S. aureus*.

3.7. Antimicrobial studies

The effects of the starting materials, the resulting complex, the reference antibiotic (chloramphenicol) and antifungal (nystatin) were evaluated against some selected microbial pathogens (four bacteria and four fungi strains). The susceptibility of the bacteria and fungi strains towards these compounds was judged by measuring the size of the growth inhibition diameter. The diameter of the zone of inhibition (mm) was used to compare the antimicrobial activity of the test compound with that of the reference antibiotic and antifungal. Results of the preliminary screening are presented in Table 5.

The results indicate that SCN^- exhibits a high activity against the pathogens, especially the fungi species. The metal complex shows higher activity compared to that of the free ligand as well as SCN. It was found to be active against all the pathogens with high inhibition zones. The complex is most active against the fungi *C. albicans 194B, C. glabrata 44B* and the bacteria species *P. aeruginosa* and *S. typhi*. The complex is also more active than the reference drug nystatin towards the fungi species. The most sensitive bacteria species was *S. typhi*. This indicates that reaction of metal ions with the ligand plays an important role in enhancing its antimicrobial activity. This increase in activity could be due to the reduction of the polarity of the metal ion by partial sharing of the positive charge with the ligand's donor atoms so that there is electron delocalization within the metal complex. This may increase the hydrophobic and lipophilic character of the metal complex, enabling it to permeate the lipid layer of the organism killing them more effectively (Tabong et al., 2016; Yuoh et al., 2015).

4. Conclusion

A Cu(II) complex with SCN^- and pyridine $[Cu_3(py)_6(SCN)_6]_n$ has been synthesized and characterized. The structure is polymorphic to $[Cu(Py)_2(SCN)_2]_n$ (Chen et al., 2005) and iso-structural with $[Ni(NCS)_2(pyridine)_2]_n$ (Neumann et al., 2014). The crystal structure consists of two crystallographically independent copper(II) atoms, of which one (Cu1) is located on a general position whereas the second (Cu2) is located on a crystallographic inversion centre. Each Cu (II) atom adopts a slightly

distorted octahedral coordination environment (CuS_2N_4) in which it is covalently bonded to two pyridine N-atoms in the axial position, two S-atoms of SCN^- and two N-atoms of SCN^- in the equatorial position. Adjacent Cu centres are bridged by two SCN^- (μ-1,3) ions resulting in a 1D polymeric chain structure. Adjacent 1-D chains are further connected to form a 2-D supramolecular layer parallel to the bc plane by alternating S1...S3, S2...S2 (3.567(1) Å) and S3...S1 (3.541(1) Å), interactions. The two-dimensional layers are further connected by off-set π–π stacking of pyridine rings, C–H...S and C–H...C interactions to form a three-dimensional supramolecular structure. The complex exhibited photoluminescent properties in the solid state at room temperature because of charge transfer from ligand to the metal. The results of the preliminary antimicrobial screening against four pathogenic bacteria and four fungi species indicate that the complex is most active against *S. typhi*.

Supporting Information
CCDC 1055785 contains the supplementary crystallographic data for the complex. The data can be obtained free of charge from The Cambridge Crystallographic Data Centre via www.ccdc.cam.ac.uk/data_request/cif. (or from the Cambridge crystallographic Data Center, 12 Union Road, Cambridge CB21EZ, UK; Fax:+44 1223/336 033; E-mail: deposit@ccdc.cam.ac.uk).

Funding
The authors received no direct funding for this research.

Author details
Feudjio Tsague Chimaine[1]
E-mail: f.chimie@yahoo.fr
Divine Mbom Yufanyi[2]
E-mail: dyufanyi@yahoo.com
ORCID ID: http://orcid.org/0000-0001-8889-611X
Amah Colette Benedicta Yuoh[1]
E-mail: colette_amah@yahoo.fr
Donatus Bekindaka Eni[1]
E-mail: donatus_eni@yahoo.com
Moise Ondoh Agwara[1]
E-mail: agwara29@yahoo.com
ORCID ID: http://orcid.org/0000-0001-9112-7637
[1] Department of Inorganic Chemistry, University of Yaounde I, P.O. Box 812 Yaounde, Yaounde, Cameroon.
[2] Department of Chemistry, The University of Bamenda, P.O. Box 39 Bambili, Bamenda, Cameroon.

Citation information
Cite this article as: Synthesis, crystal structure, photoluminescent and antimicrobial properties of a thiocyanato-bridged copper(II) coordination polymer, Feudjio Tsague Chimaine, Divine Mbom Yufanyi, Amah Colette Benedicta Yuoh, Donatus Bekindaka Eni & Moise Ondoh Agwara, *Cogent Chemistry* (2016), 2: 1253905.

Cover image
Source: Author.

References
Baca, S. G., Malaestean, I. L., Keene, T. D., Adams, H., Ward, M. D., Hauser, J., ... Decurtins, S. (2008). One-dimensional manganese coordination polymers composed of polynuclear cluster blocks and polypyridyl linkers: Structures and properties. *Inorganic Chemistry, 47*, 11108–11119. doi:10.1021/ic8014145

Bai, Y., Shang, W.-L., Dang, D.-B., Gao, H., Niu, X.-F., & Guan, Y.-F. (2008). Synthesis, crystal structure and luminescent properties of a thiocyanato bridged two-dimensional heteronuclear polymeric complex of cadmium(II) and copper(II). *Inorganic Chemistry Communications, 11*, 1470–1473. doi:10.1016/j.inoche.2008.10.016

Bai, Y., Shang, W.-L., Dang, D.-B., Sun, J.-D., & Gao, H. (2009). Synthesis, crystal structure and luminescent properties of one coordination polymer of cadmium(II) with mixed thiocyanate and hexamethylenetetramine ligands. *Spectrochimica Acta Part A: Molecular and Biomolecular Spectroscopy, 72*, 407–411. doi:10.1016/j.saa.2008.10.033

Banerjee, S., Drew, M. G. B., & Ghosh, A. (2003). Construction of coordination polymers of cadmium(II) with mixed hexamethylenetetramine and terephthalate or thiocyanate ligands. *Polyhedron, 22*, 2933–2941. doi:10.1016/S0277-5387(03)00404-2

Batten, S. R., Harris, A. R., Murray, K. S., & Smith, J. P. (2002). Crystal engineering with mercuric chloride. *Crystal Growth & Design, 2*, 87–89. doi:10.1021/cg0155696

Bruker. (2001). *SMART (Version 5.625), SADABS (Version 2.03a) and SHELXTL (Version 6.12)*. Madison, Wisconsin, USA.: Bruker AXS Inc.

Chattopadhyay, S., Bhar, K., Choubey, S., Khan, S., Mitra, P., & Ghosh, B. K. (2012). A new luminous end-to-end thiocyanato bridged heptacoordinated coordination polymer of lead(II) containing a tetradentate Schiff base. *Inorganic Chemistry Communications, 16*, 21–24. doi:10.1016/j.inoche.2011.11.019

Chattopadhyay, S., Drew, M. G. B., Diaz, C., & Ghosh, A. (2007). The first metamagnetic thiocyanato-bridged one-dimensional nickel(ii) complex. *Dalton Transactions, 24*, 2492–2494. doi:http://dx.doi.org/10.1039/B702814H http://dx.doi.org/10.1039/b702814h

Chen, G., Bai, Z.-P., & Qu, S.-J. (2005). catena -Poly[[dipyridylcopper(II)]-di-μ-thiocyanato]. *Acta Crystallographica Section E Structure Reports Online, 61*, m2718–m2719. doi:10.1107/S1600536805036998

Das, K., Datta, A., Sinha, C., Huang, J.-H., Garribba, E., Hsiao, C.-S., & Hsu, C.-L. (2012). End-to-end thiocyanato-bridged helical chain polymer and dichlorido-bridged copper(II) complexes with a hydrazone ligand: Synthesis, characterisation by electron paramagnetic resonance and variable-temperature magnetic studies, and inhibitory effects on H. *ChemistryOpen, 1*, 80–89. doi:10.1002/open.201100011.

Demir, S., Yilmaz, V. T., Sariboga, B., Buyukgungor, O., & Mrozinski, J. (2010). Metal(II) nicotinamide complexes containing succinato, succinate and succinic acid: Synthesis, crystal structures, magnetic, thermal, antimicrobial and fluorescent properties. *Journal of Inorganic and Organometallic Polymers and Materials, 20*, 220–228. doi:10.1007/s10904-010-9340-2

Dhaveethu, K., Ramachandramoothy, T., & Thirunavukkarasu, k. (2013). Microwave-assisted synthesis of mixed ligand complexes of Zn(II), Cd(II) and Hg(II) derived from 4-aminopyridine and nitrite ion: Spectral, thermal and bilogical investigations. *Journal of the Korean Chemical Society, 57*, 341–351. doi:10.5012/jkcs.2013.57.3.341

Du, M., Li, C. P., Liu, C. S., & Fang, S. M. (2013). Design and construction of coordination polymers with mixed-ligand synthetic strategy. *Coordination Chemistry Reviews, 257*, 1282–1305. http://dx.doi.org/10.1016/j.ccr.2012.10.002

Eddaoudi, M., Moler, D. B., Li, H., Chen, B., Reineke, T. M., O'Keeffe, M., & Yaghi, O. M. (2001). Modular chemistry: Secondary building units as a basis for the design of highly porous and robust metal–organic carboxylate frameworks. *Accounts of Chemical Research, 34*, 319–330. doi:10.1021/ar000034b

Etaiw, S. E.-D. H., & El-bendary, M. M. (2013). The Influence of copper-copper interaction on the structure and applications of a metal-organic framework based on cyanide and 3-chloropyridine. *Journal of Inorganic and Organometallic Polymers and Materials, 23*, 510–518. doi:10.1007/s10904-012-9808-3

Etaiw, S. E. H., & Abdou, S. N. (2016). Double stranded helical organo-lead 3D-supramolecular coordination polymer containing copper cyanide and phenanthroline ligand as antimicrobial agent. *Journal of Inorganic and Organometallic Polymers and Materials, 26*, 117–126. doi:10.1007/s10904-015-0301-7

Forood, B., Flatt, B. T., Chassaing, C., & Katritzky, A. K. (2002). 2-aminopyridine derivatives and combinatorial libraries thereof. *United States Patent US 6458789 B1, Lion Bioscience AG*.

Gerlach, D. L., Nieto, I., Herbst-Gervasoni, C. J., Ferrence, G. M., Zeller, M., & Papish, E. T. (2015). Crystal structures of bis- and hexakis[(6,6′-dihydroxybipyridine)copper(II)] nitrate coordination complexes. *Acta Crystallographica Section E Crystallographic Communications, 71*, 1447–1453. doi:10.1107/S205698901502037X

Henninger, S. K., Jeremias, F., Kummer, H., & Janiak, C. (2012). MOFs for use in adsorption heat pump processes. *European Journal of Inorganic Chemistry, 2012*, 2625–2634. doi:10.1002/ejic.201101056.

Hong, Z. (2008). Synthesis, crystal structures, and antimicrobial activity of two thiocyanato-bridged dinuclear copper(II) complexes derived from 2,4-dibromo-6-[(2-diethylaminoethylimino)methyl]phenol and 4-nitro-2-[(2-ethylaminoethylimino)methyl]phenol. *Transition Metal Chemistry, 33*, 797–802. doi:10.1007/s11243-008-9113-8

Hu, X., Li, Y., Wang, Y., Du, W., & Guo, J. (2009). Synthesis, spectroscopic properties, and structures of copper(II) and manganese(II) complexes of pyridine-2,6-dicarboxylate and 1,10-phenanthroline. *Journal of Coordination Chemistry, 62*, 3438–3445. doi:10.1080/00958970903093686

Janiak, C. (2003). Engineering coordination polymers towards applications. *Dalton Transactions, 14*, 2781–2804. doi:10.1039/B305705B

Kabesova, M., & Gazo, J. (1980). Structure and classification of thiocyanates and the mutual influence of their ligands. *Chemicke Zvesti, 34*, 800–841.

Kurdziel, K., Głowiak, T., Materazzi, S., & Jezierska, J. (2003). Crystal structure and physico-chemical properties of cobalt(II) and manganese(II) complexes with imidazole-4-acetate anion. *Polyhedron, 22*, 3123–3128. http://dx.doi.org/10.1016/j.poly.2003.07.004

Laachir, A., Bentiss, F., Guesmi, S., Saadi, M., & El Ammari, L. (2016). Crystal structure of bis[2,5-bis(pyridin-2-yl)-1,3,4-thiadiazole-$\kappa^2 N^2, N^3$]bis(thiocyanato-κ S)copper(II). *Acta Crystallographica Section E Crystallographic Communications, 72*, 1176–1178. doi:10.1107/S2056989016011713

Li, L., Liang, J., & Tian, G. (2011). Synthesis and structure of a thiocyanato-bridged one-dimensional cdII coordination polymer. *Journal of Chemical Crystallography, 41*, 44–47. doi:10.1007/s10870-010-9834-3

Lu, J., Liu, H.-T., Zhang, X.-X., Wang, D.-Q., & Niu, M.-J. (2010). Important roles of weak interactions: Syntheses and supramolecular structures of four CoII/NiII-thiocyanato compounds. *Zeitschrift für anorganische und allgemeine Chemie, 636*, 641–647. doi:10.1002/zaac.200900286.

Małecki, J. G., Machura, B., Świtlicka A., Gron, T., & Bałanda, M., (2011). Thiocyanate manganese(II) complexes with pyridine and its derivatives ligands. *Polyhedron, 30*, 766–753.

Neumann, T., Jess, I., & Näther, C. (2014). catena-poly[[bis(pyridine-κN)nickel(II)]-di-μ-thiocyanato-κ(2) N:S;κ(2) S:N]. *Acta Crystallographica Section E: Structure Reports Online, 70*, m196–m196. doi:10.1107/S1600536814009611

Prins, L. J., Reinhoudt, D. N., & Timmerman, P. (2001). Noncovalent synthesis using hydrogen bonding. *Angewandte Chemie International Edition, 40*, 2382–2426. doi:10.1002/1521-3773(20010702)40:13<2382:AID-ANIE2382>3.0.CO;2-G

Rapheal, P. F., Manoj, E., & Kurup, M. R. P. (2007). Copper(II) complexes ofN(4)-substituted thiosemicarbazones derived from pyridine-2-carbaldehyde: Crystal structure of a binuclear complex. *Polyhedron, 26*, 818–828. doi:10.1016/j.poly.2006.09.091

Reddy, P. A. N., Nethaji, M., & Chakravarty, A. R. (2002). Synthesis, crystal structures and properties of ternary copper(II) complexes having 2,2′-bipyridine and α-amino acid salicylaldiminates as models for the type-2 sites in copper oxidases. *Inorganica Chimica Acta, 337*, 450–458. http://dx.doi.org/10.1016/S0020-1693(02)01108-8

Rowsell, J. L. C., & Yaghi, O. M. (2004). Metal–organic frameworks: A new class of porous materials. *Microporous and Mesoporous Materials, 73*, 3–14. doi:10.1016/j.micromeso.2004.03.034.

Sheldrick, G. M. (1997). *SHELXS-97 and SHELXL-97*. Germany: University of Gottingen.

Shen, L., & Feng, X. (2002). Synthesis and crystal structure of a novel polymeric thiocyanato-bridged heteronuclear complex of copper(II) and cadmium(II). *Structural Chemistry, 13*, 437–441. http://dx.doi.org/10.1023/A:1020509403583

Shi, J.-M., Xu, W., Zhao, B., Cheng, P., Liao, D.-Z., & Chen, X.-Y. (2005). A 2D thiocyanato-bridged copper(II)-manganese(II) bimetallic coordination polymer with ferromagnetic interactions. *European Journal of Inorganic Chemistry, 2005*, 55–58. doi:10.1002/ejic.200400335

Shirdel, H., Marandi, F., Jalilzadeh, A., Huber, S., & Pfitzner, A. (2015). effects of direction of bridging of thiocyanato on the dimension of coordination polymers: Synthesis, characterization and single-crystal X-ray structure determination of $[Cd(4,4'\text{-dm-}2,2'\text{-bpy})(NCS)_2]_n$ and $[Cd(4,4'\text{-dmo-}2,2'\text{-bpy})(NCS)_2]_n$ coordination polymers. *Chinese Journal of Structural Chemistry, 3*, 1135–1144.

Tabong, C. D., Yufanyi, D. M., Paboudam, A. G., Nono, K. N., Eni, D. B., & Agwara, M. O. (2016). Synthesis, crystal structure, and antimicrobial properties of [diaquabis(hexamethylen etetramine)diisothiocyanato-kN]nickel(II) Complex. *Advances in Chemistry, 2016, Article ID 5049718*, 8 pages. doi:http://dx.doi.org/10.1155/2016/5049718

Trivedi, M., Pandey, D. S., & Rath, N. P. (2009). catena -Poly[[(pyridine-κ N)copper(II)]-μ 3 -pyridine-2,6-dicarboxylato-$\kappa^3 O^2 : O^{2'}$, N , $O^6 : O^{6'}$]. *Acta Crystallographica Section E Structure Reports Online, 65*, m303–m304. doi:10.1107/S1600536809005212.

Whitesides, G. M., & Boncheva, M. (2002). Beyond molecules: Self-assembly of mesoscopic and macroscopic components. *Proceedings of the National Academy of Sciences, 99*, 4769–4774. doi:10.1073/pnas.082065899.

Wohlert, S., Wriedt, M., Jess, I., & Nather, C. (2011). Chloridotetrapyridinecopper(II) dicyanamidate pyridine disolvate. *Acta Crystallographica Section E Structure Reports Online, 67*, m695. doi:10.1107/S1600536811016187

Yang, G. B., & Sun, Z. H. (2013). Tuning the structural topologies of two luminescent metal-organic frameworks through altering auxiliary ligand. *Inorganic Chemistry Communications, 29*, 94–96. http://dx.doi.org/10.1016/j.inoche.2012.12.022

You, Z.-L., & Zhu, H.-L. (2005). A novel thiocyanate-bridged dinuclear cadmium(II) complex: di-[mu]-thiocyanato-bis((methanol){4-nitro-2-[2-(dimethylamino) ethyliminomethyl]phenolato}cadmium(II)). *Acta Crystallographica Section C, 61*, m397–m399. doi:10.1107/S0108270105021906

Yue, Y.-F., Fang, C.-J., Gao, E.-Q., He, C., Bai, S.-Q., Xu, S., & Yan, C.-H. (2008). Four thiocyanato-bridged cadmium(II) polymeric complexes based on open chain diazine ligands. *Journal of Molecular Structure, 875*, 80–85. doi:10.1016/j.molstruc.2007.04.002.

Yuoh, A. C. B., Agwara, M. O., Yufanyi, D. M., Conde, M. A., Jagan, R., & Eyong, K. O. (2015). Synthesis, crystal structure, and antimicrobial properties of a novel 1-D cobalt coordination polymer with dicyanamide and 2-aminopyridine. *International Journal of Inorganic Chemistry, 2015, Article ID 106838*. doi:http://dx.doi.org/10.1155/2015/106838

Zaworotko, M. J. (2001). Superstructural diversity in two dimensions: Crystal engineering of laminated solids. *Chemical Communications, 1*, 1–9. doi:10.1039/B007127G

***Cogent Chemistry* (ISSN: 2331-2009) is published by Cogent OA, part of Taylor & Francis Group.**

Hindawi Publishing Corporation
Advances in Chemistry
Volume 2016, Article ID 5049718, 8 pages
http://dx.doi.org/10.1155/2016/5049718

Research Article

Synthesis, Crystal Structure, and Antimicrobial Properties of [Diaquabis(hexamethylenetetramine)diisothiocyanato-κN]nickel(II) Complex

Che Dieudonne Tabong,[1] Divine Mbom Yufanyi,[2] Awawou Gbambie Paboudam,[1] Katia Nchimi Nono,[1] Donatus Bekindaka Eni,[1] and Moise Ondoh Agwara[1]

[1]*Department of Inorganic Chemistry, Faculty of Science, University of Yaoundé I, P.O. Box 812, Yaoundé, Cameroon*
[2]*Department of Chemistry, Faculty of Science, The University of Bamenda, P.O. Box 39, Bambili, Bamenda, Cameroon*

Correspondence should be addressed to Moise Ondoh Agwara; agwara29@yahoo.com

Received 23 April 2016; Revised 10 June 2016; Accepted 13 June 2016

Academic Editor: Renal Backov

A nickel(II) complex with hexamethylenetetramine and thiocyanate ion as coligands has been synthesized and characterised by infrared spectroscopy and ultraviolet-visible spectroscopic techniques. The crystal structure of the complex was determined by single crystal X-ray diffraction and the ligands were found to coordinate terminally through N-atoms. The ligand and the complex were screened for their activity against resistant strains of bacteria (*Salmonella enteric*, *Shigella flexneri*, *Escherichia coli,* and *Staphylococcus aureus*) and fungi (*Candida albicans*, *Candida krusei*, *Candida parapsilosis,* and *Candida neoformans*).

Dedicated to Professor Moise Ondoh Agwara on his 60th anniversary

1. Introduction

Recently, the design and synthesis of novel coordination compounds, inorganic-organic hybrid materials, and coordination polymers with desired physicochemical properties are at the frontiers of inorganic chemistry research [1–6]. To achieve this goal, the rational design of particular structures employing different synthetic approaches needs to be developed, followed by a study of the structure-property relationships. The rational choice of building blocks, metal centres and ligands, is of crucial importance in the deliberate construction of coordination networks and the design of metal-based supramolecular architectures [7, 8]. Among the ligands employed in the construction of these networks, hexamethylenetetramine (HMTA), as a potential tetradentate ligand or hydrogen bond acceptor, seems quite suitable in self-assembly systems.

Hexamethylenetetramine is a commercially available organic molecule which possesses three fused rings in the chair conformation similar to the cage-like structure of adamantine [9]. It is cheap, ecofriendly, and readily available for reactions with many hydrated salts. It forms molecular complexes, with varied coordination patterns ranging from monodentate [10], bridging [11, 12], nonchelating to hydrogen-bonded frameworks [13–15], inducing the formation of one-, two-, and three-dimensional framework structures. Biologically, HMTA has several uses like a cosmetic biocide in eye make-up preparation, preservative in lotions and creams, or antiseptic agent for the treatment of urinary tract infections [16, 17].

Among the inorganic anions serving as coligands, thiocyanate SCN^- (an ambidentate ligand) is very important due to its great tendency to combine with a variety of metal ions, forming either thiocyanato (M-SCN) or isothiocyanato (M-NCS) complexes and also bridges metal ions. In addition, the antagonism between the ligands HMTA and SCN^- (neutral and ionic) as well as the solvent molecules influence in the coordination sphere is fundamental in supramolecular

assembly [18–22]. Hence, the nature of these complexes depends on the interplay between the metal ion, the counter ion, and HMTA [23].

Within the scope of our ongoing research on the structure and applications of coordination compounds, based on N-, and N,O-donor heterocyclic ligands and coligands (thiocyanate, azide, etc.), we have synthesized a number of different materials and together with selected examples from the literature evaluated their antimicrobial properties [16, 23–28].

The emergence of drug-resistant bacterial and fungal strains has become a worldwide cause for concern [29, 30]. This increasing resistance of microbes to antibacterial and antifungal drugs has necessitated the search for new compounds to target pathogenic microbes [29, 30]. Several efforts have been made to develop antimicrobial agents to fight against these resistant pathogens among which are the protection of the efficacy and appropriate use of existing drugs as well as research and development of new antimicrobial agents that are not affected by the currently known, predicted, or unknown mechanisms of resistance [31–33]. The incorporation of metals into antibacterial molecules is expected to enhance the bactericidal or fungicidal properties of these drugs.

In this work, we report the synthesis and crystal structure of a nickel(II) hexamethylenetetramine complex with thiocyanate coligand. The biological activity of the complex towards some resistant pathogens, evaluated using *in vitro* assays, is also presented.

2. Experimental

2.1. Materials. $NiSO_4{\cdot}6H_2O$, hexamethylenetetramine, and ammonium thiocyanate were obtained from Sigma Aldrich. Methanol was obtained from Riedel-de Haen (Germany). The chemicals were of analytical grade and were used as such, while the solvent was distilled according to standard methods.

2.2. Synthesis of the Complex $[Ni(HMTA)_2(NCS)_2(H_2O)_2]{\cdot}H_2O$. A 15 mL methanol solution of hexamethylenetetramine (0.280 g; 2.0 mmol) was added dropwise to a 15 mL methanol/H_2O (2 : 1 v/v) solution of $NiSO_4{\cdot}6H_2O$ (0.291 g; 1 mmol) while stirring at room temperature. After stirring for 30 minutes, ammonium thiocyanate (0.156 g; 2 mmol) in 10 mL methanol was added into the solution. The mixture was further stirred for two hours and stored for a week during which time bluish-green needle-like crystals suitable for single crystal X-ray diffraction were obtained. They were filtered, washed with diethylether, and dried over silica gel in a desiccator.

2.3. Characterisation. The infrared spectrum of the complex was recorded using a Bruker ALPHA-P spectrophotometer directly on a small sample of the complex in the range 400–4000 cm^{-1} while the UV-visible spectrum of an ethanolic solution of the complex was recorded using a Bruker HACH DR 3900 UV-visible spectrophotometer at room temperature.

2.4. X-Ray Crystal Structure Determination. Intensity data for the compound was collected using a Bruker AXS Kappa APEX II single crystal CCD Diffractometer, equipped with graphite-monochromated MoKα radiation (λ = 0.71073 Å) at room temperature. The selected crystal for the diffraction experiment had a dimension of 0.25 × 0.25 × 0.2 mm^3. Accurate unit cell parameters were determined from the reflections of 36 frames measured in three different crystallographic zones by the method of difference vectors. The data collection, data reduction, and absorption correction were performed by APEX2, SAINT-Plus, and SADABS programs [38]. The structure was solved by direct methods procedure using SHELXS-97 program [39] and the nonhydrogen atoms were subjected to anisotropic refinement by full-matrix least squares on F^2 using SHELXL-97 program [39]. The positions of all the nonhydrogen atoms were identified from difference electron density map and were fixed accordingly. Hydrogen atoms were treated by a mixture of independent and constrained refinement.

2.5. Antimicrobial Tests. The *in vitro* antimicrobial activities of the metal salts, metal complex, ligands, and reference drugs were evaluated by disk diffusion and broth microdilution methods. The antimicrobial tests were carried out in the Laboratory of Phytobiochemical and Medicinal Plant Study, University of Yaoundé I, Cameroon. Four strains of bacteria (*Salmonella enteric*, *Shigella flexneri*, *Escherichia coli,* and *Staphylococcus aureus*) and four strains of fungi (*Candida albicans*, *Candida krusei*, *Candida parapsilosis,* and *Candida neoformans*) were used for this study. All the species were derived from stock cultures obtained from the Medical Bacteriology Laboratory of "Centre Pasteur du Cameroun", Yaoundé, Cameroon. Chloramphenicol and fluconazole were used as reference antibacterial and antifungal drugs, respectively.

2.5.1. Diffusion Tests. In vitro antibacterial activities of the ligand, metal salt, and the complex were evaluated using disc diffusion method. Mueller-Hinton Agar was employed as microbial growth medium. The antibacterial diffusion tests were carried out as previously reported [26].

Mueller-Hinton agar was prepared from a commercially available dehydrated base according to the manufacturer's instructions. Several colonies of each microorganism were collected and suspended in saline (0.9% NaCl). Then, the turbidity of the test suspension was standardized to match that of a 0.5 McFarland standard (corresponding to approximately 1.5×10^8 CFU/mL for bacteria or 1×10^6 to 5×10^6 cells/mL for yeast). Each compound or reference was accurately weighed and dissolved in the appropriate diluents (DMSO at 10%, methanol at 10%, or distilled water) to yield the required concentration (2 mg/mL for compound or 1 mg/mL for reference drug), using sterile glassware.

Whatman filter paper number 1 was used to prepare discs approximately 6 mm in diameter, which were packed up with aluminum paper and sterilized by autoclaving. Then, 25 μL of stock solutions of compound or positive control was

delivered to each disc, leading to 50 μg of compound or 25 μg of reference drug.

The dried surface of a Mueller-Hinton agar plate was inoculated by flooding over the entire sterile agar surface with 500 μL of inoculum suspensions. The lid was left ajar for 3 to 5 minutes to allow for any excess surface moisture to be absorbed before applying the drug impregnated discs. Discs containing the compounds or antimicrobial agents were applied within 15 minutes of inoculating the MHA plate. Six discs per Petri dish were plated. The plates were inverted and placed in an incubator set to 35°C. After 18 hours (for bacteria) and 24 hours (for yeasts) of incubation, each plate was examined. The diameters of the zones of complete inhibition (as judged by the unaided eye) were measured, including the diameter of the disc. Zones were measured to the nearest whole millimeter, using sliding calipers, which was held on the back of the inverted Petri plate. Three replicas were performed for each sample and mean values of the growth inhibition zone were calculated. Compounds were considered active when the IZ was greater than 6 mm.

3. Results and Discussion

3.1. Synthesis of the Complex. The reaction of hexamethylenetetramine, ammonium thiocyanate, and $NiSO_4 \cdot 6H_2O$ yielded the complex $[Ni(HMTA)_2(NCS)_2(H_2O)_2] \cdot H_2O$. The complex was bluish-green in colour and it was obtained in high yield, 74%.

3.2. Description of the Crystal Structure. The crystal structural data of the complex are summarized in Table 1. The ORTEP view of the crystal structure together with the atom numbering scheme is shown in Figure 1. The packing diagram of the complex and the H-bonding scheme seen along the crystallographic *b*-axis are shown in Figures 2 and 3, respectively. Selected bond distances and bond angles for the complex are presented in Table 2.

The complex crystallizes in the monoclinic crystal system with space group C*2/c*. The asymmetric unit consists of one HMTA molecule, one thiocyanate anion, one coordinated water molecule, one lattice water molecule, and one Ni(II) ion. The crystal structure of the complex reveals that the Ni(II) coordination environment is a slightly distorted octahedron (NiN_4O_2 chromophore) in which it is covalently bonded to two terminal HMTA N-atoms (Ni-N4 2.238(2) Å) in transaxial positions, two water O-atoms (Ni-O1 2.058(2) Å) and two terminal NCS^- N-atoms (Ni-N2 2.031(2) Å), in the equatorial plane. The Ni atom is located in an inversion centre. This arrangement is similar to that of related structures reported in the literature [35–37]. The NCS^- groups show almost linearity with N-C-S angle of 179.52° in the complex as previously reported for analogous Co and Mn structures [35–37]. The connection between Ni atoms and NCS groups is slightly bent with a Ni-N2-C8 angle of 172.68°. Furthermore, the O atoms of both water molecules and the N atoms of both NCS^- anions are each mutually trans to each other, as evidenced by the bond angles O1-Ni-O1 180° and N2-Ni-N2 180°, respectively. Each lattice water molecule forms three H-bonds with O-atom of a coordinated water molecule (O-H···O 2.669 Å), noncoordinated N-atom of HMTA (O-H···N 2.797 Å), and S-atom of SCN^- (O-H···S 3.310 Å). There is another H-bond between the oxygen atom of the coordinated water molecule and a noncoordinated nitrogen of a HMTA molecule (O-H···N distance = 2.806 Å). Adjacent Ni coordination centres are linked by free H_2O molecules via hydrogen bonds also involving two coordinated O-atoms of water molecules and two uncoordinated N-atoms of HMTA molecule in the hydrogen bond net, forming 1D chains. These adjacent chains are further connected to form 2D supramolecular layers parallel to the ac plane by S···N and C···C interactions. The two-dimensional layers are further connected by O-H···S and O-H···N hydrogen bonds, along the *b* crystallographic axis, to form a three-dimensional supramolecular structure. This is in agreement with literature reports [35–37]. The H-bonding motifs can be described in Etter's graph set notation as $R_2^2(12)$ and

Table 1: Crystal data and structure refinement for the complex.

Empirical formula	$C_{14}H_{32}N_{10}NiO_4S_2$
Formula weight	527.33
Temperature	100 K
Wavelength (Å)	$\lambda = 0.71073$
Crystal system	Monoclinic
Space group	C*2/c*
Unit cell dimensions	
a (Å)	18.085(4)
b (Å)	7.4019(16)
c (Å)	17.422(4)
α (°)	90
β (°)	91.527(2)
γ (°)	90
Unit cell volume	2331.4(9)
Z	4
F(000)	1112.0
Density (calculated)	1.502 Mg/m^3
Absorption coefficient	1.054 mm^{-1}
Crystal size	$0.16 \times 0.203 \times 0.501$ mm^3
Theta range for data collection	2.25 to 28.15
Indexes $(h, k, l)_{max}$	(24, 9, 23)
Reflections collected	6943
Independent and observed reflections	2681[*R*(int) = 0.0240], 2563
Completeness to theta = 26°	99.8%
Refinement method	Full-matrix least squares on F^2
Data/restraints/parameters	2681/0/158
Goodness-of-fit on F^2	1.051
Final *R* indices [$I > 2$sigma(I)]	$R_1 = 0.0269$, $wR_2 = 0.0695$
Final *R* indices (all data)	$R_1 = 0.0279$, $wR_2 = 0.0689$
Largest diff. peak and hole	0.875 and −0.567 e·$Å^{-3}$

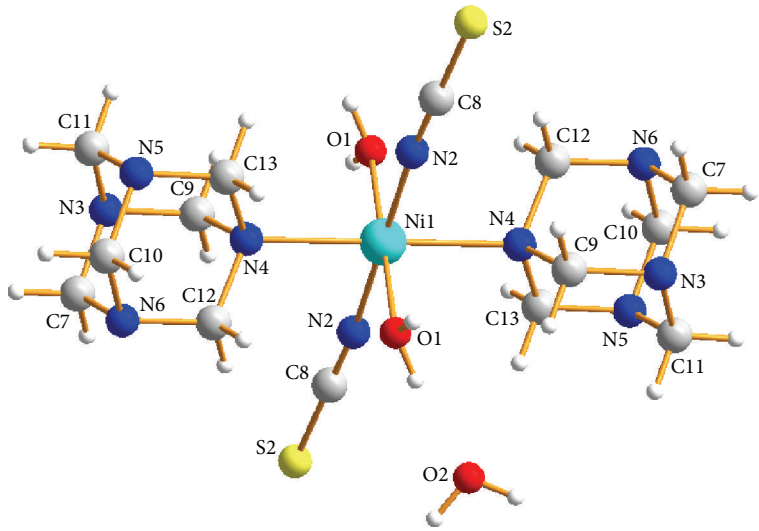

Figure 1: ORTEP view of the complex with atom numbering scheme.

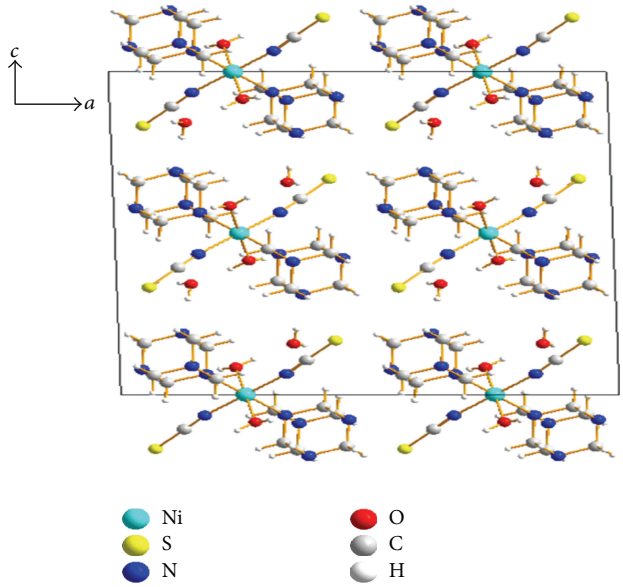

Figure 2: Packing diagram of the complex seen along the crystallographic *b*-axis.

Table 2: Selected bond lengths (Å) and angles (°) for the complex.

Ni1-O1	2.058(2)	N6-C7	1.476(2)
Ni1-N2	2.031(2)	N6-C10	1.485(2)
Ni1-N4	2.238(2)	N6-C12	1.475(2)
Ni1-O1	2.058	S2-C8	1.642(1)
Ni1-N2	2.031	N2-C8	1.161(2)
Ni1-N4	2.238	N3-C7	1.481(2)
S2-C8	1.642(1)	N3-C9	1.469(2)
N2-C8	1.161(2)	N3-C11	1.484(2)
O1-Ni1-N2	90.08	Ni1-N2-C8	172.68
O1-Ni1-N4	93.73	Ni1-N4-C9	108.74
O1-Ni1-O1	180	Ni1-N4-C12	113.34
O1-Ni1-N2	89.92	Ni1-N4-C13	112.96
O1-Ni1-N4	86.27	S2-C8-N2	179.52
N2-Ni1-N4	92.64	N4-Ni1-N4	180
N2-Ni1-O1	89.92	O1-Ni1-N2	90.08
N2-Ni1-N2	180	O1-Ni1-N4	93.73
N2-Ni1-N4	87.36	N2-Ni1-N4	92.64
N4-Ni1-O1	86.27	Ni1-N2-C8	172.68
N4-Ni1-N2	87.36	Ni1-N4-C9	108.74
Ni1-N4-C13	112.96	Ni1-N4-C12	113.34

$R_4^4(16)$ [40, 41]. The nickel atoms form linear chains running along the *b*-direction with an interlayer Ni-Ni distance of 7.402 Å, while the Ni⋯Ni distances within hydrogen-bonded chains and between adjacent chains in the same layer are 9.465 Å and 9.771 Å, respectively.

A comparison of the M-N (HMTA), M-N (NCS^-), and M-O (H_2O) bond distances for similar structures found in the literature [34–37] is shown in Table 3. The axial Ni-N (HMTA) bond length is slightly shorter than those of Co-N and Mn-N but longer than that of Cu-N. The Ni-N (NCS^-) bond length is similar to those of Co and Cu but is shorter than that of Mn. The Ni-O bond is slightly shorter than the other M-O bonds. While the Ni complex obtained has a unique coordination centre, the complexes, $[Mn(hmt)_2(H_2O)_2(NCS)_2]\cdot[Mn(H_2O)_4(NCS)_2]\cdot 2H_2O$ and $[Co(NCS)_2(hmt)_2(H_2O)_2][Co(NCS)_2(H_2O)_4]\cdot H_2O$, contain two distinct six coordinate M(II) centres alongside two lattice water molecules and one lattice water molecule, respectively. The independent uncharged components $[M(NCS)_2(hmt)_2(H_2O)_2]$, $[M(NCS)_2(H_2O)_4]$, and H_2O are linked together by three kinds of hydrogen bonds (O-H⋯N, O-H⋯O and O-H⋯S) to form a three-dimensional supramolecular structure [35–37]. On the other hand, the coordination environment of the Cu atom in the complex $K[Cu(C_6H_{12}N_4)_2(NCS)_3]\cdot 2H_2O$ is trigonal bipyramidal with

Table 3: Comparison of bond parameters for similar structures $[M(hmt)_2(H_2O)_2(NCS)_2]$ (M = Cu, Co, Mn, and Ni).

M-N (HMTA)	Bond length (Å)	M-N (NCS^-)	Bond length (Å)	M-O (H_2O)	Bond length (Å)	Ref.
Cu-N	2.09(5) 2.10(5)	Cu-N	1.98(6) 2.08(6) 1.98(7)	None	—	[34]
Mn-N	2.4213(13)	Mn-N	2.1342(15)	Mn-O	2.1865(12)	[35]
Co-N	2.341(5)	Co-N	2.058(5)	Co-O	2.104(5)	[36]
Co-N	2.3274(16)	Co-N	2.0411(19)	Co-O	2.1025(16)	[37]
Ni-N	2.238(2)	Ni-N	2.031(2)	Ni-O	2.058(2)	This work

Table 4: Relevant IR bands of the ligands and the complex.

	$\upsilon_{O\text{-}H}$	υ_{H_2O}	$\upsilon_{C\text{-}N}$	$\upsilon_{C\text{-}N}$ (SCN)	ρ_{CH_2}	$\upsilon_{M\text{-}O}$	$\upsilon_{M\text{-}N}$
HMTA	—	—	1238	—	810		
Complex	3370	3250	1232	2084	821	778	683 669

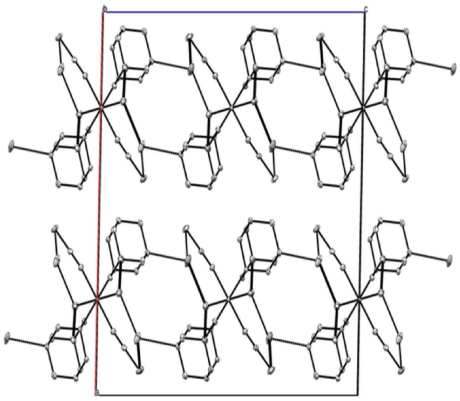

Figure 3: ORTEP representation of the H-bonding scheme of the complex seen along the crystallographic *b*-axis.

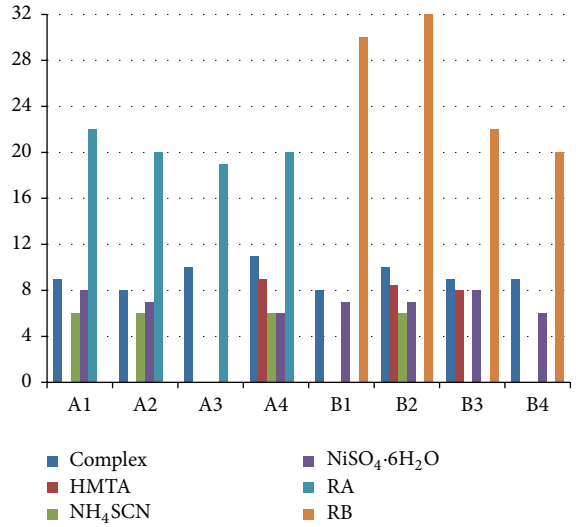

Figure 4: Histogram of inhibition zone of ligands, metal salt, and complex against bacteria.

three equatorial positions occupied by NCS groups and the axial positions by the HMTA molecules [34].

As shown by Lu et al. [37], the close distance of NCS^- groups, the large volume of HMTA ligand, and the ratio between the divalent metal and NCS^- of 2 : 1 can probably explain the absence of S···S Van der Waals' interactions in the Mn [35], Co [36], and Ni (this work) complexes.

3.3. Infrared Spectroscopy. The characteristic IR band frequencies of the ligand and complexes are presented in Table 4.

The broad band at 3250 cm^{-1} and the sharp peak at 1661 cm^{-1} are assigned to $\upsilon_{O\text{-}H}$ and $\delta_{H\text{-}O\text{-}H}$ of lattice water, respectively, while the peak at 3370 cm^{-1} is due to $\upsilon_{O\text{-}H}$ of coordinated water [42]. The CH_2 stretching vibrational band of HMTA appears at 2957 cm^{-1}. The band at 1238 cm^{-1} assigned to the C-N stretch of HMTA is shifted to 1232 cm^{-1} in the complex while the band at 810 cm^{-1} in the free ligand assigned to the CH_2 rocking vibration of HMTA is shifted to 821 cm^{-1} in the complex, indicating coordination of the ligand [27]. The sharp peak at 2084 cm^{-1} is assigned to the C-N stretching vibration of SCN [43]. The appearance of new peaks at 778 cm^{-1}, 683 cm^{-1}, and 669 cm^{-1}, respectively, indicates M-O and M-N bonding between the metal and the ligands.

3.4. UV-Visible Spectroscopy. The electronic spectrum of the nickel(II) complex exhibits two absorption bands: one band around 25,000 cm^{-1} and a second broad and split band at 15625–14514 cm^{-1}. These bands have been assigned to $^3A_{2g} \rightarrow {}^3T_{1g}(P)$ and $^3A_{2g} \rightarrow {}^3T_{1g}(F)$ transitions, respectively [44]. The ratio of 1.72 of the height of the first to that of the second band indicates an octahedral environment around the nickel(II) ion [45].

3.5. Antimicrobial Tests. The metal salt, ligands, metal complex, and reference drugs were tested for antimicrobial activity *in vitro* against four bacteria and four fungi strains. The susceptibility of the bacteria and fungi strains towards the compounds was judged by measuring the diameter of the growth inhibition zone. The results are summarized in Table 5 and displayed in a histogram (Figure 4).

HMTA was found to be active against three of the eight pathogens while the metal complexes showed increased

Table 5: Diameter of inhibition zone (mm) of the compounds against bacteria and fungi.

	A_1	A_2	A_3	A_4	B_1	B_2	B_3	B_4
Complex	9 ± 0.0	8 ± 0.0	10 ± 0.0	11 ± 0.0	8 ± 0.0	10 ± 0.0	9 ± 0.0	9 ± 0.0
HMTA	0	0	0	9 ± 1.4	0	8.5 ± 0.7	8 ± 0.0	0
NH_4SCN	6 ± 0.0	6 ± 0.0	0	6 ± 0.0	0	6 ± 0.0	0	0
$NiSO_4{\cdot}6H_2O$	8 ± 0.0	7 ± 0.0	0	6 ± 0.0	7 ± 0.0	7 ± 0.0	8 ± 0.7	6 ± 0.0
RA	22 ± 0.0	20 ± 0.0	19 ± 1.4	20 ± 0.0	—	—	—	—
RB	—	—	—	—	30 ± 0.0	32 ± 0.0	22 ± 0.0	20 ± 0.0

A_1: *Staphylococcus aureus*; A_2: *Salmonella enterica*; A_3: *Shigella flexneri*; A_4: *Escherichia coli*; B_1: *Candida albicans*; B_2: *Candida parapsilosis*; B_3: *Candida krusei*; B_4: *Candida neoformans*; RA: reference antimicrobial (chloramphenicol); RB: reference antifungal (fluconazole); —: not tested.

activity against all the pathogens. This indicates that the metal ion probably plays an important role in enhancing the antimicrobial activity of the ligand on interaction with it. The highest activity of the complex is shown against *E. coli* and *S. flexneri*. This increase in activity could be due to the reduction of the polarity of the metal ion by partial sharing of the positive charge with the ligand's donor atoms so that there is electron delocalisation within the metal complex. This may increase the lipophilic character of the metal complex, enabling it to permeate the lipid layer of the organism killing them more effectively [46].

4. Conclusion

The synthesis of a nickel-HMTA complex $[Ni(HMTA)_2(NCS)_2(H_2O)_2]{\cdot}H_2O$ has been reported. The equatorial H_2O and NCS ligands coordinate in a nonlinear manner to the central metal ion while the axial HMTA ligands are terminally coordinated to the Ni(II) ion through one N-atom each. The Ni(II) coordination environment is a slightly distorted octahedron (NiN_4O_2 chromophore). An extended three-dimensional network is assembled via H-bonding interactions involving the lattice water molecule, O-atom of a coordinated water molecule, noncoordinated N-atom of HMTA, and S-atom of SCN^-. Results of the preliminary antimicrobial screening against four pathogenic bacteria and four fungi species indicate that the complex is moderately active, with highest activity shown against *E. coli* and *S. flexneri*. The complex could be further screened *in vitro* against a wide range of pathogens.

Additional Points

CCDC 1452400 contains the supplementary crystallographic data for the complex. The data can be obtained free of charge from The Cambridge Crystallographic Data Centre via https://summary.ccdc.cam.ac.uk/structure-summary?access=referee&ccdc=1452400&authors=che.

Competing Interests

The authors declare that there is no conflict of interests regarding the publication of this paper.

Acknowledgments

The authors thank the Government of Cameroon for financial support through the Fonds d'Appuis à la Recherche.

References

[1] S. Wöhlert, T. Runčvski, R. E. Dinnebier, S. G. Ebbinghaus, and C. Näther, "Synthesis, structures, polymorphism, and magnetic properties of transition metal thiocyanato coordination compounds," *Crystal Growth and Design*, vol. 14, no. 4, pp. 1902–1913, 2014.

[2] M. J. Zaworotko, "Superstructural diversity in two dimensions: crystal engineering of laminated solids," *Chemical Communications*, no. 1, pp. 1–9, 2001.

[3] C. Janiak, "Engineering coordination polymers towards applications," *Dalton Transactions*, no. 14, pp. 2781–2804, 2003.

[4] G. R. Desiraju, "Crystal engineering: a holistic view," *Angewandte Chemie—International Edition*, vol. 46, no. 44, pp. 8342–8356, 2007.

[5] C. B. Aakeröy, N. R. Champness, and C. Janiak, "Recent advances in crystal engineering," *CrystEngComm*, vol. 12, no. 1, pp. 22–43, 2010.

[6] G. R. Desiraju, "Crystal engineering: from molecule to crystal," *Journal of the American Chemical Society*, vol. 135, no. 27, pp. 9952–9967, 2013.

[7] L. Carlucci, G. Ciani, A. Gramaccioli, D. M. Proserpio, and S. Rizzato, "Crystal engineering of coordination polymers and architectures using the $[cu(2,2'\text{-bipy})]^{2+}$ molecular corner as building block (bipy=2,2′-bipyridyl)," *CrystEngComm*, vol. 2, no. 29, pp. 154–163, 2000.

[8] S. Stepanow, N. Lin, and J. V. Barth, "Modular assembly of low-dimensional coordination architectures on metal surfaces," *Journal of Physics Condensed Matter*, vol. 20, no. 18, Article ID 184002, 2008.

[9] A. M. Kirillov, "Hexamethylenetetramine: an old new building block for design of coordination polymers," *Coordination Chemistry Reviews*, vol. 255, no. 15-16, pp. 1603–1622, 2011.

[10] M. K. Ammar, T. Jouini, and A. Driss, "Synthesis and structural characterization of dihexamethylenetetraminetetraaquocobalt(II) hexaaquocobalt(II) sulfate hexahydrate," *Journal of Chemical Crystallography*, vol. 30, no. 4, pp. 265–268, 2000.

[11] A. Ray, J. Chakraborty, B. Samanta et al., "Two new hydrothermally synthesised hexamine bridged L–M–L type coordination polymers: characterisation and magneto-structural correlation," *Inorganica Chimica Acta*, vol. 361, no. 7, pp. 1850–1860, 2008.

[12] Y. Chen, Y.-L. Wang, S.-M. Ying, and S.-L. Cai, "Poly [di-μ_2-chlorido-μ_4-hexa-methyl-ene-tetra- mine-bis-[chlorido (methanol-κO)-cadmium(II)]]," *Acta Crystallographica, Section E: Structure Reports Online*, vol. 63, no. 11, Article ID m2751, 2007.

[13] A. Trzesowska and R. Kruszynski, "The synthesis, crystal structure and thermal studies of a mixed-ligand 1,10-phenanthroline and hexamethylenetetramine complex of lanthanum nitrate. Insight into coordination sphere geometry changes of lanthanide(III) 1,10-phenanthroline complexes," *Transition Metal Chemistry*, vol. 32, no. 5, pp. 625–633, 2007.

[14] X.-L. Li, Z.-S. Lu, and D.-Z. Niu, "Bis(4-carboxypyridinium) aquapentakis(isothiocyanato-κN)iron(III) bis(pyridinium-4-carboxylate)," *Acta Crystallographica Section E*, vol. 63, no. 11, article m2640, 2007.

[15] D. Chopra, P. Dagur, A. S. Prakash, T. N. Guru Row, and M. S. Hegde, "Synthesis and crystal structure of $M(hmt)_2(H_2O)_6(NO_3)_{2.4}H_2O$ complexes, where M = Mn^{2+}, Co^{2+}," *Journal of Crystal Growth*, vol. 275, no. 1-2, pp. e2049–e2053, 2005.

[16] M. O. Agwara, M. D. Yufanyi, J. N. Foba-Tendo, M. A. Atamba, and D. T. Ndinteh, "Synthesis, characterisation and biological activities of Mn(II), Co(II) and Ni(II) complexes of hexamethylenetetramine," *Journal of Chemical and Pharmaceutical Research*, vol. 3, no. 3, pp. 196–204, 2011.

[17] L. S. Miall and Mackenzie, *A Dictionary of Chemistry*, Longmans, 1956.

[18] M. K. R. Balan, F. N. Ashok, M. Vasanthi, R. Prabu, and A. Paulraj, "Mixed ligand complexes of Nickel(II), Copper(II) and Zinc(II) with nicotinanilide and thiocyanate with some Nickel(II), Copper(II) And Zinc(II) salt," *International Journal of Life science and Pharma Reviews*, vol. 3, no. 2, pp. L67–L75, 2013.

[19] D. Fu-Tai Tuan, J. W. Reed, and R. Hoffmann, "Studies of the linkage and bonding of triatomics in transition metal complexes—part 2. NCS—complexes," *Journal of Molecular Structure: THEOCHEM*, vol. 232, pp. 111–121, 1991.

[20] M. Montazerozohori, K. Nozarian, and H. R. Ebrahimi, "Synthesis, spectroscopy, theoretical, and electrochemical studies of Zn(II), Cd(II), and Hg(II) azide and thiocyanate complexes of a new symmetric schiff-base ligand," *Journal of Spectroscopy*, vol. 2013, Article ID 718149, 9 pages, 2013.

[21] S. A. Shaker, Y. Farina, S. Mahmmod, and M. Eskender, "Zn (II) and Cd (II) mixed ligand complexes of 6-aminopurine, theophylline and thiocyanate ion, preparation and spectroscopic characterization," *Journal of Engineering and Applied Sciences*, vol. 4, no. 9, pp. 29–33, 2009.

[22] E. Czubacka, R. Kruszynski, and T. Sieranski, "The structure and thermal behaviour of sodium and potassium multinuclear compounds with hexamethylenetetramine," *Journal of Structural Chemistry*, vol. 23, no. 2, pp. 451–459, 2012.

[23] M. O. Agwara, P. T. Ndifon, and M. K. Ndikontar, "Physicochemecal studies of some hexamethylenetetramine metal(II) complexes," *Bulletin of the Chemical Society of Ethiopia*, vol. 18, no. 2, pp. 143–148, 2004.

[24] M. O. Agwara, P. T. Ndifon, D. M. Yufanyi et al., "Synthesis, characterisation and crystal structure af a three-dimensional network of an H-bonded Ni(II) hexametylenetetramine complex," *Rasayan Journal of Chemistry*, vol. 3, no. 2, pp. 207–213, 2011.

[25] C. D. Tabong, A. M. Ondoh, D. M. Yufanyi, and J. Foba, "Cobalt(II) and zinc(II) complexes of hexamethylenetetramine as single source precursors for their metal oxide nanoparticles," *Journal of Materials Science Research*, vol. 4, no. 4, pp. 70–81, 2015.

[26] A. Colette, A. M. Ondoh, D. M. Yufanyi, and D. S. Yanick Gaelle, "Synthesis, crystal structure and antimicrobial properties of an anhydrous copper(II) complex of pyridine-2-carboxylic acid," *International Journal of Chemistry*, vol. 7, no. 1, pp. 10–20, 2014.

[27] P. T. Ndifon, M. O. Agwara, A. G. Paboudam et al., "Synthesis, characterisation and crystal structure of a cobalt(II)-hexamethylenetetramine coordination polymer," *Transition Metal Chemistry*, vol. 34, no. 7, pp. 745–750, 2009.

[28] A. C. B. Yuoh, M. O. Agwara, D. M. Yufanyi, M. A. Conde, R. Jagan, and K. O. Eyong, "Synthesis, crystal structure, and antimicrobial properties of a novel 1-D cobalt coordination polymer with dicyanamide and 2-aminopyridine," *International Journal of Inorganic Chemistry*, vol. 2015, Article ID 106838, 8 pages, 2015.

[29] J. Tanwar, S. Das, Z. Fatima, and S. Hameed, "Multidrug resistance: an emerging crisis," *Interdisciplinary Perspectives on Infectious Diseases*, vol. 2014, Article ID 541340, 7 pages, 2014.

[30] WHO, *Antimicrobial Resistance: Global Report on Surveillance*, World Health Organization, Geneva, Switzerland, 2014.

[31] B. Spellberg, R. Guidos, D. Gilbert et al., "The epidemic of antibiotic-resistant infections: a call to action for the medical community from the Infectious Diseases Society of America," *Clinical Infectious Diseases*, vol. 46, no. 2, pp. 155–164, 2008.

[32] N. Beyth, Y. Houri-Haddad, A. Domb, W. Khan, and R. Hazan, "Alternative antimicrobial approach: nano-antimicrobial materials," *Evidence-Based Complementary and Alternative Medicine*, vol. 2015, Article ID 246012, 16 pages, 2015.

[33] V. Kandi and S. Kandi, "Antimicrobial properties of nanomolecules: potential candidates as antibiotics in the era of multi-drug resistance," *Epidemiology and Health*, vol. 37, Article ID e2015020, 5 pages, 2015.

[34] J. Pickardt, "The crystal structure of potassium-bis(hexamethylenetetramine)-tris-(isothiocyanato) cuprate(II)-dihydrate, $K[Cu(C_6H_{12}N_4)_2(NCS)_3] \cdot 2H_2O$, a trigonal bipyramidal cupric complex," *Zeitschrift für Naturforschung B*, vol. 36, no. 5, pp. 649–650, 1981.

[35] Q. Liu, B. Li, X. Sun, Z. Xu, and K. Yu, "Diaquabis(hexamethylenetetramine-N)bis(isothiocyanato)manganese(II) tetraaquabis (isothiocyanato)manganese(II) dihydrate," *Acta Crystallographica Section E: Structure Reports Online*, vol. 57, no. 4, pp. m151–m153, 2001.

[36] Y. Zhang, J. Li, H. Xu, H. Hou, M. Nishiura, and T. Imamoto, "Structural and spectroscopic properties of hexamethylenetetramine cobalt(II) complex: $[Co(NCS)_2(hmt)_2(H_2O)_2][Co(NCS)_2(H_2O)_4](H_2O)$," *Journal of Molecular Structure*, vol. 510, no. 1–3, pp. 191–196, 1999.

[37] J. Lu, H.-T. Liu, X.-X. Zhang, D.-Q. Wang, and M.-J. Niu, "Important roles of weak interactions: syntheses and supramolecular structures of four CoII/NiII-thiocyanato compounds," *Zeitschrift für Anorganische und Allgemeine Chemie*, vol. 636, no. 3-4, pp. 641–647, 2010.

[38] Bruker, in *APEX2*, SAINT-Plus and XPREP, Eds., Bruker AXS, Madison, Wis, USA, 2004.

[39] G. M. Sheldrick, "A short history of SHELX," *Acta Crystallographica Section A: Foundations of Crystallography*, vol. 64, no. 1, pp. 112–122, 2008.

[40] M. C. Etter, "Encoding and decoding hydrogen-bond patterns of organic compounds," *Accounts of Chemical Research*, vol. 23, no. 4, pp. 120–126, 1990.

[41] M. C. Etter, J. C. MacDonald, and J. Bernstein, "Graph-set analysis of hydrogen-bond patterns in organic crystals," *Acta Crystallographica Section B: Structural Science*, vol. 46, no. 2, pp. 256–262, 1990.

[42] C. Hee Ng, S. Guan Teoh, N. Moris, and S. Yang Yap, "Structural, infrared spectral and thermogravimetric analysis of a hydrogen-bonded assembly of cobalt(II) and nickel(II) mixed complex cations with hexamethylenetetraamine and aqua ligands: $\{[M(hmt_)_2(H_2O)_4][M(H_2O)_6]\}(SO_4)_2 \cdot 6H_2O$," *Journal of Coordination Chemistry*, vol. 57, no. 12, pp. 1037–1046, 2004.

[43] Y. Zhang, J. Li, M. Nishiura, and T. Imamoto, "Structural, spectral and thermal properties of a polymeric nickel(II) complex containing two-dimensional network," *Journal of Molecular Structure*, vol. 520, no. 1–3, pp. 259–263, 2000.

[44] F. E. Mabbs and D. J. Machin, *Magnetism and Transition Metal Complexes*, Chapman and Hall, London, UK, 1973.

[45] F. A. Cotton and G. Wilkinson, *Advanced Inorganic Chemistry, A Comprehensive Text*, Interscience Publishers, New York, NY, USA, 4th edition, 1980.

[46] Z. H. Chohan, A. Munawar, and C. T. Supuran, "Transition metal ion complexes of Schiff-bases. Synthesis, characterization and antibacterial properties," *Metal-Based Drugs*, vol. 8, no. 3, pp. 137–143, 2001.